UNIVERSITÉ DU QUÉBEC

THÈSE
PRÉSENTÉE À
L'UNIVERSITÉ DU QUÉBEC À CHICOUTIMI
POUR L'OBTENTION
DU DOCTORAT EN RESSOURCES MINÉRALES

PAR
WENJIN YANG

GÉOCHIMIE ET MINÉRALOGIE DES GRANITES DE LA REGION DE HETAI, PROVINCE DE GUANGDONG, CHINE MÉRIDIONALE

AVRIL 1993

Bibliothèque
Paul-Émile-Boulet

UQAC
Université du Québec
à Chicoutimi

Mise en garde/Advice

Afin de rendre accessible au plus grand nombre le résultat des travaux de recherche menés par ses étudiants gradués et dans l'esprit des règles qui régissent le dépôt et la diffusion des mémoires et thèses produits dans cette Institution, **l'Université du Québec à Chicoutimi (UQAC)** est fière de rendre accessible une version complète et gratuite de cette œuvre.

Motivated by a desire to make the results of its graduate students' research accessible to all, and in accordance with the rules governing the acceptation and diffusion of dissertations and theses in this Institution, the **Université du Québec à Chicoutimi (UQAC)** is proud to make a complete version of this work available at no cost to the reader.

L'auteur conserve néanmoins la propriété du droit d'auteur qui protège ce mémoire ou cette thèse. Ni le mémoire ou la thèse ni des extraits substantiels de ceux-ci ne peuvent être imprimés ou autrement reproduits sans son autorisation.

The author retains ownership of the copyright of this dissertation or thesis. Neither the dissertation or thesis, nor substantial extracts from it, may be printed or otherwise reproduced without the author's permission.

GEOCHEMISTRY AND MINERALOGY OF GRANITES IN THE HETAI AREA, GUANGDONG, SOUTH CHINA

BY

WENJIN YANG

A THESIS FOR THE DEGREE OF DOCTOR OF PHILOSOPHY AT
UNIVERSITÉ DU QUÉBEC À CHICOUTIMI, QUÉBEC, CANADA
AND
INSTITUTE OF GEOCHEMISTRY, ACADEMIA SINICA, CHINA

APRIL 1993

ABSTRACT

The Hetai Area, located in the western Guangdong Province of South China, has been affected by four orogenies, from the Caledonian (Early Paleozoic) to the Yanshanian (Late Mesozoic). Two major northeast trending faults, the Guangning-Loudin and the Wuchuan-Sihui, characterized by wide deformation zones, traverse the region. Granitic rocks, which cover about half the surface area, are related to each of the four orogenies. Previous regional studies have been premised on the importance of in situ granitization of Precambrian strata for the formation of the older granitic rocks as well as the formation of the Hetai gold deposits.

This study discusses the genesis and evolution of ten granitic intrusions from the Hetai area based on their petrography, mineralogy and geochemistry. The granites of the Hetai Area are defined as "older granites" (Caledonian and Hercynian granites) and "younger granites" (Indosinian and Yanshanian granites) for comparison. Detailed field and microscopic observations show that all granitic rocks have a magmatic flow foliation. This foliation is overprinted by various degrees of solid-state deformation in the older (Caledonian and Hercynian) granite bodies.

The geochemical analyses of granites also distinguish them into different types. The older granites are characterized mainly by peraluminous chemistry (A/CNK>1.05), high LILE/HFSE, HREE/LREE and a negative Eu anomaly, whereas the younger granites are characterized by slightly peraluminous and metaluminous chemistry (A/CNK<1.05), a significant change of LILE/HFSE, HREE/LREE and a negative Eu anomaly ranging from low to high with the calc-alkaline ----> alkaline evolution of the magma. Comparison of the granites of the Hetai Area to those of well studied world areas by selected geochemical diagrams such as (Nb+Ta) vs (V+Sc) and Rb/Sr shows that the older granites are similar to S-type granite, but the younger granites are coincident with I-type and A-type (?) granites.

Au contents are higher in younger granites than those in older granites. Au distributions in different type granites of the Hetai Area suggest that the granites derived

from basic magmas are Au enriched compared to those derived from peraluminous crustal source regions.

Chemical analyses of biotite show that biotites from the older granites contain high FeO (>22%) and Al_2O_3(>15%) but low MgO (<8%), TiO_2 (<3%) and SiO_2 (<36%), whereas those from the younger granites have high MgO (>8%), TiO_2 (>3%) and SiO_2 (>36%) but low FeO (<22%) and Al_2O_3 (<15%). In general, the biotites from older granites are characterized by Fe-biotite and their M values are < 0.45 ($M=Mg/(Mg+Fe^{2+}+Mn)$), whereas the biotites from younger granites are characterized by Mg-biotite and their M values are > 0.45 in the ternary chemical classification. The amphiboles of the younger granites are Mg-hornblende and actinolite, but there are no amphiboles in the older granites. Plagioclases from the older granites have low anorthite content (An 35-5), and those from the younger granites are characterized by high initial anorthite contents (An 70-30) becoming very low (An 15-0) with magmatic differentiation.

The crystallization temperature of different granites has been estimated by the $Fe^{2+}/(Mg+Fe^{2+})$ in biotite, and the older granites have a lower temperature (700-850 °C) than the younger granites (850-950 °C). In addition, the presence of silicate melt inclusion provides further evidence that the Hetai granites are the result of magmatic crystallization, and the homogenization temperature of silicate melt inclusion indicates that the crystallization temperature of the older granites (750-850 °C) is lower than that of the younger granites (900-950 °C).

In summary, the older granites are similar to S-type granites and they are probably the result of continent-continent collision (Early Paleozoic to Early Mesozoic), whereas the younger granites are similar to I-type and A-type granites and are produced in a subduction environment (Middle Mesozoic)---> extension environment (Late Mesozoic). A geotectonic evolution of different granites of the Hetai Area may be suggested. An Early Paleozoic continental collision folded, thickened and melted the Precambrian sedimentary rocks, producing the Caledonian and Hercynian peraluminous granites. The later geotectonic evolution was characterized by a subduction environment in the Middle-Late Mesozoic periods, so that the Indosinian and Yanshanian calc-alkaline granite series were produced and the final Yanshanian period resulted in the alkali-granite series in an extension environment possibly because of a higher subduction angle. Generally, the geochemical

evolution of the different granites shows a geotectonic evolution from the peraluminous collision-type granites to mafic and calc-alkaline subduction-type granites finally to alkaline extension-type granites in the Hetai Area.

RÉSUMÉ

Cette thèse porte sur la génèse et l'évolution des roches granitiques de la région de Hetai et sur leurs relations possibles avec la minéralisation aurifère. Cette région de la Chine Méridionale est située à l'ouest de la Province de Guangdong. La Chine Méridionale a une histoire géotectonique complexe et l'étude des granites de la région de Hetai, qui sont de différents âges, permet d'en reconstituer une partie.

La Chine Méridionale est divisée en trois grands domaines géotectoniques orientés nord-nord-est, qui sont d'ouest en est : le domaine de Nanling, le domaine du Yangtzé et le domaine Côtier. Le domaine de Nanling, ou un socle précambrien est identifié, est fortement déformé, résultat d'une collision continentale à la fin du paléozoïque- début du mésozoïque. Des granites gneissiques à biotite abondants sont associés à cette collision. Le domaine du Yangtzé est également déformé et comprend une série intrusive de gabbro, diorite à hypersthène, diorite quartzite, tonalite et de granodiorite ainsi que des roches volcaniques associées. Ce domaine et le magmatisme associé resultent d'une subduction de type Andin au Mésozoïque moyen. Le domaine Côtier, qui est recoupé par une faille majeure de direction nord-est, comprend une série ignée plutono-volcanique où les granites à feldspath alcalin dominent. Le domaine Côtier correspond à une phase d'extension de la subduction précitée à la fin du Mésozoïque. D'une façon générale, les granites de ces trois domaines ont des caractérisques minéralogiques et chimiques différents : les granites du domaine de Nanling sont de type-S, ceux du domaine du Yangtzé sont de type-I et, les granites du domaine Côtier montrent une transition du type-I au type-A. Cette classification des granites de la Chine Meridionale servira de fondement pour séparer les granites de la région de Hetai.

Quatre orogénies sont reconnues dans la région de Hetai : l'orogénie Calédonienne (580-360 Ma), l'orogénie Hercynienne (360-240 Ma), l'orogénie Indosinienne (240-190 Ma)et l'orogénie Yanshanienne (Mésozoïque supérieur, 190-65 Ma). Les roches sedimentaires, dont l'âge varie du précambrien au paléozoïque inférieur, sont

métamorphisées aux faciés des schistes verts et amphibolite. Deux failles majeures recoupent la région : la faille de Guangning-Loudin de direction nord-est et la faille de Wuchuan-Sihui de direction nord-nord-est.

Des plutons granitiques polyphasés d'âges variés occupent 50% de la superficie de cette région et 10 de ceux-ci furent étudiés. ils peuvent être divisés en deux groupes d'âge : les granites anciens et les granites récents. Les granites anciens sont des granites à biotite, dont la texture varie de oeillée à gneissique à mylonitique, qui se retrouvent associés à la zone de faille Guangning-Loudin. Leurs âges préliminaires varient du Calédonien (plutons de Shijiang, Sidong et Shiniutou) à l'Hercynien (pluton de Guangning). Les granites récents, dont la composition varie de granodiorite à granite à feldspath alcalin, sont localisée à proximité de la zone de faille Wuchuan-Sihui. Ils se divisent en trois groupes d'âges préliminaires : Hercynian (?) (pluton de Yunlougan), Indosinien (pluton de Wuchun) et Yanshanien (pluton de Sihui). Deux types d'enclaves sont identifiées dans ces granites : des enclaves sombres (biotite + feldspath) dans le pluton de Shijiang et des enclaves granodioritiques dans les plutons de Wuchun et de Sihui.

Ces roches granitiques ont souvent été interprétées par les géologues Chinois comme résultant de la granitisation des roches précambriennes. Cette hypothèse ne concorde pas avec les données de terrain qui indiquent la présence d'une foliation magmatique dans tous les granites. Dans les granites anciens elle apparaît comme relique malgré la déformation et la recristallisation à l'état solide qui produit des structures gneissiques, oeillées et mylonitiques. La nature magmatique de ces roches est confirmée par l'étude au microscope qui montre en plus, que les cristaux de plagioclase dans tous les types de granites sont zonés. De plus, certains de ces granites sont des corps polyphasés (granodiorite, monzogranite, granite) et d'autres montrent des enclaves. Le granite de Shijiang présent des enclaves sombres, qui sont possiblement des sédiments métamorphisés, tandis que les complexes de Wuchun et de Sihui sont caractérisés par des enclaves ignées granodioritiques.

Les analyses géochimiques permettent de distinguer deux grands types de granites dans la région de Hetai : les granites anciens et les granites récents. Les granites anciens sont peralumineux (paramètre-Al > 1.05), ils montrent une anomolie négative en Eu et ils

possèdent des ratios K_2O/Na_2O et "HREE/LREE" élevés et un rapport "LILE/HFSE" moyen comparativement aux granites récents. Ces derniers sont méta-alumineux et la variation des ratios MgO/(MgO+FeO), K_2O/Na_2O, Rb/Sr, "HREE/LREE" , "LILE/HFSE" ainsi que l'accroissement de l'anomalie en Eu sont capatibles avec une suite de différenciation calco-alkaline : (gabbro) --> diorite quartzique --> granodiorite --> (granite à feldspath alcalins). Lorsqu'on compare ces granites à ceux provenant de régions mieux étudiées sur des diagrammes discriminants comme (Nb+Ta) vs (V+Sc) et vs Rb/Sr, les granites anciens montrent des similitudes avec les granites de type-S tandis que les granites récents coïncident, pour la majorité, avec les granites de type-I et certains avec le type-A (?).

La composition chimique des biotites, des amphiboles et des plagioclases analysés à la microsonde permet de confimer la séparation des granites de Hetai en deux groupes. Les granites anciens ont des biotites-Fe caractérisées par les pourcentages en oxydes suivants : FeO (>22%), Al_2O_3 (>15%), MgO (<8%), TiO_2 (<3%) et SiO_2 (<36%), ainsi qu'un rapport M (<0.45) ($M=Mg/(Mg+Fe^{2+}+Mn)$). Par contre, les granites récents possèdent des biotites-Mg avec des pourcentages en oxydes suivants : FeO (<22%), Al_2O_3 (<15%), MgO (>8%), TiO_2 (>3%) et SiO_2 (>36%) ainsi qu'un rapport M > 0.45. Les granites anciens ne possèdent pas de hornblende tandis que les granites récents montrent soit une hornblende-Mg, soit une hornblende-actinolitique. Les granites anciens ont des plagioclases de calcité plus basse (An=35-5) que celle des granites récents (An=70-30) sauf dans le cas des granites à feldspath alcalins (An=15-0). Ces différences dans la minéralogie réflètent essentiellement une chimie des magmas différente pour les deux types de granite.

Les températures de cristallisation, basées sur les rapports $Fe^{2+}/(Mg+Fe^{2+})$ des biotites, sont de 950 -850 °C pour les granites récents et de 850-750 °C pour les granites anciens. Des estimés de profondeurs d'emplacement, basées sur le Al (t) des amphiboles, indiquent un niveau plus profond pour les granites anciens que pour les granites récents.

La présence d'inclusions silicatées fondues apporte un argument supplémentaire pour une origine ignée de ces granites. Ces inclusions varient en dimensions de 0.10 à 0.20 mm et sont ellipsoïdales dans les granites anciens, tandis que dans les granites récents elles varient de 0.05 à 0.15 mm et sont polygonales. Leur température d'homogénéisation est de 850-750 °C pour les granites anciens et de 950-850 °C pour les granites récents.

L'or présente des valeurs plus basses (0-5 ppb) dans les granites anciens que dans les granites récents (5-15 ppb); celles les plus élevées étant dans le gabbro de Huangtongjiang avec 15 ppb. Cette distribution suggère que les granites derivés de magmas basiques sont enrichis en or par rapport à ceux qui dérivent d'une source crustale peralumineuse. Il faut aussi noter que les granites anciens ont des valeurs d'or similaire à celles des sédiments précambriens.

L'évolution géotectonique suivante peut être suggérée pour les granites de Hetai:

1. Au paléozoïque inférieur des roches précambriennes sont plissées et métamorphisées et subissent une fusion partielle dûe à un doublement de la croûte résultant d'une collision continent-continent. Les granites peralumineaux anciens (Calédoniens et Hercyniens) sont le résultat de cette anatexie crustale. Ces granites deviennent déformés suite à l'évolution géotectonique subséquente.

2. Au Mésozoïque inférieur la subduction de la plaque océanique de Gunanhai sous le continent de Nanling à conduit à la mise en place du granite de type-I de Yunlougan.

3. Au Mésozoïque moyen-supérieur, la subduction se poursuit et les plutons de type-I d'âges Indosinien et Yanshanien inférieur se mettent en place.

4. Au Mésozoïque supérieur, l'angle de la subduction augmente, de l'extension prend place et les granites à feldspath alcalin de type Sihui (type-A ?) s'emplacent à faible profondeur.

En résumé, les granites anciens sont apparentés aux granites de type-S et resultent d'une collision continent-continent qui prend place entre le Paléozoïque inférieur et le Mésozoïque inférieur. Par contre les granites récents sont similaires aux types-I et A (?). Ils sont associés à une subduction qui débute au Mésozoïque moyen et, qui suite à une augmentation de l'angle du plan de benioff, produit une extension au Mésozoïque supérieur.

河台地区花岗岩的矿物学和地球化学
-----兼论本区上地幔岩浆作用与金的富集

（摘　要）

长英质矿物微结构构造和硅酸盐熔融包裹体的研究证明,河台花岗岩是岩浆作用的产物,固结后又经过了多次强烈的动力变形作用的迭加.总之,不是所谓的花岗岩化的结果.无论是加里东和海西期花岗岩,或是印支和燕山期花岗岩,都具有原始岩浆流动构造的特征.但是后来的动力变形作用强烈地迭加在较老的花岗岩（加里东和海西期）上.全岩和黑云母,角闪石,斜长石的地球化学分析表明,加里东期的石涧岩体,诗洞岩体,石牛头岩体和海西期的广宁岩体具有过铝和富含大离子亲石元素和强烈的Eu 负异常的特征,黑云母为 Fe-黑云母,富 Al2O3 和 FeO,不含角闪石,斜长石的 An 号码较低（An < 30）. 相反,黄铜降的辉长岩,海西期的云楼冈花岗闪长岩,印支和燕山期的伍村花岗闪长岩,巨斑二长花岗岩和四会花岗闪长岩,钾长花岗岩具有如下特征：贫铝,贫大离子亲石元素,很弱的 Eu 负异常和较富 LREE, 但是随着岩浆分异演化从辉石闪长岩,花岗闪长岩到钾长花岗岩,大离子亲石元素和 HREE 明显增高,Eu 负异常增强.黑云母主要为镁质黑云母,含镁质角闪石,斜长石的 An 组成较高但随着岩浆分异演化而变低. Rb/Sr, V, Sc, (Nb+Ta) 等元素的地球化学演化模式分析表明,加里东的石涧等岩体和海西期的广宁岩体是前寒武地层源岩在大陆型挤压碰撞环境下经过 20-30% 部分熔融的熔体原地-半原地结晶而成.相反,燕山期的四会等岩体,印支期的伍村岩体和海西期的云楼冈岩体以及黄铜降的辉长岩是在俯冲和扩张环境下上地幔来源的岩浆经高度结晶分异的系列产物.

Au 在上地幔岩浆作用形成的花岗岩中具有明显高的选择性.中子活化分析表明,黄铜降辉长岩的金含量为 7-15 ppb, 云楼冈花岗闪长岩为 8-12 ppb, 伍村巨斑二长花岗岩为 9-11 ppb, 四会碱长花岗岩为 4-6 ppb. 相反,石涧花岗岩为 0.3-3.1 ppb, 诗洞和石牛头花岗岩为 1.8-4.3 ppb, 广宁岩体为 0.8-4.5 ppb. 此外,前寒武变质地层中的金含量为 0.4-3.6 ppb. 对比可见,上地幔岩浆作用形成的花岗岩比上地壳部分熔融形成的花岗岩具有明显高的金分布背景.金的相关矢量分析表明,具有高金含量背景的上地幔岩浆的高度结晶分异演化作用将促使金与富 NaCl 和 CO2 的岩浆挥发份一起从岩浆中分离,并向低压方向（构造断裂）迁移富集成矿.所以,河台地区上地幔来源的花岗岩的成岩演化可能是本区金矿形成的一个重要途径.

ACKNOWLEDGEMENTS

This thesis is part of the CIDA (Canadian International Development Agency) joint program of Sciences de la Terre, Université du Québec à Chicoutimi (UQAC) and the Institute of Geochemistry, Chinese Academy of Sciences (IGCAS). The scholarships were provided by CIDA-China joint program.

At first, I would like to express my sincere thanks to the supervisor, Professor Edward H. CHOWN, and members of the supervision committee, Professor Gérard WOUSSEN and Professor Huanzhang LU at UQAC. This thesis was prepared under their careful supervision, and I have greatly benefited from frequent discussion with them.

Sincere thanks are extended to Professor Jayanta GUHA at UQAC and Professor Guangzhi TU at IGCAS. This project was initiated by their confidence and guidance. I also would like to express my sincere thanks to Professor Liankui WANG at IGCAS. I have greatly benefited from his guidance during previous field investigations. Many thanks to Mr. Michel TRAMBLAY, administrative assistant of the CIDA program, for the great help during the preparation of this thesis at UQAC.

I have also greatly benefited from the assistance of many professors and colleagues both in UQAC and IGCAS. They include : Profs. Pierre COUSINEAU, M. D. HIGGINS, Alain ROULEAU, Sarah-Jane BARNES, Edward W. SAWYER, Réal DAIGNEAULT and Wulf MUELLER (UQAC); Ms. Sanmei GAO, Danielle GIOVENAZZO, Jeannette SEE, Françoise LANGE, Caroline ANTONUK, Katherine BOGGS, and Mr. Denis COTE, Bernard LAPOINTE, Yvon BOUDREAULT, Paul BEDARD, Claude DALLAIRE, Pierre DOUCET, Réjean GIRARD, Jean LACROIX, Daniel BANDY-AYERA, Guoxiang CHI and Amar DAHMANI (UQAC); Profs. Jingpin CHEN, Xianpei CHEN, Xiuzhang WANG, Yimao LIU, Shaoli ZHANG, and Mrs. Jinlin SUN,

Yougzhang ZHOU, Jianjun TANG, Wenxin XU, Yaolong LIAN, Bin LAO, Junsou LIU, Guangqing LU and Mrs.Rumin PENG (IGCAS).

I also thank to my wife, Xiaoyuan GUO, for her understanding.

CONTENTS

ABSTRACT.....i
RESUME.....iv
CHINESE ABSTRACT.....viii
ACKNOWLEDGEMENTS.....ix
CONTENTS.....x
LIST OF FIGURES AND TABLES.....xvi

CHAPTER I . INTRODUCTION AND GEOLOGICAL SETTING.....1

1-1. INTRODUCTION.....1
1-1-1. Background geology of South China.....1
1-1-2. Granite classification in South China.....8
1-2. GEOLOGICAL SETTING IN THE HETAI AREA.....9
1-2-1. The principal country rocks.....11
1-2-2. Faults, shear zones and deformation.....11
1-2-3. Granitic plutons and their enclaves.....12
1-2-4. Hetai gold deposit.....14
1-2-5. Problems in the Hetai Area.....16

CHAPTER II . PETROGRAPHIC CHARACTERISTICS OF THE GRANITES.....18

2-1. INTRODUCTION.....18
2-2. PETROGRAPHIC COMPARISONS BETWEEN GRANITES OF DIFFERENT AGES.....19
2-2-1. Caledonian granitic bodies.....19
(1) Shijiang complex.....19

(2) Sidong granite....28
(3) Shiniutou granite....28
2-2-2. Hercynian granites.... 32
(1) Guangning granite....32
(2) Yunlougan pluton....35
2-2-3. Indosinian granites....35
2-2-4. Yanshanian granites....40
2-2-5. Huangtongjiang gabbro....44
2-2-6. Comparison between granites of different ages....46
2-3. IDENTIFICATION OF MAGMATIC FLOW FOLIATION AND TECTONIC FOLIATION....47
2-3-1. Magmatic flow foliation....49
2-3-2. Solid-state deformations....50
2-3-3. Myrmekite....52
2-4. SUMMARY....55

CHAPTER III . GEOCHEMISTRY OF GRANITES 57

3-1. INTRODUCTION....57
3-2. GEOCHEMICAL CHARACTERISTICS OF THE CALEDONIAN GRANITES....61
3-2-1. Shijiang granitic complex....61
(1) Geochemical features....61
(2) Relations between dark enclaves and the Shijiang host granites....66
(3) Petrogenetic model of the Shijiang complex....69
3-2-2. Sidong granite....74
3-2-3. Shiniutou granite....78
3-2-4. Geochemical comparison among the Caledonian granites....81
3-3. HERCYNIAN GRANITES....82
3-3-1. Guangning granite....86
3-3-2. Yunlougan pluton....87
(1) Geochemical features of granodiorite....87

(2) Geochemical features of pegmatite.....91
3-3-3. Geochemical comparison between the Hercynian granites.....91
3-4. INDOSINIAN GRANITES.....95
3-4-1. Geochemical features of the megacryst monzogranite.....95
3-4-2. Geochemical features of the granodioritic enclave.....96
3-4-3. Relation between the megacryst monzogranite and granodioritic enclaves...97
3-5. YANSHANIAN GRANITES.....102
3-5-1. Geochemical features of the host alkali-feldspar granite suite.....102
3-5-2. Geochemical features of the granodioritic enclave.....103
3-5-3. Evolution of the Sihui granite suite.....105
3-6. GEOCHEMICAL FEATURES OF THE HUANGTONGJIANG GABBRO.....106
3-7. GEOCHEMICAL COMPARISONS BETWEEN
OLDER GRANITES AND YOUNGER GRANITES.....113
3-7-1. Criteria to differentiate I- and S-type granites.....116
3-7-2. Trace element and REE comparisons between granite suites.....117
3-7-3. Tectonic interpretation by geochemical discriminations.....118
3-7-4. Au distribution in different granites.....128

CHAPTER IV. CHEMICAL CHARACTERISTICS OF BIOTITE,
AMPHIBOLE AND FELDSPAR.....131

4-1. INTRODUCTION.....131
4-2. CHEMICAL COMPOSITIONS OF BIOTITE.....136
4-2-1. Chemical features of biotite from the Caledonian granites.....136
(1) Biotite from the Shijiang complex.....136
(2) Biotite from the Sidong granite 138
(3) Biotite from the Shiniutou granite.....140
(4) Comparison between biotites from the Caledonian granites.....140
4-2-2. Chemical compositions of biotites from the Hercynian plutons.....141
(1) Biotite from the Guangning pluton.....141
(2) Biotite from the Yunlougan granodiorite.....143
(3) Chemical comparisons between biotites from the Gunagning
and the Yunlougan 143

4-2-3. Chemical compositions of biotite from the Indosinian granites.....146
(1) Biotites from the Wuchun megacryst monzogranite.....146
(2) Biotites from the Wuchun granodioritic enclaves.....147
4-2-4. Chemical compositions of biotites from the Yanshanian granites.....147
(1) Biotite from the Sihui alkali-feldspar granite.....147
(2) Biotite from the Sihui granodioritic enclaves.....150
(3) Geochemical evolution of biotites in the Sihui granite suite.....150
4-3. COMPARISON BETWEEN BIOTITE FROM THE HUANGTONGJIANG GABBRO AND FROM PRECAMBRIAN SEDIMENTARY ROCK.....153
4-4. COMPARISON BETWEEN BIOTITE FROM THE DIFFERENT ENCLAVES.....154
4-5. GEOCHEMICAL CHARACTERISTICS OF BIOTITE FOR DIFFERENT GRANITE TYPES IN THE HETAI AREA.....158
4-5-1. Major oxide averages of each sample by electron probe analysis.....158
4-5-2. Trace element characteristics in biotite.....159
4-6. CHEMICAL COMPOSITION OF AMPHIBOLE.....163
4-6-1. Amphibole from the Yunlougan granodiorite.....163
4-6-2. Amphibole from the Sihui granodioritic enclaves.....165
4-6-3. Amphibole from the Huangtongjiang gabbro.....167
4-6-4. Comparison between amphibole from different granitic plutons.....167
4-7. CHEMICAL CHARACTERISTICS OF FELDSPAR FROM THE HETAI GRANITES.....170
4-7-1. Chemical characteristics of feldspar from the Caledonian granites.....171
4-7-2. Plagioclase from the Hercynian granites.....173
4-7-3. Plagioclase from the Indosinian granites.....175
4-7-4. Plagioclase from the Yanshanian granites.....176
4-7-5. Comparison between plagioclase from the Huangtongjiang gabbro and from the Precambrian sedimentary rocks.....179
4-7-6. Geochemical variation of plagioclase from granites of different ages.....180
4-8. MINERAL CRITERIA FOR IDENTIFYING DIFFERENT GRANITE TYPES.....182

CHAPTER V. TEMPERATURE AND PRESSURE ESTIMATES.....184

5-1. INTRODUCTION.....184
5-2. T AND P ESTIMATES OF GRANITES
BASED ON BIOTITE AND AMPHIBOLE.....185
5-2-1. Temperature estimate based on Mg and Fe^{2+} in biotite.....185
5-2-2. Pressure estimates based on Al content in amphibole.....187
5-3. SILICATE MELT INCLUSIONS IN DIFFERENT HETAI GRANITES.....191
5-3-1. Petrographic features of silicate melt inclusions.....191
5-3-2. Change of silicate melt inclusions at high temperature.....194
5-4. FLUID INCLUSIONS IN GRANITES.....195

CHAPTER VI. DISCUSSION AND CONCLUSIONS.....200

6-1. DISCUSSION.....200
6-2. CONCLUSIONS.....207

REFERENCES.....209

APPENDIX I. DESCRIPTION OF SAMPLES.....220

APPENDIX II. METHODS OF ANALYSES.....224

APPENDIX III. TABLES OF CHEMICAL DATA OF
GRANITES AND MINERALS.....226

LIST OF FIGURES AND TABLES

1. LIST OF FIGURES

Fig.1.1. Provinces of South China 2
Fig.1.2. Three main tectonic areas of South China.....4
Fig.1.3. Sketch diagram of granite types and tectonic evolution of South China.....6
Fig.1.4. Geological map of western Guangdong Province 7
Fig.1.5. Geological map of the Hetai Area, Guangdong Province.....10
Fig.2.1. Intrusive contact between different phases in the Shijiang complex.....21
Fig.2.2. Flow fabric of aligned zoned plagioclase phenocrysts surrounding by bent mica and crushed fine-grained feldspar and quartz in the Shijiang complex.....22
Fig.2.3. Differing degrees of deformed structures in the Shijiang complex.....23
Fig.2.4. A : Myrmekite and finer-grained aggregates of mica, feldspar and quartz around the deformed plagioclase phenocrysts;
B : Myrmekite occurring on the border of plagioclase phenocrysts in the Shijiang complex.....24
Fig.2.5. A : Strain shadow of the polysynthetically twinned microcline;
B : Myrmekite produced in broken and twinned microcline phenocrysts in the later leucogranitic phases of the Shijiang complex.....25
Fig.2.6. The Shijiang complex on the Q-Af-Pl ternary classification.....26
Fig.2.7. Intrusive contact between coarse-grained and medium-fine grained phases in the Sidong complex.....29
Fig.2.8. Myrmekite occurring in alkali-feldspar of the Sidong granite.....29
Fig.2.9. Magmatic flow foliation superimposed by strong deformation in the Shiniutou granite.....30

Fig.2.10. Myrmekite occurring in twinned microcline phenocrysts of the Shiniutou granite....31
Fig.2.11. Dark enclaves aligned parallel to the magmatic flow foliation in the Guangning granite....33
Fig.2.12. Flow fabric of bent euhedral plagioclases, and interstitial quartz polygonized and elongated parallel to ductile deformation in the Guangning granite....33
Fig.2.13. Allanite enclosed by plagioclase and biotite in the Guangning granite....34
Fig.2.14. Magmatic flow of aligned amphibole and biotite, surrounded by feldspar and polygonized quartz; Yunlougan pluton....34
Fig.2.15. Flow fabric of zoned plagioclase phenocrysts surrounded by bent biotite and polygonized quartz; Yunlougan pluton....36
Fig.2.16. Granodioritic enclaves in the host megacryst monzogranite of the Wuchun pluton....36
Fig.2.17. Flow fabric of megacrysts with growth rims in the Wuchun pluton....37
Fig.2.18. Aligned zoned plagioclase phenocrysts enclosing biotite in the Wuchun pluton....37
Fig.2.19. Glomeroporphyritic aggregates of plagioclase xenocrysts in the granodioritic enclaves of the Wuchun pluton....39
Fig.2.20. Granodioritic enclave flattened parallel to magmatic foliation, slight deviation of fabric around xenolith; Sihui pluton....41
Fig.2.21. Schlieren layering of biotite and feldspar in the Sihui alkali-feldspar granite....41
Fig.2.22. Aligned zoned plagioclase phenocrysts in the Sihui alkali-feldspar granite....42
Fig.2.23. Myrmekite in the Sihui alkali-feldspar granite....43
Fig.2.24. Zoned plagioclase phenocrysts in the granodioritic enclaves of the Sihui granite suite....45
Fig.2.25. Subophitic texture of the Huangtongjiang gabbro....45
Fig.3.1. Comparison of chondrite-normalized REE diagrams between different granite types of South China....60
Fig.3.2. The Caledonian granites on the Q-Af-Pl ternary classification....63
Fig.3.3. Harker diagrams of the Shijiang complex....64
Fig.3.4. Multi-element spiderdiagrams of the Shijiang complex....67
Fig.3.5. Chondrite-normalized REE diagrams of the Shijiang complexes....68

Fig.3.6. Petrogenetic process model for the Shijiang granite complex.....69
Fig.3.7. Comparison of spiderdiagrams between the Precambrian sedimentary rocks and the Shijiang dark enclaves.....72
Fig.3.8. Comparison of chondrite-normalized REE diagrams between the Shijiang dark enclaves and the Precambrian sedimentary rocks.....73
Fig.3.9. Multi-element spiderdiagrams for the Sidong granite.....76
Fig.3.10. Chondrite-normalized REE diagrams for the Sidong granite.....77
Fig.3.11. Multi-element spiderdiagrams for the Shiniutou granite.....79
Fig.3.12. Chondrite-normalized REE diagrams of the Shiniutou granite.....80
Fig.3.13. Mol.Al2O3/(CaO+Na2O+K2O)-Al2O3/(Na2O+K2O) diagrams of the Caledonian granites.....83
Fig.3.14. Comparison between spiderdiagrams of the Caledonian granites.....84
Fig.3.15. Comparison between chondrite-normalized REE diagrams of the Caledonian granites.....85
Fig.3.16. The Hercynian granites on the Q-Af-Pl ternary classification.....88
Fig.3.17. Comparison between spiderdiagrams of the different Hercynian plutons.....89
Fig.3.18. Comparison between chondrite-normalized diagrams of the different Hercynian plutons.....90
Fig.3.19. Mol. Al2O3/(CaO+Na2O+K2O)-Al2O3/(Na2O+K2O) diagram of the Hercynian plutons.....93
Fig.3.20. Comparison between different granite types of the Hercynian.....94
Fig.3.21. The Indosinian granites on the Q-Af-Pl ternary classification.....98
Fig.3.22. Multi-element spiderdiagrams of the Wuchun granite suite.....99
Fig.3.23. Chondrite-normalized REE diagrams of the Wuchun granite suite.....100
Fig.3.24. Mol. Al2O3/(CaO+Na2O+K2O)-Al2O3/(Na2O+K2O) diagram of the Indosinian granites.....101
Fig.3.25. The Yanshanian granite suite on the Q-Af-Pl ternary classifcation.....107
Fig.3.26. Multi-element spiderdiagrams of the Sihui granite suite.....108
Fig.3.27. Chondrite-normalized REE diagrams of the Sihui granite suite.....109
Fig.3.28. Mol. Al2O3/(CaO+Na2O+K2O)-Al2O3/(Na2O+K2O) diagram of the Yanshanian granite suite.....110
Fig.3.29. The Harker diagrams of the Sihui granite suite.....111
Fig.3.30. Petrogenetic process model of the Sihui granite suite.....112

Fig.3.31. Multi-element spiderdiagrams of the Huangtongjiang gabbro.....114
Fig.3.32. Chondrite-normalized REE diagrams of the Huangtongjiang gabbro.....115
Fig.3.33. Na2O-K2O comparison between the Hetai granites and I-S type granites of Australia and southeastern Asia.....119
Fig.3.34. Mol. Al2O3/(CaO+Na2O+K2O)-Al2O3/(Na2O+K2O) diagram of different granites in the Hetai Area (after Maniar and Piccoli, 1989).....120
Fig.3.35. Comparison between spiderdiagrams of different granites in the Hetai Area...121
Fig.3.36. Comparison between chondrite-normalized REE diagrams of different granites in the Hetai Area.....122
Fig.3.37. Comparison between different granites by Pearce's (1984) diagrams.....123
Fig.3.38. Variations of Rb/Sr-(Nb+Ta) and (V+Sc)-(Nb+Ta) between granites of different ages in the Hetai Area.....124
Fig.3.39. Comparison between granites of different ages in the Wuchuan-Sihui Fault Zone.....126
Fig.3.40. (Nb+Ta) vs Rb/Sr and (V+Sc) variation diagrams between different granite types.....127
Fig.3.41. Au distribution trends in different granites of the Hetai Area.....130
Fig.4.1. Biotites from different granite types of South China on the ternary chemical classification 134
Fig.4.2. Biotites from the Caledonian granites and from the enclaves on the ternary chemical classification 137
Fig.4.3. Variation of biotite composition from the Shijiang dark enclaves and host granites.....139
Fig.4.4. Chemical variation of biotites from the Caledonian granites.....142
Fig.4.5. Biotites from the different Hercynian granites on the ternary chemical classification 144
Fig.4.6. Chemical comparison between biotites from the different Hercynian plutons...145
Fig.4.7. Biotites from the Indosinian granites their enclaves on the ternary chemical classification 148
Fig.4.8. Chemical variation of biotites from the Indosinian granites and enclaves.....149
Fig.4.9. Biotites from the Yanshanian granites anf their enclaves on the ternary chemical classification 151
Fig.4.10. Chemical variation of biotites from the Yanshanian granites and enclaves.....152

Fig.4.11. Biotites from the Huangtongjiang gabbro and from the Precambrian sedimentary rocks on the ternary chemical classification ...155
Fig.4.12. Comparison between biotites from the Huangtongjiang gabbro and from the Precambrian sedimentary rocks....156
Fig.4.13. Chemical comparison between biotites from the different enclaves....157
Fig.4.14. Biotites from different granites of the Hetai Area on the ternary chemical classification....160
Fig.4.15. Comparison between biotites from different granite types of the Hetai Area....161
Fig.4.16. Chemical classification of amphibole from the Hetai granites....164
Fig.4.17. Chemical variation of amphiboles from the Yunlougan granodiorite....166
Fig.4.18. Chemical variation of amphiboles from the Huangtongjiang gabbro....168
Fig.4.19. Comparison between amphiboles from the granites of Hetai Area and South China....169
Fig.4.20. Chemical variation of plagioclase from the Caledonian granites.... 172
Fig.4.21. Comparison between plagioclases from the different Hercynian plutons....174
Fig.4.22. Chemical variation of plagioclase from the Indosinian granite suite....177
Fig.4.23. Chemical variation of plagioclase from the Yanshanian granite suite....178
Fig.4.24. Chemical variation of plagioclases on the An-Ab-Or ternary diagram....181
Fig.5.1. Melt silicate inclusions in the Hetai granites....193
Fig.5.2. Comparison between original and heated melt silicate inclusions in different granites....196
Fig.6.1. Model of geotectonic evolution of different granite types of the Hetai Area....206

2. LIST OF TABLES

Table 1.1. Main granitic bodies in the Hetai Area, Guangdong Province.....13
Table 1.2. Ages of granitic plutons in the Hetai Area, Guangdong Province.....15
Table 2.1. Variation of rock-forming minerals from the Shijiang complex.....27
Table 2.2. Comparison of petrographic features between granites of different ages.....48
Table 3.1. Geochemical comparison between different granite types of South China.....59
Table 4.1. Comparison of biotite and amphibole from different granites of the Hetai Area and South China 183
Table 5.1. Temperature estimate by biotite, granites of the Hetai Area 193
Table 5.2. Pressure estimate by Al in amphibole, granites of the Hetai Area.....196
Table 5.3. Temperature of homogenization of silicate melt inclusions in granites of the Hetai Area 197
Table 5.4. Salinity and homogenization temperature of fluid inclusions in granites and ore deposits of the Hetai Area 199
Table 1. Major oxides of the Caledonian granites (in Appendix III).....228-229
Table 2. Trace element compositions of the Caledonian granites (in Appendix III).....230
Table 3. REE compositions of the Caledonian granites (in Appendix III).....231
Table 4. Major oxides of the Hercynian granites (in Appendix III).....232
Table 5. Trace element compositions of the Hercynian granites (in Appendix III).....233
Table 6. REE compositions of the Hercynian granites (in Appendix III).....234
Table 7. Major oxides of the Indosinian granites (in Appendix III).....235
Table 8. Trace element compositions of the Indosinian granites (in Appendix III).....236
Table 9. REE compositions of the Indosinian granites (in Appendix III).....237
Table 10. Major oxides of the Yanshanian granites (in Appendix III).....238
Table 11. Trace element compositions of the Yanshanian granites (in Appendix III).....239
Table 12. REE compositions of the Yanshanian granites (in Appendix III).....240
Table 13. Au contents in different granites of the Hetai Area (in Appendix III).....241
Table 14. Chemical compositions of biotites from the Caledonian granites (in Appendix III).....242-244

Table 15. Chemical analyses of biotites from the Hercynian granites (in Appendix III).....245
Table 16. Chemical analyses of biotites from the Indosinian granites (in Appendix III).....246
Table 17. Chemical analyses of biotites from the Yanshanian granites (in Appendix III).....247-248
Table 18. Comparison between biotites from the Huangtongjiang gabbro and from the Precambrian sedimentary rock (in Appendix III).....249
Table 19. Comparison between biotites from the different enclaves (in Appendix III).....250-251
Table 20. Trace elements and major oxide averages of biotites from granites of the Hetai Area (in Appendix III).....252
Table 21. Chemical analyses of amphiboles from granitic plutons of the Hetai Area (in Appendix III).....253-255
Table 22. Chemical analyses of plagioclases from the Caledonian granites (in Appendix III).....256-257
Table 23. Chemical comparison between plagioclases from the Hercynian granites (in Appendix III).....258
Table 24. Chemical analyses of plagioclases, Indosinian granites (in Appendix III).....259
Table 25. Chemical analyses of plagioclases, Yanshanian granites (in Appendix III).....260-261
Table 26. Chemical comparison between plagioclases from the Huangtongjiang gabbro and Precambrian metamorphosed sedimentary rock (in Appendix III).....262

CHAPTER I

INTRODUCTION AND GEOLOGICAL SETTING

1-1. Introduction

This thesis is concerned with the genesis and evolution of granitic rocks and their possible related mineralization in the Hetai Area, western Guangdong Province, South China.

1-1-1. Background geology of South China

South China consists of ten geographical provinces (Fig.1.1), and it is a composite of orogenic belts. In the light of available data, the main block of South China was formed in the Early-Middle Proterozoic era (Institute of Geochemistry, Academia Sinica, 1979; Li et al., 1989), or in the Late Proterozoic era (Hsu et al., 1990; Jahn et al., 1990). Hsu et al. (1990) considered that South China is a collage of three continental fragments, the Yangzi (the Yangtze), the Hunan (the Nanling) and the Dongnanya. According to Hsu et al. (1990), the Yangtze was separated from Gondwanaland during the Late Precambrian when an old ocean was present between the two continents. The southern margin of the Yangtze became a passive margin called the Yangtze passive margin, and the northern margin of the Nanling (Gondwana Continent) was an active margin. The Nanling was separated from a more southerly continent (Dongnanya, Southeastern Asia) in the Devonian by seafloor spreading which created a Late Paleozoic and early Mesozoic ocean (Gunanhai Ocean), and then Dongnanya became separated from Gondwanaland during the Late Permian when the Dongnanya plate moved northward to be reunited with the Nanling. The Nanling passive margin sequence was deformed by folding and overthrusting after the Late Mesozoic collision of the Nanling and Dongnanya continental plates. The suture melange resulting from this collision occurs at a few localities in coastal Fujian Province (Hsu et al., 1990).

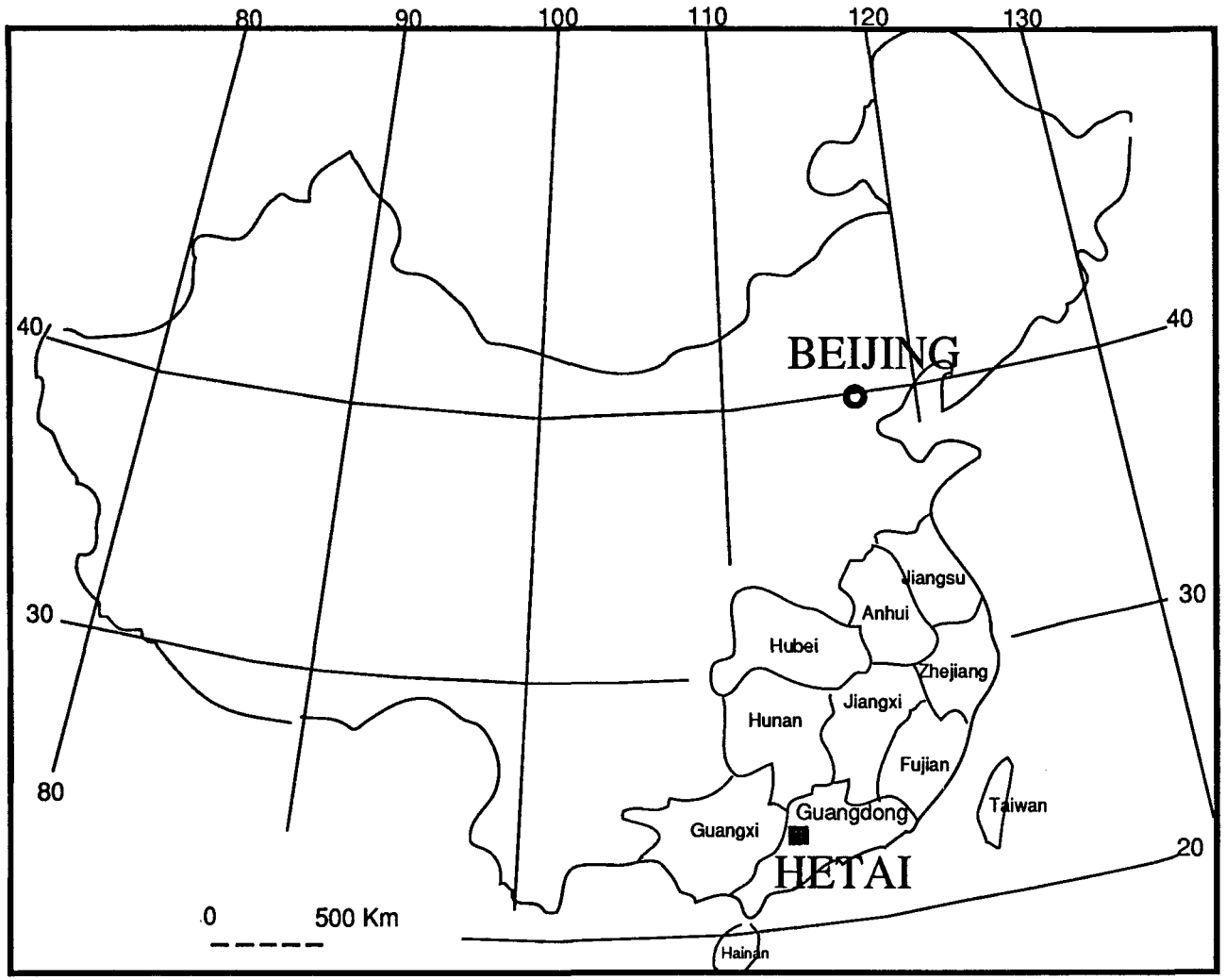

Fig.1.1. Provinces of South China

The Yangtze and the Nanling collided during the Triassic, and resulted in the deformation of the Yangtze passive margin to form the Yangtze Deformed Belt.

It appears clear that South China is not a post-Caledonian platform (Mo, 1987), but a composite of orogenic belts resulting from series of orogenic movements from Middle or Late Proterozoic to Late Mesozoic and Early Cenozoic age. However, studies of granitic magmatism and evolution divide South China into three main tectonic areas, the Yangtze Area, the Nanling Area and the Coast Area (Fig.1.2). The Nanling Area is commonly considered to represent the Precambrian basement in South China (Institute of Geochemistry, Academia Sinica, 1979; Mo, 1985). It is also characterized by a strongly compressive deformation and by a series of granites from Precambrian to Caledonian and Early Yanshanian (Late Mesozoic) in age, which may be derived by processes of continent-continent collision following the model of Harris et al. (1986). These may have been caused by the collision of the European and Asian continents in the Middle Proterozoic and Paleozoic (Institute of Geochemistry, Academia Sinica, 1979) and by the collision of the Yangtze and Nanling microcontinents in the Late Mesozoic (Hsu et al., 1990). The Yangtze Area also includes a strongly deformed belt, but is characterized by a series of Early Yanshanian (Late Mesozoic) granitic intrusives ranging from gabbro, pyroxene diorite, quartz diorite, tonalite and granodiorite and associated volcanic rocks, showing similar features to the Andino-subduction type (Pitcher, 1987). Therefore, the deformed belt and granitic magmatism of the Yangtze may be due to an ancient oceanic plate subduction beneath the Yangtze southern margin followed by a collision between the Nanling and Yangtze microcontinents during the Late Mesozoic (Hsu et al. 1990). Inland areas of the Nanling craton were intruded by Early Yanshanian granites (Institute of Geochemistry, Academia Sinica, 1979) and strongly deformed because of this continental collision. Similarly, the Zhejiang-Fujian-Guangdong Coast area is also a strongly deformed belt, but in contrast to the former, it is characterized by thrust faults and a series of granites, principally alkali feldspar granites and associated volcanic rocks, which may have resulted from the subduction of a paleo-Pacific plate (Kula) beneath the Asian continent (Guo, 1984; Wang et al., 1984a; Jahn et al., 1990) or from a Gunanhai Ocean plate (Hsu et al., 1990) beneath the Nanling continent. In addition, it may have resulted from an arc-continent collision during the Late Mesozoic and Early Cenozoic. Extension is a main feature of the Coast Area, in which alkali-feldspar granites and associated volcanic rocks were widely developed.

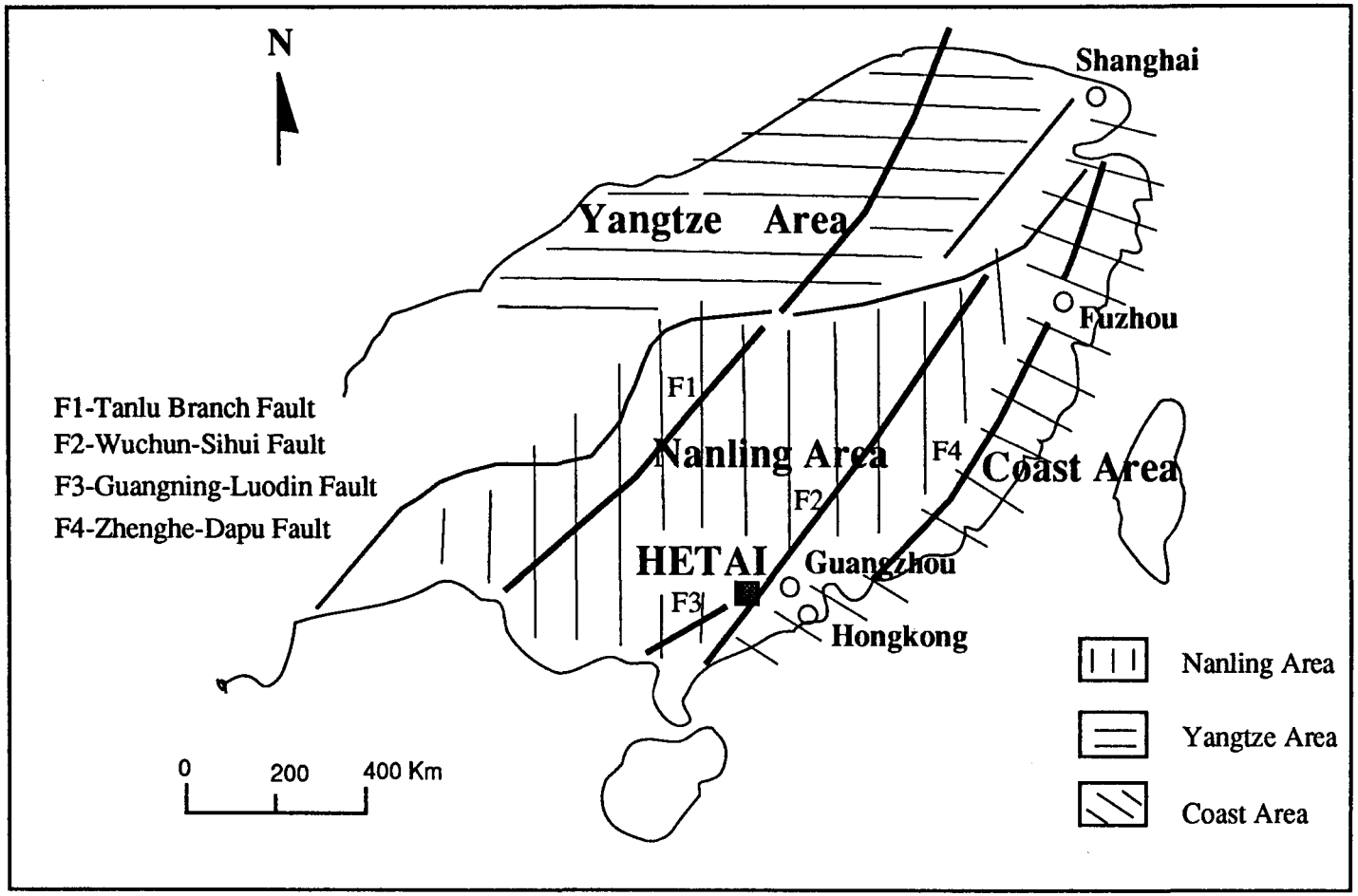

Fig.1.2. Three main tectonic areas of South China

Therefore, the South China block may be divided into three main tectonic regions, the Yangtze, the Nanling and the Coast areas (Fig.1.2) and the tectonic evolution of different type granites may be sketched as illustrated in Fig.1.3. The Nanling granites are the continent-continent collision type mainly formed in the Late Paleozoic to Late Mesozoic, whereas the Yangtze granites represent the subduction type formed mainly in the Late Mesozoic, and the Coast granites are of the extension type from Late Mesozoic to Early Cenezoic formed after long subduction.

The orogenic evolution and granitic magmatism of South China from Precambrian to Mesozoic and Cenozoic have been described by various authors (Institute of Geochemistry, Academia Sinica, 1979; Jahn et al., 1990). It is characterized by six orogenic periods each with related granitic magmatism. These are : 1) Precambrian granites (1400-1100 Ma, Sibao Movement and 1100-680 Ma, Xuefeng Movement), mainly in Guangxi and Anhui Provinces; 2) Caledonian granites (580-360 Ma) in the Nanling Area; 3) Hercynian granites (360-240 Ma) in Guangxi and Guangdong provinces; Indosinian granites (240-190 Ma) in Hunan province; 5) Yanshanian granites (190-65 Ma), which are widespread, particularly in middle-lower Yangtze Area and Coast Area; and 6) Himalayan granitic and mafic magmatism, < 65 Ma, formed chiefly in the Coast Area and Taiwan. The granite distribution becomes younger in general from the interior to the coast (from NW to SE, Fig.1.2), and the late Yanshanian and the Himalayan granites and mafic rocks occur mainly in the Zhejiang-Fujian-Guangdong coast areas and Taiwan. The principal associated volcanic rocks are composed of Yanshanian calc-alkaline and alkaline suites and Himalayan basalts, which occur in the middle-lower Yangtze Area, Zhejiang-Fujian-Guangdong Coast Area and Taiwan.

A series of faults and thrust faults with SW-NE orientation, such as the Tanlu Branch fault, Wuchuan-Sihui fault and Zhenghe-Dapu fault (Fig.1.2, Wang et al., 1984b), appear to control the spatial extent of Yanshanian granites and associated volcanic rocks, and locally deform older granites and related strata. Deformation associated with each orogenic period is distributed in zones dominated by a SW-NE orientation. The strongest deformation affects the Precambrian and Caledonian granites as well as the Precambrian and Early Paleozoic strata, which commonly display gneissic, augen and mylonitic textures such as observed in the Yunkai Mountain Deformed Belt and in the Hetai Area (Fig.1.4). In general, these deformed structures are parallel to that of the major faults. The Late Paleozoic

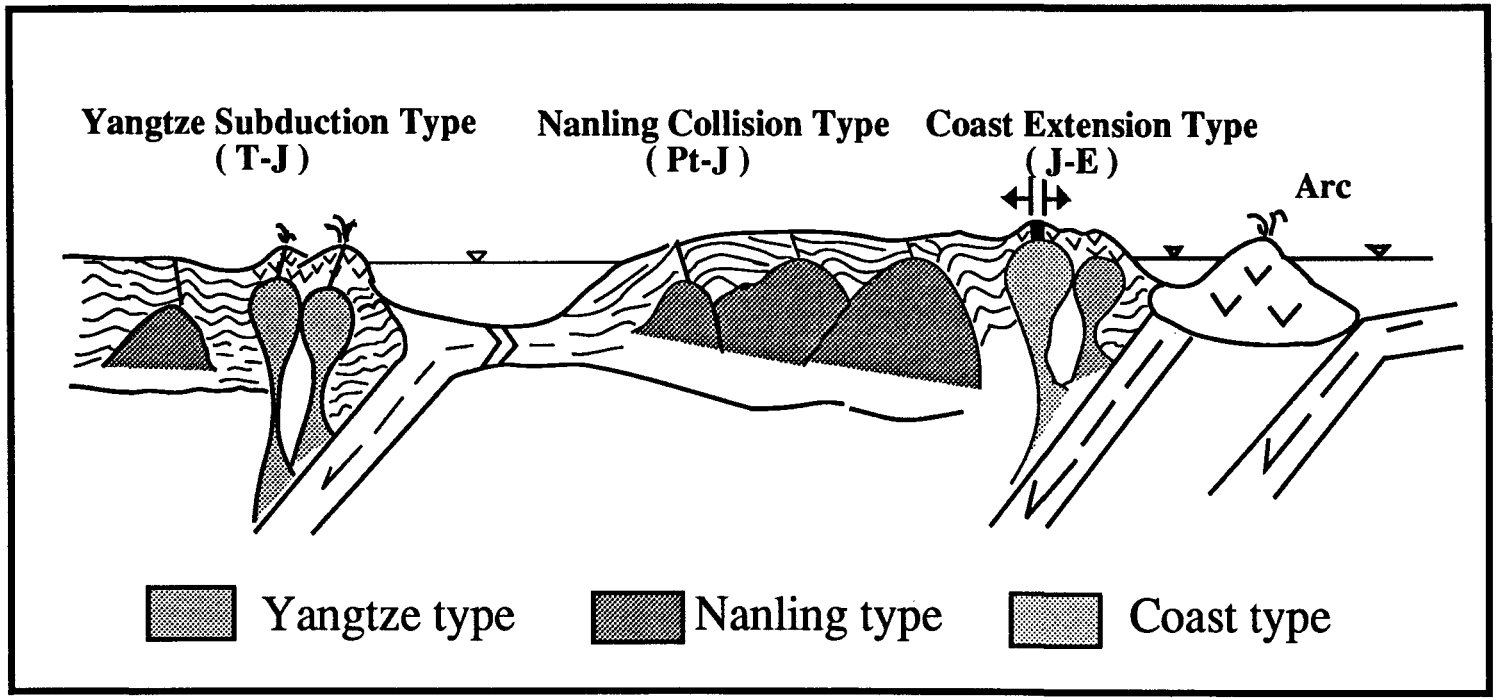

Fig.1.3. Sketch diagram of granite types and tectonic evolution of South China

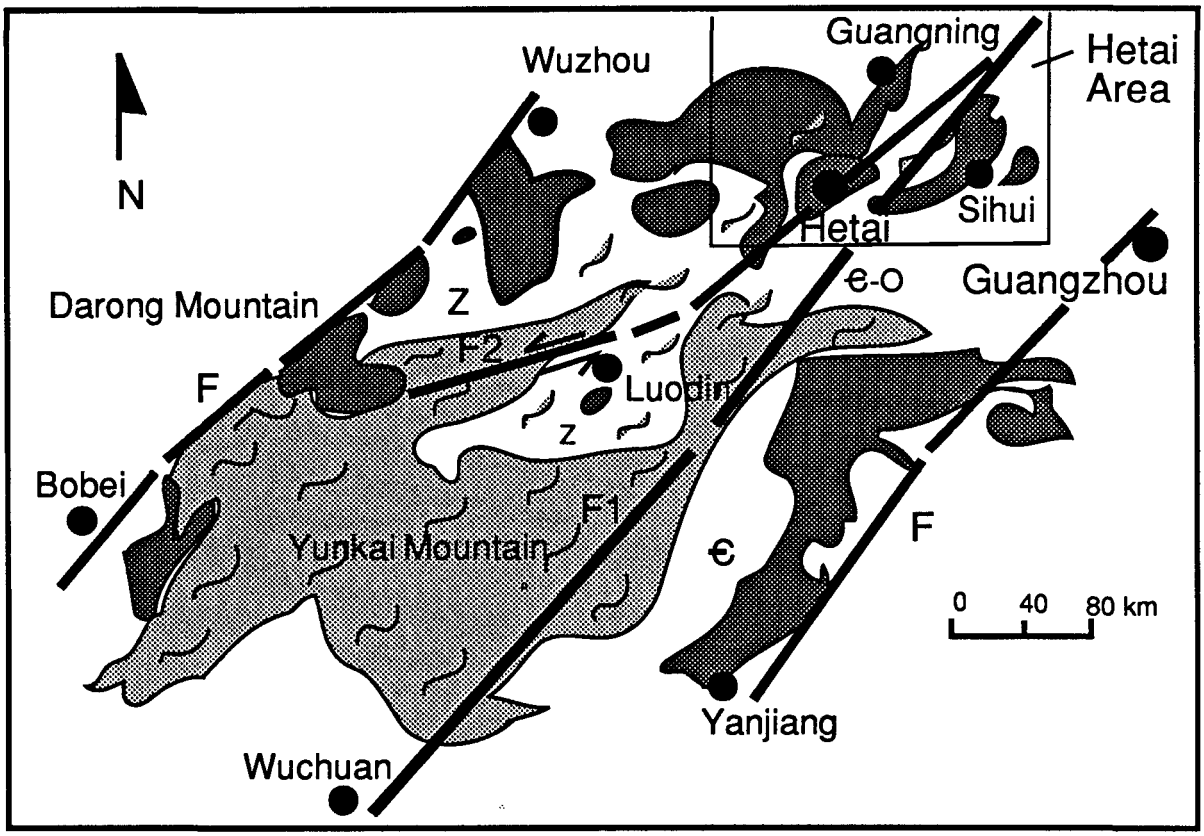

Legend

Strata* | Deformed Rocks | Granite | Fault | Locality

* Z - Zhendanian (Precambrian); Є - Cambrian; O - Ordovician

F1 - Wuchuan-Sihui Fault; F2- Guangning-Luodin Fault

Fig.1.4. Geological Map of Western Guangdong Province

(Modified from Mo and Geological Bureau of Guangdong Province, 1980)

granites and strata are also strongly deformed, and typical SW-NE oriented deformation can be observed in the Zhejiang-Fujiang-Guangdong Coast Deformed Belt (parallel to the Zhenghe-Dapu fault zone, Fig.1.2).

1-1-2. Granite classification in South China

Recent discussions on the origin of granites reflect the recognition of granite classification based on genesis. Chappell and White (1974 and 1984; White and Chappell, 1977 and 1983) divided the granites in the Lachlan Fold Belt of Eastern Australia into I-type and S-type in the light of the different postulated source rocks. The I-type and S-type classification scheme and related criteria have been widely applied to other areas. Bowden et al. (1984) further discussed the petrological, geochemical and source criteria for granite classification.

Different mineralogical and geochemical criteria have evolved, however, to determine source rocks and the geological environment of granite formation in distinct regions of China. As the widely distributed granites have associated mineralizations such as W, Sn, Nb, Ta and REE in South China, the genesis of granites has become an important issue (Institute of Geochemistry, Academia Sinica, 1979; Department of Geology, Nanjing University, 1981; Xu et al., 1984 et al.; Mo, 1985 and Wang et al., 1983, 1984c). For example, Xu et al. (1984) and Department of Geology, Nanjing University (1981) divided granitoid rocks of South China into " Syntectic" type (calc-alkaline magma) and "Reformed" type (granitization), and considered that most granitoid rocks in the Nanling Area are formed by granitization ("Reformed" type). On the other hand, Wang et al. (1983, 1984c) demonstrated that the granites occurring in the Middle-Lower Yangtze Area and the Nanling Area can be interpreted as two different genetic-evolutionary series, the Yangtze Series granites derived from the lower crust and upper mantle (like subduction-type) and with associated Fe, Cu, Au, Mo, Pb and Zn mineralizations, whereas the Nanling Series granites are mainly derived from the upper crust (like collision-type) and have associated REE, Nb, Ta, W, Sn and U mineralizations. The Yangtze Series granites were principally produced in the Mesozoic (Yanshanian, 190-65 Ma) ; whereas the Nanling Series granites were produced over a wide span of ages, from the Paleozoic to Mesozoic, but mainly in the

Caledonian (460-360 Ma) and in the Early Yanshanian (190-135 Ma). In general, the Yanshanian granites are the most important economically, because much mineralization is closely associated with this granitic magmatism.

An important division may be inferred between continental granites generated during orogenic evolution and those granites more closely associated with an anorogenic period. As the orogenic and anorogenic granites occur in a transitional region, a close relation may exist between them, not only in geological setting, but also in geochemistry. A-type granites (Collins et al., 1982; Bowden and Kinnaird, 1984) may be considered not as a source classification type such as I- and S-type, but as granites with anhydrous, alkaline and aluminous chemical characteristics. As mentioned before, the Coast granites in South China display alkalic geochemical features, but they are still close to the I-type granite series, including pyroxene diorite, quartz diorite, granodiorite and biotite granite, in geological and geochemical relations, demonstrating a cognate-evolution tendency (Yang et al., 1986a, 1986b). So it appears difficult to interpret these suites as A-type. The working area of this thesis, the Hetai Area, shown in Fig.1.2, is located in the transitional region between the Nanling Area and the Coast Area, and the granitic rocks occur as a complex assemblage of deformed biotite granites and gabbro, tonalite, granodiorite and alkali-feldspar granite from Caledonian to Yanshanian age. The genesis and evolution of granites in this area, therefore, may be compared to the larger series of granites within the tectonic background of South China.

1-2. Geological setting in the Hetai Area

The Hetai Area, located in western Guangdong Province of South China (Fig.1.1) includes Gaoyao, Guangning and Sihui counties (Figs.1.4 and 1.5), and its geological setting belongs to the northeastern part of Yunkai Mountain Foldbelt (Fig.1.4), which is characterized by a suite of Precambrian or Early Paleozoic metamorphosed strata (greenschist to amphibolite facies) and diverse granitic rocks. The general geology of the Hetai Area of western Guangdong Province is described in the following paragraphs.

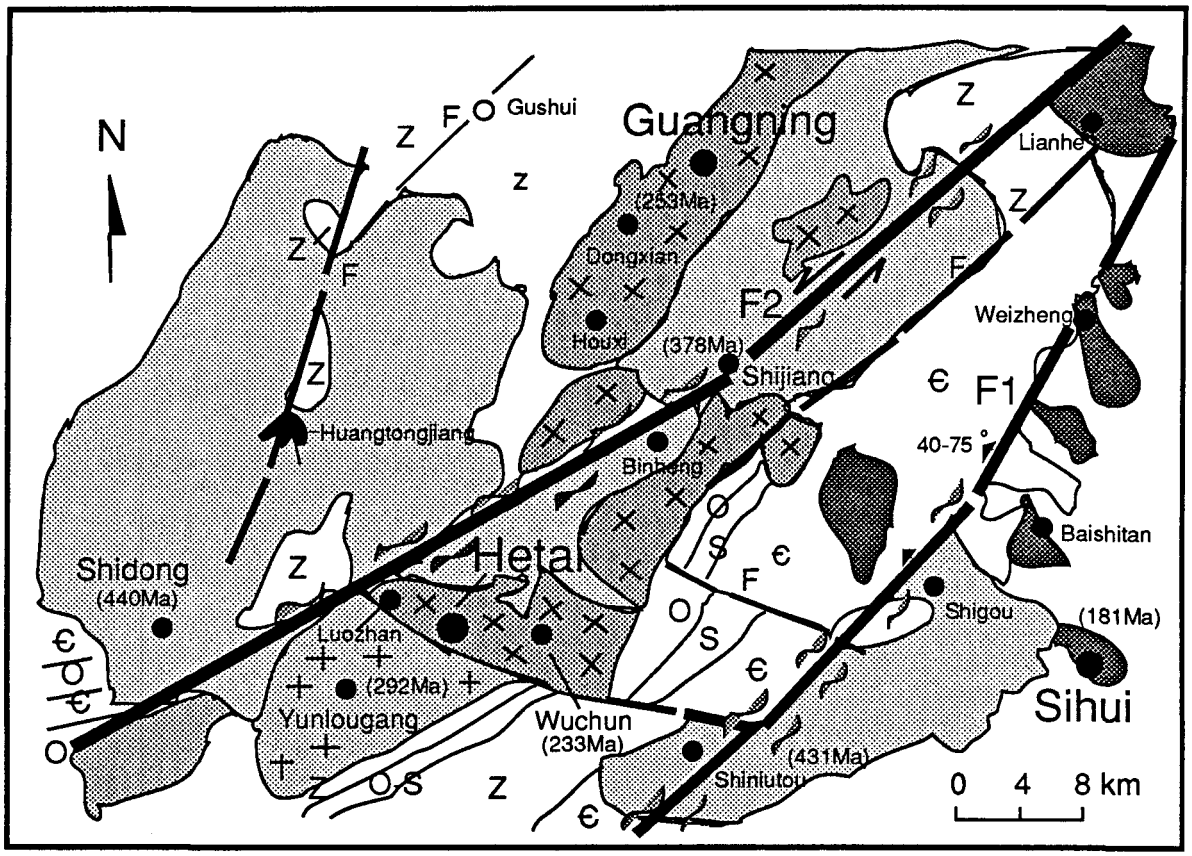

Legend

Strata*

1 2 3 4 5 6

7 8 9 10

1. Caledonian granite
2. Hercynian granite
3. Indosinian granite
4. Yanshanian granite
5. Gabbro or pyroxene diorite
6. Fault
7. Deformation zone
8. Strike-slip fault
9. Thrust fault
10. Locality

F1: Wuchun-Sihui Fault; F2 : Guangning-Luodin Fault;

* Z- Zhengdanian; Є- Cambrian; O- Ordovician; S- Silurian

Fig.1.5. Geological Map of the Hetai Area, Guangdong Province

(Modified from 719 Geological Team of Guangdong Province, 1986)

1-2-1. The principal country rocks

The principal country rocks of the Hetai Area are mainly Late-Proterozoic and Early Paleozoic (Cambrian, Ordovician and Silurian) strata. The Late Proterozoic and the Early Paleozoic are generally composed of psammitic pelitic rocks, characterized by the flysch facies (Nan, 1989) with a metamorphic grade of greenschist to amphibolite facies. The principal lithology is represented by volcanoclastic sedimentary rocks, siliceous schist, biotite-schist and phyllite. The main strata in the Hetai Area of western Guangdong Province (Nan, 1989) are listed as following :

Late Proterozoic :

Yunkai Group, about 2700-5200 m apparent thickness, including sandstone, phyllite, slate, bedded siliceous and intermediate-basic volcanoclastic sedimentary rocks, metamorphosed from the greenschist to amphibolite facies.

Early Paleozoic :

Cambrian, > 1800 m apparent thickness, displaying a comformable relationship with the underlying Zhandanian strata (Yunkai group) and including shale and sandstone, metamorphosed to the greenschist facies.

Ordovician, > 550 m apparent thickness, including phyllite, shale and sandstone, metamorphosed to the greenschist facies, overlying the Cambrian strata unconformably.

Silurian, > 420 m thickness, including dark shale, metamorphosed to the greenschist facies, displaying a conformable relationship with the underlying Ordovician strata.

1-2-2. Fault zones, shear zones and deformations

The four main fault zones in Guangdong Province are shown in Figs.1.4 and two of them pass through the Hetai Area, the NE trending Guangning-Luodin fault zone and the NNE Wuchuan-Sihui fault zone (Figs.1.4 and 1.5). The Guangning-Luodin fault zone

(Fig.1.5), about 180 km long, is a near-vertical strike-slip shear zone with a mylonitic belt about 1.5-2.0 km wide, in which the granitic rocks and Late Proterozoic and Early Paleozoic strata are deformed. Within this shear zone, the granitic rocks such as the Shijiang, Guangning and Yunlougan plutons display various deformation structures. The Wuchuan-Sihui fault zone (Fig.1.5), which is a thrust fault, controlled the extent of Yanshanian granites such as the Sihui, Baishitan and Lianhe bodies, and deformed Caledonian granitic rocks such as the Shiniutou body and related strata, and the corresponding shear zone developed a mylonitic belt more than 1000 m wide. The Shiniutou granite and country rocks are strongly deformed and present the typical structural features of mylonitization, showing augen, gneissic and mylonitic structures in the shear zone.

1-2-3. Granitic plutons and their enclaves

The Hetai Area is a part of the Caledonian to Yanshanian orogenic or deformed belt. Granites are important in this geotectonic setting, composing about one half the surface area of the whole Hetai area. In this study, the petrography, mineralogy and geochemistry of ten granitic plutons were analyzed to represent the essential tendency of the Hetai granites. Their geological characteristics are listed in Table 1.1. These granites include the Sidong, the Huangtongjiang, the Shijiang (Binhen), the Guangning, the Yunlougan, the Wuchun, the Shiniutou and the Sihui (Baishitan and Lianhe) plutons from NW to SE (Fig.1.4). Each individual body is a polyphase intrusion, and in addition, scattered dark enclaves are commonly found in the outcrops of the granites. These scattered irregular-shaped dark enclaves show reactions with the host granite. The enclaves may be roughly divided into two types usually occurring in different host granites. The first type is the granodioritic enclave, which contains plagioclase phenocrysts and occurs in the Wuchun megacryst monzogranite and in the Sihui alkali-feldspar granite. The second type is a dark enclave, which is mainly composed of biotite and plagioclase and occurs in the Shijiang complex and Guangning body. In addition, some intermediate-basic and pegmatitic dykes can usually be found within these granites and their country rocks. They are mainly oriented NNE or NW and NNW, and usually cut through both the granites and the enclosing strata. Within shear

Table 1.1. Main granitic bodies in the Hetai Area, Guangdong Province

Name of body	Surface area (km^2)*	Polyphase intrusions
Shijiang (and Binhen)	670	Homogeneous medium grained biotite granodiorite, heterogeneous banded (schlieren) granodiorite, medium-fine nebulitic granite, augen granite, dark enclaves
Shidong	900	Coarse grained biotite granite , medium-fine grained biotite granite
Shiniutou	208	Augen granite, stromatic augen granite, banded granite
Guangning	340	Biotite monzogranite
Yunlougan	150	Granodiorite, two mica-feldspar pegmatite
Wuchun	76	Megacryst monzogranite, coarse monzogranite, granodioritic enclave
Sihui (and Baishitan)	>100	Coarse grained biotite granite, medium grained alkali-feldspar granite, fine grained alkali-feldspar granite, granodioritic enclave
(Lianhe)		Coarse-medium grained alkali-feldspar granite, fine grained alkali-feldspar granite, granodioritic enclave
Huang-tongjiang	< 5	Gabbro, pyroxene diorite

* From the data of 719 Geological Team of Guangdong Province

zones, granitic rocks were deformed so that both enclaves and dykes are elongated and transposed to produce discrete bands within granites.

Based on the data of Fu (1988) and Ye (1989), the ages of these granites in the Hetai Area represent diverse eras from Caledonian to Yanshanian as listed in Table 1.2. In the light of the geochronological data for orogenic periods in South China (Institute of Geochemistry, Academia Sinica, 1979; Department of Geology, Nanjing University, 1981), the Shijiang, the Shidong and the Shiniutou granites appear to belong to the Caledonian, the Guangning granites and the Yunlougan to the Hercynian, the Wuchun granites to the Indosinian and the Sihui granites to the Yanshanian. The Huangtongjiang gabbro is not dated, but may belong to the Late Mesozoic (Indosinian or Yanshanian) according to geological and geochemical relationships with the Indosinian and the Yanshanian plutons. These age data are only used for conveniently describing each granitic body and complex, and their geochronological discrimination may depend on more precise dating results. In this study, the Shijiang, the Sidong, the Shiniutou (Caledonian) and the Guangning (Hercynian) granites are defined as "older granites", and in contrast, the Sihui (Yanshanian), the Wuchun (Indosinian) and the Yunlougan (Hercynian ?) as "younger granites", for comparison of their petrographical, geochemical and mineralogical characteristics.

1-2-4. Hetai gold deposit

The Hetai gold deposits occur between the Guangning-Luodin Fault and the Wuchun-Sihui Fault (Fig.1.5) and are within or near the Yunlougan and Wuchun plutons, as shown in Fig.1.5. The gold deposits are mainly developed in shear zones and most gold ore bodies occur in metamorphosed strata of the Precambrian or Paleozoic basement. Gold ore bodies are present in quartz-veins, and the ore mineral is in native gold which occurs as irregular grains in quartz. The associated sulfide minerals are chalcopyrite and pyrite, both rich in Au and Ag. Sericite is a major alteration product, and it is the result of dynamic metamorphism and hydrothermal metasomatism.

Table 1.2. Ages of granites in the Hetai Area, Guangdong Province

Name of pluton	Ages(Ma)	Eras	Method	References
Sihui	181±15	Yanshanian	39Ar-40Ar(biotite)	Ye, 1989
	-------Yanshanian	Orogeny (190--65 Ma) -------		(Triassic)
Wuchun	233±2	Indosinian	Rb-Sr (whole rock)	Ye, 1989
	-------Indosinian	Orogeny (240--190 Ma) -------		(Permian)
Guangning	253±36	Hercynian (or Indosinian ?)	Rb-Sr (whole rock)	Ye, 1989
Yunlougang	292	Hercynian	Pb-Pb (feldspar)	Fu, 1988
	-------Hercynian	Orogeny (360--240 Ma) -------		(Devonian)
Shijiang	378±45	Caledonian (or Hercynian?)	Rb-Sr (whole rock)	Ye, 1989
Shiniutou	431	Caledonian	39Ar-40Ar (muscovite)	Ye, 1989; Chen & Wu, 1989
Shidong	440±5	Caledonian	Rb-Sr (whole rock)	Ye, 1989
	-------Caledonian	Orogeny (580--360 Ma) -------		(Cambrian)

1-2-5. Problems in the Hetai Area

As various structures overlap in the deformed granitic rocks in the Hetai Area, the genetic relations of these granites and gold deposits are disputed, but most authors follow the hypothesis of Xu et al. (1984), Department of Geology, Nanjing University (1981) and Mo (1987 and 1989) that the granitoid rocks are the result of metamorphism of the older strata : (1) the granitoid rocks are the final products of granitization by regional metamorphism of the Precambrian basement (Mo, 1989; Dai, 1986); (2) tectonic metamorphism of older sedimentary strata within shear zone plays the most important role for gold mineralization (Chen et al., 1988; Zhou, 1992); and (3) some granites may only supply heat during gold deposit formation (Ling, 1986 and 1988; Fu, 1988 and 1989; Zhang et al., 1986; Huang, 1988, and Yuan and Huang, 1990). The theories of Mo (1987 and 1989) are premised on the importance of "fault metamorphism" and propose that, after the Caledonian geosyncline activity, most of the Nanling Area became a platformal area, and granitization took place along fault zones. These granitoids, such as the Shijiang and Guangning complexes were "reformed" by means of granitization of Caledonian basement (Mo, 1987 and 1989). In general, this hypothesis of granite genesis by granitization is based on the theoretical tectonic framework of the geosyncline and platform cycle.

Although regional studies have been premised on the importance of metamorphism (granitization) of sedimentary rocks for the formation of granitoid rocks and gold-deposits, the interpretation of granitization does not completely explain the evidence observed in the field. Consequently, the genesis of the Hetai granites is still a problem. It has been proved that granitic rocks derived from magmatic crystallization differ from those formed by granitization. Detailed field and microscope observations show that many granite bodies display magmatic flow foliation both within and outside shear zones and they are spatially closely connected with the gold deposits. The field evidence does not clearly favor a granitization origin for the Hetai granites, but rather supports the idea that the Hetai granites might be crystallized from a magma and subsequently deformed in the solid state. This may be more important, not only for the genetic interpretation of granites, but also to establish the relations between granites, deformation and gold mineralization, because studies of the granitic rocks and gold deposits have so far failed to show clear relations between the granitic rocks, gold mineralization and shear zones in the Hetai Area.

In this thesis, the mineralogy and geochemistry of ten main granitic complexes and their enclaves from the Hetai Area will be systematically investigated, in order to develop fundamental evidence for the genetic interpretation of the granites and their possible relation to gold mineralization. First, the microstructure of the main rock-forming minerals will be described and the petrographic characteristics of different granites will be compared. The geochemical characteristics of bulk rocks and the principal rock-forming minerals such as biotite, amphibole and plagioclase will be analyzed in detail. The analyzed granitic samples of the Hetai Area plot in the QAP ternary classification by IUGS (1989) based on the CIPW calculation of whole rock and on the principal mineral contents in thin section. The different granite types and their evolution of different granite series will be interpreted. Generally, these data may be regarded as important evidence, in order to distinguish the genetic type of granites and to characterize the geochemical pattern of magma evolution of granites in the Hetai Area. In addition, the possible relationships between granite and gold mineralization may be more clearly analyzed based on a genetic classification of granites.

Although the Hetai Area has been mapped in detail (by 719 Geological Team of Guangdong Province, 1986), structural information is not available, particularly for the granitic intrusions. Sampling of the granites is constrained by the deep laterite cover over much of the terrain. Sampling for this project was limited to available active or inactive quarries and deeply incised river valleys. For this reason, all phases of the intrusion present at each site were sampled, as well as the major population of xenoliths. The presence of cognate xenoliths in some intrusions allowed sampling of a wide range of compositions. The granites were examined for general textural fabrics, indicating probable temporal generation of structures. Relations between granite fabrics and regional structures remain conjectural.

The author started field work on South China granites in 1982, and analyzed about 1000 granitic samples with his colleagues in Institute of Geochemistry, Academia Sinica. This earlier work lay a useful basis for this study. The author, and his co-workers, began to make field investigations and to collect granite samples in the Hetai area in 1986, and 60 samples were analyzed in China and the rest in Chicoutimi, Canada. In 1990, the author came UQAC to further study the mineralogy and geochemistry of the Hetai granites. The analyzed samples in this thesis are representative because they include typical plutons and polyphase intrusions in the Hetai area.

CHAPTER II

PETROGRAPHIC CHARACTERISTICS OF THE GRANITES

2-1. Introduction

The texture and mineral assemblage are essential to demonstrate the structural evolution of the granitic rocks as well as their differentiation trends. Primary magmatic features are directly observed if a post-solidification dynamic deformation is not superimposed or if they are not destroyed by the later deformation. Most granites in the Hetai Area give a first impression that they have undergone strong dynamic processes. The primary magmatic features are obscured by the superimposition of solid-state deformation after magma solidification and may have been ignored. This superimposition of deformation on the magmatic fabric is considered to be the result of regional metamorphism, and the petrographic features of the older granites such as the Shijiang, Shiniutou, Sidong and Guangning granites are usually ascribed to different metamorphic grades within the development of regional metamorphism (Mo, 1987 and 1989; Dai, 1986). The first impression may be important on discussing granite genesis, but the essential phenomena must be described in detail. First, the primary magmatic features need to be separated from the deformational features, in order to describe the petrographic primary magmatic characteristics and to examine the petrogenesis of the Hetai granites. The deformational characteristics may then be considered.

2-2. Petrographic comparisons between granites of different ages

Mesostructural and microstructural observations show that the Hetai granites are all characterized by a primary magmatic flow foliation with superimposed solid-state deformation foliations. These granites, which are polyphase intrusions, display different degrees of deformation depending on their age and location. In general, dynamic deformation of the older (Caledonian and Hercynian) granites is very strong especially within fault zones, varying from gneissic to mylonitic texture. In contrast, dynamic deformation of the Indosinian and Yanshanian granites is very weak, and primary magmatic foliations are clearly preserved. Petrographic comparison between polyphase granite intrusions of different ages, and in differing degrees of deformation, is a significant base to consider the petrogenetic aspects of the granites.

2-2-1. Caledonian granitic bodies

The Caledonian granitic bodies, the Shijiang, Sidong and Shiniutou (see Tables 1.1 and 1.2), are distributed in the Guangning-Loudin Deformed Zone and the Wuchuan-Sihui Deformed Zone, respectively (Figs.1.4 and 1.5).

(1) Shijiang complex

The Shijiang complex is characterized by a series of strongly deformed polyphase intrusions which are located within the Guangning-Loudin deformed zone (Fig.1.5). These deformed polyphase intrusions are usually divided in the field into homogeneous biotite granodiorite, heterogenerous stromatic or banded granodiorite, augen granite and mylonitic granite (Table 1.1). In addition, dark colored enclaves are found in all phases of the intrusion. Relict magmatic features are the intrusive contact between phases (Fig.2.1) and magmatic flow foliation such as the flow arrangement of zoned plagioclase phenocrysts (Fig.2.2), which is still discernible although superimposed by a strong tectonic foliation. The smaller biotites are usually enclosed within plagioclase phenocrysts, indicating magmatic crystallization. The strong deformations are characterized by mesostructures such

as gneissic, stromatic, banded, augen and mylonitic structures (Fig.2.3), broken and elongated plagioclase phenocrysts and bent biotite (and muscovite), crushed fine-grained feldspar and quartz oriented around relict plagioclase phenocrysts (Fig.2.3). In addition, myrmekite is widely observed in all deformed phases, particularly in the later leucogranite, and it commonly occurs in deformed feldspar phenocrysts (Fig.2.4). Microcline predominates in the late leucogranite intrusive phase, but because of the strong shearing, it is commonly broken and shows strain (Fig.2.5). Myrmekite is produced in microcline phenocrysts (Fig.2.5). The granitic intrusions are usually mylonitized when they occur within shear zone and the original igneous felsic and mafic minerals become more microgranular and more oriented with tectonic deformation.

The various rocks evolve from granodiorite, monzogranite to granite areas on the Q-Af-Pl ternary classification (Fig.2.6) by IUGS (1989) based on thin section observation and CIPW chemical calculation. The mineral content in the Shijiang complex is characterized by a regular variation (Table 2.1). Biotite and plagioclase decrease but microcline and quartz increase with evolution. At the same time, grain size increases and the rock changes from dark to light in appearance. Biotite (and muscovite) occurs as long brown-red laths, usually forming a biotite and muscovite band around plagioclase phenocrysts (Fig.2.2). Aligned zoned plagioclase phenocrysts outline the magmatic foliation, but they are crushed and elongated into finer-grained aggregates by the superimposition of deformation (Figs.2.2, 2.4 and 2.5). In addition, the polysynthetically twinned crystals commonly display strain shadows (Fig.2.4), also the result of solid-state deformation. Microcline and quartz increase with the evolution of the intrusion and they also present evidence of solid-state deformation, such as undulatory extinction, wide strain shadows, crushed fine-grained aggregates and myrmekite around the elongated phenocrysts. The accessory minerals are zircon and garnet, no amphibole and sphene are present in this complex.

The dark enclaves from the Shijiang complex are designated 'dark biotite-feldspar enclave' because they are mainly composed of biotite (25 %) and feldspar which includes plagioclase (50 %, An=50-30), orthoclase (10 %), quartz (10 %) and muscovite (5 %). The accessory minerals are mainly garnet and zircon. This type of enclave appears dark-coloured with a fine-grained texture in hand specimen. Brown-red coloured biotite forms small laths with a rough orientation. Plagioclase is subhedral, and some grains present thin

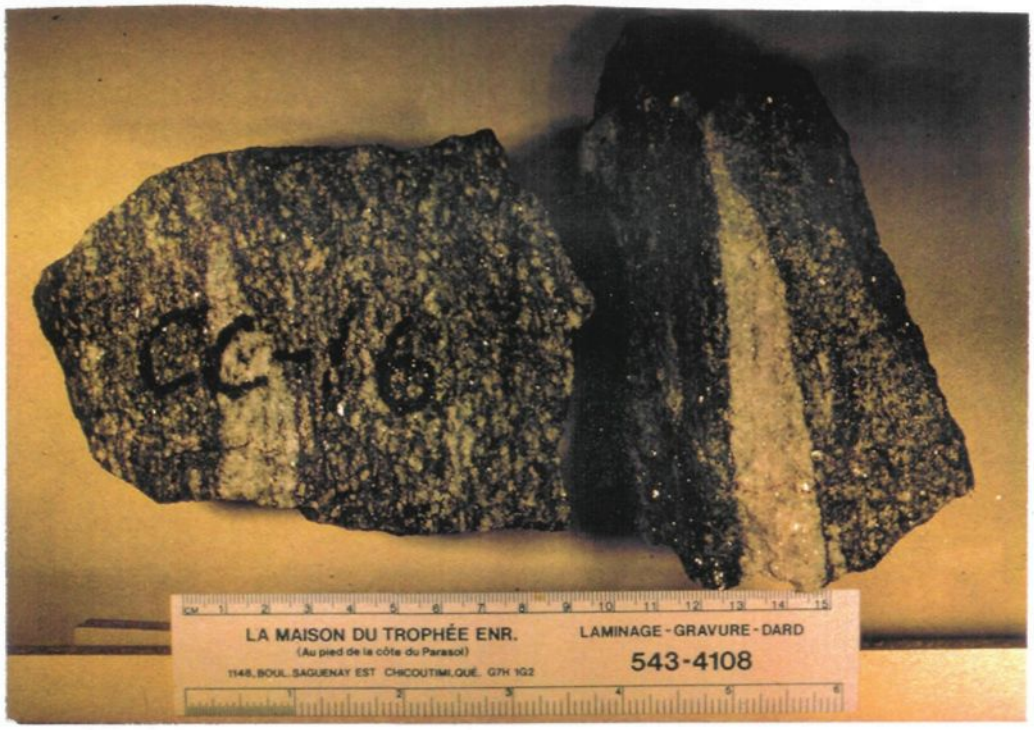

Fig.2.1. Intrusive contact between different phases in the Shijiang complex.

Note : Light-colored granitic dykes intruded into biotite granodiorite phase.

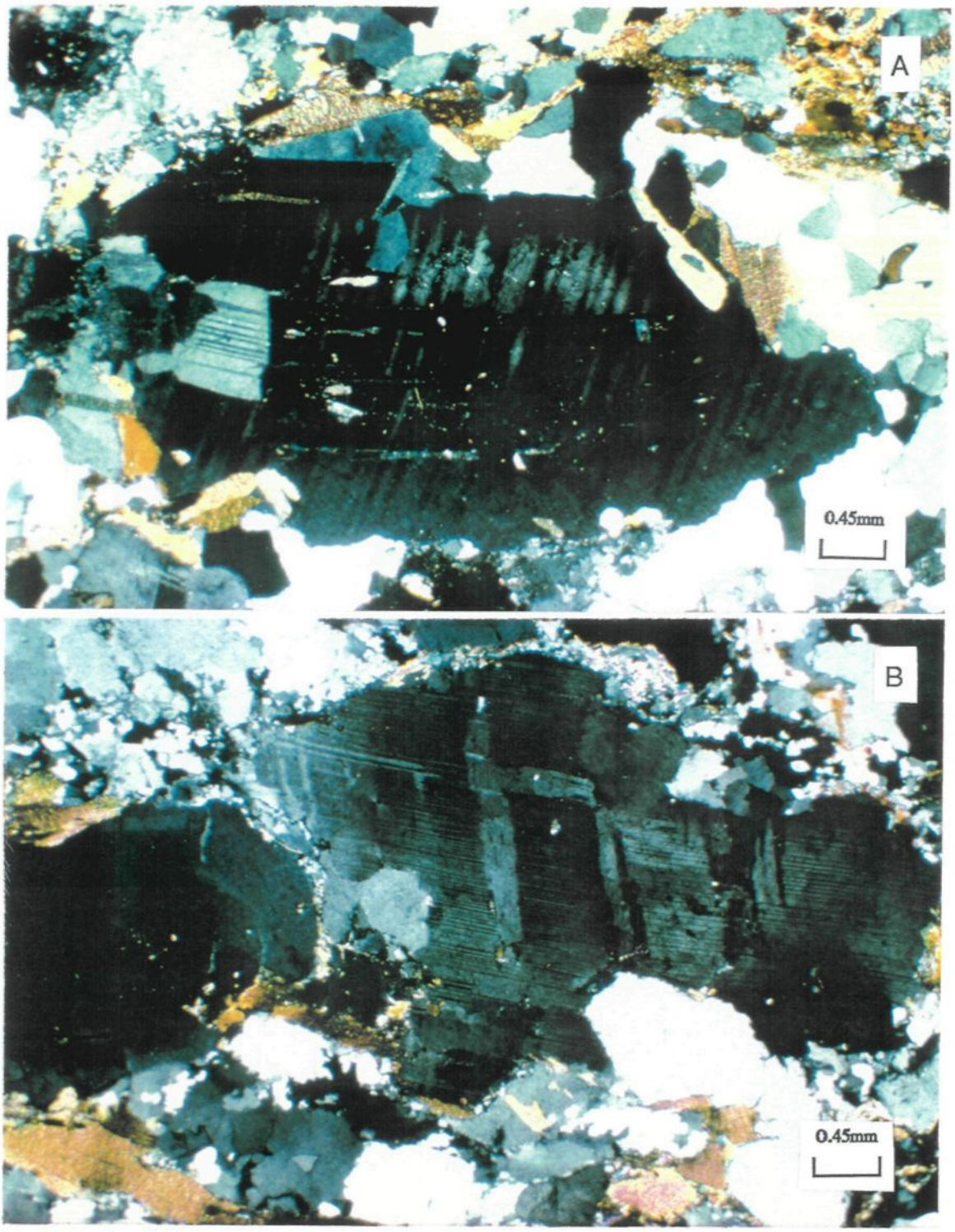

Fig.2.2. Flow fabric of aligned zoned plagioclase phenocrysts surrounded by bent mica and crushed fine-grained feldspar and quartz in the Shijiang complex.

A: Roughly oriented biotite slabs and strongly polygonized quartz;

B: Extreme cataclasis of quartz and feldspar around plagioclase phenocryst

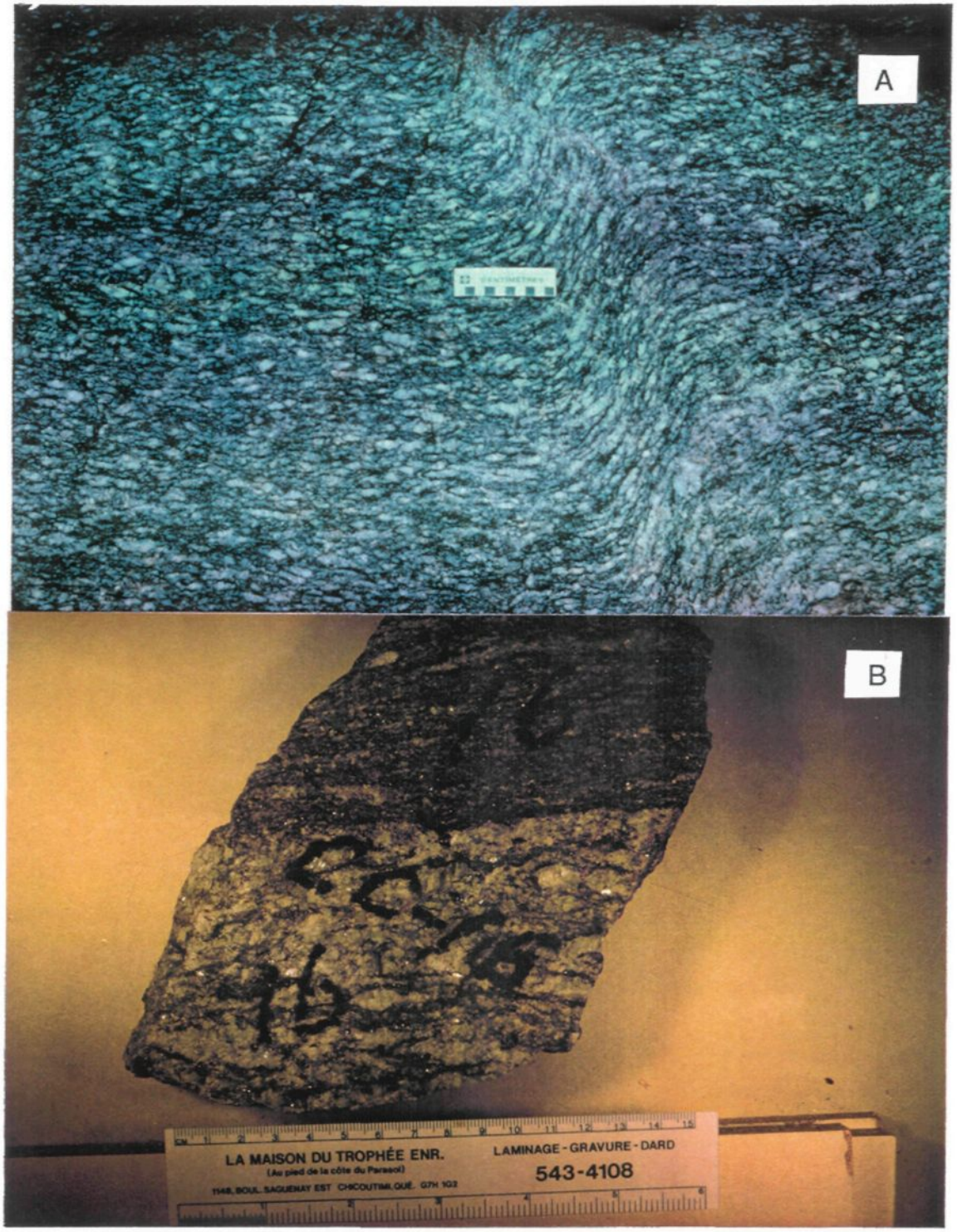

Fig.2.3. Differring degrees of deformed structures in the Shijiang complex.

A: Alternating dark- and light-colored bands, showing augen texture in light-color

B: Gneissic, augen and banded structures;

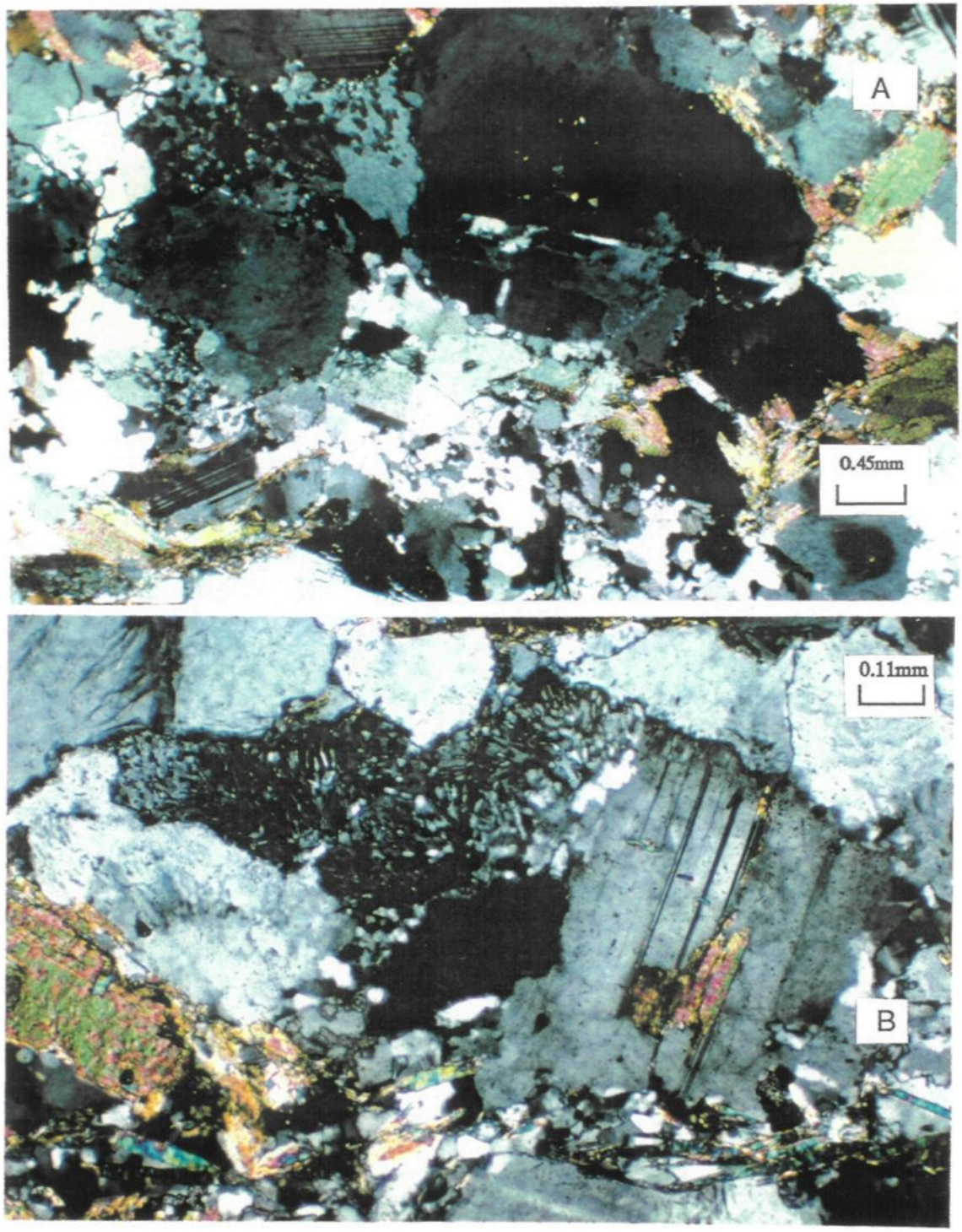

Fig.2.4. A : Myrmekite and finer-grained aggregates of mica, feldsapr and quartz around the deformed plagioclase phenocrysts; and B: Myrmekite occurring on the border of plagioclase phenocryst in the Shijiang complex.

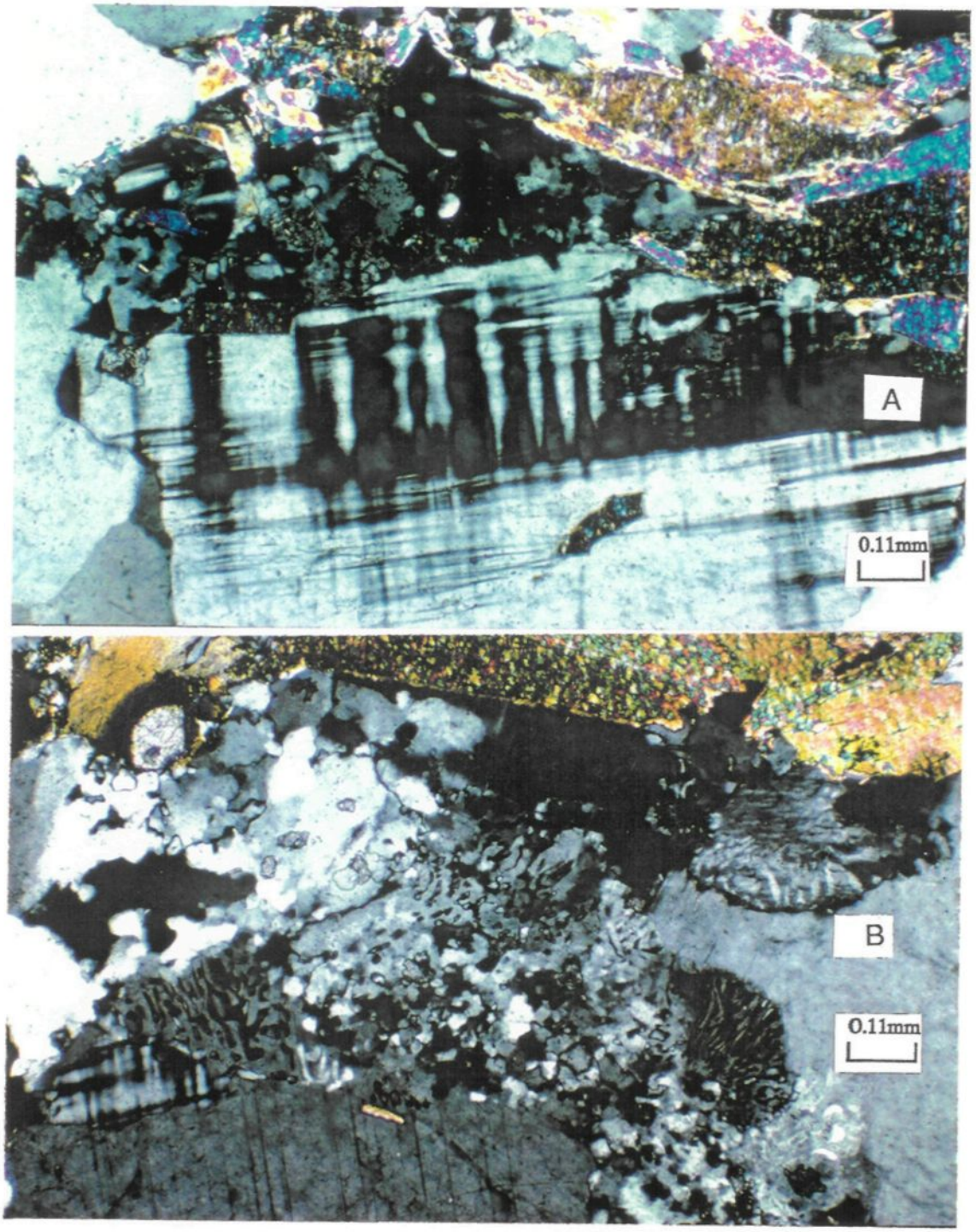

Fig.2.5. A: Strain shadow of the polysynthetically twinned microcline; and
B: Myrmekite produced in broken and twinned microcline phenocrysts in the late leucogranitic phases of the Shijiang complex.

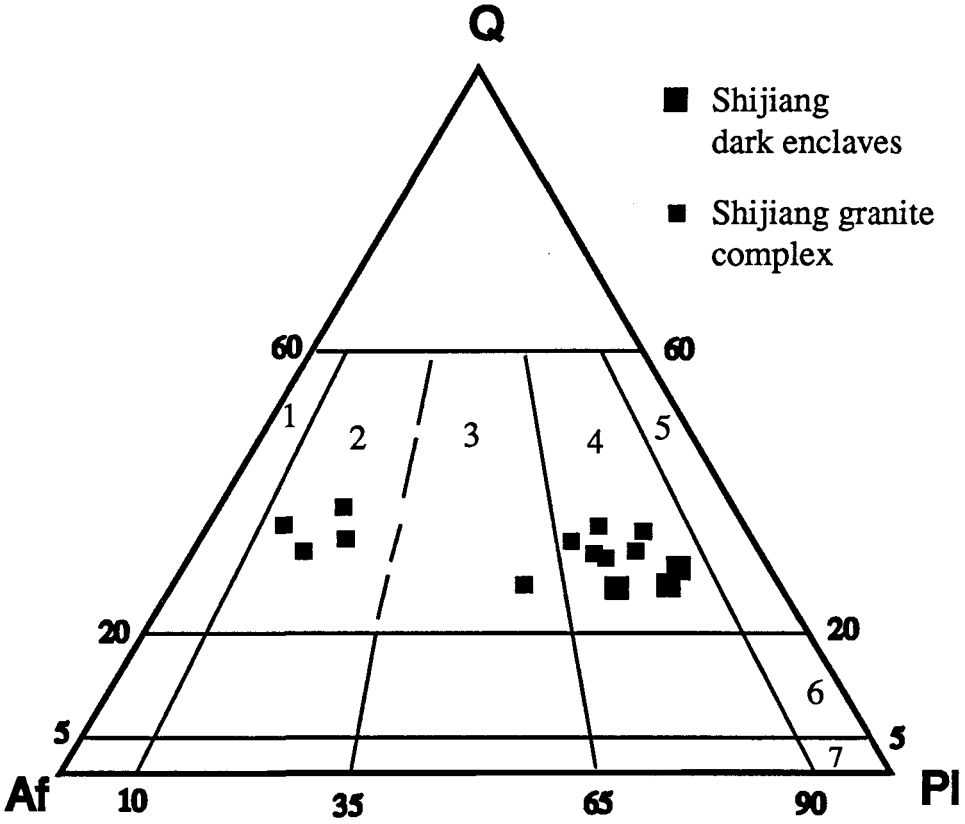

1.Alkali-feldspar granite; 2.Orthoclase granite; 3.Monzogranite
4.Granodiorite; 5.Tonalite; 6.Quartz diorite; 7. Diorite or Gabbro

Fig.2.6. The Shijiang granite complex and dark enclaves on the Q-Af-Pl ternary classification by IUGS (1989)

Table 2.1. Variation of rock-forming minerals from the Shijiang complex

Rock	Biotite	Mus	Pl (An)	Or	Q	Accessory minerals
	(%)					
Dark enclave (3*)	25	5	50 (50-30)	10	10	Gar+Zir
Homogeneous biotite granodiorite (3)	20	5	45 (35-30)	10	15	Gar+Zir
Heterogeneous stromatic biotite granodiorite (3)	15	5	40 (30-25)	20	20	Gar+Zir
Banded biotite monzogranite or biotite granite (3)	10	5	15 (30-20)	45	30	Gar+Zir
Augen biotite granite (3)	5	5	15 (25-15)	50	30	Gar+Zir

* Number of samples

polysynthetic twins and flexural structure. Orthoclase and quartz occur in rounded granular shape.

In general, these dark enclaves may be considered possibly as : (1) host rock xenoliths, possibly unmelted source rock (from the Precambrian metamorphosed sedimentary rocks), or (2) an earlier intrusive phase. However, petrographic observation shows that the rock-forming minerals do not have characteristic igneous habits. So, the dark enclaves may be regarded as metasedimentary xenoliths, possibly unmelted source rocks of the Shijiang polyphase intrusives.

(2) Sidong granite

The Sidong complex is composed of two intrusive phases, coarse-grained biotite granite and medium-fine-grained biotite granite. The coarse-grained phase is intruded by the fine-grained phase with 1 cm wide band of biotite at the contact (Fig.2.7). The magmatic flow foliation is shown by the arrangement of euhedral plagioclase and biotite crystals. The principal rock-forming minerals consist of biotite (5 %), plagioclase (30 %, An <15), microcline (30 %) and quartz (35 %). Biotite occurs as brown-red small laths. Minor muscovite and garnet are present. Plagioclase crystals are broken, and quartz and microcline display undulatory extinction, which may result from solid-state deformation and produce myrmekite at the margins of feldspar crystals (Fig.2.8). Deformation is relatively weak but increases toward the center of Guangning-Loudin deformed zone.

(3) Shiniutou granite

The Shiniutou body also appears to have been strongly deformed. In contrast to the Shijiang complex, the Shiniutou granite is relatively simple, and is dominated by biotite granite. The rock-forming minerals are biotite (3%), muscovite (5%), plagioclase (20%, An <15), microcline (40%) and quartz (32%). The magmatic flow foliation in this pluton may be reflected by the schlieren layering of biotite, feldspar and quartz (Fig.2.9a) and by the alignment of remnant plagioclase phenocrysts (Fig.2.9b), although they are partly obscured by strong solid-state deformation. The solid-state deformation is characterized by broken and crushed feldspar, presenting a typical augen and mylonitic texture (Fig.2.9b). Most brown-red biotite and muscovite grains are clustered in aggregates, which are oriented along

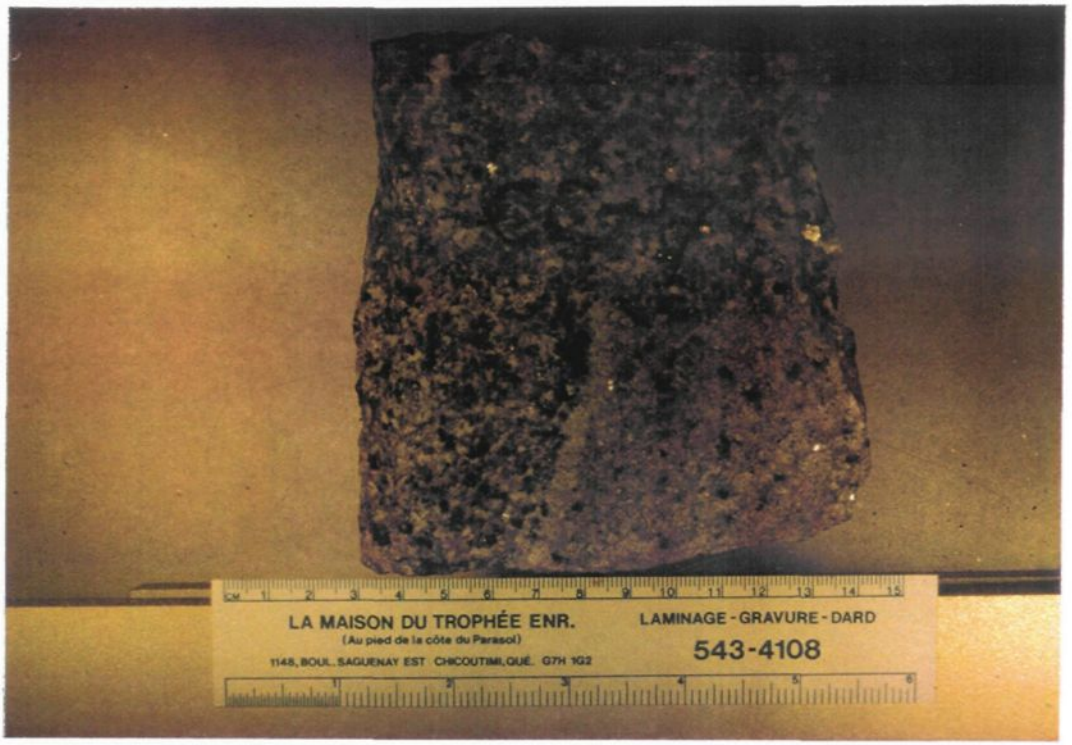

Fig.2.7. Intrusive contact between coarse-grained and medium-fine-grained phases in the Sidong complex

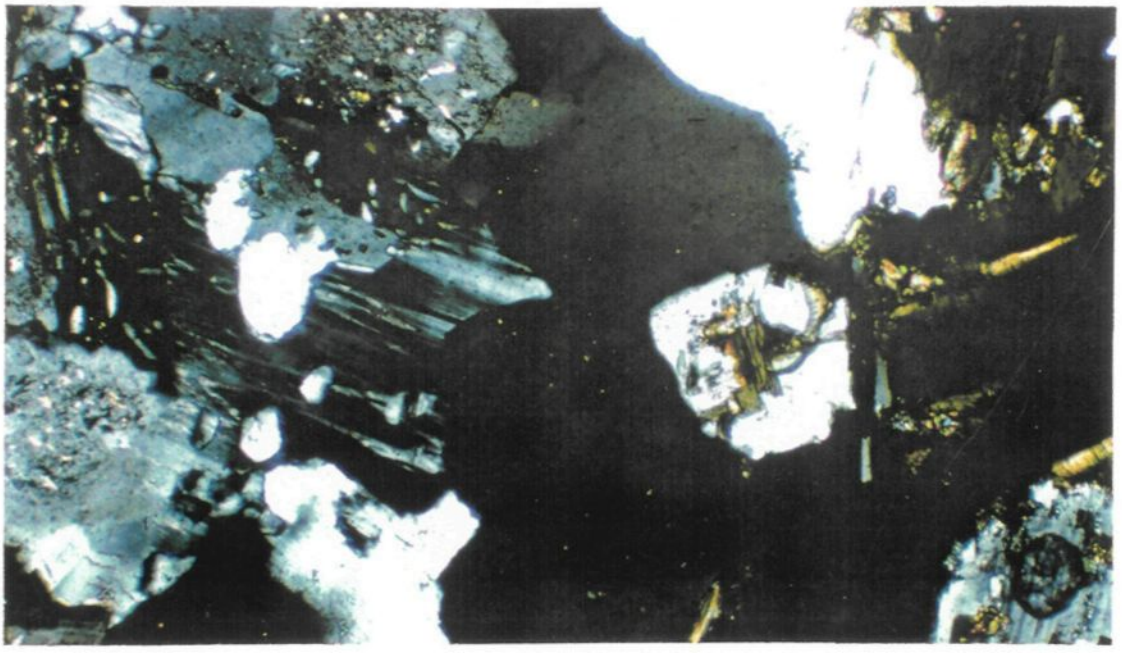

Fig.2.8. Myrmekite occurring in alkali-feldspar of the Sidong granite

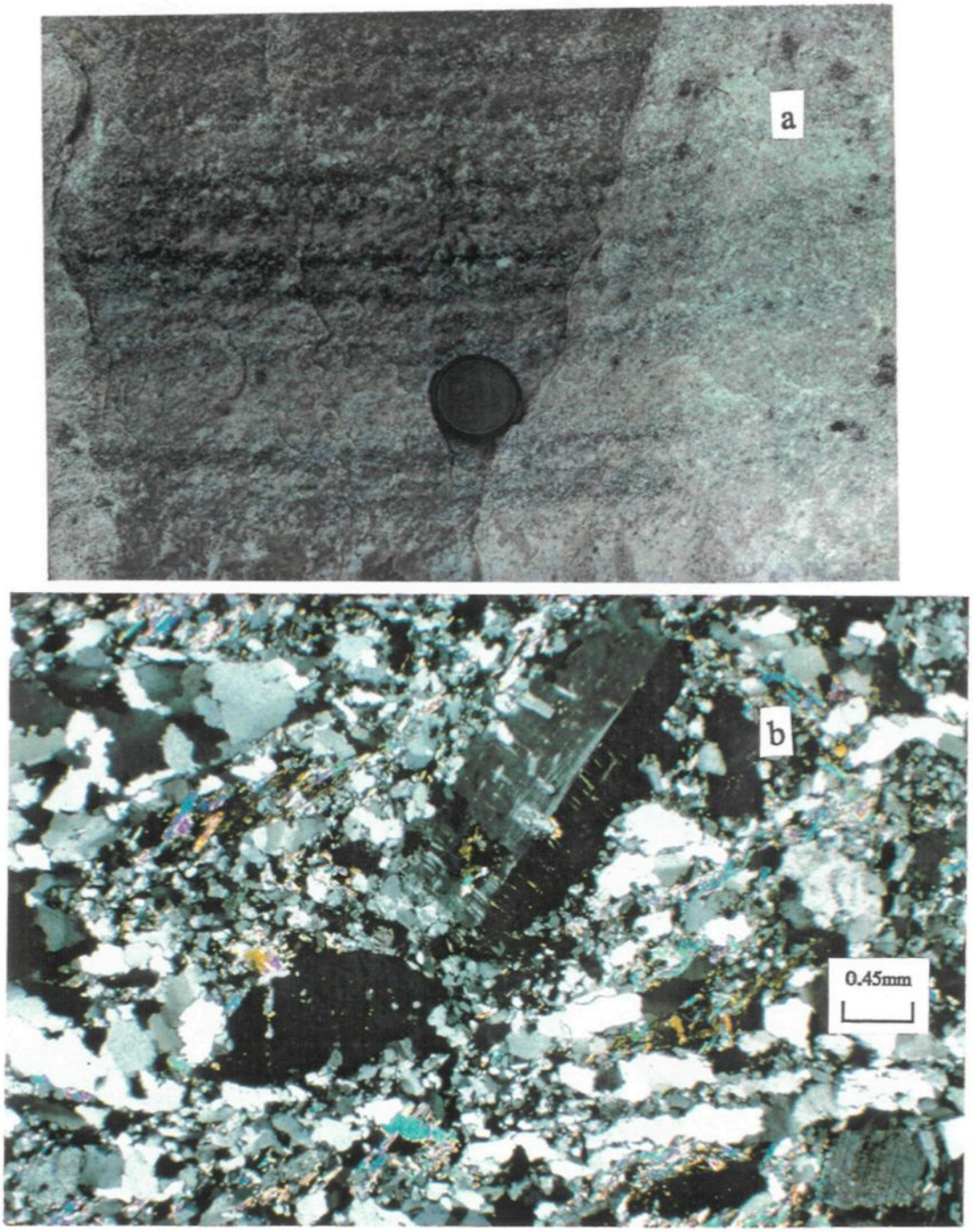

Fig.2.9. Magmatic flow foliation superimposed by strong deformation in the Shiniutou granite. a : Schlieren layering ; b : Flow arrangement of remnant plagioclase phenocrysts surrounded by crushed fine-grained aggregates of mica, feldspar and quartz.

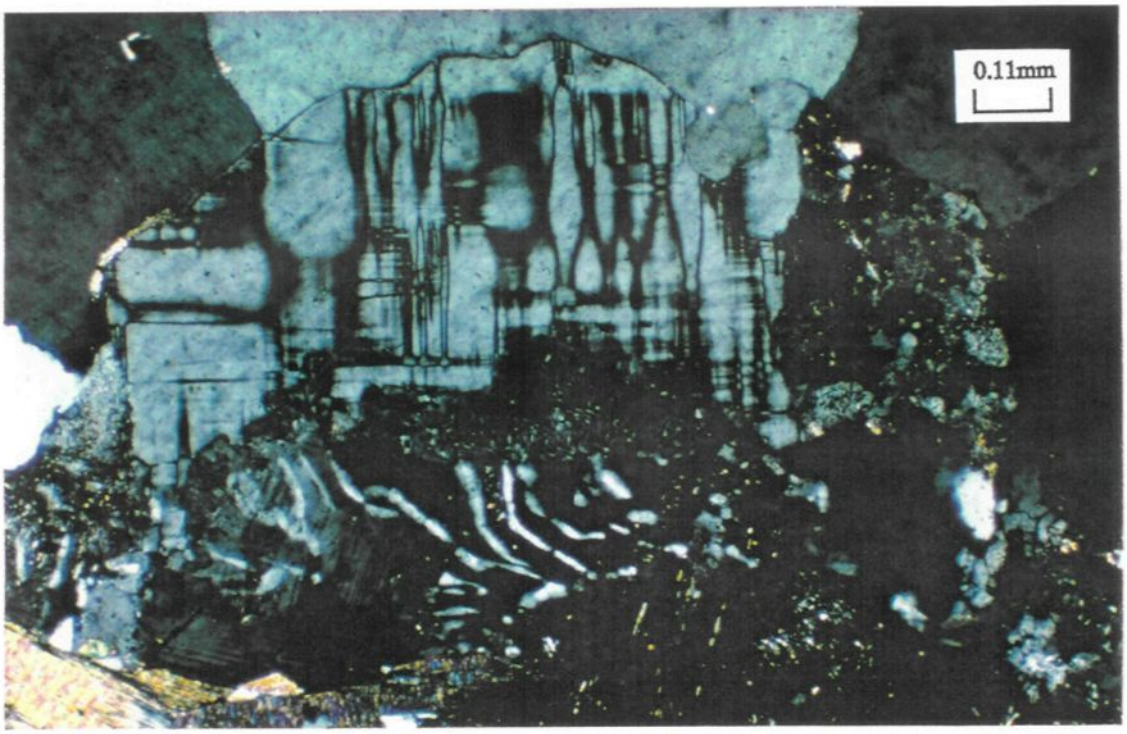

Fig.2.10. Myrmekite occurring in twinned microcline phenocrysts of the Shiniutou granite

remnant elongate feldspar phenocrysts (Fig.2.9b). The smaller biotites are enclosed inside plagioclase phenocrysts, as a result of primary magma crystallization. Most microclines were crushed into microgranular aggregates and strain shadows, producing myrmekite (Fig.2.10). The strongly crushed microgranular aggregates of quartz and feldspar display undulatory extinction and the myrmekite is distributed in the pressure shadow position. Accessory minerals are zircon, garnet and apatite, but no amphibole and sphene occur in the rock.

2-2-2. Hercynian granites

The Hercynian granites include the Guangning and Yunlougan plutons (Tables 1.1 and 1.2). Both arelocated in the Guangning-Luodin Fault Deformed Zone (Figs. 1.4 and 1.5).

(1) Guangning granite

The Guangning pluton is characterized by biotite monzogranite, which contains dark enclaves (Fig.2.11). The Guangning granite presents an equigranular texture and homogeneous appearance, and the euhedral plagioclases display a magmatic flow fabric (Figs.2.11 and 2.12). Solid-state deformation is also present and it seems to strengthen the alignment of feldspar and biotite. The superimposed solid-state deformation resulted in crushing of the euhedral feldspar and quartz which were elongated into finer-grained aggregates, usually distributed around the remnant host feldspar (plagioclase porphyroclasts) (Fig.2.12).

The rock-forming minerals include biotite (8 %), muscovite (2 %), plagioclase (35 %, An=15-30), microcline (25 %) and quartz (30 %). Accessory minerals include allanite, epidote and garnet. Allanite and epidote, which are usually enclosed in plagioclase and biotite (Fig.2.13), are commonly regarded as an evidence of primary magmatic crystallization and they usually reflect a magma derived from a subduction environment (Zen and Hammarstron, 1984 and 1986; Farrow et Barr, 1992). Brown-red coloured biotites are lath shaped, and smaller biotites are usually enclosed by plagioclase and microcline, as a result of magmatic crystallization. Biotites are usually crushed and sheared, becoming finer bent

Fig.2.11. Dark enclaves aligned parallel to magmatic flow foliation in the Guangning granite

Fig.2.12. Flow fabric of bent euhedral plagioclases, and interstitial quartz is polygonized and elongated parallel to ductile deformation in the Guangning granite

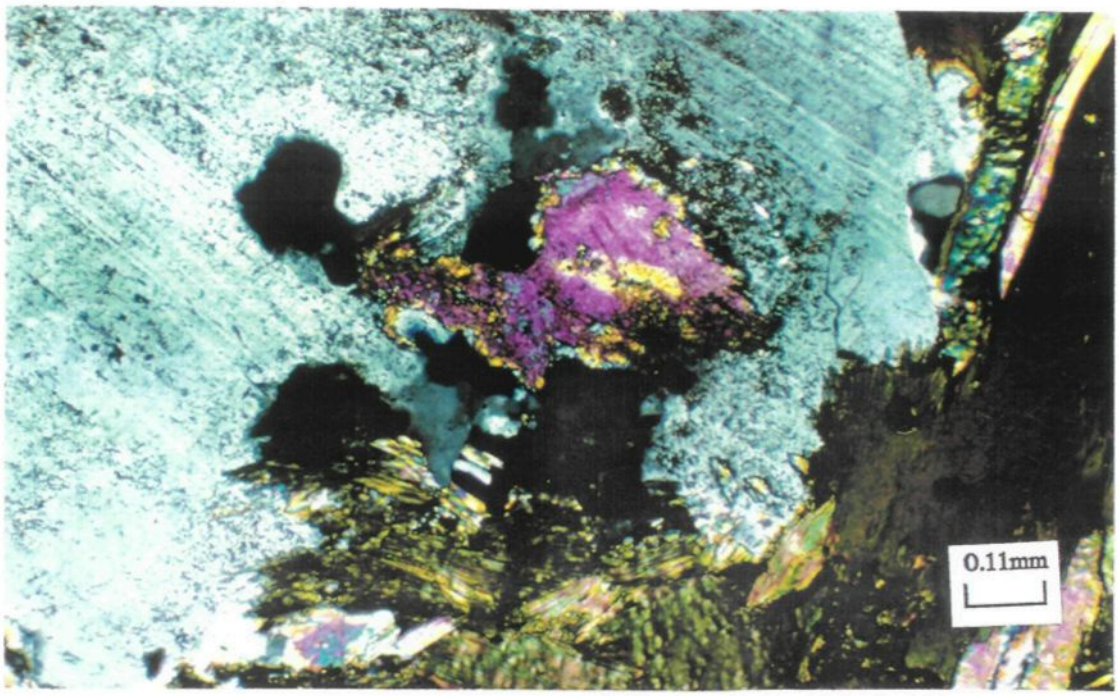

Fig.2.13. Allanite enclosed by plagioclase and biotite in the Guangning granite

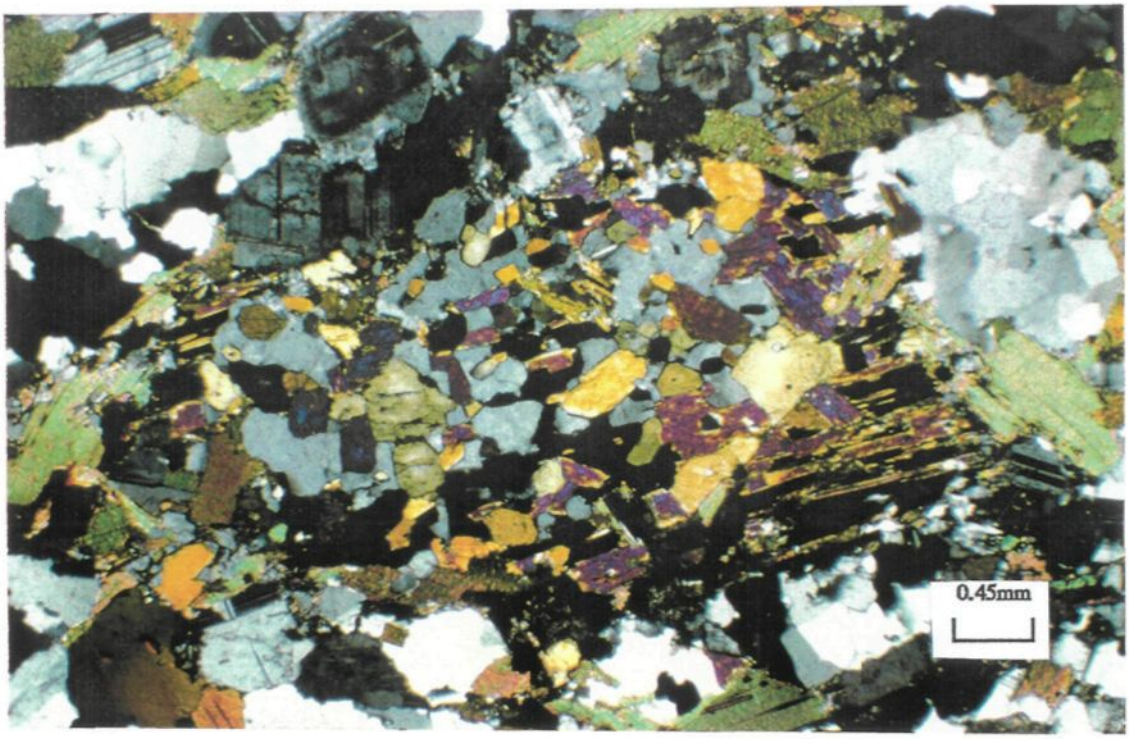

Fig.2.14. Magmatic floliation of aligned amphibole and biotite, and they are surrounded by feldspar and polygonized quartz in the Yunlougan pluton

aggregates as a result of solid-state deformation. Polysynthetically twinned zoned plagioclase crystals are crushed and elongated. The crushed finer-grained aggregates of feldspar and quartz are usually distributed around the remnant plagioclase phenocrysts (plagioclase porphyroclasts). Microcline and quartz display undulatory extinction, and the twinned microcline shows obvious strain shadow in which myrmekite was produced.

(2) Yunlougan pluton

The Yunlougan pluton, which is one of the wall rocks of the Hetai gold deposit, is an intrusion dominated by granodiorite. The granodiorite is equigranular and relatively homogenerous in outcrop. Aligned mafic minerals (amphibole and biotite, Fig.2.14) and zoned plagioclase phenocrysts outline a well-defined flow foliation (Fig.2.15).This magmatic foliation is overprinted by a strong dynamic deformation, defined by crushed feldspar and bent micas (Fig.2.15).

The rock-forming minerals of the Yunlougan granodiorite consist of amphibole (5 %), biotite (12 %), plagioclase (55 %, An=30-50), microcline (8 %) and quartz (20 %). The accessory minerals are mainly allanite, sphene, magnetite and zircon. Green-coloured amphibole occurs in small grain surrounded by biotite. Some small amphiboles and biotites were enclosed by plagioclase phenocrysts during the magmatic crystallization. Biotite is brown-green coloured and long slab shape, and is usually concentrated in biotite-rich bands. Most biotites are deformed, presenting a flexural strain feature. Plagioclase is zoned, and most are strained and broken (Fig.2.15). Microcline and quartz are locally crushed, occurring as finer-grained aggregates with undulatory extinction. Myrmekite usually occurs in deformed microcline and is present as ribbons of quartz (and little albite). These finer-grained aggregates and myrmekites are usually oriented, and then form an obvious strain shadow.

2-2-3. Indosinian granites

The Wuchun body belongs to the Indosinian period based on the available age data (Table1.2). The Wuchun body is distributed along a NW strike fault which was developed between two major fault zones, the Guangning-Luodin and Wuchuan-Sihui (Fig.1.5).

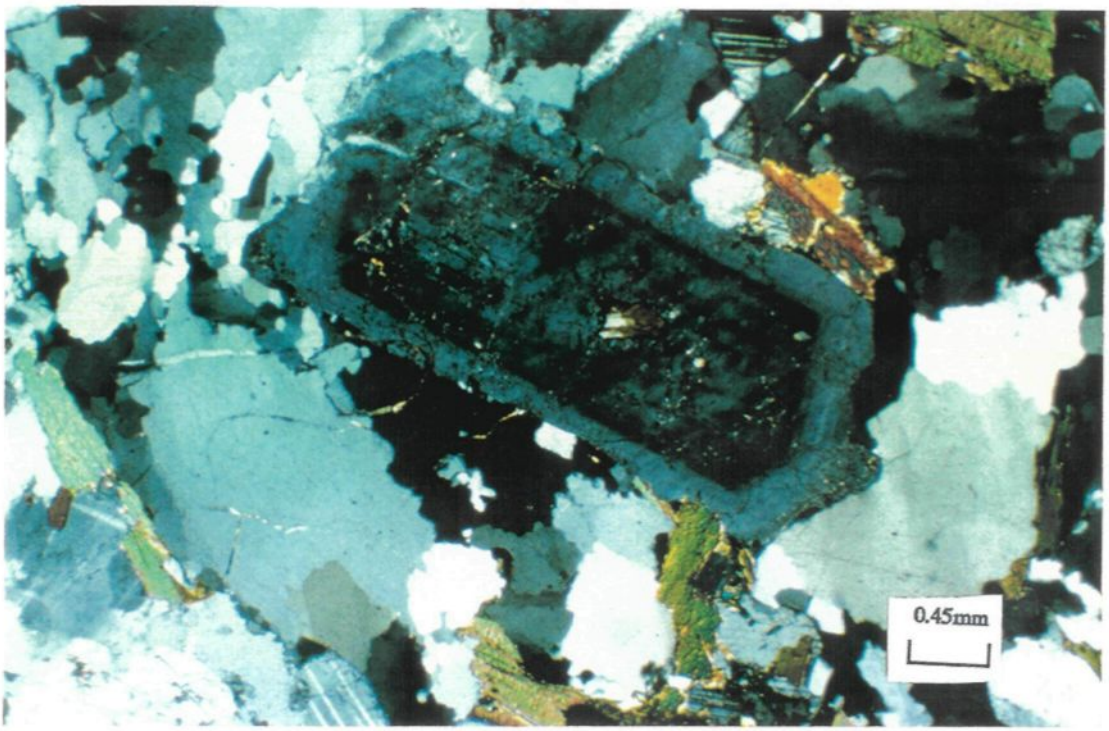

Fig.2.15. Flow fabric of zoned plagioclase phenocryst surrounded by bent biotite and polygonized quartz in the Yunlougan pluton

Fig.2.16. Granodioritic enclave in the host megacryst monzogranite of the Wuchun pluton

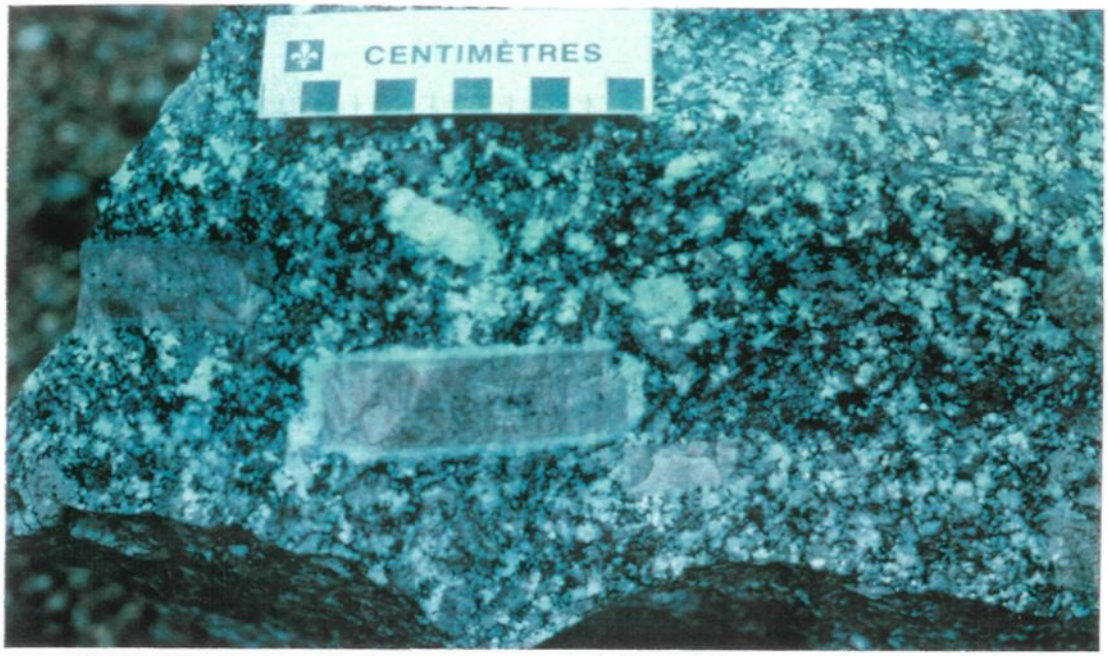

Fig.2.17. Flow fabric of megacrysts with growth rim in the Wuchun pluton

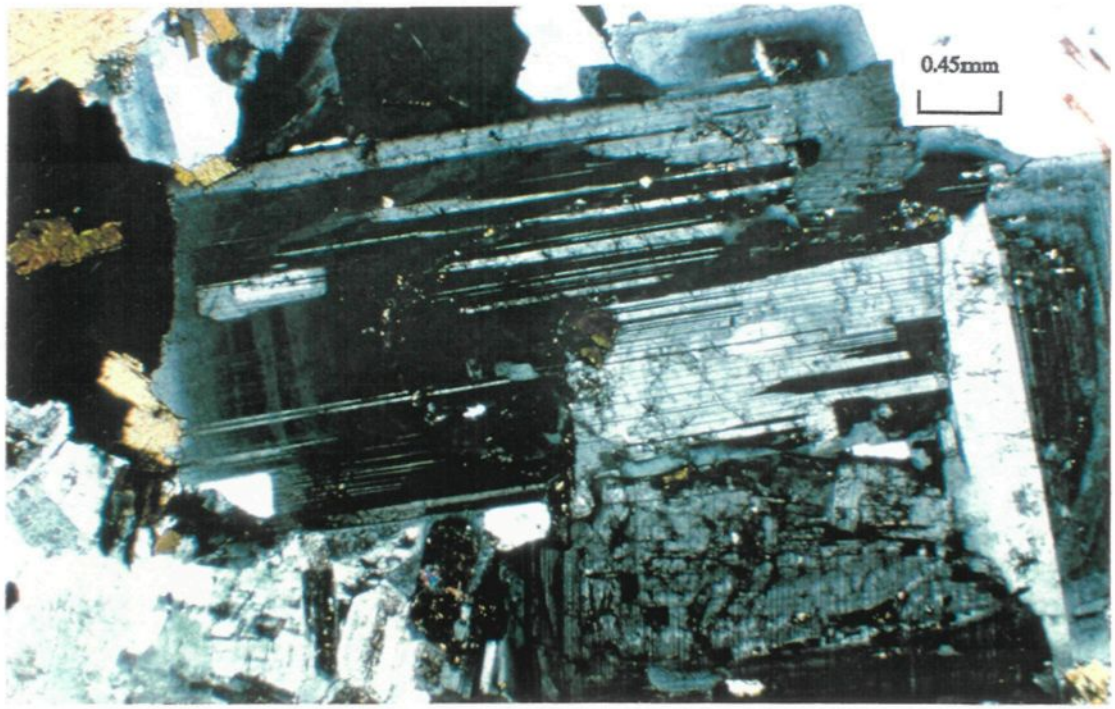

Fig.2.18. Aligned zoned plagioclase phenocrysts enclosing biotite in the Wuchun pluton

The Wuchun body is a light rose-coloured porphyritic monzogranite with granodioritic enclaves (Fig.2.16). It is also a host-rock of the Hetai gold deposit. The porphyritic monzogranite contains plagioclase phenoclasts, which are about 2-10 cm large (Fig.2.17). The magmatic flow foliations are characterized by flow arrangement of these bigger feldspar phenoclasts (Fig.2.17). In contrast to the Caledonian and Hercynian granites, the Wuchun body is undeformed and the igneous minerals retain original crystal shape and primary magmatic flow foliation.

The rock-forming minerals of the Wuchun monzogranite include biotite (5 %), plagioclase (30 %, An=5-35), orthoclase (35 %) and quartz (30%). The accessory minerals are sphene, allanite, zircon and magnetite. Brown-green coloured biotite occurs in small laths, and some smaller biotites are enclosed inside plagioclase and arranged along the growth zones of plagioclase (Fig.2.18) during magmatic crystallization. Amphibole is partly altered to chlorite. Plagioclase is characterized by large zoned and polysynthetically twinned phenocrysts, which are aligned in a magmatic flow foliation (Fig.2.18). The plagioclase has an andesine (An=40) core with an outer rim of albite (An=5) or an outer rim of orthoclase (Figs.2.17 and 2.18). This may reflect the early accumulation of plagioclase and then a change of magmatic composition during crystallization. Orthoclase is inequigranular and some occurs as large phenocrysts. The large orthoclase also has a growth rim of albite and quartz, and it displays the light rose core and white border (albite and quartz) in hand-specimen (Fig.2.17). Both the plagioclase or orthoclase core and albite and quartz outer rim enclose small biotite grains, demonstrating that albite and quartz rims are the products of magma crystallization and not the results of sodium replacement (Dai, 1986).

The granodioritic enclaves occurring in the Wuchun monzogranite have irregular shape and size (about 5-30 cm) (Fig.2.16). There are reaction zones between the enclaves and host monzogranite. The granodioritic enclaves seem undeformed and retain an igneous habit. The enclaves contain amphibole (2 %), biotite (18 %), plagioclase (55 %, An=25-40), orthoclase (10 %) and quartz (15 %). Amphibole is strongly altered to chlorite. Biotite is brown-green colored and lath shaped, and smaller biotites are usually enclosed by feldspar and quartz. These granodioritic enclaves contain about 5% large plagioclase xenocrysts (An=40-60). These plagioclases occur in glomeroporphyritic aggregates (Fig.2.19). The plagioclase xenocrysts are characteristically zoned, in which smaller biotite crystals are enclosed and distributed within plagioclase growth zones (Fig.2.18). The small plagioclases,

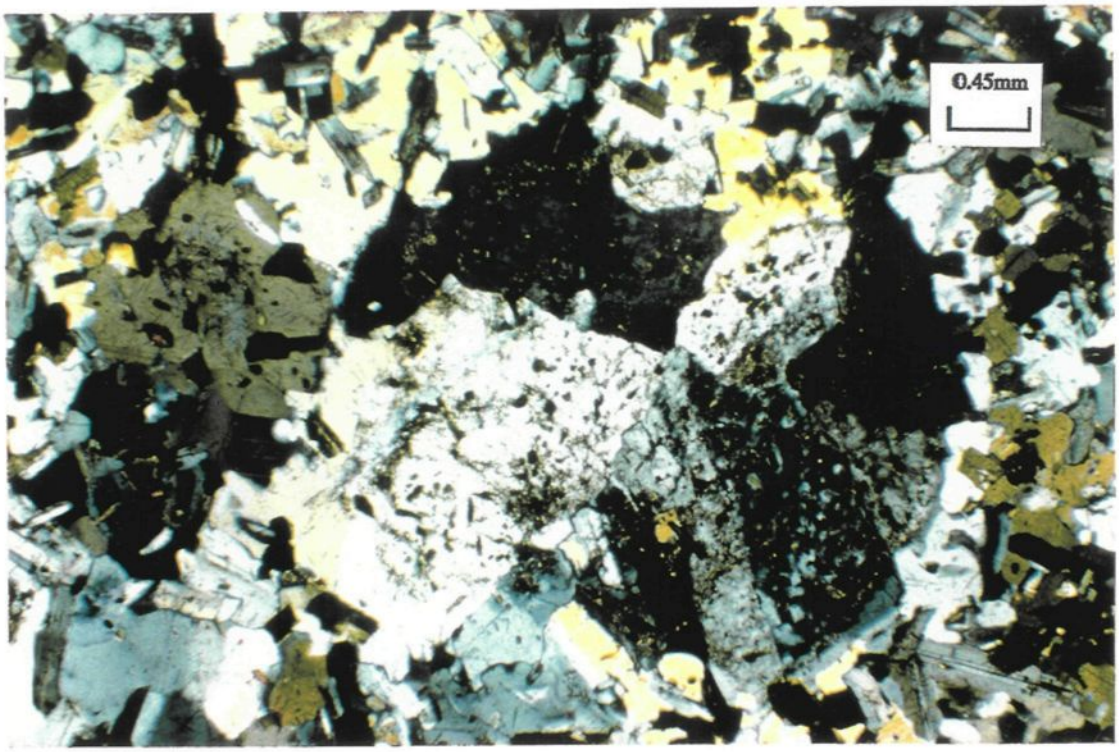

Fig.2.19. Glomeroporphyritic aggregates of plagioclase xenocrysts in the granodioritc enclaves of the Wuchun pluton

about 45 % (An=25-40), are polysynthetically twinned with a hypidiomorphic texture, and they also enclose euhedral biotite. Orthoclase and quartz occur as fine grained granular and xenomorphic texture, and also enclose euhedral biotite. The big plagioclase xenocrysts may be derived from an earlier formed magma, because they obviously differ from the other plagioclase of the granodioritic enclaves in texture and structure as well as in chemical composition.

2-2-4. Yanshanian granites

The Sihui complex, which belongs to the Yanshanian period based on the available age data (Table 1.2), is distributed along the Wuchuan-Sihui Fault Zone (Fig.1.5).

The Sihui complex includes the Sihui, Baishitan and Lianhe bodies (Fig.1.5), characterized by a suite of light rose coloured biotite alkali-feldspar granites. The granites are polyphase intrusions, containing coarse-grained alkali-feldspar granite, medium-grained alkali-feldspar granite and fine-grained alkali-feldspar granite. In addition, it contains dark granodioritic enclaves (Fig.2.20). The magmatic flow foliations are represented by flow aligned feldspar and biotite, in some places forming schlieren layering (Fig.2.21). The granodioritic enclaves are also aligned with magmatic flow foliation (Fig.2.21). Mafic minerals decrease from the granodioritic enclave to the host alkali-feldspar granitic rocks. These intrusive phases are not deformed, but their spatial distribution is controlled by the strike (NNE) of the Wuchuan-Sihui Fault Zone (Fig.1.5).

Except for the dark granodioritic enclaves, the composition of the Sihui alkali-feldspar granite series is relatively constant, composed of biotite (5 %), plagioclase (15 %, An =10-45), microcline (45 %) and quartz (35 %). The accessory minerals are mainly magnetite, sphene and zircon. The few amphiboles are mostly altered to chlorite. Brown-green biotite occurs in small laths, usually around magnetite. Some biotite is enclosed by the feldspar and quartz. In the coarse-grained alkali-feldspar granite, some plagioclase phenocrysts display zoned and patchy features (Fig.2.22) and obviously differ from other small polysynthetically twinned plagioclases with equigranular grains. Myrmekite occurs on the border of both plagioclase and K-feldspar (Fig.2.23). Microcline and quartz usually

Fig.2.20. Flattened granodioritic xenolith parallel to magmatic foliation and slight deviation of fabric around xenolith of the Sihui pluton

Fig.2.21. Schlieren layering of biotite and feldspar in the Sihui alkali-feldspar granite

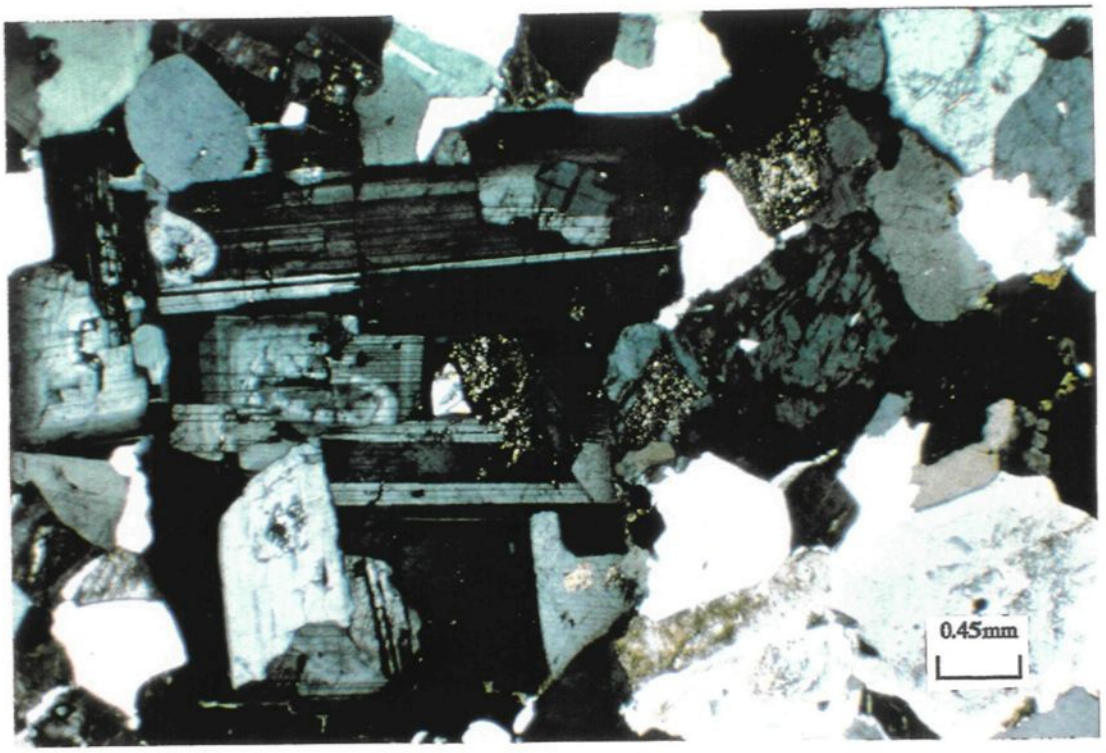

Fig.2.22. Aligned zoned plagioclase phenocrysts in the Sihui alkali-feldspar granite

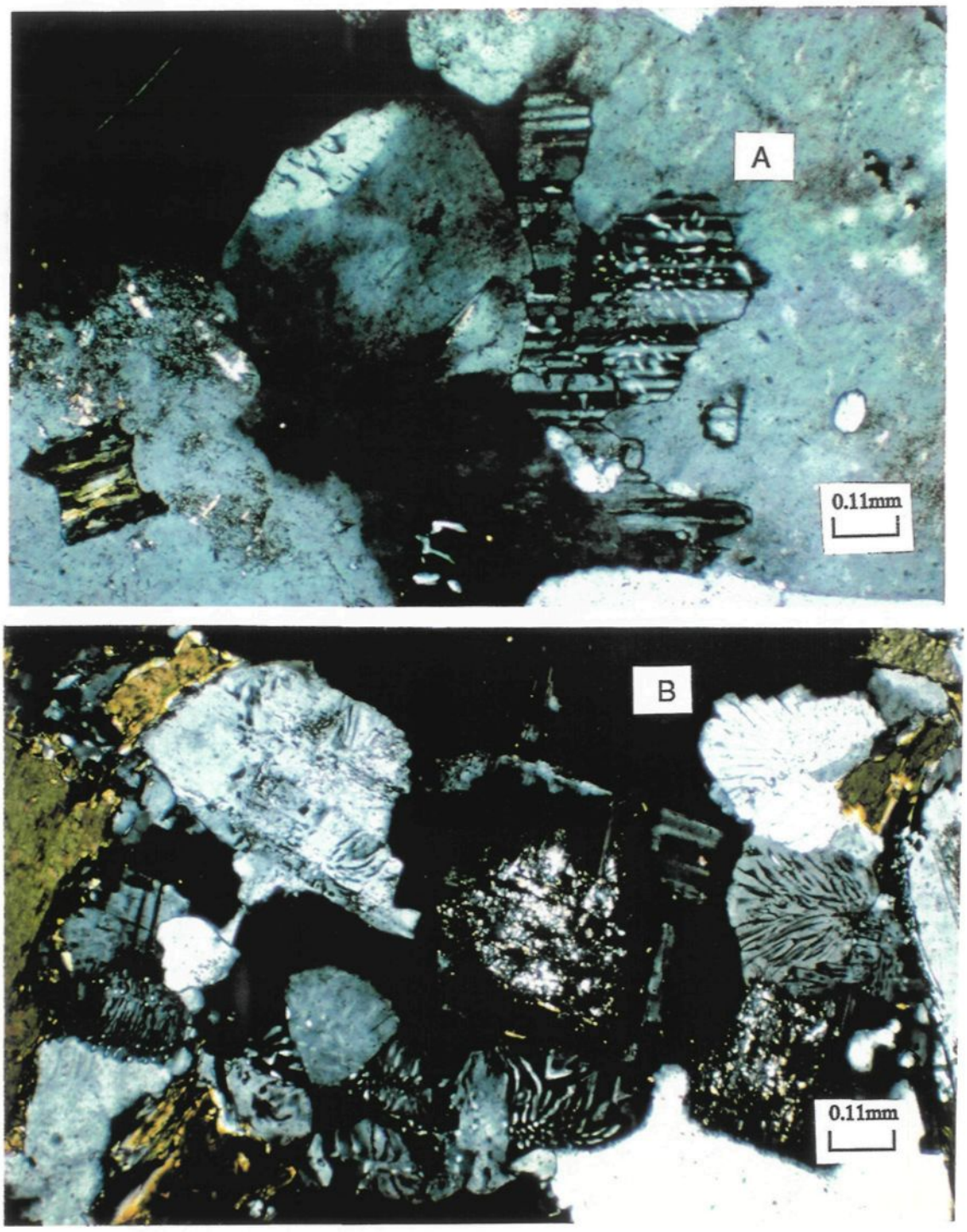

Fig.2.23. Myrmekite in the Sihui alkali-feldspar granite. A: Myrmekite in polysyntheticly twinned plagioclase; B: Myrmekite in K-feldspar

present a hypidiomorphic to xenomorphic texture, and a graphic intergrowth texture is commonly observed. This myrmekite seems different from that in the older granites, and may be produced by a different mechanism.

The granodioritic enclaves in the Sihui complex display irregular shape and different size (5-20 cm) in outcrop, but are aligned parallel to the magmatic flow foliation of the host alkali-feldspar granite (Fig.2.20). The enclaves have not been deformed and retain their original magmatic habits as do the host granites. They have a fine-grained porphyritic texture, and the phenocrysts all are composed of zoned plagioclase (Fig.2.24). The principal rock-forming minerals include amphibole (2 %), biotite (8 %), plagioclase (60 %, An=30-45), orthoclase (10 %) and quartz (20 %). The accessory minerals are magnetite, zircon and sphene. Green coloured amphibole occurs in long prisms and brown coloured biotite occurs in small laths. In outcrop, these mafic minerals display the flow fabric and combine with felsic minerals to form schlieren layering. Biotite and amphibole usually cluster around magnetite. Matrix plagioclase is hypidiomorphic and all plagioclases have an outer rim of alkali feldspar and quartz on their border (Fig.2.22). Albite, orthoclase and quartz show xenomorphic texture. According to the texture and composition (anorthite), the zoned plagioclase phenocrysts may result from an earlier accumulation.

2-2-5. Huangtongjiang gabbro

The Huangtongjiang gabbro occurs within the Sidong biotite granite near the Guangning-Loudin Fault deformed zone (Fig.1.5). There is no available age data for it. It is a basic stock (< 0.5 km2) and is of particular interest as a reference to the granites with mafic enclaves because it may be regarded as a sample of a more primitive magma and because it contains high Au contents (about 15 ppb). This body includes two intrusive phases, medium-fine grained gabbro and pyroxene diorite. They appear dark-green in colour with an inequigranular texture. Their microstructures are characterized by typical subophitic texture, granular pyroxene and amphibole existing in a triangular framework formed by long laths of plagioclase (Fig.2.25). This body appears undeformed and the magmatic texture is well preserved. In this, it is similar to the other rocks of the Indosinian or Yanshanian magmatic suites.

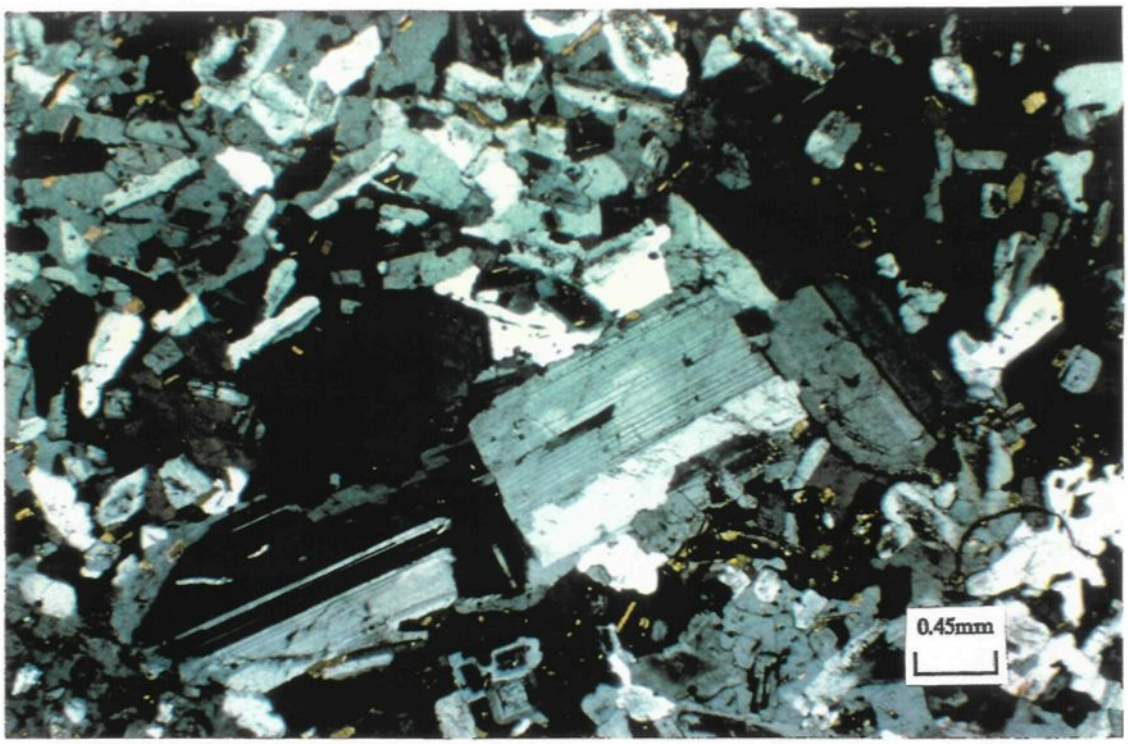

Fig.2.24. Zoned plagioclase phenocrysts in granodioritic xenolith of the Sihui granite suite

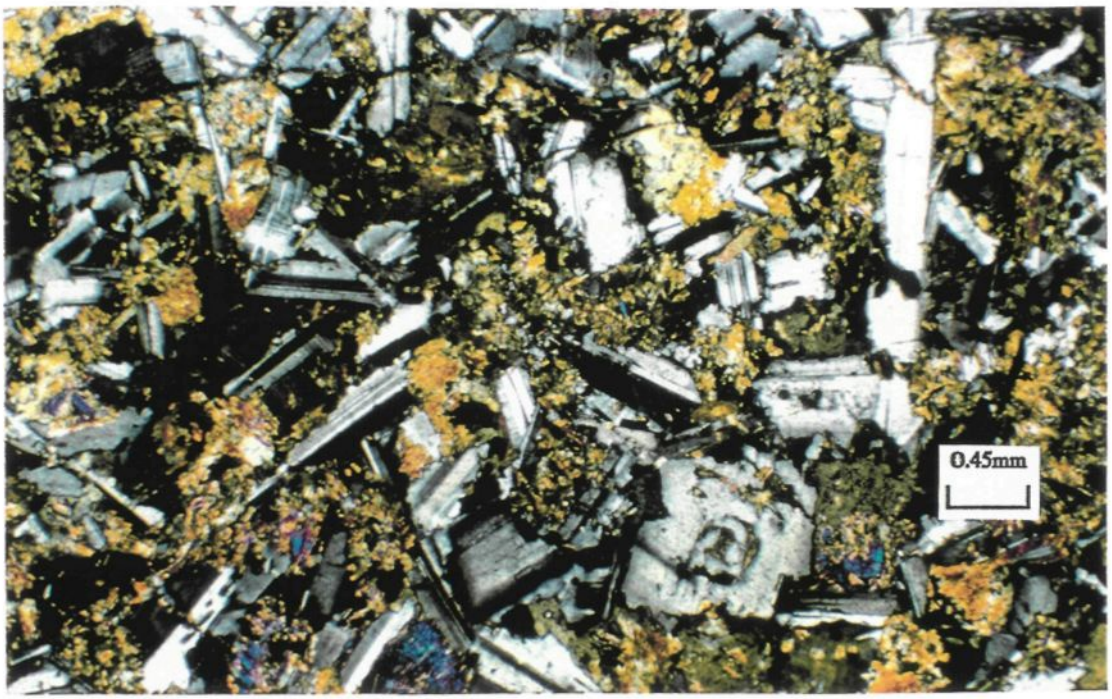

Fig.2.25. Subophitic texture of the Huangtongjiang gabbro

The rock-forming minerals of the gabbro include pyroxene (5-8 %), amphibole (35 %), biotite (5 %), plagioclase (50 %, An=50-70), orthoclase (1-2 %) and quartz (1-3 %). The accessory minerals mainly are magnetite and apatite. Pyroxene and magnetite usually occur within the larger amphibole crystals and within the triangular framework of plagioclase laths (Fig.2.25). Amphibole is predominant and occurs as large laths and small granular grains. The large amphibole grains usually enclose other minerals, but the smaller grains occur in the triangular framework of plagioclase. Biotite is dark brown in colour and occurs as very small grains with pyroxene and magnetite. Most of plagioclases show polysynthetically twinned laths with slight zoning.

2-2-6. Comparison between the granites of different ages

The petrographic descriptions of individual bodies show clearly that magmatic crystallization and flow foliations are a common phenomenon. However, the extent of solid-state deformation is very different between the granites of different ages. The Caledonian and Hercynian (older) granites have a strongly developed solid-state deformation, whereas the Indosinian and Yanshanian (younger) granites are very weakly deformed at best. Comparatively, the petrographic features of the younger granites clearly differ from the older granites. Granites vary from equigranular to porphyritic texture from the Caledonian and Hercynian to the Indosinian and Yanshanian, which may imply that the depths of magma emplacement became shallower from the Caledonian to the Yanshanian. Of course, the other factor is that the older granites were strongly deformed. In addition, alkali-feldspar becomes predominant in the Indosinian and Yanshanian granites as a result of changing magmatic composition. The three Caledonian bodies analyzed (the Sidong, Shijiang and Shiniutou) all are characterized by biotite+muscovite+garnet mineral assemblage, indicating the peraluminous features of the source rocks. The Hercynian bodies are different, the Guangning biotite monzogranite having a biotite+ muscovite+ garnet+ allanite(epidote) mineral assemblage, whereas the Yunlougan granodiorite having a mineral assemblage of hornblende+ biotite+ sphene+ allanite(epidote)+ magnetite, but both are strongly deformed. However, the Indosinian and Yanshanian bodies display the hornblende+ Mg-biotite+ sphene+ magnetite mineral assemblage. This may suggest that they have a different source. In addition, the petrographic features of the two types of enclaves are different, and individual enclaves suggest certain petrogenetic relations with their host granite. The

enclaves from the Wuchun and Sihui granites have a certain similarity in petrographic features, especially in mineral assemblage and igneous texture, but the enclaves from the Shijiang complex display metamorphosed sedimentary rock textures rather than igneous textures.

The enclaves of the Wuchun and the Sihui granites are probably earlier intrusive phases of pluton, and they may be considered as cognate xenoliths because both have similar igneous mineral assemblage and have not been deformed. In addition, the presence of Ca-rich plagioclase xenocrysts may indicate that the Wuchun granodioritic enclaves are related to a more basic magma source, such as the Huangtongjiang gabbro. So, it is reasonable to infer that the Wuchun and the Sihui enclaves may be inherited from the magma source similar to the Huangtongjiang gabbro. In contrast, the dark enclaves of the Shijiang complex may be an unmelted source rock, which have been deformed with the host complex, and the petrographic and mineral assemblage present a gradational relation with host intrusive rocks.

Generally, the Hetai granites display a variation trend from Caledonian, through Hercynian and Indosinian to Yanshanian with tectonic evolution, reflected by both their mineral assemblage and their deformation features. The petrographic features from the granites of different ages are compared in Table 2.2.

2-3. Identification of magmatic flow foliation and tectonic foliation

Previous genetic consideration has been focussed on the premise that these granitic rocks are formed by granitization during regional metamorphism (Mo, 1987; Dai, 1986). Because of this premise, previous studies were mostly based on the theory of regional metamorphism, and the petrographic phenomena in fact have not been investigated in detail, particularly the identification of primary magmatic structures. The complex textures and structures in these granitic rocks have been regarded as the result of regional and tectonic metamorphism (Mo, 1987 and 1989; Dai, 1986) and the magmatic structural features were ignored.

Are the Hetai granites characterized by magmatic structures, and are they superimposed by later dynamic solid-state deformation ? The mesostructural and

Table 2.2. Comparison of petrographic features between granites of different ages

Age	Body	Mineral assemblage	Magmatic feature	Deformation feature
Caledonian				
	Shijiang Sidong Shiniutou	Brown-red biotite +muscovite +garnet	Intrusive contact flow fabric of zoned plagioclase	Very strong cataclasis mylonitic texture deformation myrmekite
Hercynian				
	Guangning	Brown-red biotite +muscovite+allanite	Flow fabric of zoned plagioclase	Strong cataclasis mylonitic texture
	Yunlougan	Brown-green biotite+ hornblende+sphene +allanite	Flow fabric of zoned plagioclase	Strong cataclasis gneissic texture
Indosinian				
	Wuchun	Brown-green biotite+ hornblende+sphene +magnetite	Flow fabric of zoned plagioclase and alkali-feldspar with growth rime	Slight
Yanshanian				
	Sihui Baishitan Lianhe	Brown-green biotite+ hornblende+sphene +magnetite	Flow fabric of feldspar and biotite, plagioclase and alkali-feldspar with growth rims	Slight
	Huangtong-jiang gabbro	Pyroxene+hornblende +brown-green biotite +magnetite	Subophitic texture	Slight

microstructural inverstigations show that many of the directly perceived petrographic phenomena imply superimposed foliations, but the primary magmatic features such as intrusive contacts and flow foliation can be still identified in spite of the deformation. So, it is reasonable to suggest that the granitic rocks of the Hetai Area are generally formed by magmatic processes and have had solid-state deformation superimposed on them during later tectonic movements. Therefore, the detailed observations of petrographic phenomena must be considered before discussing geochemical characteristics, because it gives the first evidence on which the petrogenesis of granitic rocks are usually modeled.

2-3-1. Magmatic flow foliation

The identification of magmatic foliations is very important (Paterson and Tobisch, 1988, 1989 and Paterson et al., 1989). Magmatic foliations in granitic rocks are characterized by oriented primary minerals. The Hetai granites consist of different complexes (Table 1.1), each of which contains different intrusive phases and displays differing degree of deformation. Most of the granite bodies, such as the Sidong, Shijiang, Guangning, Wuchun and Sihui, show intrusive contact relations in outcrop, and the feldspar and biotite display a flow orientation parallel to contact zones between different granitic phases (Figs.2.1 and 2.7). The later intrusive phase is richer in felsic minerals and intersects the earlier phase in a wedge shape (Figs.2.1 and 2.7).

Intrusive contact phenomena are the most direct evidence for identifying magmatic intrusion, and the other main criterion of magmatic flow is the preferred orientation of primary igneous minerals. For example, one of the strongest criteria is that of oriented euhedral K-feldspar and plagioclase, because feldspars generally do not grow as euhedral crystals in unmelted metamorphic rocks (Vernon, 1968, 1986, and 1991; Vernon et al., 1983; Vernon and Collins, 1988). Consequently, solid-state growth cannot explain the alignment or crystal shapes (Paterson and Tobisch, 1989 and Paterson et al., 1989). In the Hetai granites, the flow orientations of zoned plagioclase are commonly observed in thin sections of the Shijiang, Guangning, Yunlougan, Wuchun and Sihui granites (Figs. 2.2, 2.9, 2.12, 2.15, 2.17, 2.18, 2.22 and 2.24), and the best example is the megacrysts of zoned feldspar in the Wuchun body which display evident magmatic flow orientation (Fig.2.17).

Mafic minerals such as biotite and amphibole are oriented in planes in the Yunlougan granodiorite (Fig.2.14), indicating a magmatic foliation. These mafic mineral flow foliations are similar to those observed in the Yangtze pyroxene diorite-quartz diorite-tonalite-granodiorite series in South China. Bateman et al. (1983) and Bateman (1985) observed that in the contact zone of granites with country rocks, mafic minerals show an alignment especially in tonalites and diorites. Except for this, biotite is usually aligned by solid-state foliations in the Hetai granites.

Schlieren layering is a feature in the Shiniutou (Fig.2.9) and the Sihui complexes (Fig.2.21). The felsic minerals and biotite form parallel bands. Schlieren layering is regarded as a clear indicator of magmatic flow in the granitic rocks (Paterson and Tobisch, 1989 and Paterson et al., 1989; Reid and Hamilton, 1987). Barriere (1981) considered that schlieren layering in granitic rocks is due to flow sorting rather than gravitational sorting, which does not directly reflect the direction of magma flow (Wager and Brown, 1967). Gravitational sorting may usually occur in some relative basic rocks such as pyroxene diorite and quartz diorite in the Yangtze Area , but for most granites, the schlieren layering may be due to magmatic flow foliation. Such schlieren layering can be also observed from the Nanling, the Yangtze and the Coast granites in South China.

The elongate dark enclaves may be also regarded as important evidence for magmatic foliation. As shown in the Wuchun and Sihui granites, the granodioritic enclaves are parallel to flow foliation of the host granitic magma (Fig.2.20), and they contain also Ca-rich xenocrysts in them (Fig.2.19). Host magmatic flow foliations usually deflect around the dark enclaves (Fig. 2.20), because the enclaves behaved as fragments of solid rock.

It is clear that primary magma structures such as flow foliations can still be identified, although a later deformation has been superimposed in some instances on the primary fabric.

2-3-2. Solid-state deformations

Solid-state deformation consists of dynamic brittle to ductile processes as the granites are subjected to overthrust and strike-slip shear zones. The brittle processes result in

microfracturing and displacements resulting in new shapes and sizes of crystals. Field investigations of the Hetai granites show that the Shijiang, Guangning and Shiniutou granites display prominent gneissic, augen and mylonitic structures (Figs.2.3, 2.4, 2.9, 2.12 and 2.15), with structural orientation sub-parallel to the Guangning-Luodin and Wuchun-Sihui Fault Zones. Microstructural observations show that the larger zoned plagioclase phenocrysts were broken (and displaced), or recrystallized into finer-grained aggregates, and the remaining phenocrysts are usually enclosed by finer-grained aggregates of broken feldspar, quartz and mica (Figs.2.2, 2.9, 2.12 and 2.15). The plagioclase phenocrysts present primary magmatic flow foliation and the solid-state foliation was superimposed on it. The broken feldspar, quartz and mica are distributed around the relict plagioclase phenocryst parallel to the dynamic deformation direction, and the elongation of aggregates contribute to the deformation foliation.

The ductile processes usually result in the formation of subgrains, kink bands, deformation lamellae, ribbon texture and undulatory extinction (Hibbard, 1979 and 1987). In addition, the elongation of the feldspar during the ductile process may be an important phenomenon. The plagioclase in the Guangning granite is evidently elongate and slightly displaced (Fig.2.13), showing ductile deformation. Quartz and mica are the most subject to solid-state deformation, and polygonized and undulatory extinction quartz, ribbon and mica kinking are widely observed in the Shijiang, Shiniutou, Guangning and Yunlougan plutons (Figs.2.2, 2.9, 2.12 and 2.15). These finer-grained aggregates of feldspar, quartz and mica show the plastic state of shearing, and always display flow-like features, passing around the bigger plagioclase phenocrysts and parallel to the dynamic deformation. Vernon et al. (1986) and Paterson et al. (1989, Paterson and Tobisch, 1989) considered that the plastic deformation of quartz undulatory extinction and mica kinking is a typical result of solid-state foliation. The quartz, which is the last rock-forming mineral to crystalize in most granites is extremely sensitive to post-crystallization deformation, and demonstrates the time of deformation.

The primary schlieren layering in the Shijiang and Shiniutou bodies is greatly affected by later deformation, showing folded schlieren layering, heterogeneous stromatic and banded foliations even mylonitic foliation in the strongest deformation zone (Figs.2.3 and 2.9).

The alignment of elongate dark enclaves can be found in the Wuchun, Shihui and Guangning granites, indicating a magmatic flow foliation, but the dark enclaves in the Shijiang complex are strongly flattened and elongated by dynamic deformation. The deformed dark enclaves usually occur as gneissic and lenticular shapes. Vernon and Collins (1988) considered that lenticular layering may resemble layering produced by extreme magmatic elongation of microgranitoid enclaves, but the lenticular elongation of dark enclaves observed in outcrops of the Guangning granite (Fig.2.11) is most probably the result of tectonic deformation. Deformation foliations pass through enclaves with slight refraction where the enclaves and host granite have different compositions and textures. Aplite or lamprophyre dykes are usually folded or broken into fragments.

2-3-3. Myrmekite

Myrmekite is commonly present in the Hetai granites, both in the deformed and undeformed granites, and it may be divided into two types :

(1) Myrmekite from the undeformed granites such as the Wuchun megacryst monzogranite and the Sihui alkali-feldspar granite usually occurs as quartz lobes fringing an alkali-feldspar phenocryst. This type of myrmekite has sharp contacts, generally grows into the undeformed alkali-feldspar, and is present as quartz ribbon and drops in the border of alkali-feldspar (Fig.2.23), forming a mosaic structure with alkali-feldspar seen in hand-specimen from the Wuchun and the Sihui body. This myrmekite is similar to that of the alkali-feldspar granite (miarolite) in the Coast Area, South China (Yang et al. 1985; Yang et al., 1986b).

(2) Another type of myrmekite is widely developed in deformed granitic rocks such as the Shijiang, Guangning, Yunlougan and Shiniutou granites (Figs.2.4, 2.5, 2.8 and 2.10). This type of myrmekite always occurs around a phenocryst of microcline-microperthite and is present as curved lobes on the margin of microcline-microperthite phenocrysts. In addition, some myrmekites also exist in the center of microcline phenocryst and occur as quartz lobes, ribbon and drop impression, even in the twinned microcline produced when microcline is deformed (Figs.2.5 and 2.10). In general, this type of myrmekite occurs most

commonly in zones parallel to the foliation, suggesting that the myrmekite aggregates were produced during ductile solid-state deformation.

Comparing these two different types of myrmekites, it is clear that they are the result of different geological occurrences. The former is present in non-deformed granites and the later is developed in deformed granites. Therefore, they may be produced by different mechanisms, respectively.

Several mechanisms for producing myrmekite in deformed and undeformed granites are proposed. Hibbard (1979, 1987) suggested that all myrmekite in mesoscopically undeformed granites is due to crystallization of water-saturated, pressure-quenched magma, based on his observation of crystal faces and zoning in the plagioclase of some myrmekitic aggregates and on his general model of late magmatic crystallization in granites. This is the opposite of conventional hypotheses of replacement of K-feldspar in the solid state (Phillips,1980; Vernon et al.,1983), requiring that myrmekite in deformed granites is due to crystallization of small amounts of water-saturated magma in a largely crystallized rock, in response to 'micro pressure-quenching' during deformation. Whereas Hibbard (1979 and 1987) considered that, in undeformed granite or in deformed granite, the strong K partitioning into the aqueous phase is a major reason, which results in coprecipitation of K-feldspar with plagioclase and quartz, allows myrmekite crystallization from the remaining melt during pressure-quenching, and promotes precipitation of K-feldspar from the K-rich aqueous phase around the myrmekite. Hibbard believed that myrmekite was produced from a melt developed in the late stage of magma development or during the deformation, and that the pressure-quenching is an essential condition. However, Simpson and Wintsch (1989) inferred that local increases in both stress and strain localize the development of myrmekite, because local increases in strain energy would cause replacement of K-feldspar by plagioclase and quartz, via components in a fluid, and they suggested that temperature, pressure and chemical activities control the occurrence of myrmekite, but that strain energy localizes the reaction at sites of high normal stress. Vernon (1991) considered that strain energy may not be a major contributor to the advance of the growth interface of the myrmekite colony and to the nucleation of myrmekite, and that deformation appears to contribute indirectly, by facilitating access of fluids to growth sites, thereby altering the local chemical environment and promoting the development of myrmekite. In general, Vernon (1991) inferred that the development of myrmekite in deformed granites is attributed to

solid-state replacement processes accompanying deformation, because the large interfacial area of the myrmekitic intergrowth allows fluids to penetrate and promote boundary movement during recrystallization, and that the myrmekite grows at sites of locally high stress and is one of the main contributors to the development of foliation.

The microstructural observations show that, in the Hetai Area, the myrmekites in undeformed granites usually display optical continuity between myrmekitic quartz and primary quartz (Fig.2.23), whereas the myrmekites in deformed granites have undulatory extinction, without obvious crystal faces (Figs.2.4, 2.5, 2.8 and 2.10), and they have been produced in some granitic rocks that were deformed well after magma solidfication without developing a melt. In addition, these myrmekites always grow into remnant microcline phenocrysts and occurs most commonly in zones parallel to the foliation, normal to local zones of maximum shortening, demonstrating dynamic solid-state deformation more than chemical replacement. So, the myrmekite produced in undeformed granites may be due to quartz precipitation during late volatile-rich magma crystallization in response to pressure-quenching; whereas the myrmekite in deformed granites in the Hetai Area may be the result of the deformation and the finer-grained aggregates of broken quartz and little feldspar (albite) may invert and fill the expansion zones and fractures in microcline produced by shearing. In general, both in underformed granite and in deformed granite, the precipitation of quartz from K-feldspar or microcline as a result of pressure change may be a major factor for producing myrmekite, that is, the pressure change (pressure-quenching or compressive shearing) may play a more important role than chemical replacement.

In general, the microstructural investigations indicate that the Caledonian and Hercynian granites in the Hetai Area have a superimposed solid-state deformation. The solid-state deformation in the Hetai granites may be a brittle to ductile process, but not a melting processes. The brittle processes of dynamic deformation after granitic magma consolidation in the Hetai Area resulted in igneous minerals such as feldspar and quartz being broken and displaced and micas bent. The ductile process resulted in polygonized quartz and feldspar. In addition, myrmekite is produced inside and between deformed minerals (such as microcline). The physical deformation mechanism is well developed in the Hetai granites.

2-4. Summary

The Caledonian granites are dominated by biotite granites and the mineral assemblages include such aluminous minerals as biotite+muscovite+garnet, but no hornblende and sphene. They display primary magmatic characteristics, but have a strong superimposed solid-state deformation. The Shijiang polyphase intrusive rocks show an evolutionary magmatic trend shown by the mineral variation in the complex. The Caledonian granites in the Hetai Area may be provisionally classified as S-type (Chappell and White, 1974; Chappell, 1984) or the Nanling type granite (Zhang et al., 1984; Yang et al., 1986a) on the basis of their mineral assemblage.

The Hercynian granites in the Hetai Area are characterized by both magmatic crystallization and dynamic solid-state deformation. However, the mineral assemblage of the Guangning monzogranite is different from the Yunlougan granodiorite. The Guangning body is characterized by the assemblage biotite+muscovite+garnet+allanite(epidote), whereas the Yunlougan granodiorite by hornblende+biotite+sphene+allanite (epidote)+garnet. According to the classification of Chappell and White (1974) and Chappell (1984), the Gaungning body may be similar to S-type, but it contains allanite and epidote, demonstrating that parts of a deeper source magma (I-type) may participate in the petrogenetic process. In contrast, the Yunlougan granodiorite may be mainly derived from a deeper source magma (I-type). Allanite, epidote and garnet coexist in both the Guangning and the Yunlougan granites, reflecting a possible mixture of source materials for the Hercynian granites of the Guangning-Loudin Fault Deformed Zone.

After comparing textural features of the rock-forming minerals of the Wuchun host monzogranite and their granodioritic enclaves, it seems clear that a close relation may exist between granodioritic enclaves and the megacrystic monzogranite. The mineralogical trend from the granodioritic enclave to megacrystic monzogranite suggests a cognate relation between them such that the granodioritic enclave is an earlier intrusive phase and the megacrystic monzogranite is a later product, derived from the same magma. Furthermore, the xenocrysts of Ca-rich plagioclase in the granodioritic enclaves may indicate that the source magma is basic.

Sihui K-felaspar granites may be the result of later magma evolved from the same magma as the enclave. It is reasonable to infer that they may both be derived from a deeper source possibly related to basic magmatic activities such as the Huangtongjiang gabbro in the Hetai Area. Combined with the Wuchun granite, the intermediate-basic enclaves may be used to examine the entire magmatic evolution.

The relationship of mineral assemblages in granitic rocks to the intensive variables of the original magma has been discussed in many papers (Ishihara, 1977; Chappell and White, 1974; Didier et al.,1982; and Yang et al., 1986a), and it is well known that granites derived from the peraluminous crustal source regions (S-type) are characterized mainly by Al-rich silicate+Fe-biotite (+little Fe-hornblende) assemblage, whereas granites derived from deeper source regions are composed of Ca-rich silicate+Mg-biotite+Mg-hornblende assemblage. Comparatively, mineral assemblage of the older granites (Caledonian and Hercynian biotite granites) may be similar to those derived from a peraluminous crustal region (S-type), whereas that of the younger granites (Yanshanian and Indosinian granites and Hercynian Yunlougan granodiorite) may be derived from a deeper source region (I-type). So, it may be considered, on the basis of petrography, that the older granites may be derived mainly from a peraluminous source rock like S-type granites, whereas the younger granites are derived from the deeper sources (I-type) and may belong to a series from calc-alkali to alkali evolution.

CHAPTER III

GEOCHEMISTRY OF THE GRANITES

3-1. Introduction

The granites of the Hetai Area are classified into a series of suites of rocks of different ages from Caledonian through Hercynian and Indosinian to Yanshanian. In this chapter, these granitic rocks will be further characterized by geochemistry, in order to develop the geochemical relations within individual bodies and suites and to discuss the evolution and genesis of the separate series.

Geochemical discussions on genetic classifications of granites depend mainly on the features of element abundance and assemblage compared with cosmic and earth abundances. According to the estimate of the compositions of the upper and lower crust by Shaw et al. (1986), the lower crust has less Si, K, Nb, Rb and Zr but more Ti, Fe, Mg, Co, Cr, Cu, Ni, Sc, V and Y than the upper crust. This result may be regarded as an important reference when discussing geochemistry of source rocks of different granite types. In addition, the compatible and incompatible properties of elements may cause a change in their content during magma evolution (Wall et al., 1987). The abundance of certain elements in granites may be variable in different geotectonic settings, although the granites may belong to certain genetic classifications. For example, S-type granites are high in Cr and Ni but low in Sr relative to the I-type granites in the Lachlan Fold Belt (White and Chappell, 1977 and 1983). In contrast to the Lachlan Fold Belt, the granites of South China are high in F, Li, Rb, Sn, W, Nb and Ta but low in Co, Ni, Zn and Sr, and are believed to be derived from aluminous crustal source rocks; whereas those which are high in Co, Ni, Zn and Sr but low in F, Li, Rb, Sn, W, Nb and Ta, are believed to be derived from the lower crust and upper mantle (Wang et al., 1983 and 1984c; Yang et al., 1986b). These studies show that the difference between two areas may be due both to the lack of chemical uniformity and to the different geotectonic environment of granite generation. Pearce et al. (1984) used trace element discrimination diagrams of Y-Nb, Yb-Ta, Rb-(Y+Nb) and Rb-(Y+Ta) for the

tectonic interpretation of granites, and divided granites into four main groups: ocean ridge granites (ORG, low Rb, high Y+Nb and Yb+Ta), volcanic arc granites (VAG, low Rb, Y+Nb and Yb+Ta), within plate granites (WPG, high Rb, Y+Nb and Yb+Ta) and collision granites (COLG, high Rb but low Y+Nb and Yb+Ta). Collision granites can be further subdivided into continent-continent, arc-continent and arc-arc according to the type of collision. Maniar and Piccoli (1989) divided granites into different groups categorized by tectonic environment by using a series of petrochemical plots such as Mol.Al_2O_3/(Na_2O+K_2O)-Al_2O_3/(CaO+Na_2O+K_2O) (Mol.A/NK-A/CNK) diagram. Brown et al (1984) analyzed the trace element variations of granites in modern subduction zones with respect to arc maturity in time and space and used multi-element spiderdiagrams (Rock, 1987) normalized to primitive mantle to interpret the tectonic associations of granite suites as four groups represented by different element assemblage features : (1) primitive calcic arc granite with low LIL (Large-Ion Lithophile) and HFS (High-Field Strengh) elements, (2) normal calc-alkaline continental arc granite with enhanced LIL elements and low HFSE/LILE ratios, (3) mature alkali-calcic arc granite with high LIL and HFS elements and HFSE/LILE ratios, and (4) back-arc/anorogenic alkaline granite with the highest HFS elements.

Thus it is clear that the element assemblage of granites can reflect different tectonic environments of granite genesis and these geochemical discrimination diagrams will be used as a reference for discussing different granite types in the Hetai Area. Earlier work has shown that the different granite types in South China such as the Nanling, the Yangtze and the Coast granites have been distinguished by geochemical features and mineral assemblages (Table 3.1 and Fig.3.1). These geochemical data are used as a reference for the Hetai granites, because the Hetai granites can be directly compared with these granites on the basis of a common geotectonic background.

For easy comparison with available results, a series of multi-element spiderdiagrams and REE distribution patterns of the Hetai granites were normalized to primitive mantle (Taylor, 1979; Taylor and McLennan, 1985) and to chondrite (Henderson, 1984), respectively. In addition, Rb/Sr, Sc, V, Nb and Ta will be used for distinguishing different granite types in the Hetai Area. An earlier study (Yang et al., 1988a) suggested that the geochemical behaviour of Nb and Ta may vary in different granites. For example, Nb decreases in the Nanling granite series (collision-type) but increases in the Yangtze granite

Table.3.1. Geochemical comparison between different granite types of South China *

Nanling Granite Type :

Na_2O >3.0 %, K_2O >3.5-4.0 %, SiO_2 68.0-74.0 %
Mol. $Al_2O_3/(K_2O+Na_2O+CaO)$ >1.05
Sr, Ni, V and Sc low, Rb, Sn, W and Ta high
REE and Nb high ---> low with granite series evolution
LREE/HREE ratios are low, $\partial Eu < 0.40$
Initial $^{87}Sr/^{86}Sr$ ratios > 0.710, $\partial^{18}O > 10$ ‰
Fe-biotite+ Fe-hornblende+ muscovite+ garnet
Sn, W, Ta, Nb and REE mineralization

Yangtze Granite Type :

Na_2O=3.0-4.0 %, K_2O=2.0-3.0 %, SiO_2 50.0-65.0 %
Mol. $Al_2O_3/(K_2O+Na_2O+CaO)$ near 1.0
Sr, Ni, V and Sc are high, Rb, Sn, Nb and Ta are low
REE contents are moderate, LREE/HREE ratios are high, ∂Eu >0.80
Initial $^{87}Sr/^{86}Sr$ ratios <0.710, $\partial^{18}O < 10$ ‰
Mg-biotite+ Mg-hornblende+ sphene+ epidote
Fe, Cu, Au and Mo mineralization

Coast Granite Type :

Na_2O 3.0-->4.5 %, K_2O 2.5-->5.0 %, SiO_2 50.0 --> 76.0 %
Mol. $Al_2O_3/(K_2O+Na_2O+CaO) < 1.0$
Sr, Ni, V and Sc high---> very low; but Rb, Sn and Nb very low ---> very high
REE moderate ---> very high, LREE/HREE ratios high ---> low, ∂Eu 1.1 --> 0.20
Initial $^{87}Sr/^{86}Sr$ ratios < 0.710, $\partial^{18}O < 8$ ‰
Mg-biotite+ Mg-hornblende (+ arfvedsonite)
Au, Nb and REE mineralization

---

* (from Yang, 1986)

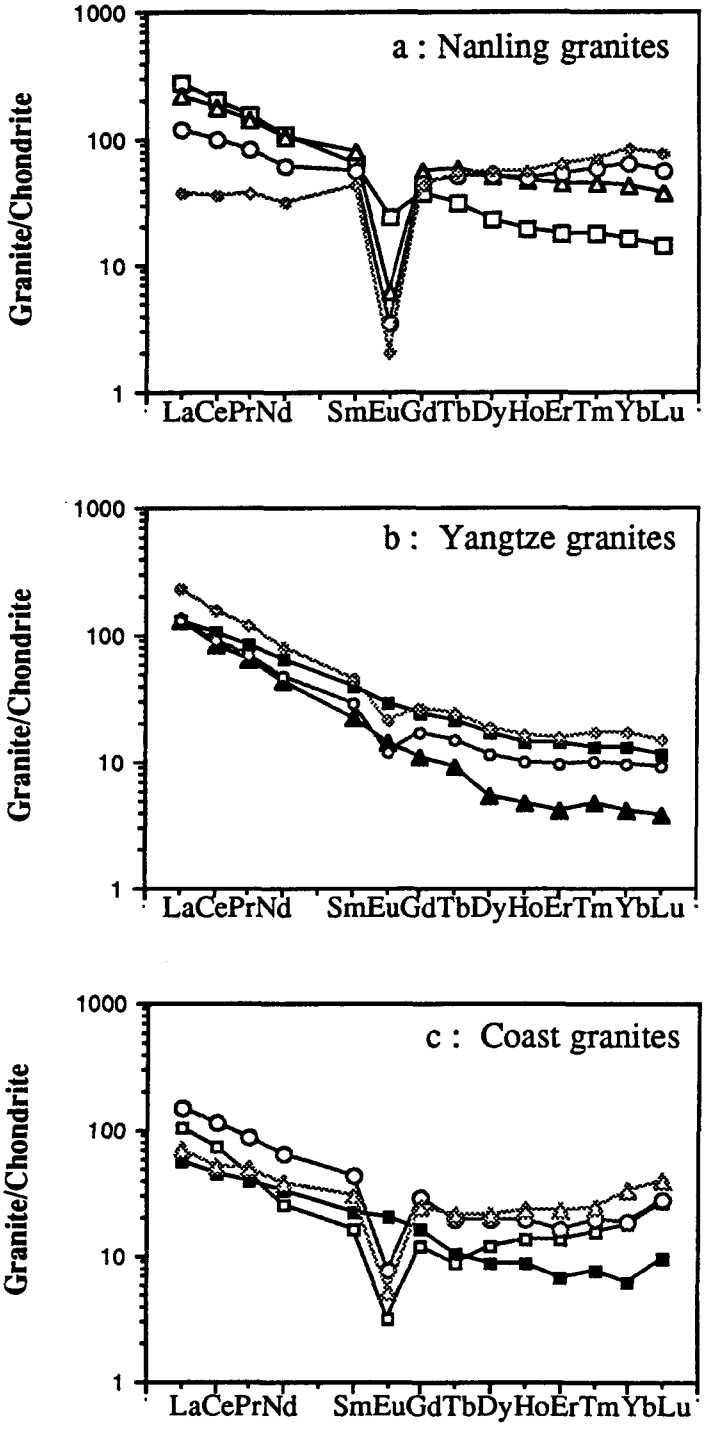

Fig. 3.1. Comparison between chondrite-normalized REE diagrams of different type granites of South China
(data from Yang, 1986)

series (subduction- and extension-types) with granite evolution (Yang et al., 1988a). This geochemical feature of Nb may characterize the different granitic evolution trends in specific tectonic environments. In addition to Rb/Sr, Nb and Ta, the Sc and V are chosen as important indicators for granite classification, because they do not usually form independent minerals during granite evolution. So, Sc and V may reflect the natural difference of source rocks and magma evolution of different granite types more sensitively. In this chapter, the geochemical features of the individual granites in the Hetai Area will be described in order of different ages from Caledonian and Hercynian (Older granites) to Indosinian and Yanshanian (Younger granites) and compared with other granites in South China. The average major oxide content of granites from South China (Institute of Geochemistry, Academia Sinica, 1979) may be used as a reference for discussing geochemical trends of the Hetai granites, although the average may not be a good standard value. As well, the individual bodies and polyphase intrusions will be classified in some selected geochemical illustrations such as (Nb+Ta) vs Rb/Sr, Sc and V, in order to distinguish their source rocks and discuss their magma evolution. Furthermore, the geochemical characteristics of the Hetai granites will be compared geochemically with the results from well studied world areas as well as from South China, in order to discuss tectonic associations of different granite types in the Hetai Area.

3-2. Geochemical characteristics of the Caledonian granites

The chemical compositions of the three analyzed Caledonian granitic bodies, the Shijiang, the Sidong and the Shiniutou (Fig.1.5), listed in Appendix III (Tables 1, 2 and 3), will be compared geochemically, in order to understand their geochemical characteristics and use them as petrogenetic indicators.

3-2-1. Shijiang granitic complex

(1) Geochemical features

The Shijiang complex consists of a series of polyphase intrusions previously discussed, including 'dark enclaves', homogeneous biotite granodiorite, heterogeneous

stromatic (schlieren) granodiorite, banded granite and augen granite based on field observation. They are located in the granodiorite, monzogranite and granite areas in the QAP ternary classification (Fig.3.2) based on CIPW calculation and principal mineral contents.

The bulk rock chemical compositions (Table 1) show regular variations among the different intrusive phases, SiO_2 increasing from 64.34-->73.63 % and K_2O 1.73-->6.05 , but inversely, TiO_2 decreasing from 1.00-->0.14, Fe_2O_3 1.02-->0.01, FeO 4.73-->1.17, MnO 0.09-->0.02, MgO 2.51-->0.24, CaO 4.27-->1.02 and Al_2O_3 16.47-->13.37. Na_2O and P_2O_5 vary irregularly, but the K_2O/P_2O_5 and K_2O/Na_2O ratios increase from 11-->106 and 0.44->2.62, respectively. Similarly, the CIPW parameters show increasing qz (quartz index, 22->35), ag (alkaline index, 0.47->0.81) and DI (differentiation index, 65->91) with the variation.

The Al-parameters, Mol. $Al_2O_3/(CaO+Na_2O+K_2O)$ (Mol. A/CNK), vary from 1.03-1.15. In particular, their Al-parameters decrease regularly from the dark enclaves through homogenerous biotite granodiorite to augen biotite granite (Table 1). This variation is related to decreasing Al_2O_3 and K_2O enrichment with the evolution of granite complex. In addition, the MgO/(MgO+FeO) ratios also decrease regularly from 0.39 to 0.17 with the evolution, but $Fe_2O_3/(Fe_2O_3+FeO)$ is commonly low (<0.20), indicating a lower fO_2.

It is clear from Table 2 that some trace elements display a regular variation, such as V decreasing from 115-->31 (ppm), Sc 14.8-->4.0 , Zr 158-->39 and Hf 6.6-->1.4, but U increasing from 0.8-->14 and Th 6.7-->27. Generally, Rb increases but Sr decreases through a complex development, although their variations are very limited.

Harker diagrams are used to demonstrate that the rocks of the complex stem from the evolution of a cognate magma. The Shijiang complex displays regular variations in Harker diagrams between SiO_2 and selected oxides and elements (Fig.3.3). For example, SiO_2 has a close positive relation with K_2O, Rb, Ba, Pb, U, Th, Y, Yb, Tb, Lu, K_2O/Na_2O, K_2O/P_2O_5 and Rb/Sr, but a negative relation with MgO, FeO, TiO_2, CaO, MnO, Al_2O_3, Na_2O, Zn, Sc, V, Ga, Nb, Zr, Hf, Sr, Eu, La/Sm and La/Yb from dark-colored enclaves, through homogeneous biotite granodiorite, to augen biotite granite. Such a regular geochemical variation implies that these different intrusion phases evolved from a common magma. Particularly, K_2O, U, Th and Pb show great enrichment but MgO, TiO2, V, Sc, Eu and Zn obvious depletions with SiO_2 increase, demonstrating the evolution trend

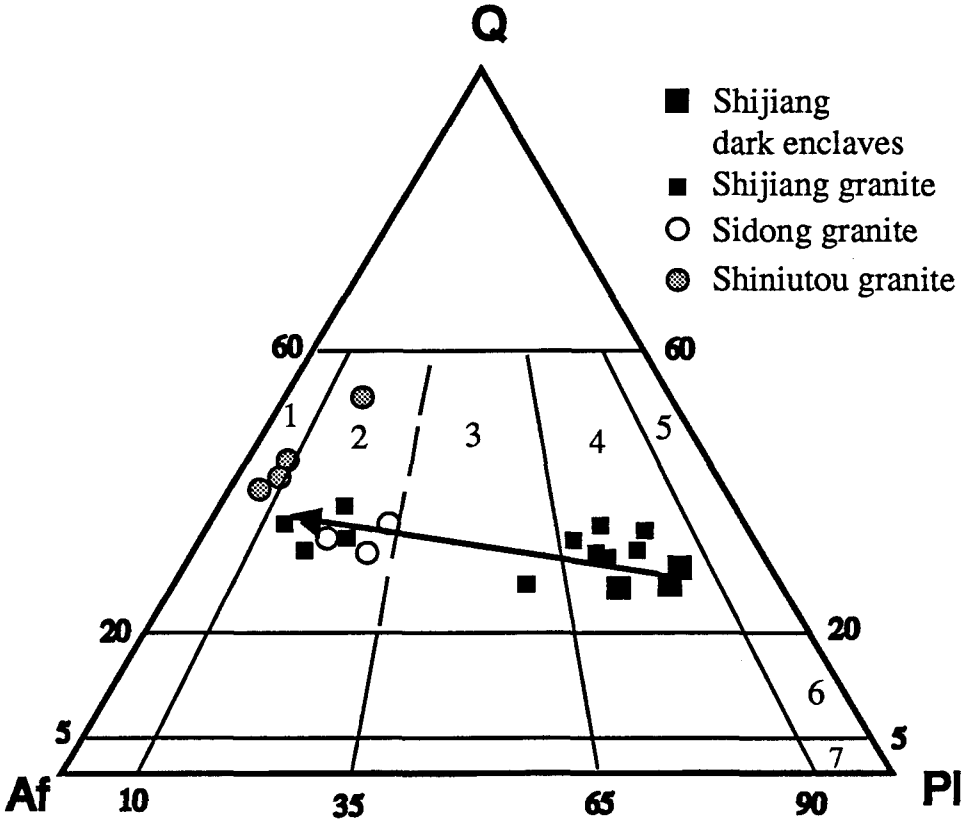

1.Alkali-feldspar granite; 2.Orthoclase granite; 3.Monzogranite
4.Granodiorite; 5.Tonalite; 6.Quartz diorite; 7. Diorite or Gabbro

Fig.3.2. The Caledonian granites on the Q-Af-Pl ternary classification by IUGS (1989)

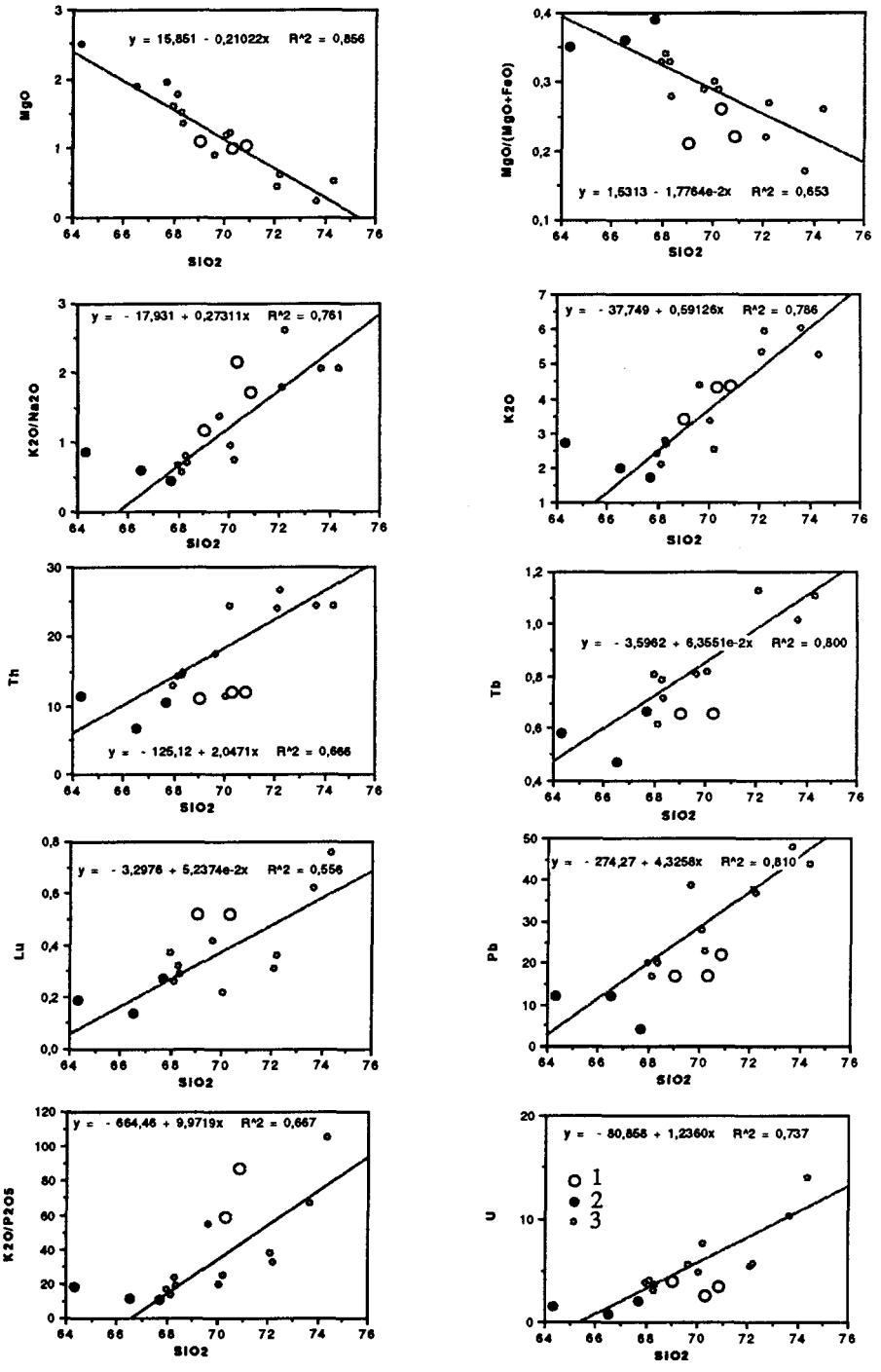

Fig. 3.3. The Harker diagrams of the Shijiang complex.

1: Precambrian sedimentary rock; 2 : Dark enclaves; 3 : Shijiang granites

Fig.3.3. continued

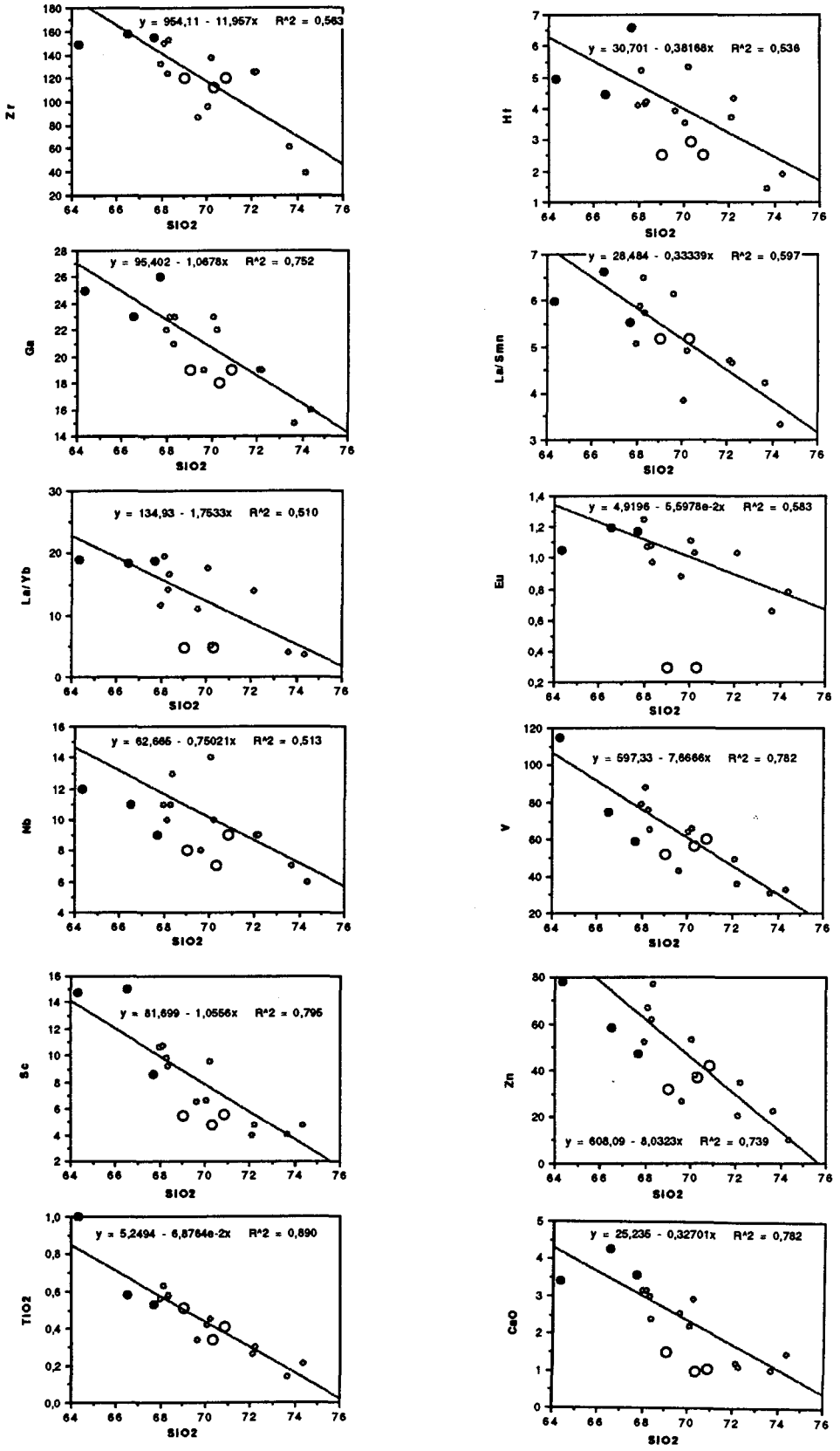

of the Shijiang complex. Solid-state deformation appears to have played a physical role on the solidified granitic rocks, but no obvious chemical modification resulted.

The multi-element spiderdiagrams of the Shijiang complex also display an evolution trend (Fig.3.4), and show the LILE-rich distribution, which is characterized by Rb, Th, U, K and Ta enrichments and Nb, Sr and Ti depletions. Such element distribution usually reflects the chemical features of crustal source rocks. The regular changes of increasing Ba and decreasing Ti further demonstrate the evolution trend of the granitic complex, although both elements are depleted.

REE in the Shijiang complex (Table 3) present relatively stable high contents. The ratios of La/Sm and La/Yb are high, implying relative enrichment of light REE, but regularly decrease from 19.0 --> 3.6 with increasing SiO_2 through the evolution of the granitic complex (Fig.3.3). The chondrite-normalized REE patterns display obvious inclined-right trends (Fig.3.5), and the negative Eu anomaly is weak but becomes stronger with SiO_2 increase and with the evolution of the complex (Figs.3.3 and 3.5). It is difficult to establish genetic relations directly with the chondrite-normalized REE patterns, because these patterns display transitional features compared to different granite types in South China (Fig.3.1). The major oxides and trace elements as well as petrographic features suggest that the Shijiang complex may be classified as S-type, but the source rocks may include igneous materials according to their REE features.

(2) Relations between dark enclaves and the Shijiang host granites

The enclaves in the Shijiang complex may possibly be unmelted source rock according to their petrographic characteristics, because they do not have magmatic appearance and differ greatly from other mafic enclaves in granites (Cantagrel et al., 1984; Chen et al. 1989 and 1990; Blundy and Sparks, 1992). If the enclaves are an original sedimentary rock, they may not have a certain chemical relation with the polyphase intrusives. If the enclaves are unmelted source rock, they not only appear to be in equilibrium with granitic rock, but also represent a specific geochemical relation with polyphase intrusions. This geochemical relation between them can be examined in the Harker diagrams (Fig.3.3). It is clear from the Harker diagrams (Fig.3.3) that the samples of dark enclaves generally plot at an end of the

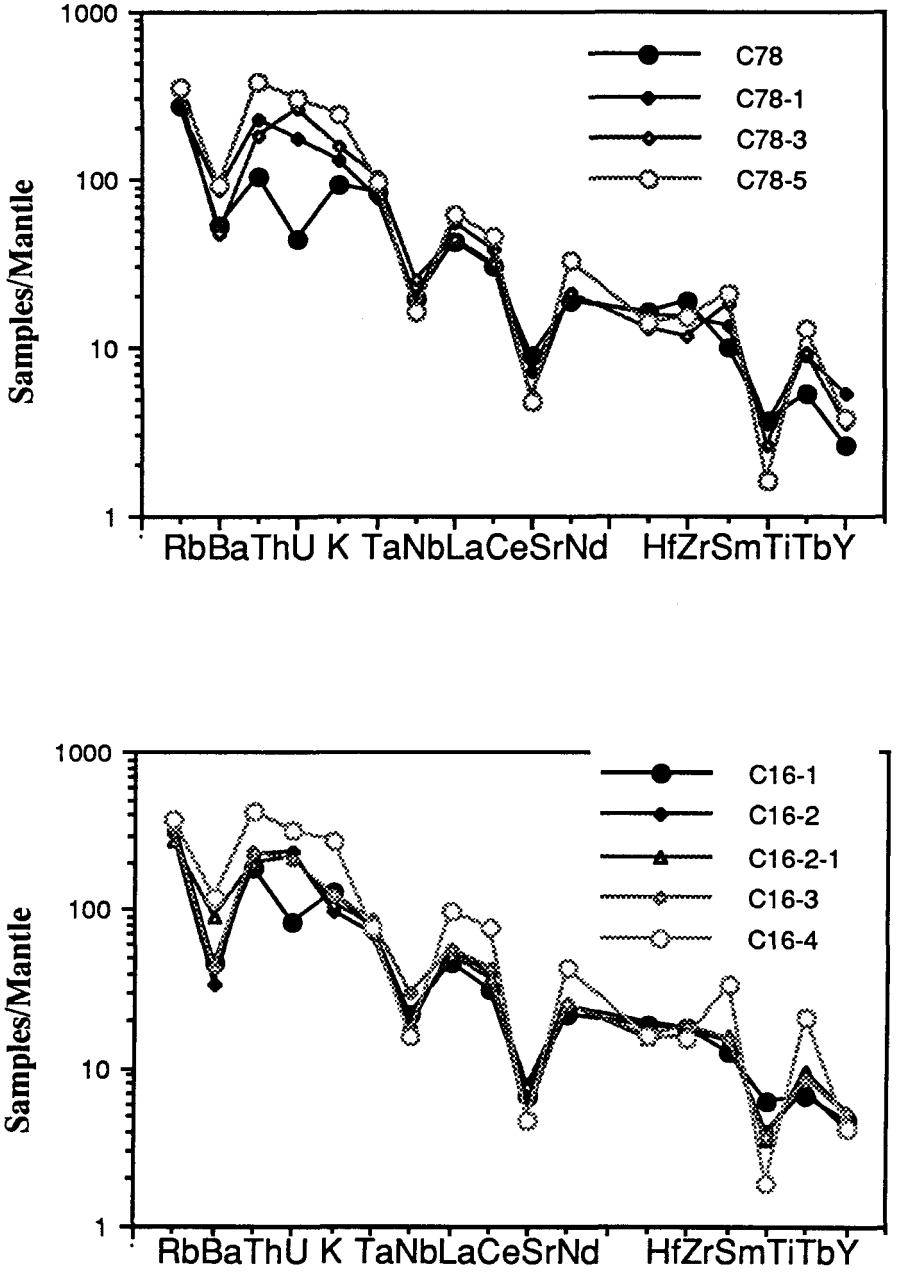

Fig. 3.4. Multi-element spiderdiagrams of the Shijiang complex

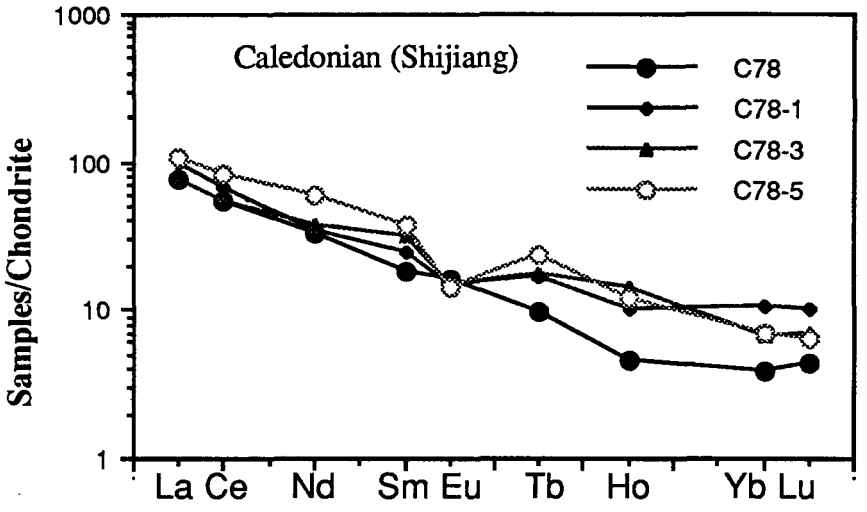

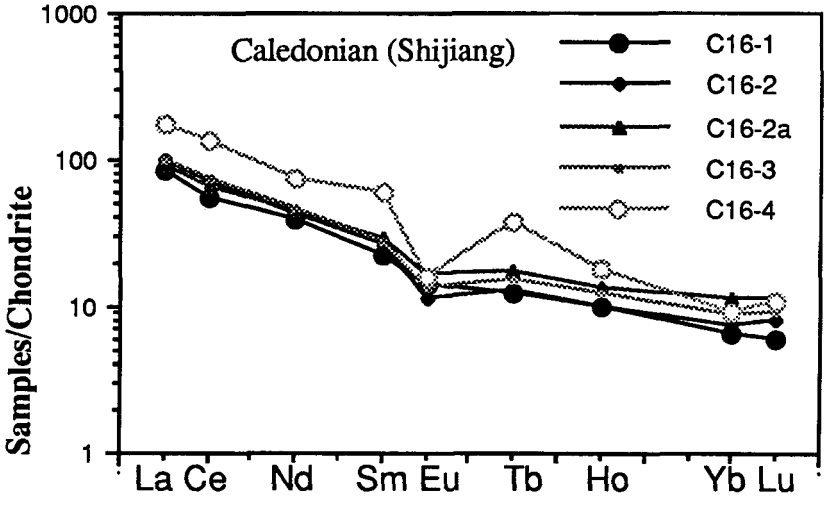

Fig. 3.5. Chondrite-normalized REE diagrams of the Shijiang complexes

chemical evolution line of the Shijiang complex, and are high in mafic oxides and related elements (such as Zn, V, Sc) but low in K_2O, K_2O/Na_2O, Pb and LIL element contents. It is possible that the dark enclaves may be an unmelted source rock of the Shijiang complex, but more chemical analyses of the dark enclaves and the Precambrian sedimentary rocks are needed for further proof of the exact geochemical relation between them.

The abundances of Rb and Sr in the Shijiang complex vary in a limited scale, from 133-209 ppm and from 69-160 ppm, respectively, with development of the complex, although both display a regular variation with increasing SiO_2 (Fig.3.3). Other differentiated elements such as Ba, V, Sc and Nb also vary in a limited scale through the granite complex (Fig.3.3). Such a limited variation of differentiated elements is different from the Nanling granite series which are developed by fractional crystallization such as the Guposhan and Xihuashan granites in South China (Chi, 1992; Xia et al., 1985). In general, Rb increases but Sr decreases in the Nanling granite series during fractional crystallization. The presence of this different tendency implies that the Shijiang complex magma may be produced by a partial melting process and has not been subjected to extensive fractional crystallization.

From these geochemical features, it is more reasonable to consider that the dark enclaves are possibly the unmelted source rock and are in equilibrium with granitic melts at the temperature and pressure of the anatectic environment, because refractory magnesium-ferrous components are enriched in unmelted phases during melting processes. Clearly, the chemical compositions of the 'dark enclaves' can be regarded as one end component in the Shijiang complex, and every intrusive phase may be derived from the same source rock.

(3). Petrogenetic model of the Shijiang complex

Trace element variations will be examined in order to establish the processes of granite generation for the Shijiang complex. The two-element variation diagram method proposed by Hanson (1978) is used to distinguish the processes of fractional crystallization or partial melting. Two trace elements with contrasting values of D (bulk distribution coefficient between the solid phases and the melts) must be used in this method, because separation between these two elements reflects the variation tendency during the

granite generation processes more sensitively. Rb vs Sr is usually used as an indicator in this method. The geochemical features of Rb and Sr in their correlation diagram (Fig.3.6) demonstrate that Rb contents increase with Sr decrease during the evolution, and they have a good negative corelation (R=0.760). In addition, Rb and Sr have evident Kd values (element distribution coefficient between the minerals and the melt) for most rock-forming minerals in normal granitic rocks, biotite (Rb : 3.26, Sr : 0.12), plagioclase (0.048, 2.84), K-feldspar (0.659, 3.87) and garnet (0.0085, 0.015) according to the data of Hanson (1978). Clearly, for all these minerals except biotite, Sr has much higher Kd than Rb. In fact, the exact proportion of these minerals involved in the processes of granite generation is difficult to determine, but they can be roughly estimated by the content of these minerals in the related intrusive phases. Based on the statistics of thin section and CIPW calculation, the proportion of main minerals in the 'dark enclaves' may be estimated as follows : plagioclase : K-feldspar : quartz : biotite : garnet = 50 : 10 : 10 : 24 : 1. Taking this proportion and the Kd values of Hanson (1978), the D values (bulk distribution coefficient) of Rb and Sr may be calculated, about 0.571 and 2.612, respectively. According to Hanson (1978), for a fractional crystallization model, it is

$$\lg C(l) - \lg C(o) = F \lg(D-1) ;$$

and for partial melting model, it is

$$\lg C(l) - \lg C(o) = -\lg[D(1-F)+F] ;$$

where, C(l) is the content of an element in the melt; C(0) is the content of an element in the original parent; F is the weight fraction of melt relative to original parent; D is the bulk distribution coefficient.

According to the correlation of Rb and Sr in Fig.3.6, it may be calculated that, with 1% fractional crystallization or 99% partial melting, the magma contains contents about 150 ppm Rb and about 160 ppm Sr, which may represent contents near the original parent rock. Then the two curves can be plotted for the two different processes of fractional crystallization and partial melting respectively (Fig.3.6). These two curves display different tendencies. Curve 3, representing the fractional crystallization model, indicates that when Rb increases to a maximum (about 210 ppm), Sr sharply decreases to 35 ppm, which differs from the actual data (curve 1). It is evident from Fig.3.6 that the fractional crystallization

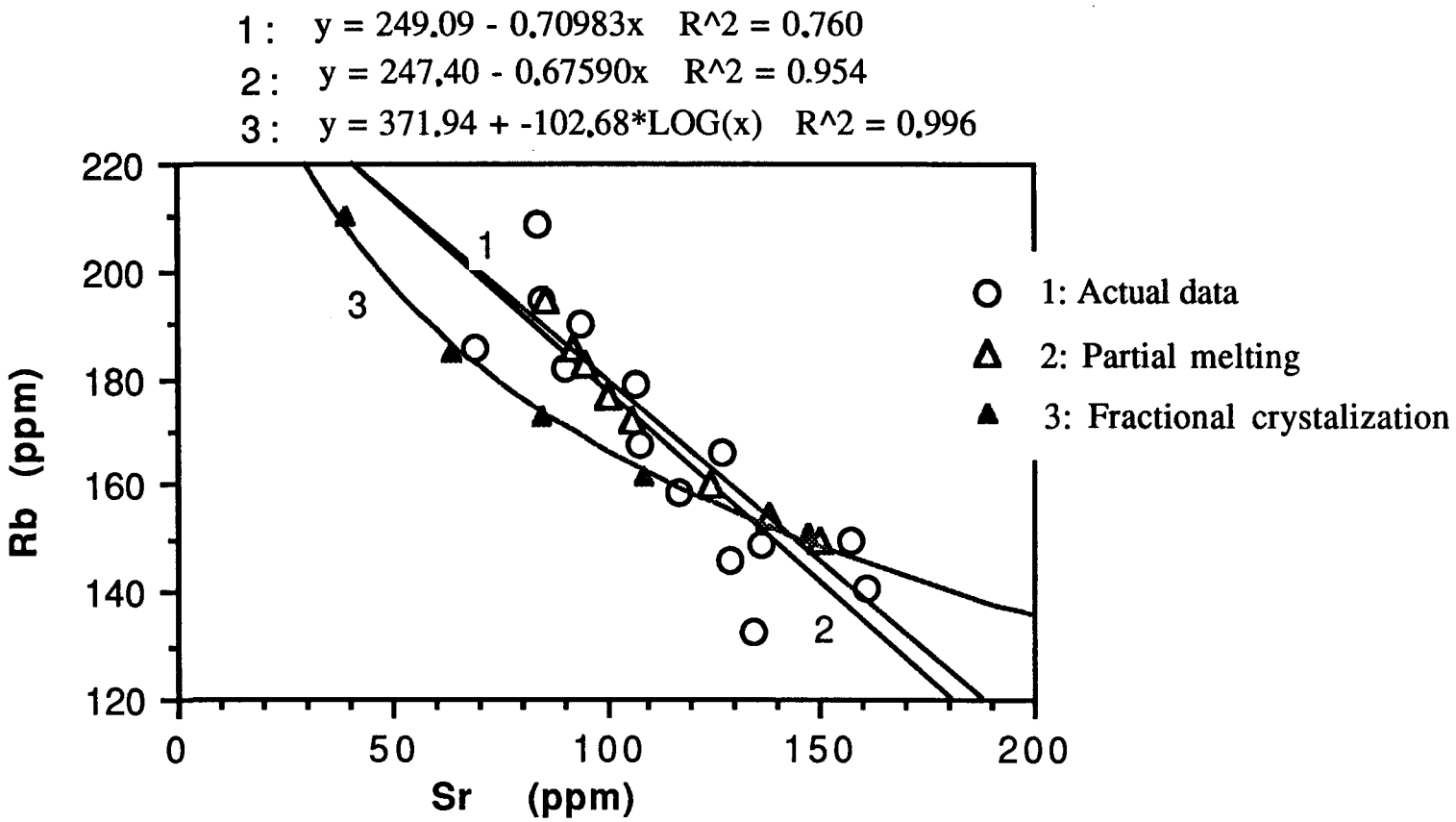

Fig.3.6. Petrogenetic process model of the Shijiang granite complex

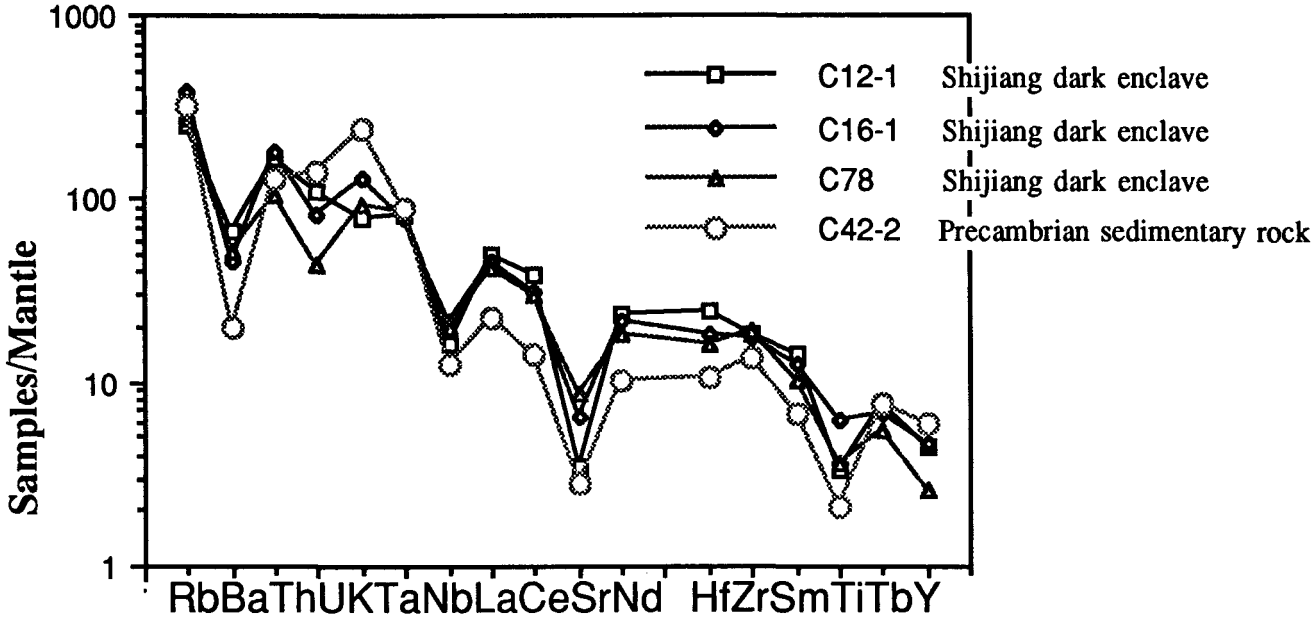

Fig.3.7. Comparison between spiderdiagrams of the Precambrian sedimentary rocks and the Shijiang dark enclaves

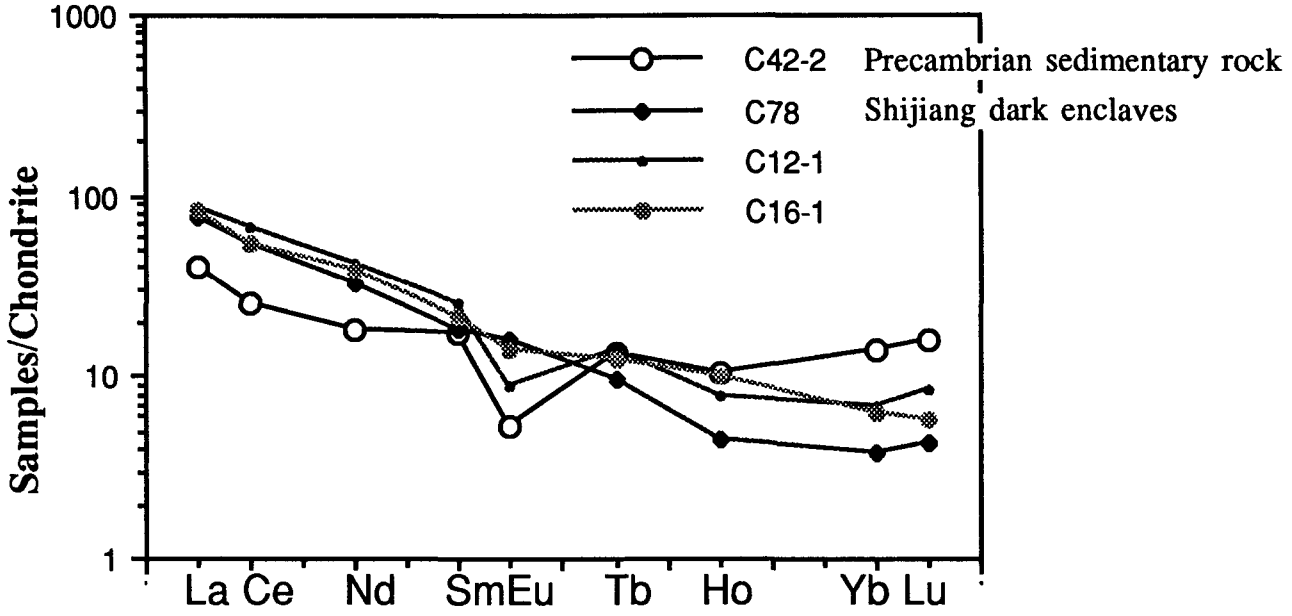

Fig.3.8. Comparison between chondrite-normalized REE diagrams of the Shijiang dark enclaves and Precambrian sedimentary rocks

model does not fit the actual curve (1) of the Shijiang complex. In contrast, Curve 2, representing the partial melting model, fits the data much better than fractional crystallization, and is consistent with the actual curve (1) in Fig.3.6. The partial melting process seems able to produce the largest Rb content (210 ppm) at the lowest Sr content (75 ppm), and Sr is decreased gently with increasing Rb during the process of partial melting. This appears favourable to the data from the Shijiang complex in Fig.3.6. The partial melting process may be the principal petrogenetic mechanism for the evolution of the Shijiang complex.

Comparing dark enclaves with the composition of Precambrian metamorphosed sedimentary rocks (Tables 1, 2 and 3; Figs. 3.7 and 3.8) shows geochemical similarities and evolutional relations between them, so the Precambrian metamorphosed sedimentary rocks may be assumed to be possible source rocks for the Shijiang complex. For this, it is estimated that the melt fraction (F) relative to parent rock is about 0.3, that is, the geochemical composition of melts produces such granitic rocks when about 30 % of the source rocks melt. The melting events of the Precambrian metamorphosed sedimentary rocks probably occurred during the processes of continent-continent collision. In continent collision, the Precambrian metamorphosed sedimentary rocks in a lower plate may be melted at depth greater than 20 km (He,1987; Sevigny et al., 1989; Condie, 1989), because of temperature increase.

3-2-2. Sidong granites

The samples from the Sidong body include two intrusive phases, medium-grained biotite granite and fine-grained biotite granite. The Sidong granites (Table 1) contain higher SiO_2 (> 73 %), Na_2O (> 3.22) and K_2O (3.88-4.92) and lower P_2O_5 (0.03), Al_2O_3 (12.72-13.59), TiO_2 (0.13-0.14) and MgO (< 0.1) compared with the major oxide averages of granites of South China (Institute of Geochemistry, Academia Sinica, 1979). In addition, the chemical compositions display regular variation between the two phases of the intrusion, SiO_2 (73.55->76.66), K_2O (3.88->4.92) increasing but FeO (1.67->0.68), MgO (0.5-regular >0.01) and CaO (2.00->0.87) decreasing from medium-grained granite to fine-grained granite. This variation may indicate that the Sidong polyphase intrusion is characterized by a normal differentiation evolution.

The CIPW calculations for both phases present high qz (33-36), ag (0.71-0.88) and DI (85-95) parameter, and in QAP ternary classification, they plot in the normal granite area (Fig.3.2). Their Al-parameters (Mol.A/CNK) are 1.0-1.05. The MgO/(MgO+FeO) and Fe_2O_3/(Fe_2O_3+FeO) ratios are relatively low, about 0.01-0.04 and 0.12-0.28 respectively, reflecting the lower mafic components.

The Sidong granites (Table 2) contain low Ni (11-14 ppm), Cr (10-15), V (10-16), Sc (1.2-3.4), Zn (10 -12), Ga (12-15) and Sr (22-27), but high Ba (864-919), Hf (6.0-6.2), Ba/Sr (31-57) and Rb/Sr (4.6-6.6). Such trace element assemblage is characteristic of the chemical composition of upper crustal source rocks (Shaw et al. 1986; Wang et al. 1984c) or sedimentary source rocks (Chappell and White, 1974). The very high Ba and Ba/Sr in granite particularly reflect the features of sedimentary source rocks, and indicate that the Sidong granites may be crystallized from an evolved magma because Ba is a strongly imcompatible element (D<<1) in magma crystallization (Liu et al., 1984).

The multi-element spiderdiagrams normalized to primary mantle of the Sidong granite characterize the LILE-rich type (Fig.3.9), Rb, Ba, Th, U, K and Hf contributing to the high positive distribution, whereas Nb, Sr and Ti display strong depletion. Enrichment of Rb, Ba, Th, U, K and Hf in granite usually demonstrates a richer lithophile-element source rock, or higher maturity of crustal and magma evolution. Similarly, the strong depletions of Ti and Sr may be due both to low chemical background contents of source rocks and magma evolution, because these two elements are strongly compatible (D>>1). However, strong Nb depletion may be caused by magma differentiation, because Nb decreases with magma crystallization in the Nanling Series granite (S-type) as Nb formed independent minerals such as samarskite in the early stage, compared with the granites in South China (Wang et al. 1984c; Yang et al. 1988a).

REE contents in Table 3 are generally low and the ratios of La/Sm are relatively high (6.2-7.2) but La/Yb low (4.7-5.8), as a consequence of HREE enrichment. The chondrite-normalized (Henderson, 1984) REE patterns display a nearly symmetrical V-model and a negative Eu anomaly (Fig.3.10). These REE features suggest that the Sidong granite is similar to the Nanling granites and may be the result of differentiated magmas derived from the crustal source rocks (see Fig.3.1).

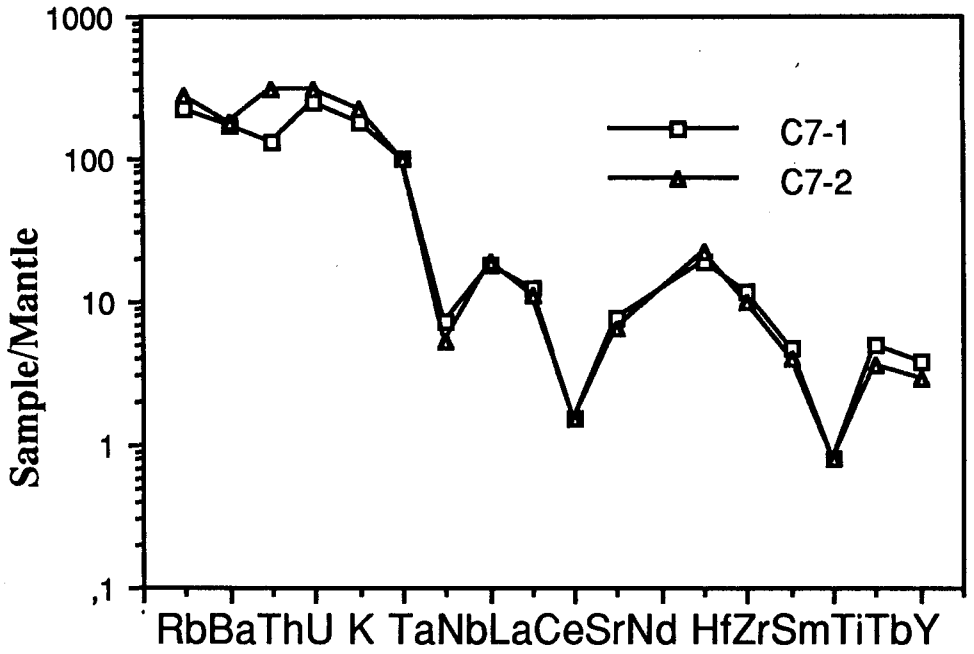

Fig. 3.9. Multi-element spiderdiagrams of the Sidong granites

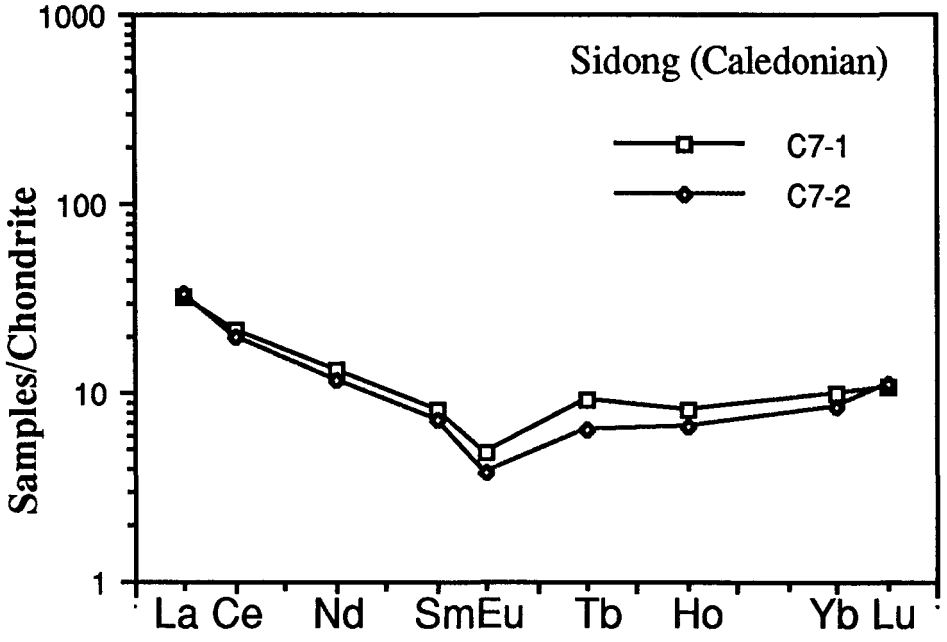

Fig. 3.10. Chondrite-normalized diagrams of the Sidong granites

3-2-3. Shiniutou granite

The Shiniutou complex is dominantly composed of biotite alkali-feldspar granites and four samples were analyzed (Table 1). The Shiniutou granites contain high SiO_2 (72.65-76.25) and K_2O (4.20-5.18), but low Na_2O (2.39-2.82). Other major oxides such as TiO_2 (0.05-0.26), Fe_2O_3 (1.02-2.24), FeO (0.66-1.52), MgO (0.01-0.89) and CaO (0.58-1.39) are low but display a relatively wide variation. Anomalously high P_2O_5 contents (0.13-0.15) result in relatively low ratios of K_2O/P_2O_5 (28-33), but K_2O/Na_2O ratios (1.56-5.43) are high.

The granites have high parameters of qz (39-49), ag (0.43-0.79) and DI (82-94), and plot in the alkali-feldspar granite area in the QAP ternary classification (Fig.3.2). The Al-parameters (A/CNK) are greater than 1.1. The ratios of MgO/(MgO+FeO) and Fe_2O_3/(Fe_2O_3+FeO) vary widely, 0.01-0.37 and 0.14-0.62 respectively, reflecting unstable evolution or possibly late alteration.

Similarly, trace element contents of the Shiniutou granite (Table 2) vary widely and generally show high Rb (241-369 ppm), U (5-51), Th (10-20) and Y (24-40), but low Cr (10), Ni (20-41), V (15-34), Sc (3-5), Zn (10-17), Ba (70-292) and Sr (18-53). Some HFS elements such as Nb (6-11), Ta (3-4), Zr (41-110) and Hf (3-5) have relative low contents. Such a trace element assemblage is similar to an upper crustal composition (Shaw et al, 1986; Wang et al., 1984c) and implies that the Shiniutou granites may be derived from crustal source rocks. The lower Ba abundance may be due to late fluid alteration during deformation and conversion of feldspar and biotite into sericite.

The multi-element spider-diagrams of the Shiniutou granite show it to be of the LILE-rich type (Fig.3.11). The evident enrichment of Rb, Th, U and K but obvious depletion of Sr and Ti may be related to a more evolved magma derived from upper crustal source rocks with high maturity. Particularly, Ta enrichment represents a geochemical trend of normal granite in a more differentiated stage. The separation of Ta and Nb is present in the Nanling Series granites (S-type) in South China (Yang et al., 1988a). The Nb depletion is shown in the spiderdiagrams.

REE contents in the Shiniutou complex (Table 3) are generally low. The La/Sm and La/Yb ratios are low, 1.41-4.70 and 2.79-6.83 respectively, presenting the granite

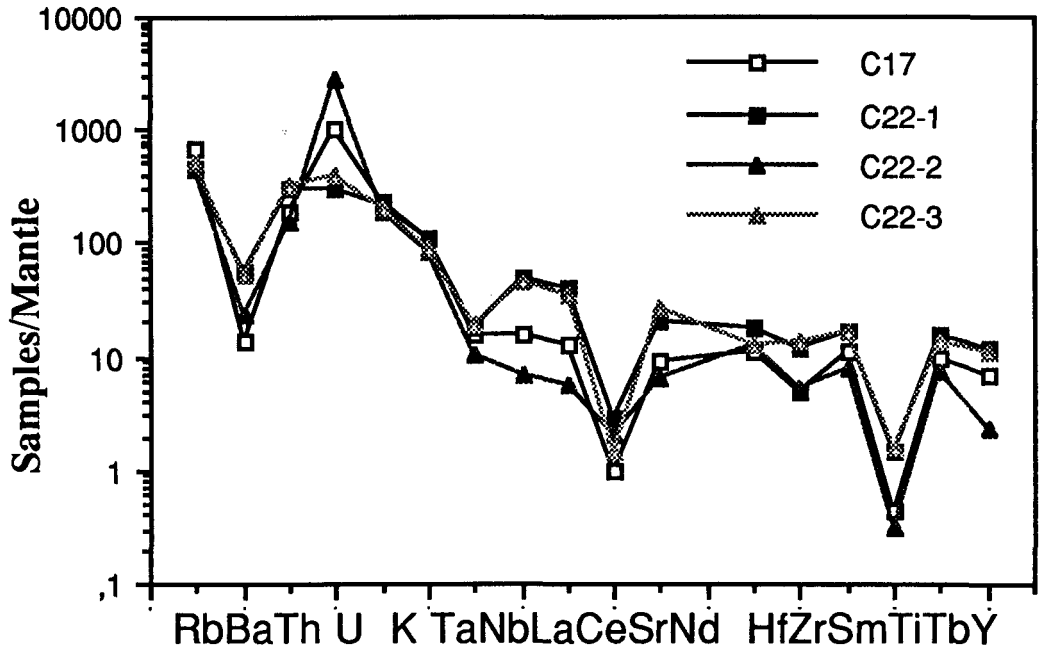

Fig. 3.11. Multi-element spiderdiagrams of the Shiniutou granites

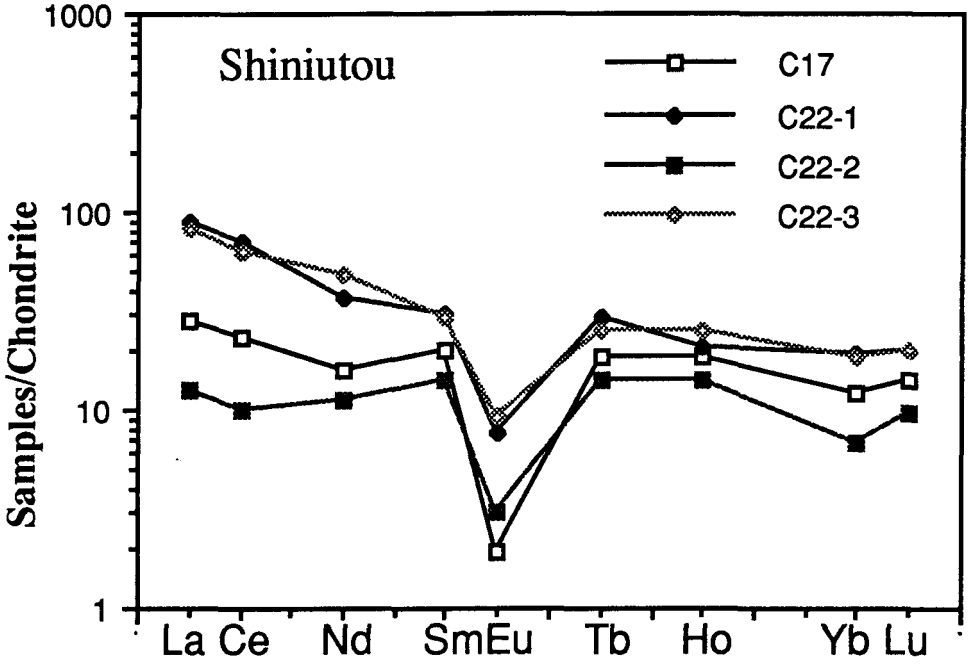

Fig. 3.12. Chondrite-normalized REE diagrams of the Shiniutou granite

as a HREE-rich type. The chondrite-normalized REE distribution patterns (Fig.3.12) display a very strong negative Eu anomaly, giving a near-symmetrical V-shaped model. These REE distribution patterns are similar to those of the Nanling granites in South China, and it may also demonstrate that the Shiniutou granites resulted from a highly evolved magma derived from crustal source rocks.

3-2-4. Geochemical comparison among the Caledonian granites

Plotting all the Caledonian samples in the Mol. $Al_2O_3/(Na_2O+K_2O)$-$Al_2O_3/(CaO+Na_2O+K_2O)$ (A/NK-A/CNK) diagram (Fig.3.13) shows that the Shijiang granitic rocks are located in the metaluminous to peraluminous saturation areas, coincident with the CCG (Continental collision granite) and CAG (continental arc granite) areas (Maniar and Piccoli, 1989); the Sidong granitic rocks in the metaluminous saturation area, coincident with the CEUG (continental epeirogenic uplift granite) (Maniar and Picolli, 1989). All samples are plotted in peraluminous area, coincident with the CCG (continental collision granite) area (Maniar and Piccoli, 1989). Although these granitic rocks display peraluminous features, the difference is still reflected in their degree of aluminum saturation. The Al-parameter (A/CNK) value of the Sidong granite is 0.99-1.02 and that of the Shiniutou granite is 1.13-1.61, but both are coincident with CCG and CEUG areas (Maniar and Piccoli, 1989). However, the Shijiang samples have Al-parameter values from 1.03-1.17 and plot in the CCG and CAG areas (Maniar and Piccoli, 1989), evolving from the peraluminous area to near metaluminous area with development of the complex (Fig.3.13). Thus, the source rocks of Shijiang granitic complex may be produced by a different mechanism from the others, because it is generally considered that aluminous variations tend to become peraluminous (muscovite occurring in the later stage) in the calc-alkali series with fractional crystallization of magma (Pitcher, 1987). The decreasing aluminum trend with evolution in the Shijiang complex differs from the calc-alkali series evolution and may imply that partial melting processes may be the petrogenetic mechanism for development of the Shijiang complex.

All three Caledonian bodies have a common feature of LIL element enrichment and are relatively rich in K, Rb, U, Th and Ta, but depleted in Nb, Ti and Sr compared in the spider-diagrams (Fig.3.14). In addition, they are similar to Precambrian metamorphosed sedimentary rock (Fig.3.14). These common features of element distribution indicate that

their source rocks had a common chemical background probably in the crust. However, some chemical disparities exist between the three granitic bodies. For example, high K_2O is a common feature in both the Sidong and the Shiniutou granites in contrast with the more evolved rocks of the series in the Shijiang complex. Barium (Ba), which increases gradually in the Shijiang complex, is particularly enriched in the Sidong body but depleted in the Shiniutou body. The different trace element distribution between three bodies may be the result of chemically non-uniform source rocks, or different petrogenetic processes. The Shijiang complex is produced mainly by partial melting, whereas the Sidong and the Shiniutou granites may be the result of fractional crystallization, because contrasting elements like Rb and Sr display an evident separation in these granites.

Similarly, the chondrite-normalized REE patterns of the earlier phases of the Shijiang complex (Fig.3.15) are evidently richer in LREE and differ from those of the Sidong and Shiniutou, which have typical REE pattern of the Nanling granites. For this, the Shijiang granites are difficult to explain as S-type granites. In spite of the difference of petrogenetic mechanism, another factor may be that igneous rocks contribute partly to the aluminous crustal source rocks of the Shijiang granites, so their REE patterns show some features of I-type granites. However, the later phase of the Shijiang complex is similar in REE distribution pattern to the Sidong and Shiniutou granites and to the Precambrian metamorphosed sedimentary rock (Fig.3.15).

3-3. Hercynian granites

The Hercynian granites include the Guangning and the Yunlougan plutons, both located in the Guangning-Luodin Fault Zone (Fig.1.5). The samples collected from the Guangning body are medium-grained biotite monzogranite, but the samples collected from the Yunlougan body are granodiorite. In addition, a later pegmatite occurring as a dyke cross cutting the granodiorite was also analyzed for contrast. The chemical compositions of the Hercynian granites are listed in Appendix III (Tables 4, 5 and 6) for direct comparison.

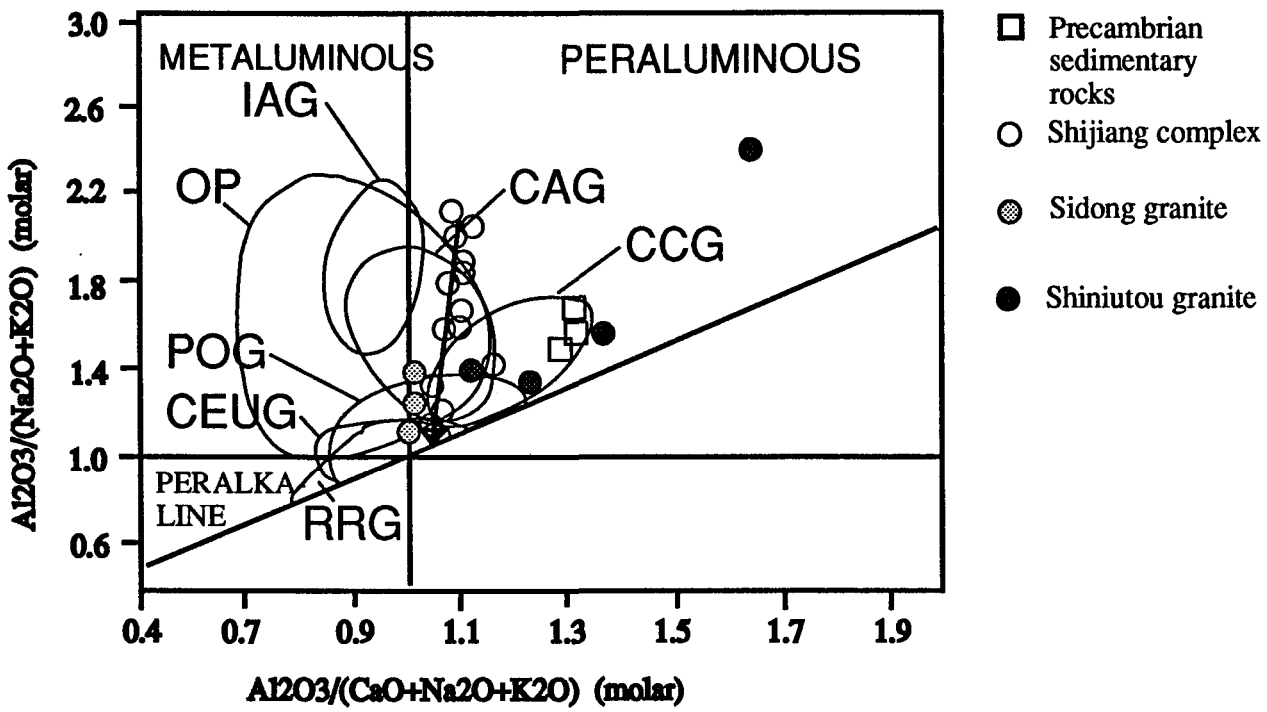

IAG=island arc granite, CAG=continental arc granite,
CCG=continental collision granite, POG=post-orogenic granite
RRG=rift-related granite, CEUG=continental epeirogenic uplift
granite, OP=oceanic plagiogranite (after Maniar and Piccoli, 1989)

Fig. 3.13. Mol. Al2O3/(CaO+Na2O+K2O)-Al2O3/(Na2O+K2O) (A/CNK-A/NK) diagram of the Caledonian granites

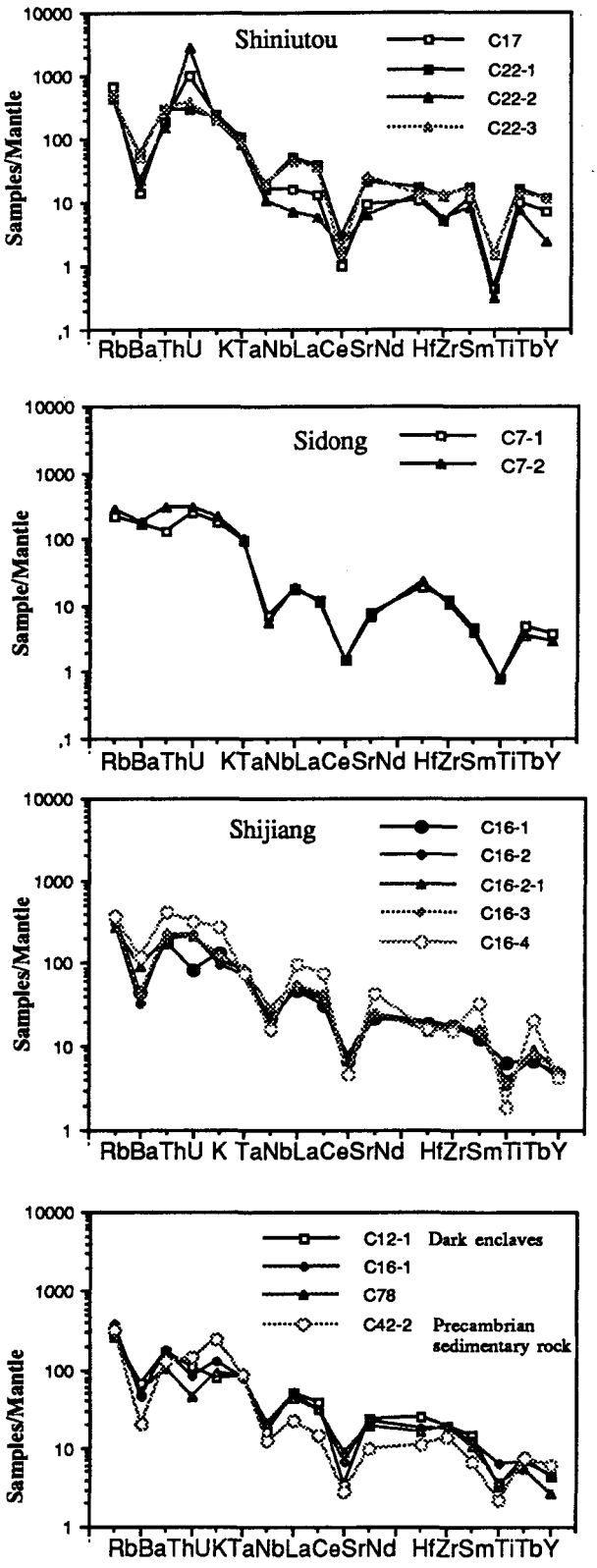

Fig. 3.14. Comparison between spiderdiagrams of the Caledonian granites

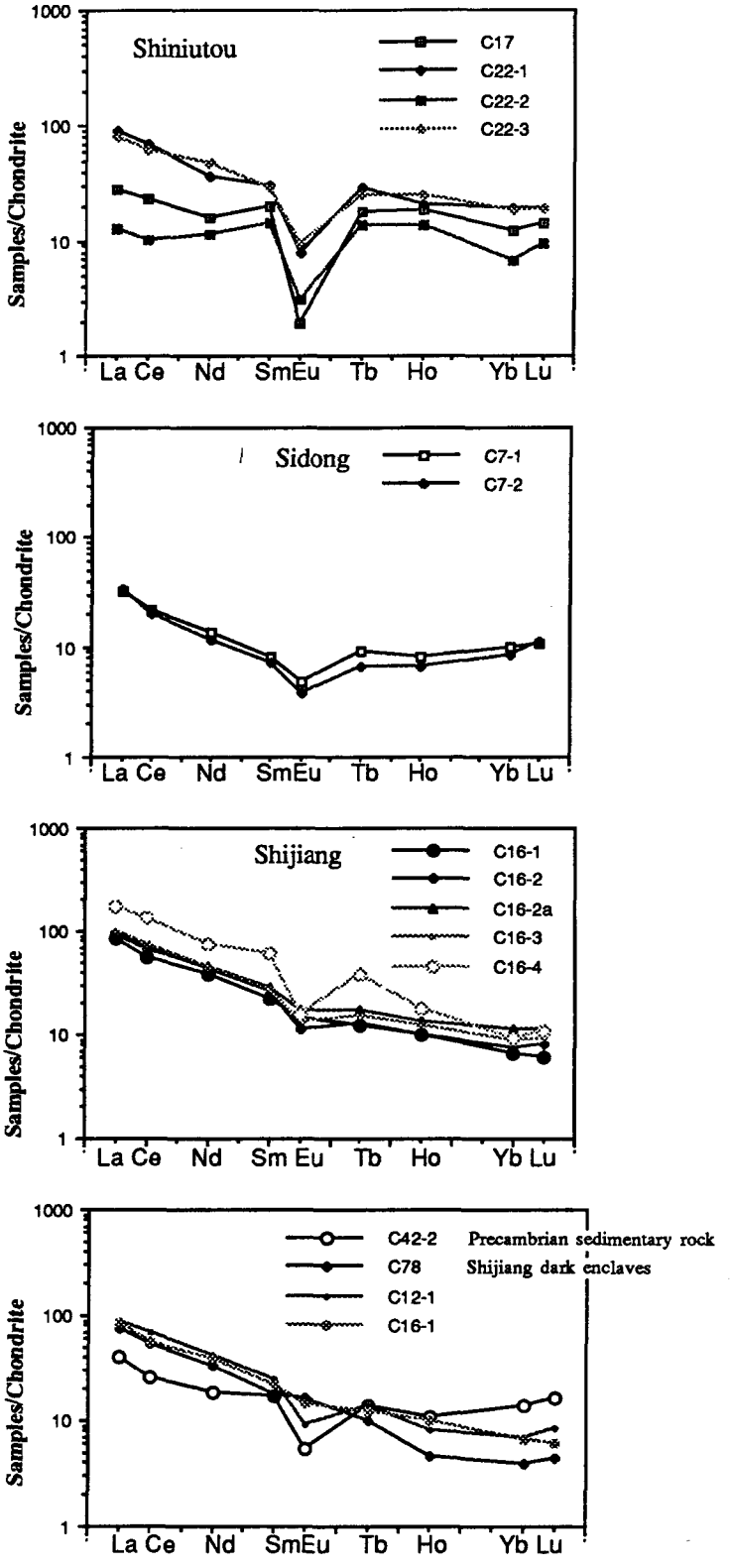

Fig.3.15. Comparison between chondrite-normalized REE diagrams of the Caledonian granites

3-3-1. Guangning granite

The Guangning pluton presents a relatively homogeneous chemical composition (Table 4), and it has slightly lower SiO_2 (69.13-71.74 %) and K_2O (3.64-4.23) contents than the average granite in South China. Na_2O contents are moderate, but MgO (0.66-1.00), FeO (1.80-2.22), TiO_2 (0.31-0.41), P_2O_5 (0.14-0.15), CaO (1.69-2.54) and Al_2O_3 (14.72-15.88) are relatively higher. The ratios of K_2O/Na_2O and K_2O/P_2O_5 are lower, 1.09-1.26 and 16.2-28.2 respectively.

The CIPW parameter shows moderate qz (29-31), ag (0.58-0.69) and DI (78-85), and the samples are located in the monzogranite area in the QAP ternary classification (Fig.3.16). The Al-parameters (A/CNK) are >1.05. The $Fe_2O_3/(Fe_2O_3+FeO)$ ratios are relative low, from 0.15-->0.21, reflecting lower fO_2, but MgO/(MgO+FeO) is slightly higher, 0.27-0.31, representing a slight enrichment of mafic components.

Trace elements in the Guangning pluton (Table 5) are characterized by high Rb (186-225 ppm), U (7-15) and Th (15-17), and moderate Sc (5.9-7.7), V (33-57), Ga (20-21), Zn (38-65), Ba (303-437), Zr (88-107), Nb (10-12) and Ta (3.4-4.9), but relatively low Sr (72-83), Ni (13-31) and Cr (12-43). The primary mantle-normalized curves in the spiderdiagram (Fig.3.17a) display strong positive anomalies for Rb, Th, U and Ta, but evident depletion of Sr and Ti. Nb and Ba depletions are weak and their normalized values are higher than 10. Such element assemblages and spiderdiagram model a LILE-rich type, and represent an early stage product of granite evolution when compared with the Nanling granite series, because of higher Nb and Ba content. These trace elements reflect the geochemical features of aluminous crustal source rocks.

The content of REE (Table 6) is moderate, but La/Sm and La/Yb ratios are high, 4.71-5.25 and 10.10-13.65 respectively, presenting a slight enrichment of light REE. The chondrite-normalized patterns (Fig.3.18a) display a slightly inclined-right curve, but the Eu negative anomaly is strong, reflecting possible fractional crystallization of plagioclase in magma evolution. Similarly, the REE distribution also indicates that the Guangning monzogranite represents an early stage of granite evolution when compared with the Nanling granite series in South China (Fig.3.1), and it implies that the source magma of the Guangning granite may be partly contaminated by deeper source materials because of slight

LREE enrichment. In addition, allanite and epidote occurring as primary accessory minerals in the Guangning granite may be the result of the mixed magma crystallization, because they are not usually produced in a pure S-type source environment. Allanite and epidote usually concentrate light REE, so that the Guangning granite presents relatively high light REE values.

3-3-2. Yunlougan pluton

The samples of the Yunlougan pluton are located in the granodiorite area in the QAP ternary classification (Fig.3.16), whereas the analyzed sample of pegmatite is in the alkali-feldspar granite area (Fig.3.16).

(1) Geochemical features of the granodiorite

The granodiorite has relatively low SiO_2 (65.26-67.31 %) and K_2O (2.27-2.39) contents (Table 4), but high MgO (1.7-1.9), FeO (4.03-4.36), TiO_2 (0.53-0.68), P_2O_5 (0.16), CaO (3.00-4.30), Al_2O_3 (15.36-16.75) and Na_2O (3.08-3.16) contents. The ratios of K_2O/Na_2O and K_2O/P_2O_5 are low, 0.74-0.76 and 14.2-14.9 respectively. The ratio of $Fe_2O_3/(Fe_2O_3+FeO)$ is moderate, about 0.12, but the MgO/(MgO+FeO) is high, 0.28-0.32. The CIPW parameters of the granodiorite have low qz (25-28), ag (0.46-0.50) and DI (65-69). The Al-parameter (A/CNK) is about 1.05.

Trace elements in granodiorite (Table 5) show high V (93-96 ppm), Sc (12-14), Cu (52-56), Zn (54-85), Ba (403-745), Sr (161-172), Zr (188-192), Hf (5.0-6.0) and Y (29-31), but low Rb (112), Pb (14-16) and U (3-5). The distribution curves in the spiderdiagrams (Fig.3.17b) show a positive Th anomaly, whereas LIL elements such Rb, U and K present no evident enrichment. Nb, Sr and Ti are depleted, but their normalized values at 10 are relatively high. Such an element distribution suggests that the granitic magma is derived from an igneous source.

The REE content is higher (Table 6), and the high La/Sm and La/Yb ratios, 7.3 and 15.7 respectively, presenting an enrichment of light REE. The chondrite-normalized REE patterns display a slightly inclined-right model and Eu shows a weaker negative anomaly (Fig.3.18b). This REE distribution in the Yunlougan granodiorite is similar to the Yangtze

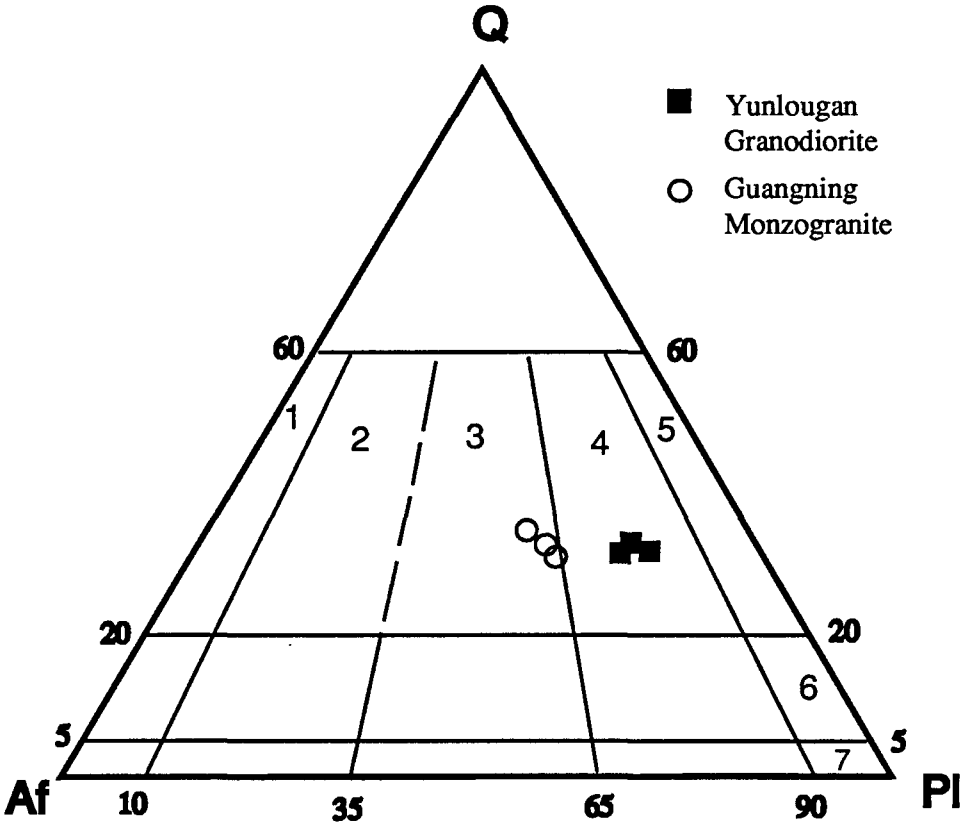

1.Alkali-feldspar granite; 2.Orthoclase granite; 3.Monzogranite
4.Granodiorite; 5.Tonalite; 6.Quartz diorite; 7.Diorite or Gabbro

Fig. 3.16. The Hercynian granites on the Q-Af-Pl ternary classification by IUGS (1989)

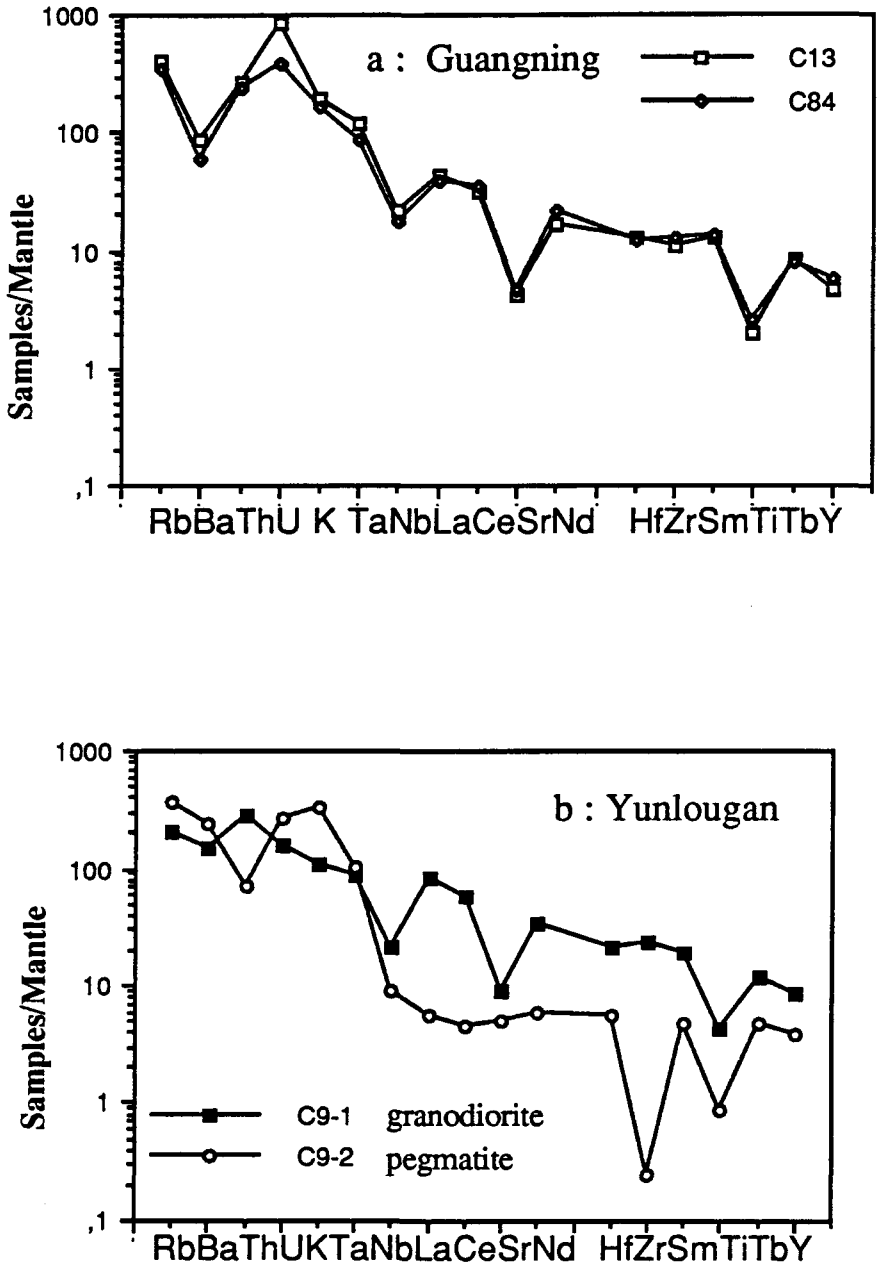

Fig. 3.17. Comparison between spiderdiagrams of the different Hercynian plutons.
a : Guangning pluton; b : Yunlougan pluton

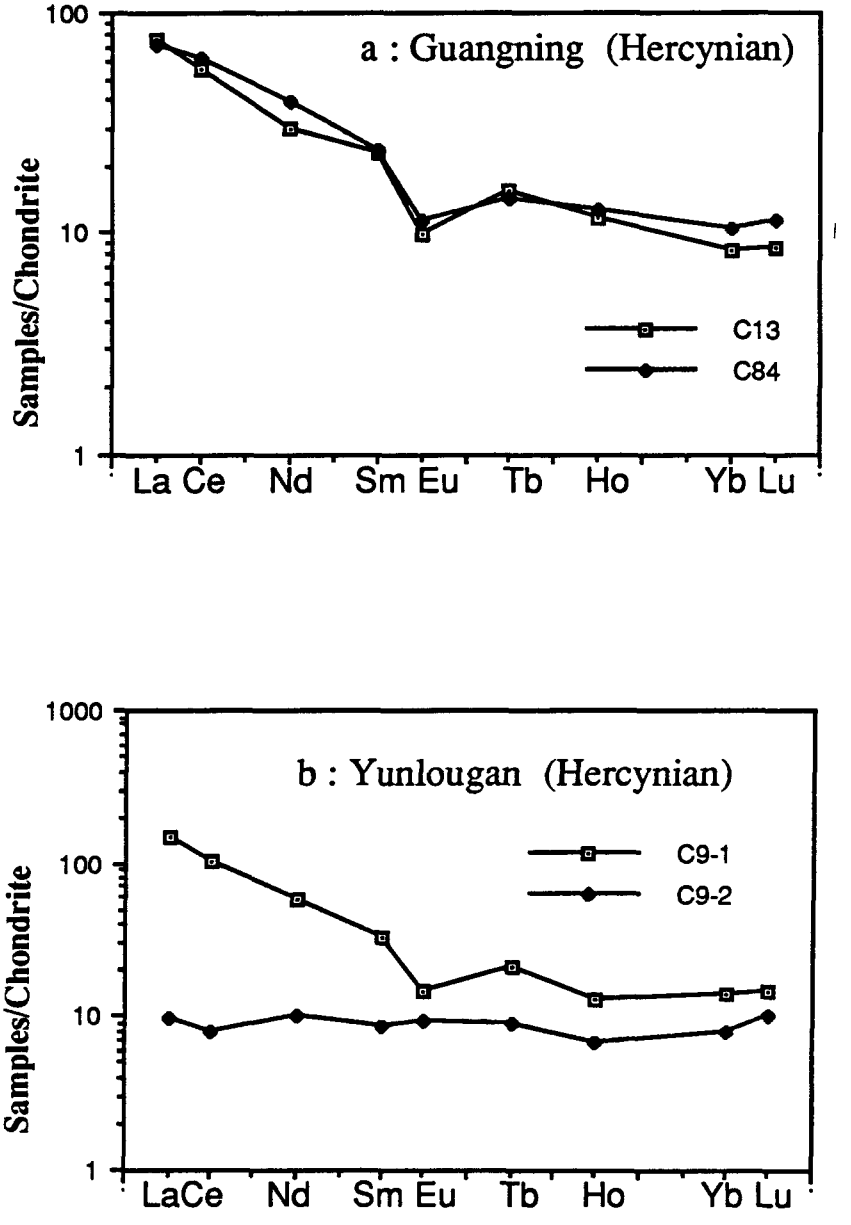

Fig.3.18. Comparison between chondrite-normalized REE diagrams of the different Hercynian plutons. a : Guangning pluton; b : Yunlougan pluton

Series granites of South China and compatible with magmas derived from deeper source rocks (I-type).

(2) Geochemical features of pegmatite

In contrast to the granodiorite, the pegmatite is characterized by high SiO_2 (73.31 %) and K_2O (7.13), but low MgO (0.3), FeO (1.11), TiO_2 (0.14), P_2O_5 (0.06), CaO (0.58), Al_2O_3 (13.34) and Na_2O (2.24) (Table 4). The K_2O/Na_2O and K_2O/P_2O_5 ratios are very high. The CIPW parameters show high qz (32), ag (0.85) and DI (94). The Al-parameter is about 1.07. The $Fe_2O_3/(FeO+Fe_2O_3)$ and MgO/(MgO+FeO) ratios are very low, about 0.01 and 0.21, reflecting a low mafic component.

The pegmatite contains low Sc (3.2 ppm), Ga (14), Zn (10), Sr (90), Nb (5), Zr (2), Hf (1.5), U (5) and Th (5), but high Ba (1244), Pb (59) and Rb (198) (Table 5) . In the multi-element spiderdiagram, it is characterized by positive Rb, Ba, U and K anomalies, but evident depletion of Th, Zr and Ti. In addition, the primary mantle-normalized values of Nb, La, Ce, Sr, Nd, Hf, Sm, Tb and Y all are less than 10, displaying a low platform in the spiderdiagram (Fig.3.17b). Generally, it shows high LILE but low HFSE feature in the multi-element spiderdiagram.

The REE abundance of the pegmatite (Table 6) is very low, and ratios of La/Sm and La/Yb are close to 1. The chondrite-normalized pattern (Fig.3.18b) is relatively flat with no Eu anomaly.

3-3-3. Geochemical comparison between the Hercynian granites

The geochemical features of the Hercynian granites present a series of differences between the Guangning biotite monzogranite and the Yunlougan granodiorite in major oxides, trace elements and REE. The comparison between the Guangning and Yunlougan plutons in the Mol. A/NK-A/CNK diagram (Fig.3.19) shows the different trends. The Guangning samples have Al-parameter (A/CNK) value about 1.07-1.14 and plot in the peraluminous area (Fig.3.19), coincident with the CCG (continent collision granite) and

CAG (continent-arc granite) areas (Maniar and Piccoli, 1989). The Yunlougan granodioritic samples have Al-parameter value about 1.03-1.06, and also plot in the peraluminous area (Fig.3.19), but they are coincident with the CAG (continental arc granite) and IAG (island arc granite) areas (Maniar and Piccoli, 1989). The Guangning granite may be the result of continental collision environment, whereas the Yunlougan granodiorite was produced in the subduction environment.

The Guangning biotite monzogranite has higher K_2O, Rb, Pb, K_2O/Na_2O and Rb/Sr, but lower MgO, TiO_2, V, Sc and Zn than the Yunlougan granodiorite. In the Rb/Sr-(V+Sc) diagram (Fig.3.20), the Yunlougan granodiorite is located in the high V+Sc but low Rb/Sr area, whereas the Guangning monzogranite is the reverse. The element distribution difference is also reflected in the trace element spiderdiagrams and REE diagrams (Figs.3.17 and 3.18). The Guangning monzogranite displays the features of the Nanling Series granites (S-type) (Wang et., 1984c) and of mature continental arc granites with high LILE but relatively low HFSE and a high LILE/HFSE ratio (Brown et al. 1984), but the Yunlougan granodiorite displays the features of the Yangtze Series granites (I-type) with a low LILE abundance and a low LILE/HFSE ratio.

The pegmatite sample has an Al-parameter value about 1.07 and plots in the peraluminous area (Fig.3.19), coincident with the POG (post-orogenic granite) area (Maniar and Piccoli (1989). The geochemical compositions of the pegmatite are clearly different from the Yunlougan granodiorite, althouth it occurs within the granodioritic body. The presence of different element assemblages and their distribution (Figs. 3.17, 3.18 and 3.20) suggest that the pegmatite may result from a more evolved magma derived from crustal source rocks, because it is geochemically very similar to the late granitic dykes evolved from the Nanling Series granites (Wang et al. 1984c). So, it may be genetically related to the Guangning monzogranite as shown in Figs. 3.17, 3.18 and 3.20, because a similar pegmatite can be found in the Guangning-Henshan granitic complex with Nb and Ta mineralization (Huang, 1988).

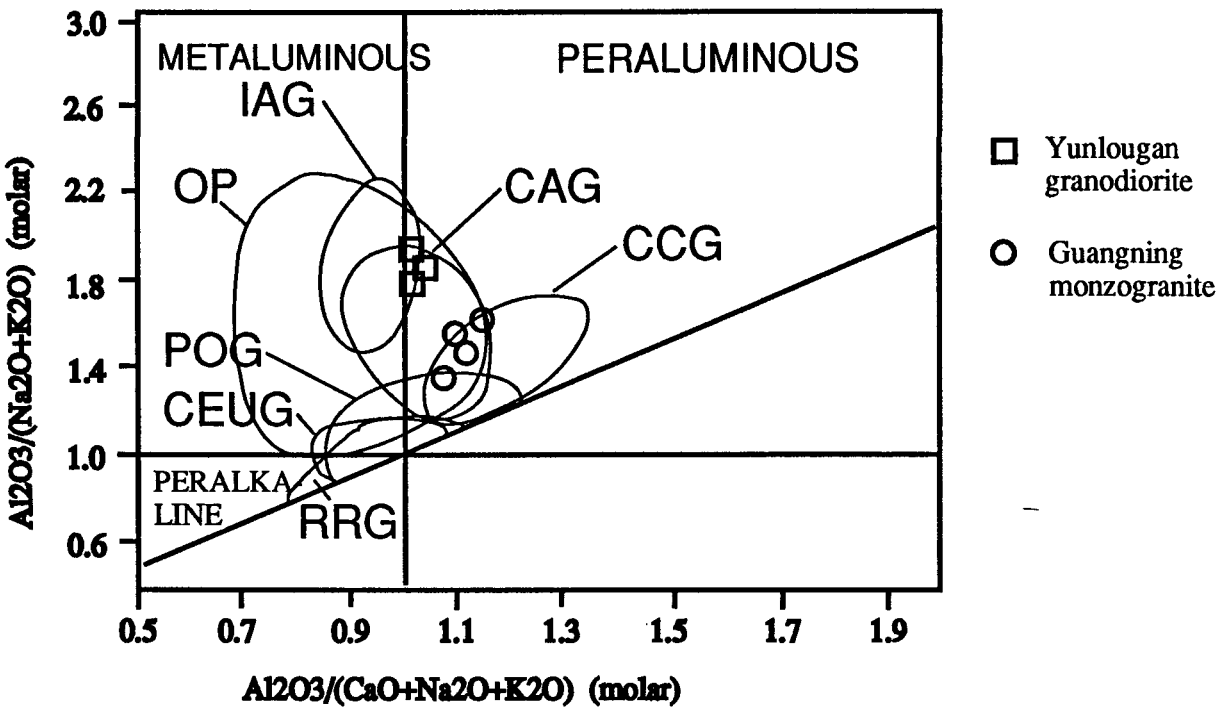

IAG=island arc granite, CAG=continental arc granite,
CCG=continental collision granite, POG=post-orogenic granite
RRG=rift-related granite, CEUG=continental epeirogenic uplift
granite, OP=oceanic plagiogranite (after Maniar and Piccoli, 1989)

Fig. 3.19. Mol. Al2O3/(CaO+Na2O+K2O)-Al2O3/(Na2O+K2O) (A/CNK-A/NK) of the Hercynian granites

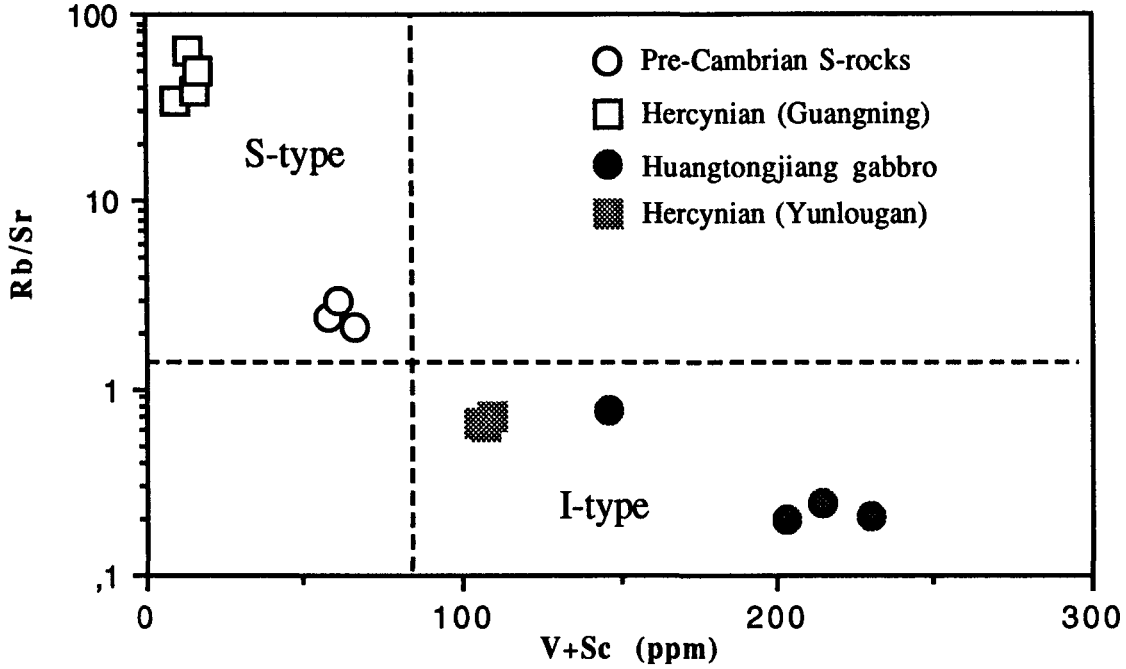

Fig.3.20. Comparison between different granite types of the Hercynian

3-4. Indosinian granites

The Indosinian granites in the Hetai area are represented by the Wuchun pluton, a megacryst monzogranite which contains granodioritic enclaves. In the QAP ternary classification, the samples of the megacryst monzogranite are located in the monzogranite area and the enclave samples located in the granodiorite area (Fig.3.21) based on the CIPW calculation and mineral analyses. The chemical compositions of the megacryst monzogranite and granodioritic enclaves are compared in Appendix III (Tables 7, 8 and 9).

3-4-1. Geochemical features of the megacryst monzogranite

The chemical compositions of the megacryst monzogranite (Table 7) are characterized by high K_2O (4.37-4.40 %), Na_2O (3.51-3.63) and CaO (2.08-2.30) but slightly lower SiO_2 (70.38-71.39) contents relative to average South China granites (Institute of Geochemistry, Academia Sinica, 1979). MgO, FeO, TiO_2, P_2O_5 and Al_2O_3 have average contents. The K_2O/Na_2O and K_2O/P_2O_5 ratios are moderate, 1.20-1.25 and 36 respectively, but the MgO/(MgO+FeO) and $Fe_2O_3/(Fe_2O_3+FeO)$ ratios are relative low, 0.19-0.22 and 0.22-0.24 respectively. The Al-parameters (A/CNK) are low, about 0.99, although the content of Al_2O_3 is relative high (about 14.50%). Relative to CaO and Na_2O, K_2O is significant in the petrochemical evolution of the Wuchun megacryst monzogranite.

The trace element contents of the megacryst monzogranite (Table 8) are characterized by high Co (90 ppm), Ni (76), Cu (862), Nb (19), Ta (6.8), Zr (105), U (10) and Th (17) contents. It is interesting to note that both Sr (190) and Rb (230) are high. In addition, V (54) is relatively high, too. This may be explained by the coexistence of Ca-rich plagioclase and K-feldspar phenocrysts, because these elements are generally affected by the fractional crystallization of Ca-rich plagioclase and K-feldspar (and albite) at different stages of magma evolution. The accumulation of Ca-rich plagioclase may at first concentrate the elements related to Ca from the magma, and later K-feldspar crystallizes from this differentiated magma as interstitial growths or outer rims on plagioclase which are enriched in elements related to potassium. In addition, the albite component is separated as an independent phase, and it further encloses the K-feldspar, forming the alkali-feldspar zoning.

This may result from a rapid decrease of the temperature during late magma crystallization. This situation is very similar to the Coast Area granites in South China (Yang et al., 1986b). The relative enrichment of mafic components in the Wuchun monzogranite indicates that the source magma may have been derived from the upper mantle. The multi-element spiderdiagram (Fig.3.22) shows that not only LIL elements but also HFS elements such as La, Ce, Nd, Hf, Zr and Sm have a high contribution. In addition, Nb, Sr and Ti show weak depletions in the spiderdiagram. This element distribution feature is very similar to the mature alkali-arc granite and back-arc/anorogenic alkaline granite (Brown et al., 1984).

The contents of REE are moderate and the La/Sm and La/Yb ratios are high, 5.09-5.60 and 8.26-14.04 respectively, showing slight enrichment of light REE (Table 9). The chondrite normalized REE patterns (Fig.3.23) display an inclined-right pattern and a weak negative Eu anomaly. Normal magma evolution leads to the enrichment of heavy REE and a strong negative Eu anomaly. However, LREE enrichment and a weak negative Eu anomaly occurring in the Wuchun monzogranite may reflect not only a deep magma source, but also imply the contribution of Ca-rich plagioclase accumulation to it.

3-4-2. Geochemical features of the granodioritic enclaves

In contrast to the host megacryst monzogranite (Table 7), the granodioritic enclaves are characterized by lower SiO_2 (64.65 %) and K_2O (2.32), but higher MgO (2.27), MnO (0.18), FeO (4.48), TiO_2 (0.77), CaO (3.75), P_2O_5 (0.25) and Na_2O (3.78) contents. The K_2O/Na_2O and K_2O/P_2O_5 ratios are very low, 0.55-0.61 and 9.1-16.2 respectively. The Al_2O_3 content (15.76) is higher, but the Al-parameter (A/CNK) value is low, about 1.0. The $Fe_2O_3/(Fe_2O_3+FeO)$ ratios are low, 0.17-0.18, but MgO/(MgO+FeO) high, 0.34-0.38.

The trace element contents are characterized by high Ni (61 ppm), Cr (116), V (99), Sc (10.7), Zn (93), Nb (16) and Zr (141), but lower Pb (13-15) and Ba (275-293) (Table 3.10) . U is very high, about 72 ppm, but Th is low, only 11 ppm, and both Sr (243) and Rb (248) are high, similar to the host monzogranite. The LILE and HFSE in the spiderdiagram (Fig.3.22) display high distribution. Particularly, U displays a strong positive anomaly, and Nb, Sr and Ti only a very weak depletion. These trace element geochemical features are very similar to the host megacryst monzogranite, and show their relationship to the megacryst

monzogranite. Xenocrysts of Ca-rich plagioclase can be found in the enclaves, and they obviously differ from other feldspars by their texture and their chemical composition. Clearly, the presence of xenocrysts of Ca-rich plagioclase may imply the participation of mafic components to the enclaves and that a more basic intrusive phase existed before the granodioritic enclave crystallization. The Ca-rich plagioclase suggests the presence of a more basic intrusive phase possibly similar to the Huangtongjiang gabbro. The plagioclase in the enclaves and the host rock commonly have an outer alkaline rim. The contrasting element enrichment in the enclave may be caused by the coexistence of Ca-rich plagioclase xenocrysts and alkali-feldspar.

The REE contents are relative high, as are the La/Sm and La/Yb ratios, 5.60 and 14.04 respectively, presenting a relative enrichment of light REE (Table 9). The chondrite normalized pattern (Fig.3.23) is inclined to the right with a weak Eu anomaly. These features of REE distribution are similar to the Yangtze granites (Fig.3.1) and support the idea that the source magma is derived from the upper mantle and may be evolved from a basaltic magma.

3-4-3. Relation between the megacryst monzogranite and granodioritic enclaves

Both the granodioritic enclaves and the host megacryst monzogranite have low Al-parameter (A/CNK) values, and the Al-parameter value decreases from the granodioritic enclaves (1.02-1.06) to the host megacryst monzogranite (0.98-0.99). The granodioritic enclaves are located just within the peraluminous area in the Mol. A/NK-A/CNK diagram (Fig.3.24) and are coincident with the CAG (continental arc granite) area (Maniar and Piccoli, 1989), and the host megacryst monzogranites plot in the metaluminous area and are coincident with the POG (post-orogenic granite) area (Maniar and Piccoli, 1989) (Fig.3.24). So, the granodioritic enclaves and the host megacryst monzogranite may be produced from a subduction or an extension environment. Comparison between the host megacryst monzogranite and granodioritic enclave in Tables 3.8, 3.9 and 3.10 and in related geochemical diagrams (Figs.3.22, 3.23 and 3.24) clearly shows that geochemical similarities between them as well as their evolutionary features can be related by the regular trend of some associated elements such as Sc, V, Rb, Sr and REE. This type of

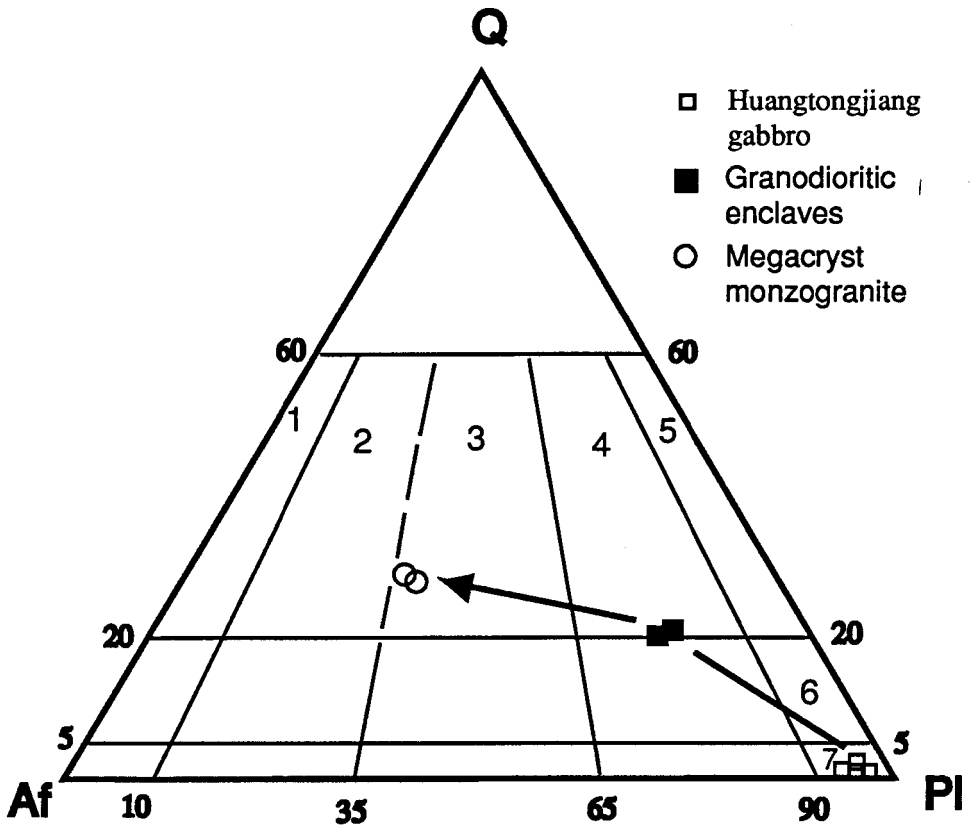

1.Alkali-feldspar granite; 2.Orthoclase granite; 3.Monzogranite
4.Granodiorite; 5.Tonalite; 6.Quartz diorite; 7.Diorite or Gabbro

Fig. 3.21. The Indosinian granites on the Q-Af-Pl ternary classification by IUGS (1989)

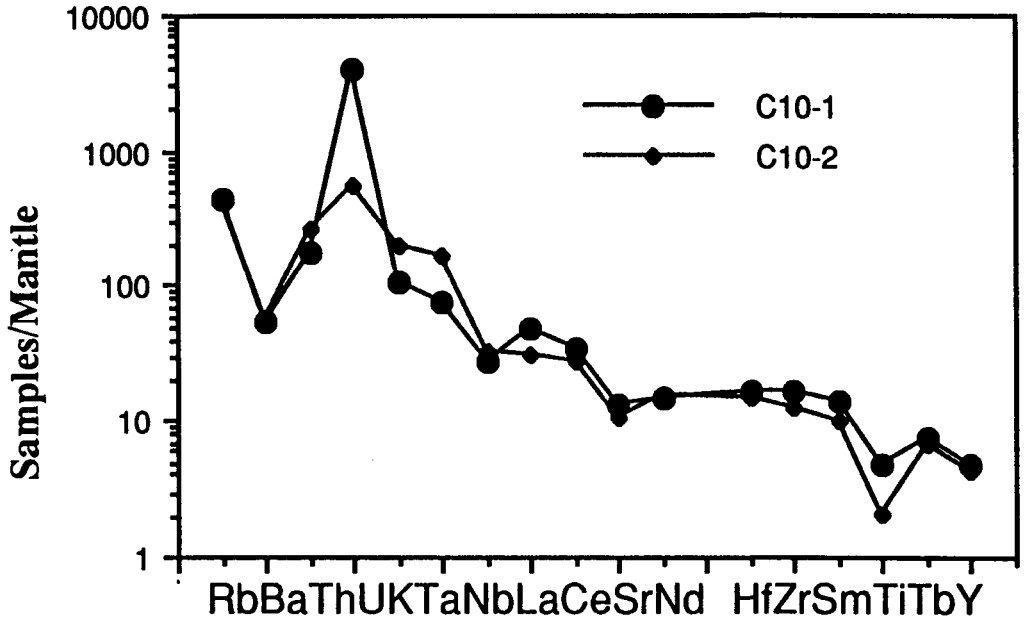

Fig. 3.22. Multi-element spiderdiagrams of the Wuchun granite suite

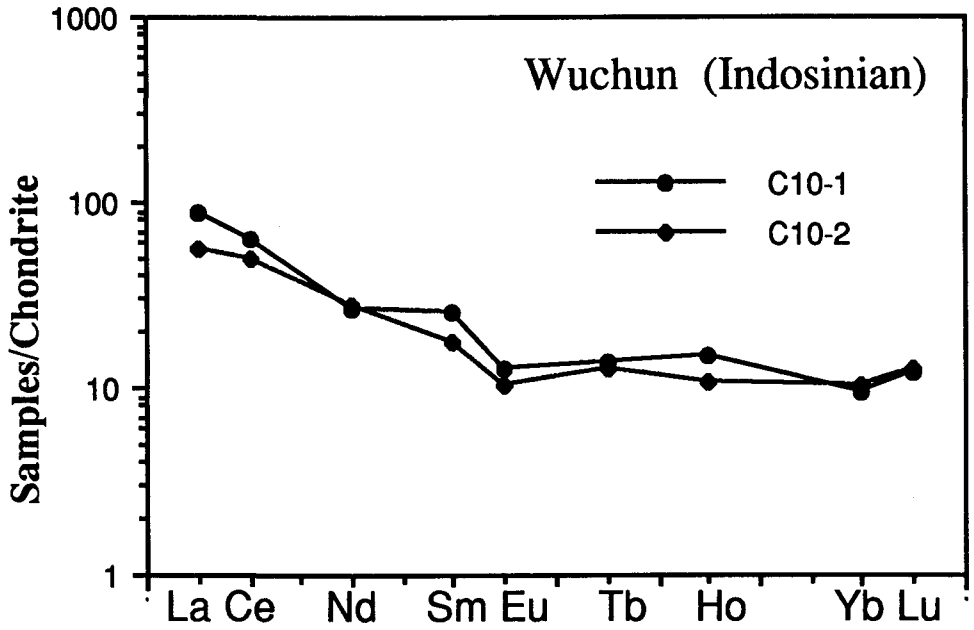

Fig. 3.23. Chondrite-normalized REE diagrams of the Wuchun granite suite

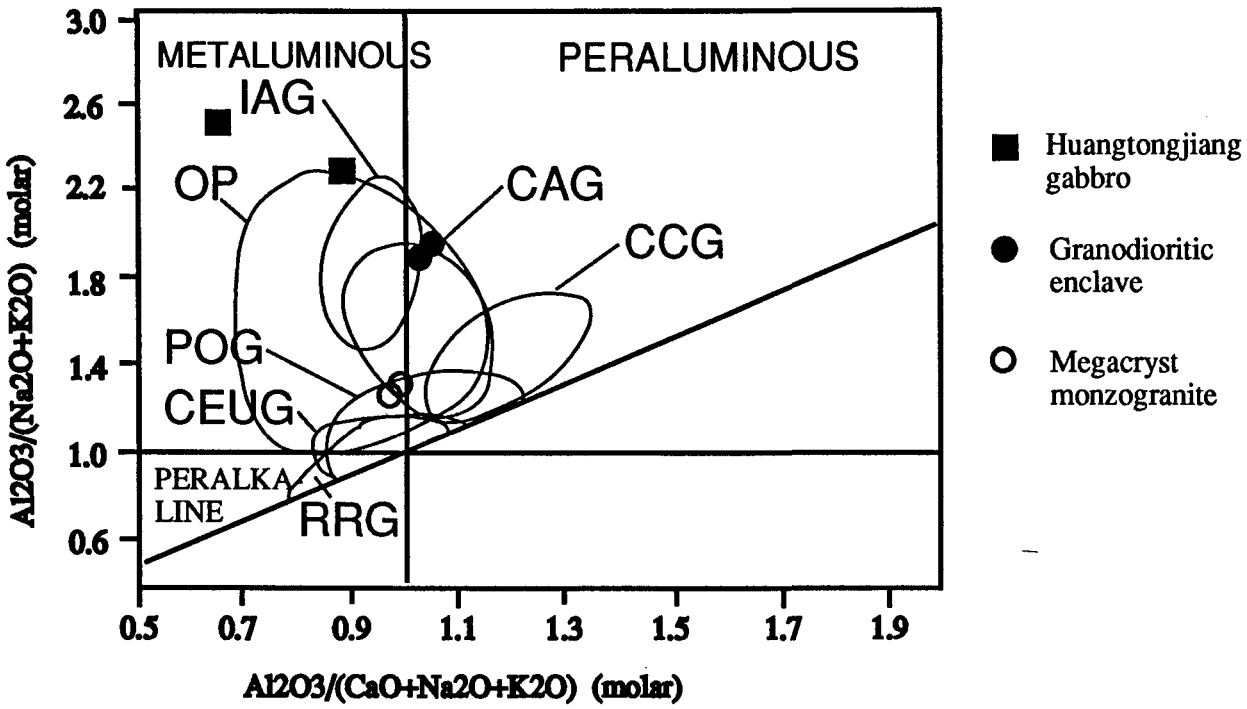

IAG=island arc granite, CAG=continental arc granite,
CCG=continental collision granite, POG=post-orogenic granite
RRG=rift-related granite, CEUG=continental epeirogenic uplift
granite, OP=oceanic plagiogranite (after Maniar and Piccoli, 1989)

Fig. 3.24. Mol. Al2O3/(CaO+Na2O+K2O)-Al2O3/(Na2O+K2O) (A/CNK-A/NK) of the Indosinian granites

granodioritic enclaves is comparable to other mafic enclaves in granites (Cantagrel et al., 1984; Chen et al. 1989 and 1990; Blundy and Sparks, 1992). These geochemical features demonstrate the mantle contribution to the granitic magma evolution during early stages of extension (Feeley and Grunder, 1991; Sutcliffe et al., 1990). It is reasonable to infer that the granodioritic enclaves are an earlier intrusive phase, and the host megacryst monzogranite is evolved from the same source magmas which are associated with basaltic magmas from upper mantle.

3-5. Yanshanian granites

The Yanshanian granites in the Hetai Area are represented by the Sihui complex, which includes the Sihui, Baishitan and Lianhe plutons (Fig.1.5). They are polyphase intrusions composed of coarse- to fine-grained biotite alkali-feldspar granites which commonly contain granodioritic enclaves. Their chemical compositions are listed in Appendix III (Tables 10, 11 and 12).

3-5-1. Geochemical features of the host alkali-feldspar granite suite

All samples of these granites are characterized by high SiO_2 (73.99-76.49 %), Na_2O (3.40-4.55) and K_2O (3.68-4.97), but very low MgO (0.29-0.01), FeO (1.27-0.37), TiO_2 (0.23-0.07), CaO (0.79-1.30) and P_2O_5 (0.06-0.01) contents (Table 10). The K_2O/Na_2O and K_2O/P_2O_5 ratios are high, 0.81-1.46 and 73-423, respectively, but the MgO/(MgO+FeO) ratio very low, from 0.01-0.10. The $Fe_2O_3/(Fe_2O_3+FeO)$ ratios vary greatly from 0.02-0.62. The CIPW parameters show high qz (32-36), ag (0.82-0.87) and DI (90-95), and all samples plot in the alkali granite area in the QAP ternary classification (Fig.3.25). The Al_2O_3 contents vary from 12.71-13.66, and their Al-parameter (A/CNK) values are <1.0.

The trace elements (Table 11) are characterized by high Rb (216-272 ppm), Nb (12-61), Ta (4.0-11.4), U (6-37), Th (17-37) and Y (19-63), but low Ni (13-31), Cr (10-27), Sc (1.8-8.2), V (10-34), Zn (10-36), Sr (19-105) and Zr (22-119). Some elements such as Cu (21-318) and Ba (19-440) show large variations. The multi-element spiderdiagrams

(Fig.3.26) reflect the high concentration of LILE and HFSE, and the normalized values of Rb, Th, U, K, Ta and La, Ce are >100 and >10 respectively. Nb is weakly depleted, but Sr, Ba and Ti are strongly depleted. Generally, the spiderdiagram patterns show enrichment of LIL elements and HFS elements. This element distribution indicates that the Sihui alkali-feldspar granites are very similar to the Coast granites in South China and represent more differentiated magmas (Yang et al., 1986b), because the differentiated and contrasting elements such as K, Rb, Nb vs Sr, V, Sc, Zn, Ti display an evident separation trend, compared with the spiderdiagram patterns of Brown (1984), which suggests that they may be similar to those from a mature continental arc environment.

The REE contents in the Sihui alkali-feldspar granites (Table 12) are moderate, but the La/Sm and La/Yb ratios decrease rapidly from coarse- to fine-grained phases, 8.36->1.25 and 12.31->0.72 respectively, indicating a relative enrichment of heavy REE with evolution. The chondrite normalized REE patterns (Fig.3.27) display a nearly symmetrical V-shape (slightly inclined left) and a strong negative Eu anomaly. In addition, the HREE is more enriched and Eu more depleted in the REE distribution patterns with the series evolution from coarse-grained to fine-grained phases. Such an evolutionary trend in the REE distribution further characterizes the magmas as products of a more evolved differentiation. Their evident similarity with the Coast alkali-feldspar granites of South China (Fig.3.1) also suggests that the Sihui alkali-feldspar granites may belong to a more differentiated magma series derived from the upper mantle and intruded into an extension environment.

3-5-2. Geochemical features of the granodioritic enclaves

Granodioritic enclaves are distributed throughout the Sihui alkali-feldspar granites. The chemical compositions (Table 10) may be compared to the host alkali-feldspar granites. The enclaves are obviously lower in SiO_2 and K_2O, but higher in Na_2O, MgO, FeO, MnO, TiO_2, Al_2O_3, P_2O_5 and CaO. The K_2O/Na_2O and K_2O/P_2O_5 ratios are lower, about 0.39 and 10 respectively, and MgO/(MgO+FeO) is higher, 0.25-0.31. The $Fe_2O_3/(Fe_2O_3+FeO)$ ratio is very high, about 0.44. Al_2O_3 contents in the enclaves are higher (15.88), but Al-parameter (A/CNK) value is low, about 0.99.

Trace elements in the granodioritic enclaves (Table 11) are characterized by high V (83 ppm), Sc (9.4), Zn (54), Sr (243), Zr (253), Hf (8.3),Y (45), U (12), Th (18) and Nb (13), but lower Ni (13) and Cr (10). Rb contents (138 ppm) are lower than the host granites, but abundances are relatively high for granodiorite. As with the host alkali-feldspar granite, the multi-element spiderdiagrams of the enclaves (Fig.3.26) also display high LILE values, but obvious K depletion. In addition, Ba, Nb, Sr and Ti are depleted, although their normalized values are relatively high. The spiderdiagrams for the granodioritic enclaves are generally similar to the host alkali-feldspar granites (Fig.3.26), and show a LILE and HFSE enrichment trend. Therefore, the granodioritic enclaves may also be derived from a mature arc environment when compared with the patterns of Brown et al. (1984). However, mafic components and some elements such as Sr, V and Sc are more concentrated in the granodioritic enclaves than in the host alkali-feldspar granites, possibly reflecting differences in evolutionary stage, the granodioritic enclaves being the earlier intrusive phase of a cognate magma series.

The granodioritic enclaves are characterized by the high REE contents and slightly higher ratios of La/Sm and La/Yb, indicating LREE enrichment (Table 12). The chondrite normalized REE pattern (Fig.3.27) displays an inclined right form with a moderate negative Eu anomaly. This trend is similar to the early intermediate phase of the Coast granite series which usually represents the deeper source magmas (or I-type). In addition, it also reflects the possible accumulation of Ca-rich plagioclase in the magma.

These geochemical features demonstrate the mantle contribution to granitic magma evolution (Feeley and Grunder, 1991). It is reasonable to infer that the granodioritic enclaves represent an earlier intrusive phase, and evolved from the same magma as the host alkali-feldspar granites.

In the Mol.A/NK-A/CNK diagram (Fig.3.28), both the granodioritic enclaves and host alkali-feldspar granites plot in the metaluminous area, but the granodioritic enclaves are coincident with the CAG (continental arc granite) area (Maniar and Piccoli, 1989), and the host alkali-feldspar granites fall in the POG (post-orogenic granite) area (Maniar and Piccoli, 1989), reflecting the tectonic evolution from a subduction environment to an extension environment of the Yanshanian granite series.

3-5-3. Evolution of the Sihui granite suite

Petrographic observations indicate that the granodioritic enclaves are part of an earlier intrusive phase of the host alkali-feldspar granite in the Sihui complex. Their chemical compositions (Tables 10, 11 and 12) show regular geochemical variations between the granodioritic enclaves and the host alkali-feldspar granites. Multi-element spiderdiagrams (Fig.3.26) show that both the host alkali-feldspar granites and the granodioritic enclaves are characterized by an enrichment of LIL and HFS elements and a very weak depletion of Nb, although K is low in the granodioritic enclaves. Rb, Th, K, Ta and Nb increase but La, Ce, Sr, Nd, Hf, Zr, Sm, Ti and Tb decrease from granodioritic enclaves to the host alkali-feldspar granites. Similarly, the chondrite normalized REE patterns display an evolution (Fig.3.27), in that the negative Eu anomaly becomes more obvious and LREE decreases but HREE increases from granodioritic enclaves to the host alkali-feldspar granites. These regular geochemical variations indicate that the granodioritic enclaves are cognate to the host alkali-feldspar granites and derived from the same magma.

Harker diagrams (Fig.3.29) of selected elements also display regular variations with SiO_2 increasing during the evolution of the complex. For example, Ti, Sc, V, Ni, Sr, Hf, Zr, La and Ce gradually decrease, whereas K, Rb, Th, Nb and Ta increase from the granodioritic enclaves through the coarse-grained alkali-feldspar granite to the fine-grained alkali-feldspar granite. The regular relation in the Harker diagrams may be helpful to establish a possible model of element variation during magma evolution. Two elements with contrasting geochemical behaviour such as Rb and Sr are chosen in a two-element variation diagram and are used to reflect the geochemical processes during magma evolution. The proportion of rock-forming minerals can be estimated based on CIPW calculation and mineral analyses for the host granite, Biotite : K-feldspar : plagioclase : apatite =5 : 50 : 10 : 1. Taking this proportion and the Kd values provided by Hanson (1978), the bulk distribution coefficient (D) of Rb and Sr are calculated as 0.421 and 2.103 respectively. The calculation as in the Shijiang complex, for a partial melting model, is :

$$C(l)/C(0)=1/[D(1-F)+F],$$

and for a fractional crystallization model, is :

$$LgC(1)-LgC(0)=(D-1)LgF.$$

According to the Harker diagram (Fig.3.29), it may be supposed that the lowest Rb content 120 ppm and the highest Sr content 300 ppm represent a situation of 99% partial melting or 1% fractional crystallization, and then two contrasting curves can be made to represent the two different processes (Fig.3.30). Comparing the actual data (points) with these curves, it is clear that the fractional crystallization model better fits the actual situation, because the partial melting process is unable to produce a high Rb content (275 ppm) when the Sr content is 50 ppm. Thus, the fractional crystallization model is more suitable for explaining the magma evolution of the Sihui complex. Clearly, the petrogenetic development of the Sihui granite complex is different from that of the Shijiang (Caledonian) granite complex.

3-6. Geochemical characteristics of the Huangtongjiang gabbro

The Huangtongjiang gabbro occurs within the Sidong granite, and includes gabbro and pyroxene diorite. The analytical data are listed in Tables 10, 11 and 12 (Appendix III), and all samples plot in the gabbro area in the QAP ternary classification (Fig.3.25).

The Huangtongjiang body is characterized by very low SiO_2 (49.42-52.67 %) and K_2O (0.51-0.77), but high MgO (7.34-9.38), MnO (0.13-0.16), FeO (4.85-6.88), Fe_2O_3 (1.38-2.13), TiO_2 (0.46-1.14) and CaO (10.53-13.78) contents (Table 10). The K_2O/Na_2O and K_2O/P_2O_5 ratios are very low, 0.24-0.27 and 9-17 respectively, but MgO/(MgO+FeO) ratios are very high, about 0.54-0.66, displaying the magmatic features of basalt. The $Fe_2O_3/(Fe_2O_3+FeO)$ ratios are about 0.22-0.23, reflecting a high fO_2. The CIPW parameters show very low qz (0-6.09), ag (0.24-0.46) and DI (20-46).

Al_2O_3 contents are high (15.14-16.77), and in the Mol. $Al_2O_3/(Na_2O+K_2O)$-$Al_2O_3/(CaO+Na_2O+K_2O)$ diagram, samples plot in high $Al_2O_3/(Na_2O+K_2O)$ but low $Al_2O_3/(CaO+Na_2O+K_2O)$ area (Fig.3.28), the Al-parameter very low, from 0.5-0.9, presenting the strongest aluminum undersaturation in rocks of the Hetai Area.

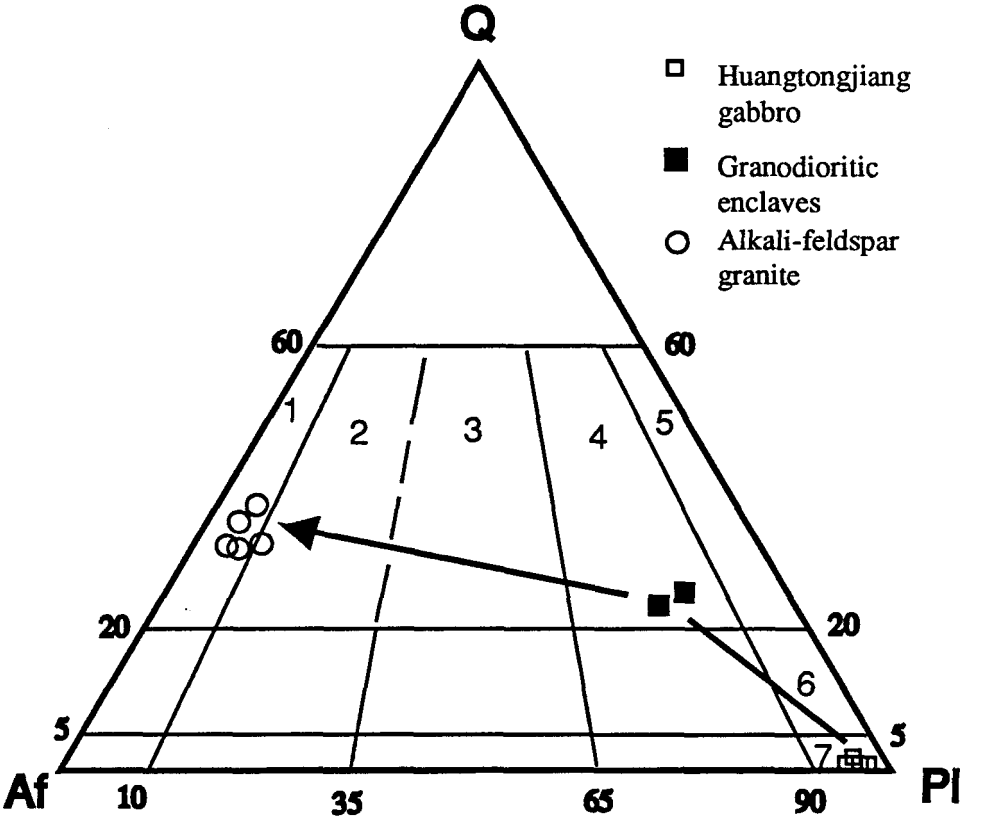

1.Alkali-feldspar granite; 2.Orthoclase granite; 3.Monzogranite
4.Granodiorite; 5.Tonalite; 6.Quartz diorite; 7.Diorite or Gabbro

Fig.3.25. The Yanshanian granites on the Q-Af-Pl ternary classification by IUGS (1989)

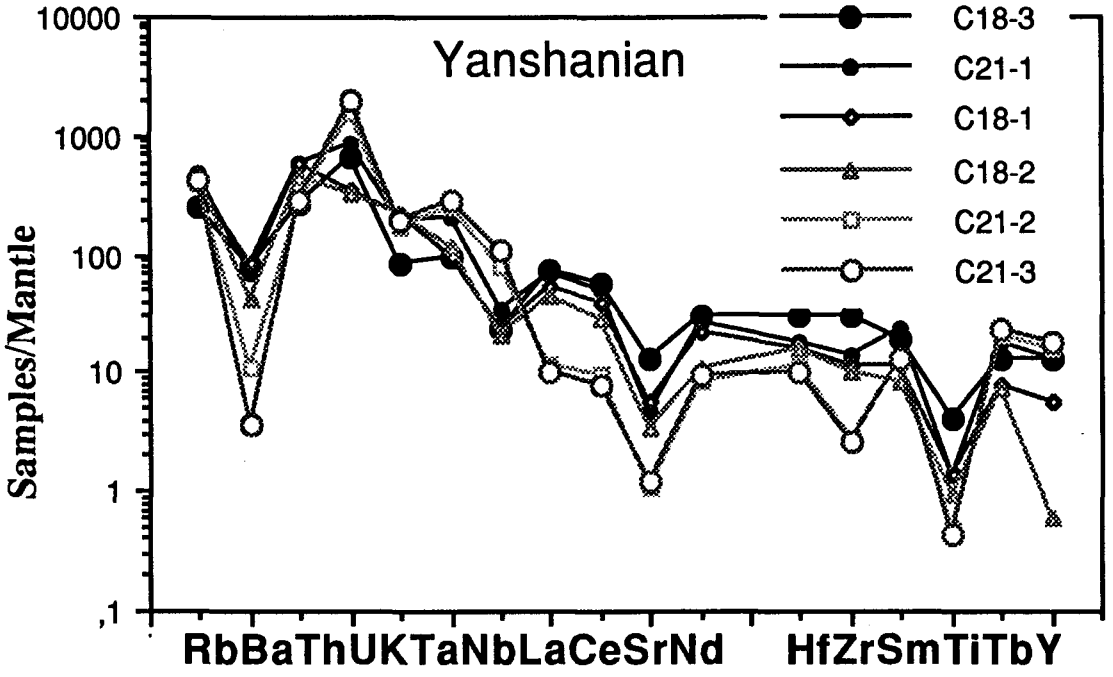

Fig. 3.26. Multi-element spiderdiagrams of the Sihui granite suite

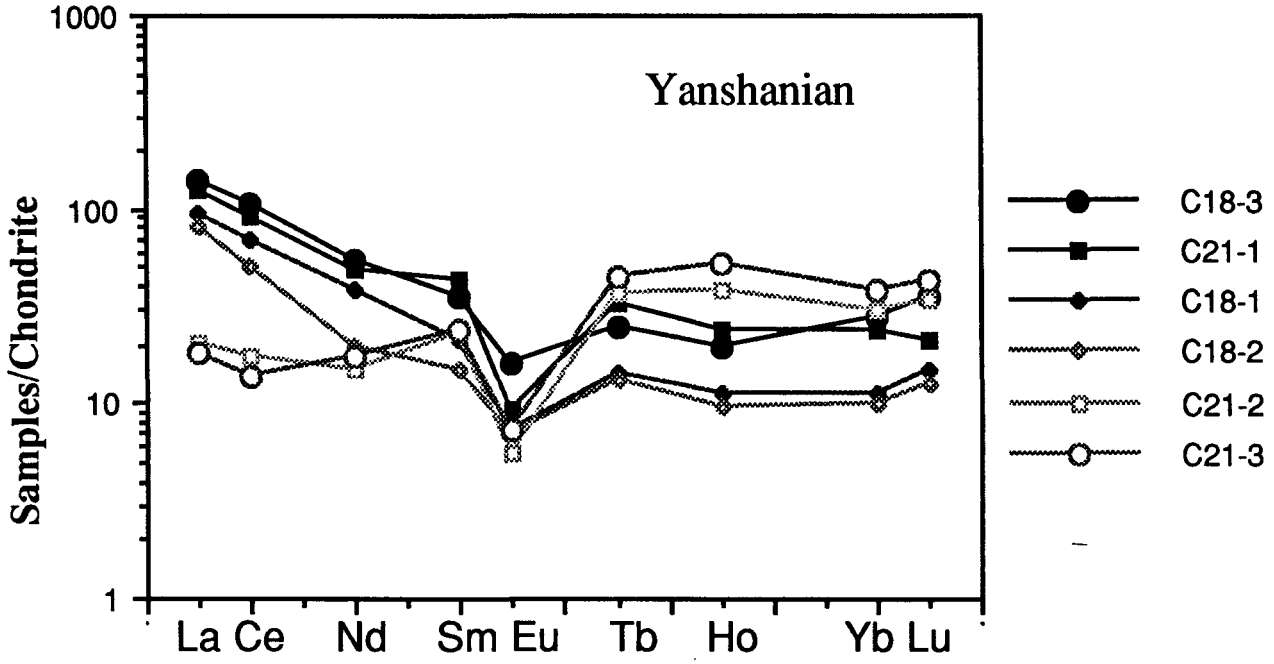

Fig.3.27. Chondrite-normalized REE diagrams of the Sihui granite suite

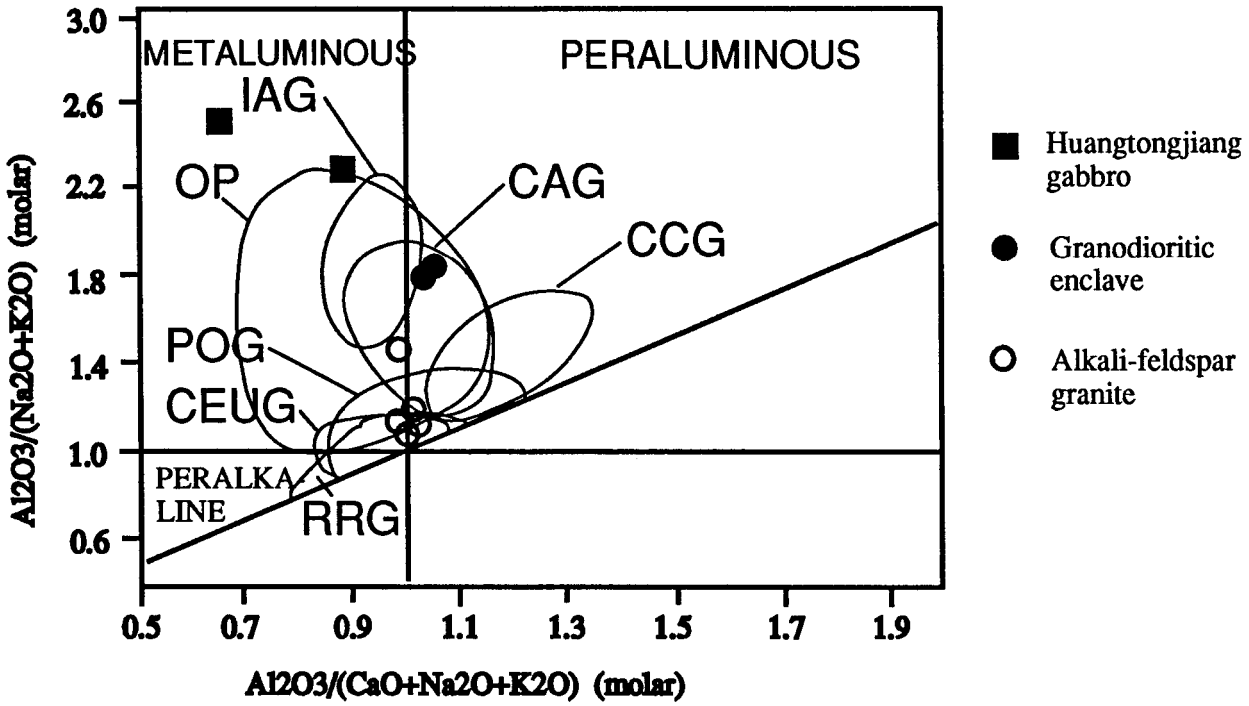

IAG=island arc granite, CAG=continental arc granite,
CCG=continental collision granite, POG=post-orogenic granite
RRG=rift-related granite, CEUG=continental epeirogenic uplift
granite, OP=oceanic plagiogranite (after Maniar and Piccoli, 1989)

Fig. 3.28. Mol.Al2O3/(CaO+Na2O+K2O)-Al2O3/(Na2O+K2O) (A/CNK-A/NK) of the Yanshanian granites

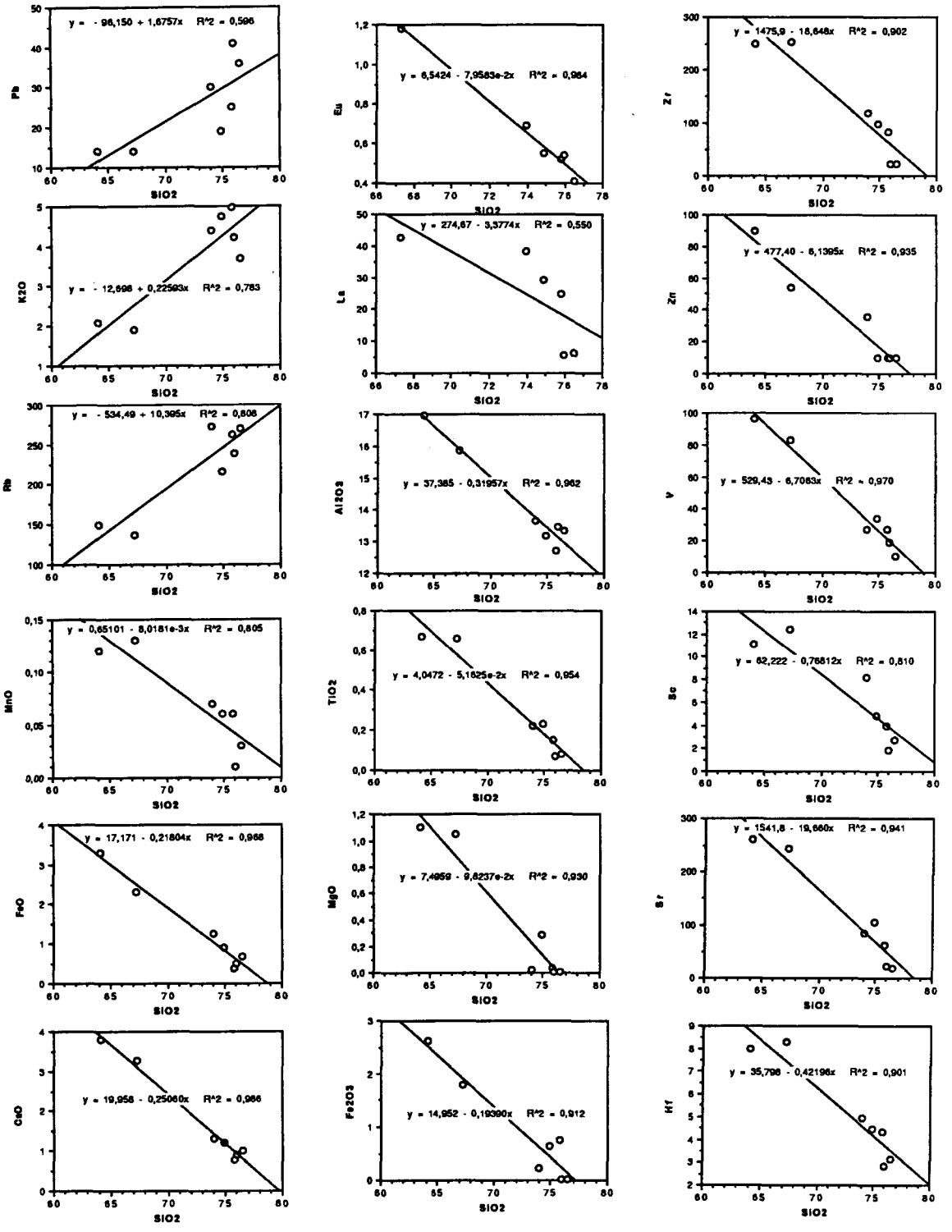

Fig. 3.29. The Harker diagrams of the Sihui granite suite

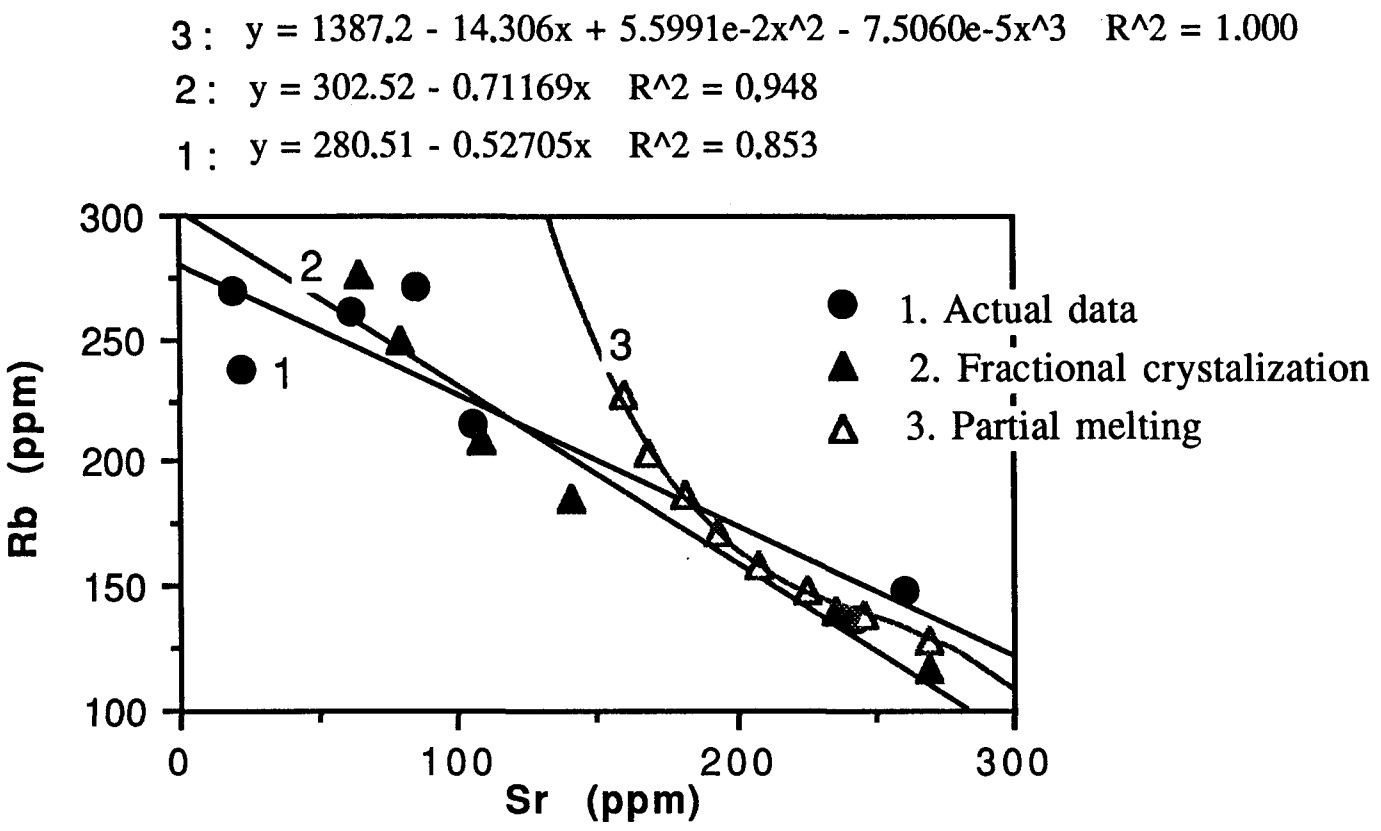

Fig.3.30. Petrogenetic process model of the Sihui granite suite

Trace elements (Table 11) are characterized by high Ni (62-130 ppm), Cr (83-284), V (162-197), Sc (32-41), Cu (81), Zn (38-61) and Sr (113-128), but low Rb (24-32), Cs (1-3), Pb (4-9), Nb (3-4), Ta (0.9-1.2), Zr (24-59), Hf (1.2-2.5), U (0.5-1), Th (1.7-4.5), Ba (39-144) and Ga (16-19) contents. The assemblage of trace elements reflects the high mafic component but very low LIL elements, suggesting that their source magmas may be derived from the upper mantle. Most elements in the multi-element spiderdiagrams (Fig.3.31) display very low values and the curve is divided into two different segments, with the values less than 100 and 10, respectively. Ba and Nb are relatively more depleted but only Ti presents a weak depletion. Comparison of with the patterns of Brown et al. (1984) suggests that the Huangtongjiang gabbro may be produced in a primitive island arc or a continental arc environment.

REE abundances (Table 12) are very low, as are La/Sm and La/Yb ratios which are close to 1.0. The chondrite-normalized REE distribution patterns (Fig.3.32) present a nearly horizontal line with no negative Eu anomaly. Such patterns are similar to that of calc-alkali basalt (Henderson, 1984), demonstrating that the source magma of this body is a calc-alkaline basalt. Consequently, the Huangtongjiang gabbro may be regarded as an important indicator of an upper mantle magma source for the Hetai granites.

3-7. Geochemical comparisons between older and younger granites

The chemistry of granites reflects both the chemical compositions of source rocks and the geological evolution of granites and their geotectonic settings. Other suites of granites which co-exist in a certain geological setting which cannot be derived from the same granitic magma. The Hetai Area includes the granites of different ages from Caledonian and Hercynian (older granite) to Indosinian and Yanshanian (younger granite), and it is impossible that they evolved from the same magma chamber whether their source rocks are the same or not. The geochemical comparisons between granites of different ages may still be significant, because the chemistry of granites may result from a repeated geotectonic environment. First, the different genetic types of the Hetai granites will be identified by means of the geochemical comparisons between granites of the same and different ages, and

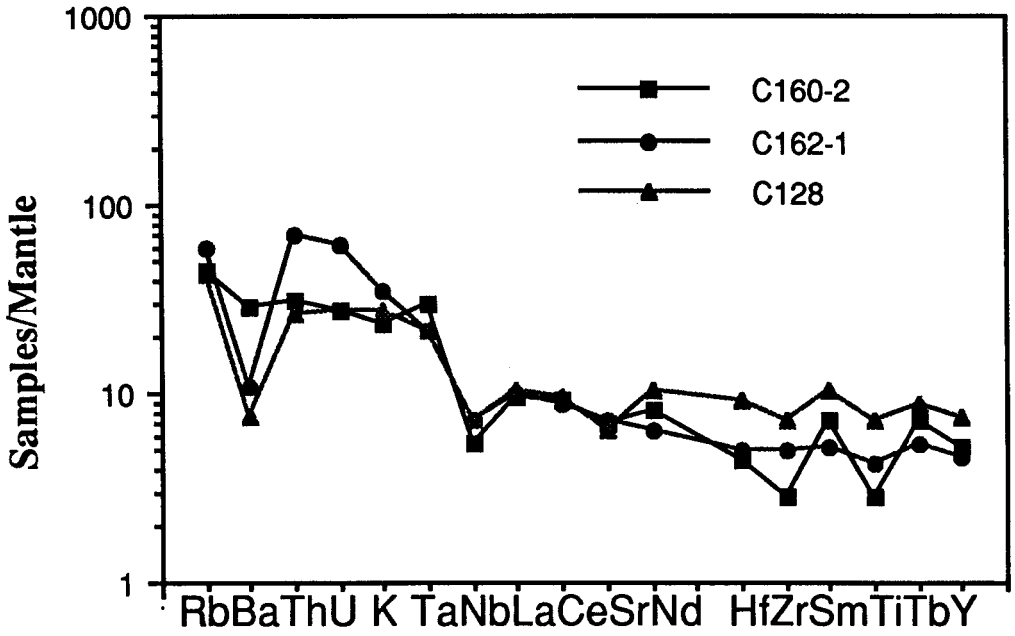

Fig.3.31. Multi-element spiderdiagrams of the Huangtongjiang gabbro

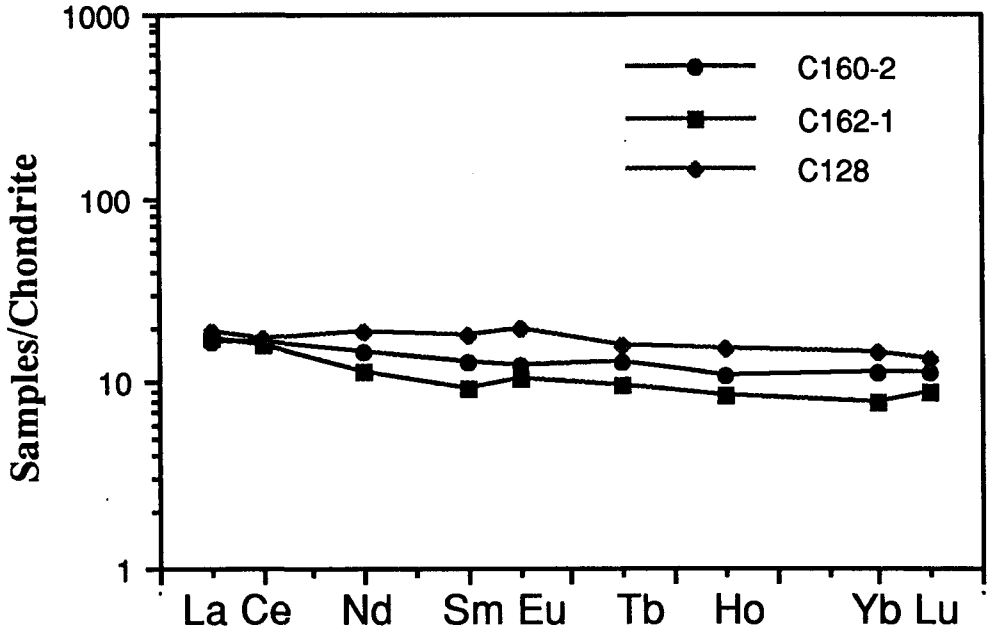

Fig.3.32. Chondrite-normalized REE diagrams of the Huangtongjiang gabbro

then the relations between granite generation and regional geotectonic evolution will be discussed.

3-7-1. Criteria to differentiate I- and S-type granites

Chappell and White (1974, and 1984) suggested that S-type granites are low in Na, Ca and Sr relative to the I-type. However, when Cobbing et al. (1986) used a projected line of demarcation on K_2O vs Na_2O plots based on the criteria of Chappell and White (1974 and 1984) to discriminate granites of Southeast Asia, he considered that the element variations between I-type and S-type granites of Southeast Asia are different from those of the Lachlan Fold Belt (Fig.3.33), although they can be distinguished by the same I-S line. This difference suggests that a geochemical variation may be present between different tectonic settings, although source rocks may be similar. The Hetai granites display three different distribution features in the K_2O vs Na_2O diagram (Fig.3.33). The older granites (Caledonian and Hercynian granites) plot mainly in the area of from low to high K_2O/Na_2O, and most overlap the transitional area between S- and I-type from the Lachlan area of Australia; whereas the earlier phases of younger granites are located in the area of higher Na_2O but low K_2O and belong to the I-type. Their later phases (megacryst monzogranite and alkali-feldspar granite) are distributed in the area of high K_2O and higher Na_2O coincident with I-type. It seems difficult to separate the Hetai granites into different genetic type using S-I line of Australia (Chappell and White, 1984; Cobbing et al., 1986) from Fig.3.33, because most samples plot in the I-type field. The Hetai granites show two different trends (Fig.3.33). The older granites show a negative correlation between K_2O and Na_2O, and the general geochemical evolution shows varying K_2O but a relatively stable Na_2O content; whereas the younger granites show a positive correlation between K_2O and Na_2O, and the geochemical evolution shows K_2O more obviously enriched with magmatic evolution (SiO_2 increase) (Fig.3.33). These different trends suggest that the older granites may be derived from the crustal source rocks which may have a varying geochemical composition; and the younger granites may be derived from a deeper source magma which has a more stable geochemical background. Magmatic evolution leads to greater K_2O enrichment, and consequently, the granites crystallized from an I-type source magma

evolved as a more differentiated granite series in which K_2O enrichment relative to SiO_2 increase plays a more important role than Na_2O increase.

In addition, the Hetai granites may also be divided into different types by means A/NK-A/CNK diagram and the Al-parameter (A/CNK) about 1.05 may be regarded as a better limiting value for the Hetai Area (Fig. 3.34), which differs from 1.0 of Maniar and Piccoli (1989). It can be seen from Fig.3.34 that the older granites are located mainly in the peraluminous area and are coincident with the CCG (continental collision granite), CCG (continental arc granite) and CEUG (continental epeirogenic uplift granite) areas (Maniar and Piccoli, 1989), whereas the younger granites as well as the Huangtongjiang gabbro plot mainly in the metaluminous area and coincident with the IAG (island arc granite), CAG (continental arc granite) and POG (post-orogenic granite) areas (Maniar and Piccoli, 1989).

3-7-2. Trace element and REE comparisons between granite suites

Trace elements in individual granites of the Hetai Area show significant indications of source rocks and granite evolution. The enrichment of different element assemblages may represent the different source regions of granites but also may reflect the different petrogenetic evolution process the granite has undergone. The distributions of elements in granites of different ages may also display significant changes although the granite source region may be substantially the same type. The individual discussions of genesis in the preceding sections suggest that the older granites are derived from crustal regions (S-type); whereas the younger granites are derived from deeper (lower crust and upper mantle) source materials (I-type), and the alkali-feldspar granites are particularly highly differentiated. The multi-element spiderdiagrams from granites of different ages are compared in Fig.3.35, and it can be seen that (1) the element distribution of the older granites differs from the younger granites ; (2) the later group, particularly the Yanshanian granites display the highest contents of both LILE and HFSE; whereas the older granites show relatively low content and slight inclined-right curve. In general, both LILE and HFSE become more enriched from Caledonian (older granite) to Yanshanian (younger granite). In addition, their chondrite-normalized REE distribution patterns display significant changes (Fig.3.36). Generally, the REE distribution patterns of the older granites (with the exception of the Shijiang complex) display lower LREE/HREE and a strong negative Eu anomaly. The

younger granites display higher LREE/HREE and a weak negative Eu anomaly, but patterns of the Yanshanian granites are characterized by symmetrical V-shaped curves of low LREE/HREE with a strong negative Eu anomaly.

3-7-3. Tectonic interpretation by geochemical discrimination

Pearce (1984) used trace element discrimination diagrams for the tectonic interpretation of granites, and subdivided granites into four groups in Nb-Y, Ta-Yb, Rb-(Y+Nb) and Rb-(Yb+Ta) diagrams. Samples of the Hetai granites plotted in these diagrams (Fig.3.37) display considerable overlap, and they are difficult to distinguish by Pearce's tectonic discrimination diagrams. However, since a plate collision event is a long dynamic process which might pass from an initial stage of oceanic lithosphere subduction through a period of continental orogeny and crustal thickening to a period of stabilized continental lithosphere, a large number of source regions for collision magmas is implied and overlap with other tectonic settings is predictable. In addition, because Rb and Nb generally present an evolutionary trend during differentiation of granite magmas, in some granite complexes, the Rb and Nb abundance vary from early to late in an evolution series.

Rb/Sr, (Sc+V) and (Nb+Ta) will be used as geochemical discrimination parameters to identify the source rocks and to interpret the magma and evolution of the Hetai granites. The use of Rb/Sr in place of Rb may magnify contrasting geochemical trends, in order to separate different granites. Because Sc and V usually do not form independent minerals in granitic magma processes, they may effectively reflect geochemical trends of magma and specific source rocks and tectonic evolutions of granites.

First, the granites of different ages are discriminated in the diagrams of (Nb+Ta) vs Rb/Sr and (Sc+V) (Fig.3.38). The Caledonian granites plot in the areas of high Rb/Sr but low (Sc+V) and (Nb+Ta). The Hercynian granites once again separate into two, the Guangning biotite monzogranite falls in the area of relative high Rb/Sr but low Sc+V and Nb+Ta, whereas the Yunlougan granodiorite in the area of low Rb/Sr and Nb(+Ta) but high Sc+V. The Indosinian and Yanshanian granodioritic enclaves are located in the low Rb/Sr and Nb+Ta but high Sc+V, and their Indosinian (Wuchun) host megacryst monzogranites and the Yanshanian host alkali K-feldspar granites are distributed in the areas of high Rb/Sr

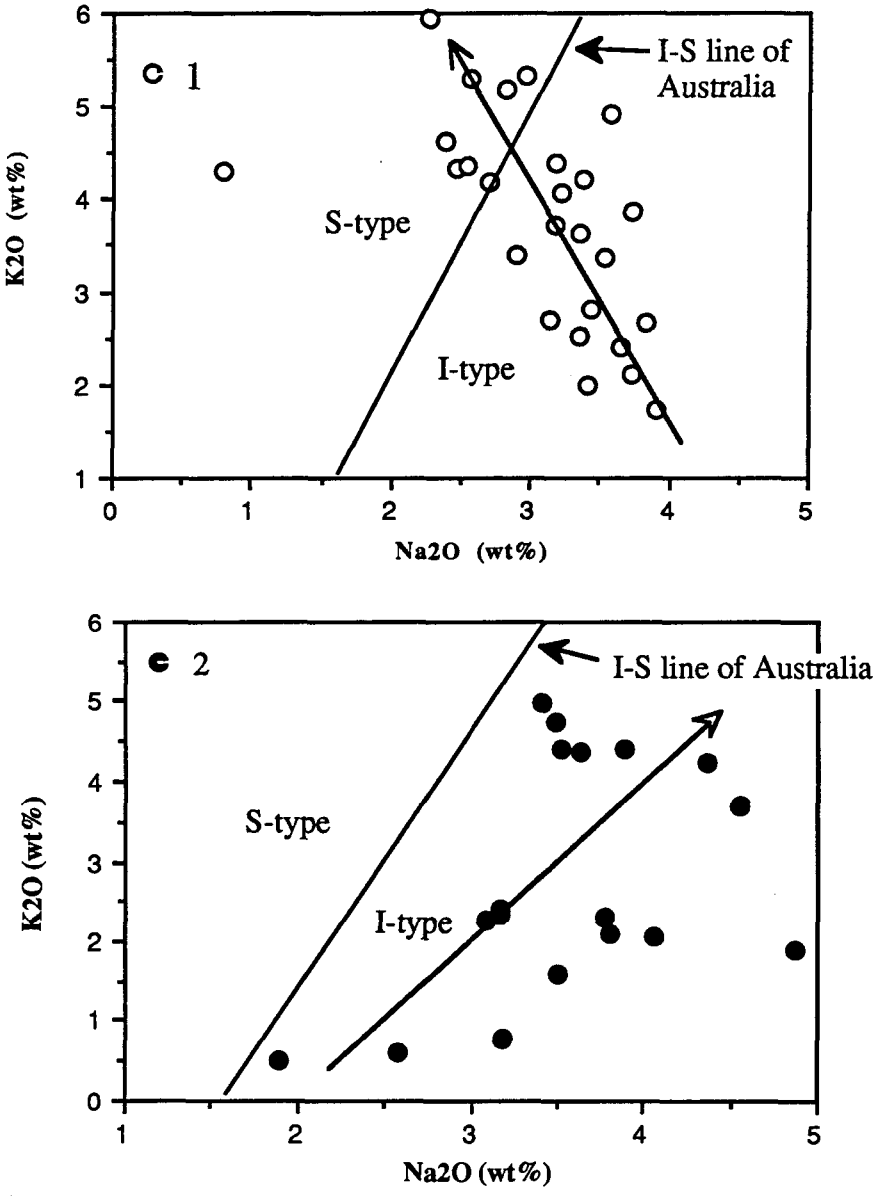

Fig. 3.33. Na2O-K2O comparison between the Hetai granites and I-S type granites of Australia and southeastern Asia. 1 : Older granites; 2 : Younger granites (After Chappell and White, 1984;Cobbing et al., 1986)

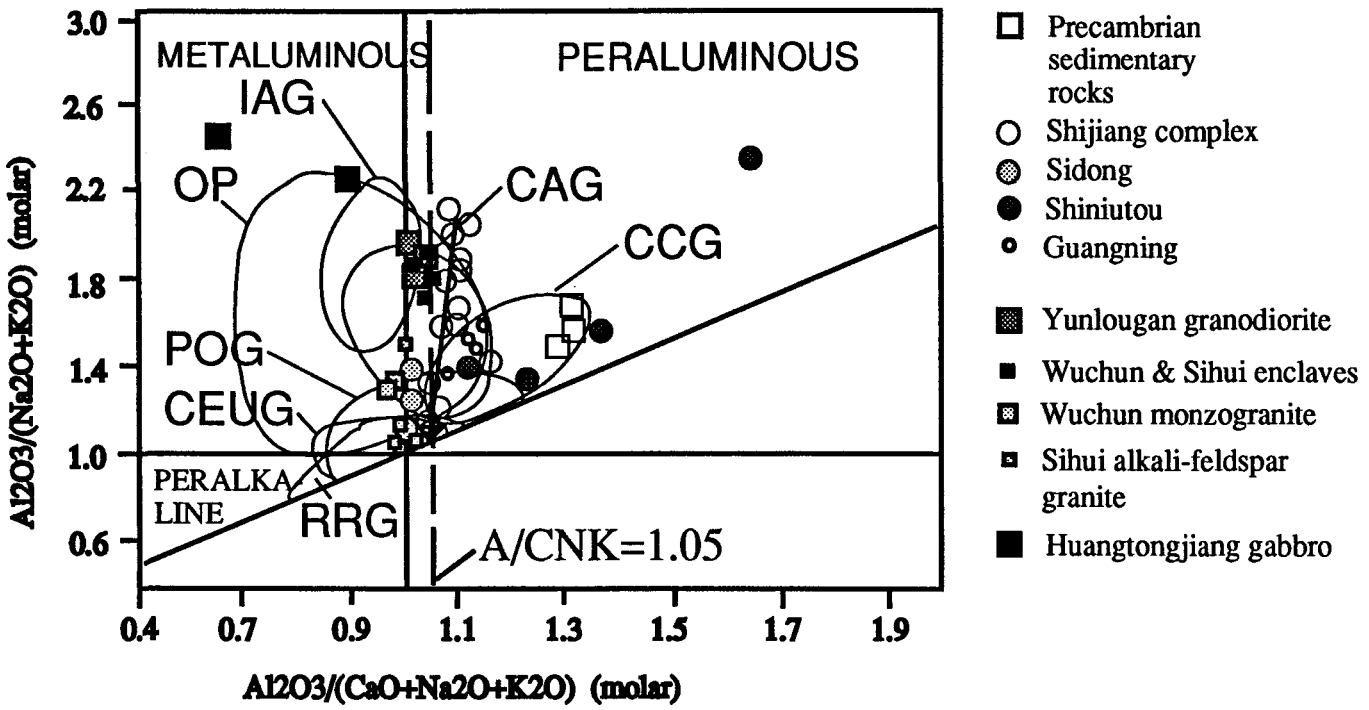

IAG=island arc granite, CAG=continental arc granite,
CCG=continental collision granite, POG=post-orogenic granite
RRG=rift-related granite, CEUG=continental epeirogenic uplift
granite, OP=oceanic plagiogranite (after Maniar and Piccoli, 1989)

Fig. 3.34. Mol. Al2O3/(CaO+Na2O+K2O)-Al2O3/(Na2O+K2O) (A/CNK-A/NK) diagram of different granites in the Hetai Area

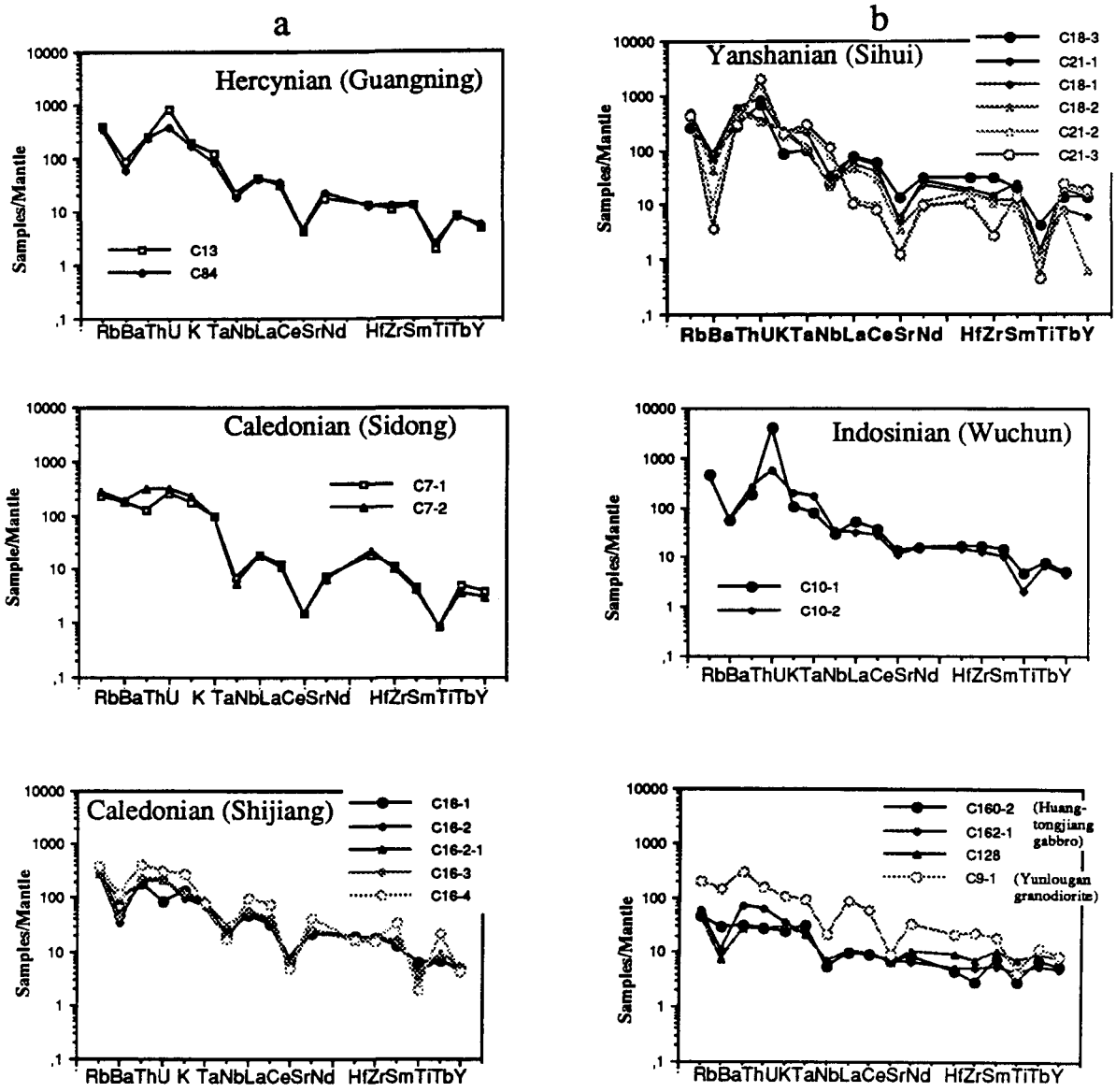

Fig.3.35. Comparison between spiderdiagrams of different granites in the Hetai Area.

a : Older granites; b : Younger granites

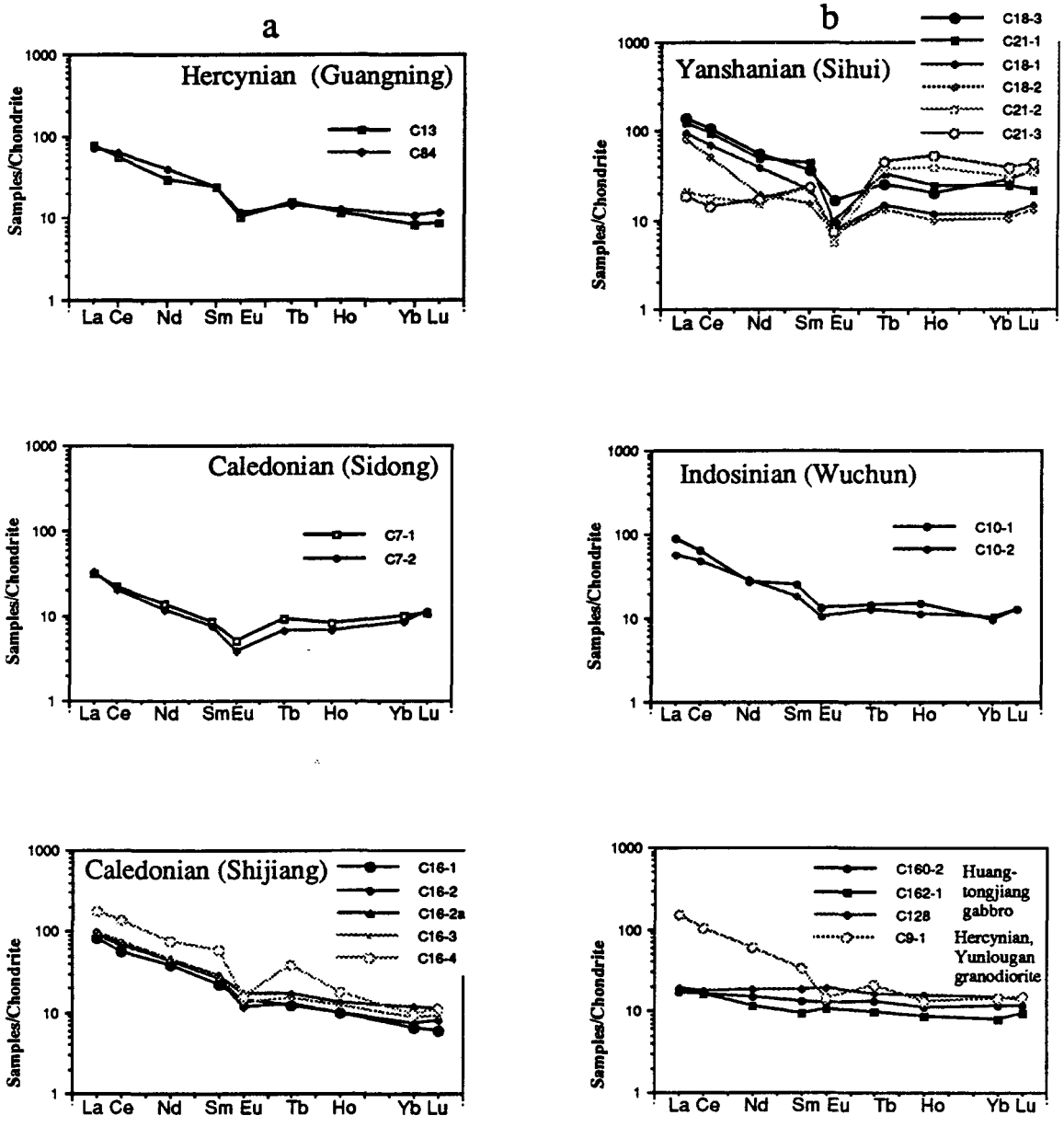

Fig.3.36. Comparison between chondrite-normalized REE diagrams of different granites in the Hetai Area. a : Older granites; b : Younger granites

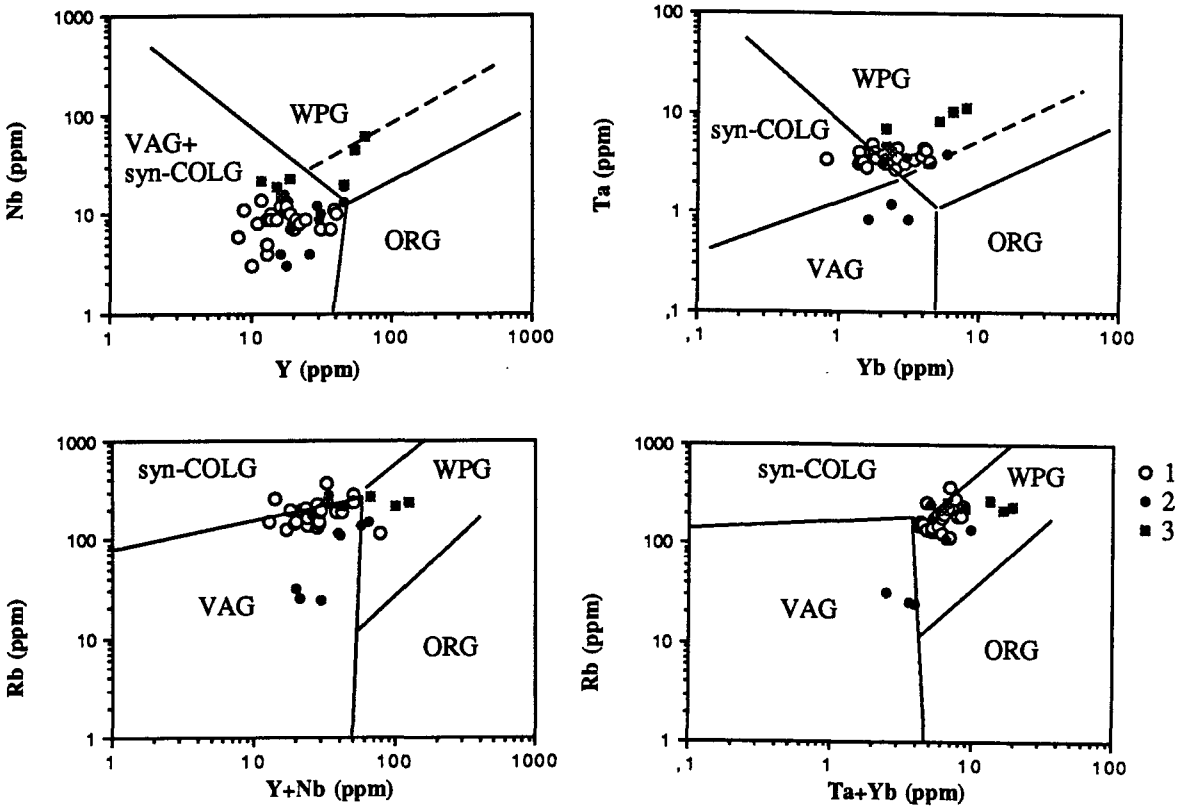

Fig.3.37. Comparison between different granites by Pearce's (1984) diagrams.
1 : Older granites; 2 : Younger granodiorites and gabbro; 3 : Younger granites
syn-COLD=syn-collision granite; VAG=volcanic arc granite; WPG=within plate granite; ORG=ocean ridge granite

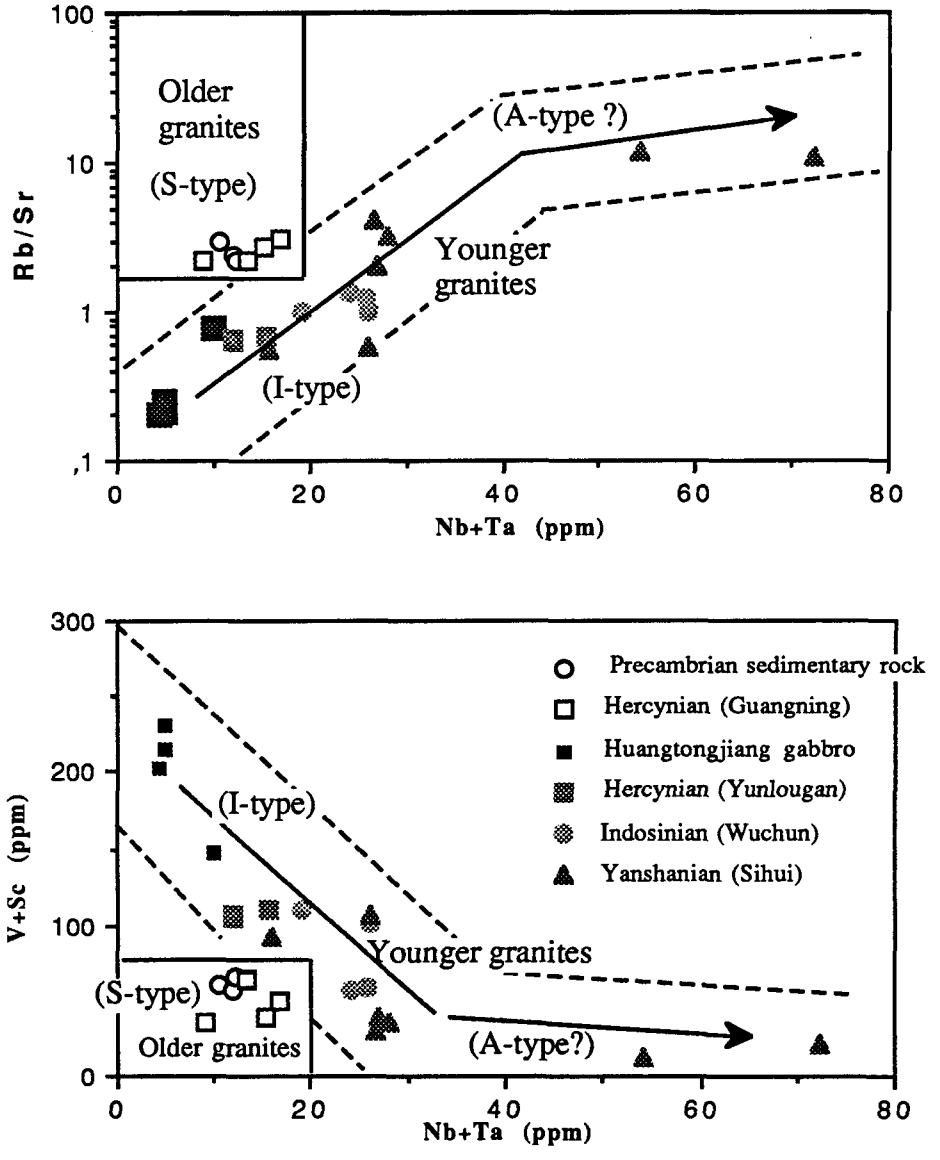

Fig. 3.38. Variations of Rb/Sr-(Nb+Ta) and (V+Sc)-(Nb+Ta) between granites of different ages in the Hetai Area

and Nb+Ta but very low Sc+ V. In addition, the Huangtongjiang gabbros are located in the areas of the lowest Rb/Sr and Nb+Ta but the highest Sc +V (Fig.3.38).

Furthermore, comparison between granites of different ages in the Wuchuan-Sihui Fault Zone shows that the Yanshanian granite suite (Sihui granite suite) is very different from the Caledonian granites (Shiniutou granite) in Rb/Sr-Sc+V and -Nb+Ta diagrams (Fig.3.39). It displays a different distributions of Rb/Sr, Sc+V and Nb+Ta, although they have similar SiO2 and K2O contents, demonstrating the different genesis and evolution between the older granites and younger granites.

All the Hetai granites are compared in Fig.3.38, and it is clear that the older granites are concentrated in a limited area of high Rb/Sr and Nb+Ta but low Sc+V; whereas the younger granites are distributed over a wider area from low Rb/Sr and Nb+Ta but high Sc+V to high Rb/Sr and Nb+Ta but low Sc+V. This implies that the younger granites may be derived from the same basaltic magma source and belong to a calc-alkaline to alkaline geochemical series. When the granite data is compared with data from other well studied areas such as the Lachlan Foldbelt, Australia (Chappell,1984; Wyborn, 1981; Collins et al., 1982), Japan and Korea (Tsusue et al., 1989), East Malaysia (Vogt and Flower, 1989) and South Africa (Kleemann and Twist, 1989) in the Nb+Ta vs Rb/Sr and Sc+V geochemical discrimination diagrams (Fig. 3.40), it is interesting that the known S-type examples are mainly located in a limited area of high Rb/Sr and Nb+Ta but low Sc+V, whereas the I-type examples are distributed in the area of low Rb/Sr and Nb+Ta but high Sc+V , and A-type samples in the area of very high Rb/Sr and Nb+Ta but very low Sc+V. In general, this compares well with different types of the Hetai granites, with a slight difference for A-type samples, because in the Hetai Area, the alkali-feldspar granites with high Rb/Sr and Nb+Ta but low Sc+V may be the result of differentiation of an igneous source magma (I-type), rather than a independent alkaline magma source like most A-type granites (Collins, 1982).

After comparing the Hetai granites with other examples, it may be inferred that the older granites may be derived from a continental collision environment, whereas the younger granites are produced in a subduction environment and the alkali-feldspar granites result from an extension environment. For the continental collision environment, the remelting of the aluminous crustal rocks may be a major process for granite formation, but not metamorphic replacement as this type of granite usually contains higher LIL elements

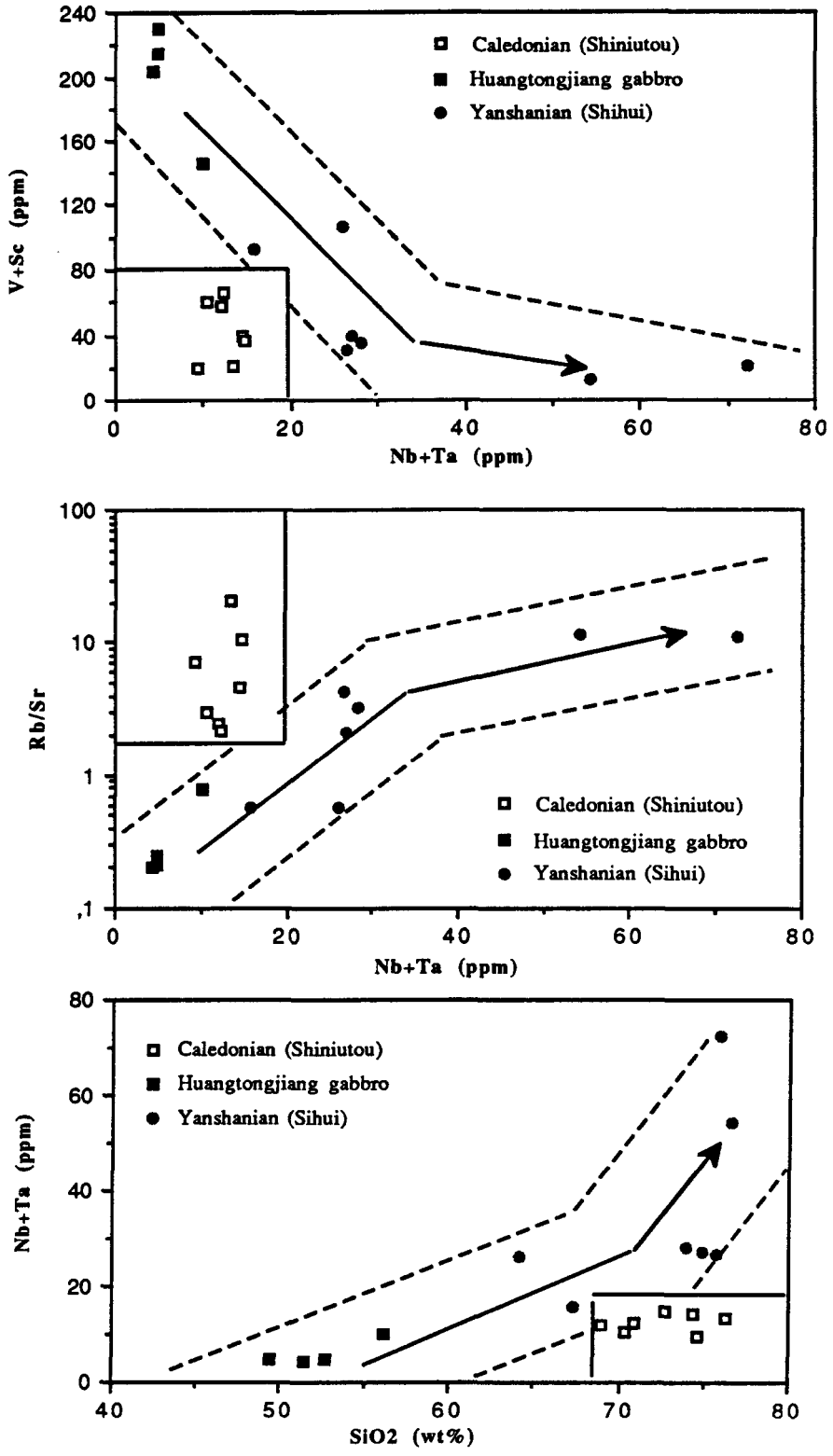

Fig. 3.39. Comparison between granites of different ages in the Wuchun-Sihui Fault Zone

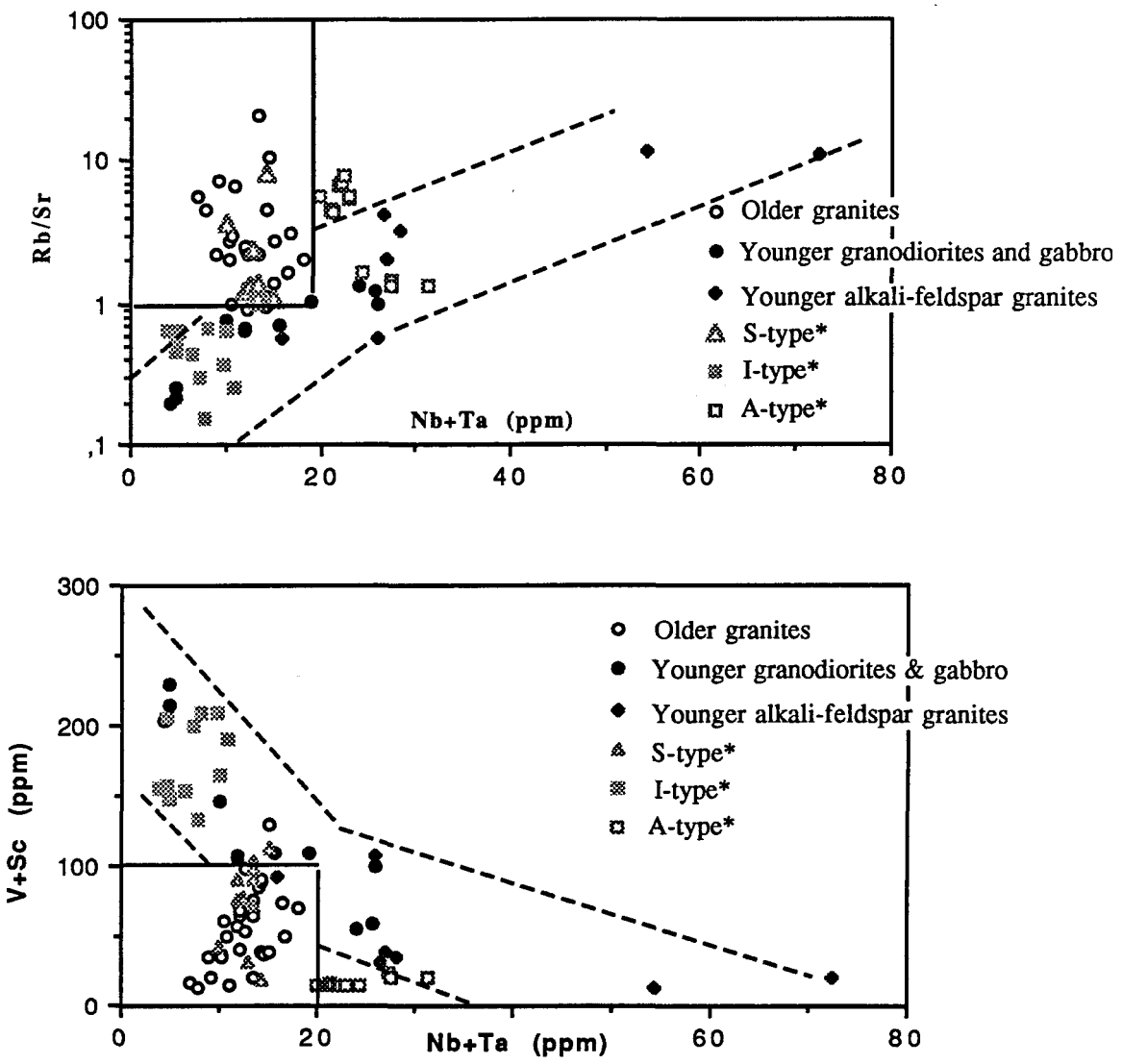

Fig. 3.40. (Nb+Ta) vs Rb/Sr and (V+Sc) variation diagrams between different granite types
* after Chappell (1984), Collins et al. (1982), Tsusue et al. (1989), Vogt & Flower (1989) and Kleemann et al. (1989)

but low HFS elements and mafic components. The subduction-derived magmas may differentiate and evolve to form granites, which are originally characterized by higher mafic components and lower LIL elements. The granitic magmas produced in the extension environment appear to have evolved from deeper source magmas and the alkali-feldspar granites may be produced from a more differentiated magma, which has both high HFS and LIL elements. The granite evolution series of the Sihui complex suggests that the extension environment may be related to the last stage of the subduction process, as these more differentiated granites are characterized by high LIL and HFS elements, demonstrating evolutionary features.

3-7-4. Au distribution in different granites

The Precambrian metamorphosed sedimentary rocks are regarded by many geologists as the ultimate gold source for the Hetai gold deposits (Dai, 1986; Chen et al. 1988; Fu, 1988; Zhou, 1992). As a result, the Au distribution in the different granites has not been considered. A brief survey of Au contents of the different granites of the Hetai Area is presented here, in order to suggest any possible relation between Au enrichment and different granite types.

The Au contents in the various granites (Table 13, see Appendix III) show different trends. The Au contents in the Shijiang dark enclaves are very low, 0-2.5 ppb, lower even than those in the Precambrian metamorphosed sedimentary rocks, 2.5-3.6 ppb. Similarly, Au contents in the Caledonian Shijiang and Sidong granites show low but stable contents from 0.3-3.1 ppb, except for the Shiniutou granite which has a greater variation, from 1.8-42.9 ppb. The Guangning (Hercynian) biotite monzogranite also has low Au contents, only 0.8-4.5 ppb, whereas the Yunlougan granodiorite has higher Au contents, 8.2-12 ppb. The Au contents of the Wuchun (Indosinian) granodioritic enclave vary from 4.1-13 ppb, and those of the megacryst monzogranite vary from 9.6-11 ppb. The Sihui (Yanshanian) granites vary from 1.6-6.8 ppb Au for the granodioritic enclaves, and 3.3-6.6 ppb Au in the alkali-feldspar granite. The Huangtongjiang gabbro has the highest Au contents, 7.5-15 ppb.

Putting all data in the diagrams (Fig.3.41) of SiO_2-Au, MgO/(MgO+FeO)-Au, K_2O-Au, K_2O/Na_2O-Au, Rb/Sr-Au, (Nb+Ta)-Au, Sc-Au and V-Au, it can be seen that Au

distribution in different granites displays certain regular trends. First, the older granites compare with the Precambrian metamorphosed sedimentary rocks in the lower Au distribution areas, whereas the younger granites are distributed in the higher Au area, demonstrating that, in the Hetai Area, the Au contents of the older granites (Collision type) is obviously lower than that of the younger granites (Subduction-Extension type). Secondly, Au variation trends in the subduction-extension type granites show a regular decrease with increase of SiO_2, K_2O, Nb+Ta and Rb/Sr, but show positive correlations with MgO/(MgO+FeO), Sc and V. Thus, Au contents decrease with granite differentiation. The Huangtongjiang gabbro presents the highest Au distribution. It may be inferred that the higher Au distribution in the younger granites derived from deeper source regions is closely related with basic magmatism. Thus, the granites derived from the deeper source region are more likely to play a role for gold mineralizations in the Hetai Area than the older granites.

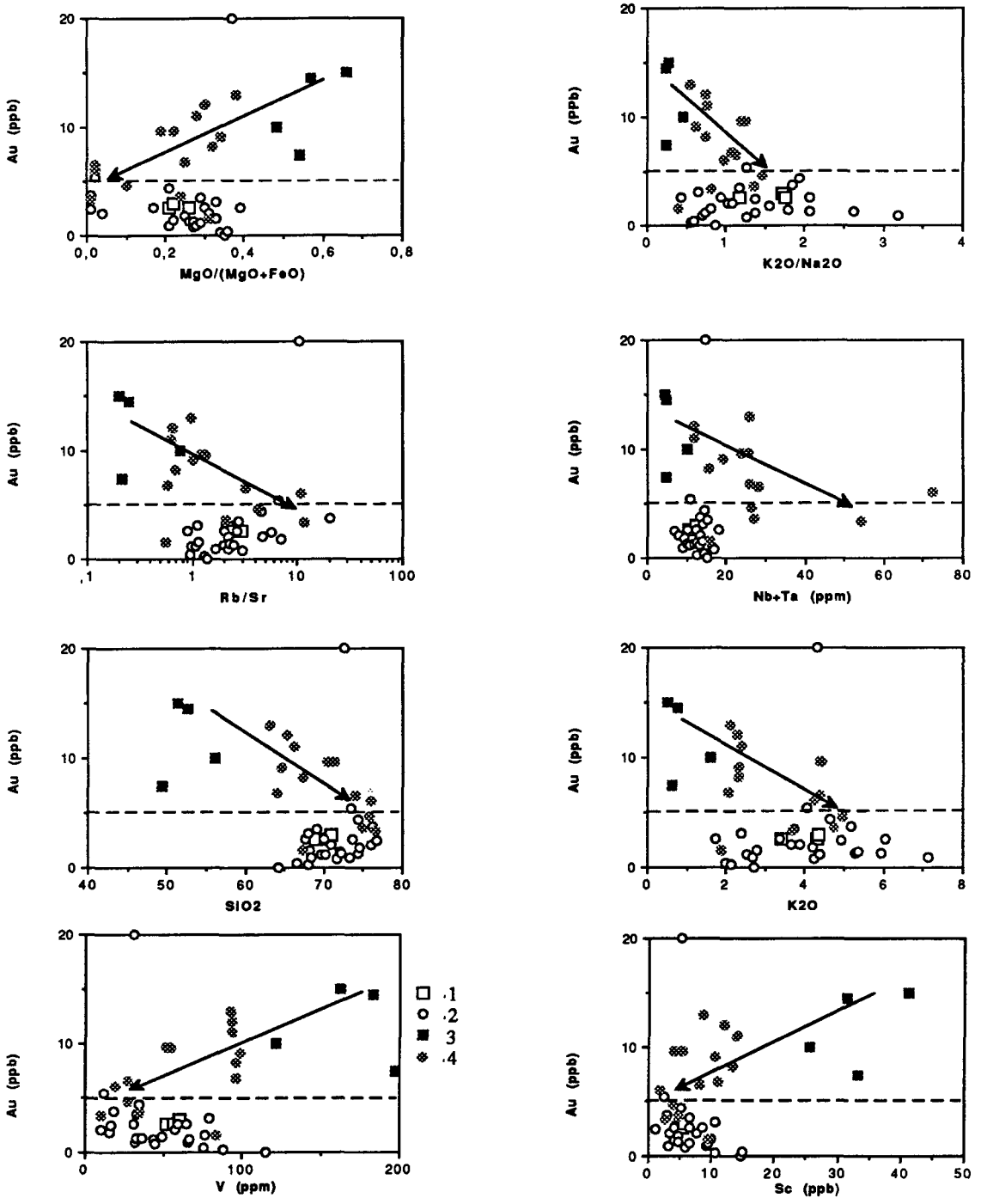

Fig. 3.41. Au distribution trends in different type granites of the Hetai Area.

1 : Precambrian sedimentary rocks; 2 : Older granites;

3 : Huangtongjiang gabbro; 4 : Younger granite suites

CHAPTER IV

CHEMICAL CHARACTERISTICS OF BIOTITE, AMPHIBOLE AND FELDSPAR

4-1. Introduction

Biotite, amphibole and feldspar are common rock-forming minerals of granites, and they are representative of Si+Mg(Fe) and Si+Al compositions in the granite system, respectively. In particular, biotite and feldspar cover the entire process of granite crystallization, so their chemical characteristics reflect both the magmatic evolution and the source of the magma. Amphibole, in contrast to biotite and feldspar, is not as widely distributed in granites, but its presence is significant to interpret magma genesis. Amphibole is common in I-type granites, but rare in S-type suites. Biotites from the Hetai granites are systematically examined because of their wide distribution and sensitive response to physico-chemical variation in the granite system.

Controls on the composition of igneous biotite are only imperfectly known (Speer, 1982), and in most cases, understanding of magmatic evolution of a pluton is necessary to understand the behavior of the biotite. Heinrich (1946) first noted a correlation between the chemical composition of biotites and different kinds of host rocks and presented the variation of chemical compositions of igneous biotites with rock type in a MgO--(Fe_2O_3+TiO_2)--(FeO+MnO) ternary diagram, showing that biotites from different rock types have restricted but not unique compositional fields. Foster (1960) further interpreted the chemical compositions of trioctahedral micas and proposed a crystal chemical classification of micas in the Mg--Al(VI)+Fe^{3+}+Ti^{4+}--Fe^{2+}+Mn ternary diagram, subdividing biotite into Mg-biotite and Fe-biotite. Wones (1965) proved the relations

between Mg^{2+} and Fe^{2+} components in biotite and T (temperature), fO_2 (oxygen fugacity) and fH_2O (water fugacity) of magma crystallization by means of high temperature and pressure experiments, and indicated that Mg-biotite is more stable than Fe-biotite under high temperature conditions. Later, Wones (1981) and Naney (1980) compared the associated mineral assemblage and chemical compositions of biotites with host granites, and suggested that mafic minerals (biotite and amphibole) may be regarded as indicators of intensive variables (T, P, fO_2 and fH_2O) in granitic magmas. Ague (1989) discussed the distribution of Fe and Mg between biotite and amphibole in granitic rocks, and indicated the effects of temperature and presssure on biotite and amphibole composition. These results laid the foundation for the study of geochemical features of biotites in granites.

Chemical compositions of biotites from granites have been used as indicators of magma evolution. For example, Dodge et al. (1968, 1969) studied the chemical features of biotite and hornblende from granitic rocks of the Central Sierra Nevada Batholith, California, and found that the biotites have uniform major element compositions with $Fe^{2+}/(Fe^{2+}+Mg)$. Kanisawa (1972, 1976) and Czamanske (1986) studied biotites and hornblendes from granitic rocks in Southwestern Japan, and showed that the chemical composition of biotites and hornblendes may be used as indicators of magma source. Weiss and Troll (1989) calculated the T, P, fO_2 and fH_2O based on the chemical compositions of biotite, amphibole and feldspar from the Ballachulish Igneous Complex, Scotland, and demonstrated the crystallization evolution trend of a monzodiorite--quartz diorite suite. Cocherie et al. (1984) used the chemical compositions of biotite and amphibole as well as trace elements in rocks to reveal the evolution trends of granitoids in the Variscan calc-alkaline plutonism of western Corsica, France. Henderson et al. (1989) analyzed the biotite and amphibole as well as isotopic compositions of whole rocks from the Red Hill Alkaline Igneous Complex in New Hampshire, U.S.A, and indicated that the alkaline complex may be formed by emplacement of fractionated magmas derived from a lower-level magma chamber which initially contained a basaltic parent magma. Farrow and Barr (1992) analyzed the hornblendes from diorite, quartz diorite, tonalite and granodiorite in the southeastern Cape Breton Highlands, Nova Scotia, and they suggested that these hornblendes contain high Al2O3 because they crystallized at high pressure from an Al2O3 rich magma derived from a continental margin subduction zone.

The distinctive character of the ferric-ferrous ratio of biotites and the relation between the ratio and the oxide assemblages have been used by Ishihara (1977) and Ishihara et al. (1977) to characterize his magnetite-series and ilmenite-series of granitic rocks in Japan, and Whelan (from Speer, 1982) subsequently showed that I-type granites have higher oxygen fugacity, but there is so far insufficient data on biotites to develop this hypothesis of genetic classification of granites. The FeOt and MgO of biotites from granites of South China (Hong, 1982) show that Mg-biotite and Fe-biotite are closely related to different granite types.

In an attempt to characterize the relationships between chemical composition of biotites and different suites of granites, Yang et al. (1986a, 1988a and 1988b) analyzed biotites from many granite complexes in South China and compared them with biotites from some well studied areas such as Lachlan Fold Belt of Australia, Japan and Nevada, indicating that the different genetic type granites can be distinguished by different chemical signatures of biotites in Mg--Al(VI)+Fe^{3+}+Ti^{4+}--Fe^{2+}+Mn ternary chemical classification (Fig. 4.1). The Mg-biotite, lower in FeO, Al_2O_3, Li, Rb, Zn, Sn, W, Nb, Ta and REE, suggests the host granites derived from the lower crust or upper mantle source region such as the Yangtze and Coastal granites in South China; whereas Fe-biotite, higher in Al_2O_3, Li, Rb, Zn, Sn, W, Nb, Ta and REE, suggests the granites generated from peraluminous crustal source regions such as the Nanling granites in South China. Yang et al. (1986a, 1988a, 1988b) established a series of geochemical criteria for biotites in order to distinguish various granites in South China. This earlier work on biotite is an important reference for the Hetai Area, because it is located in the same geotectonic setting of South China.

The chemical features of biotites may also be used as metallogenic indicators in granites. Mason (1978) analyzed the chemical compositions of biotites and amphiboles of the porphyry copper-bearing and barren granitic plutons of Papua New Guinea, and on the basis of their $Fe_t/(Fe_t+Mg)$ content variation, he concluded that the mineralized granites have high oxygen fugacities but the barren plutons have low oxygen fugacities. Similarly, the studies of tin-bearing granites in the Blue Tier Batholith of Tasmania (Groves, 1972) indicate that the Sn content of biotites from granites associated with Sn mineralizations is higher than that of biotites from barren granitic plutons. Yang et al.(1988a, 1988b) noted that there is a positive correlation between Sn, W, Nb, Ta and REE contents of biotites and

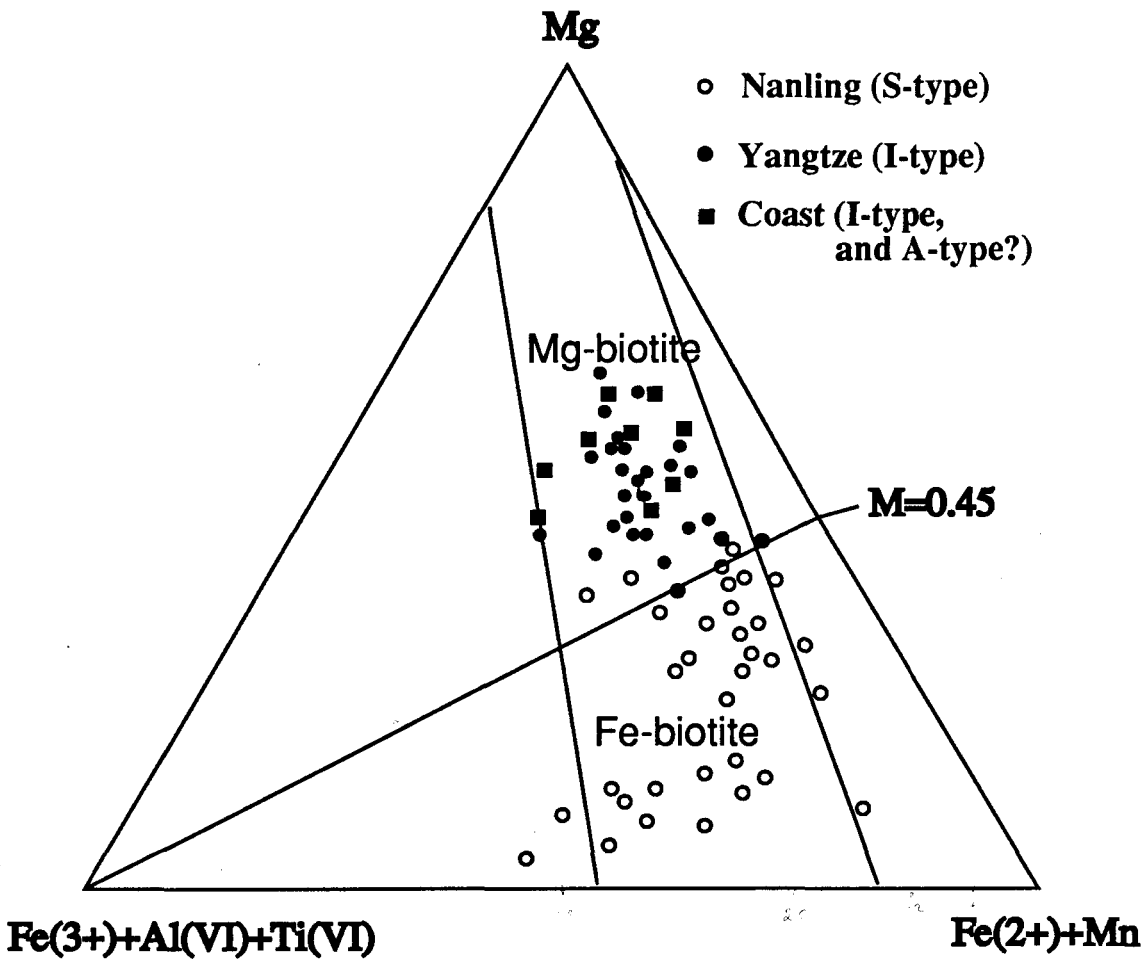

Fig.4.1. Biotites from different granite types of South China on the ternary chemical classification (Foster, 1960; data from Yang,1986)

their host rocks in the South China granites, and the biotites rich in these trace elements usually indicate a high mineralization potential for the host granites.

It is clear from research results that some elements and element ratios such as Mg, Fe, Al and $Mg/(Mg+Fe^{2+})$ are useful for discussing chemical compositions of mafic rock-forming minerals in granites. According to the crystal chemistry of biotite and amphibole, the substitutions between Si <--Al and Mg<--Fe^{2+} may lead to a series of significant geochemical changes and may establish a certain geochemical relationship between mafic minerals (biotite and amphibole) and granite types. The chemical variations of biotite and amphibole are controlled not only by their crystal chemical properties but also by the chemical composition of granitic magmas. In addition, Ti may substitute for Si or Mg depending on Al contents of the magma, so a significant geochemical relationship exists between Ti and Al during granite evolution. Therefore, SiO_2, Al_2O_3, TiO_2, MgO, FeO and MgO/FeO, $Mg/(Mg+Fe^{2+}+Mn)$ and Al(VI)/Ti in biotite and amphibole may be regarded as important indicators for discussing geochemical changes in mafic minerals and for distinguishing granite type and evolution. On the other hand, CaO, Na_2O and K_2O, which are the principal components of feldspar, also are important for discussing geochemical characteristics of feldspar associated with different granite types and evolution.

Few biotites from the Hetai granites have been analyzed (Dai, 1986), but no detailed studies performed. Biotite is widely distributed in the Hetai granites, often in all phases of polyphase intrusions, but amphibole only occurs in some granite bodies. Considering the significance of biotite and amphibole chemistry for distinguishing granite suites, the chemical compositions of biotites from individual granite bodies of the Hetai granites have been analyzed and compared with those from different granite types of South China and other areas in a series of related discrimination diagrams, in order to establish geochemical criteria for distinguishing granite types. The feldspars were also analyzed, in order to characterize the granite types.

Major oxides of biotite, amphibole and feldspar were analyzed by means of the electron microprobe at UQAC, and these major oxides and some trace elements such as Li, Rb, Zn, Ni, Co and F of selected biotite minerals were also determined by wet chemical analyses at the Institute of Geochemistry, Academia Sinica. Electron probe analyses of biotites does not distinguish Fe^{3+} but consider only total Fe. For this study, Fe^{2+} and Fe^{3+}

contents of biotites were obtained by means of the wet chemical analyses of selected biotite concentrates.

4-2. Chemical compositions of biotites

As the biotites are present in all granites of the Hetai Area, the chemical compositions of biotites from the individual granite bodies are described in the following age order : Caledonian, Hercynian, Indosinian and Yanshanian.

4-2-1. Chemical features of biotites from the Caledonian granites

Biotite is the predominant mafic mineral in the Caledonian granites, and the samples determined are respectively collected from the Shijiang, Sidong and Shiniutou granite bodies. Their chemical compositions are compared directly in Appendix III (Table 14).

(1) Biotites from the Shijiang complex

The biotites from the Shijiang granite series (Table 14) generally contain low SiO_2 (34.21-36.35 %), TiO_2 (1.15-2.87) and Fe_2O_3 (1.87-2.09), but high Al_2O_3 (17.06-19.18). The TiO_2/Al_2O_3 ratios are low, 0.13-0.16. In contrast to biotites from the Sidong and the Shiniutou granites, the Shijiang biotites contain relatively high MgO (7.30-8.91) but low FeO (19.86-22.04), so the ratios of MgO/FeO are relatively high (0.33-0.44). All biotites from the Shijiang complex plot in the Fe-biotite area but near the classifying line, and their magnesium parameter M is commonly less than 0.45 in the ternary chemical classification of biotites (Fig.4.2), similar to biotites from the Nanling granites and from S-type granites.

It is clear from Table 14 that biotites from dark enclaves contain higher MgO (8.71-11.09) but lower FeO (17.50-19.78) than those from the Shijiang intrusive series. In addition, they present relatively higher SiO_2 (35.15-37.89 %) but lower TiO_2 (2.34-2.98) than those of host granite. The TiO_2/Al_2O_3 ratios are lower (0.13-0.17) but MgO/FeO

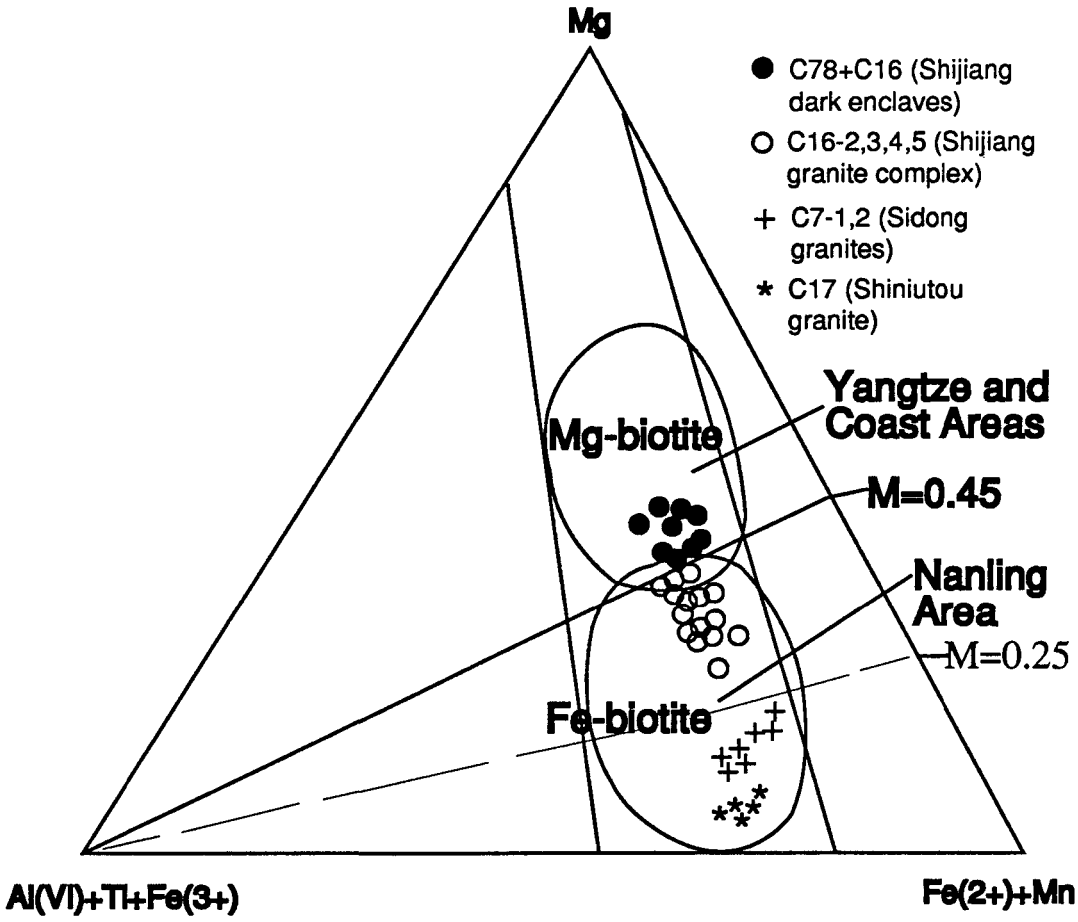

Fig.4.2. Biotites from the Caledonian granites and from their enclaves on the ternary chemical classification
(After Foster, 1960 and Yang et al., 1986a)

relatively high (0.45-0.57), and in the ternary chemical classification of biotite (Fig.4.2), these biotites plot in the transitional area between Mg- and Fe-biotite with M values from 0.44 to 0.49. The calculated chemical formulas of the Shijiang biotites are characterized by an aluminum component, Al(VI) about 0.62-0.82 and Al(VI)/Ti ratios > 2.0, confirming that the source rocks of the Shijiang granites are characterized by a peraluminous composition.

The chemistry of the biotites from the Shijiang host granites and their enclaves may be explained as : (1) the result of derivation from source rocks which are partly mixed with I-type materials and their biotites may contain higher Mg components because Mg has priority over Fe in occupying sites in the biotite crystal structure when amphibole is not formed; and (2) temperatures not high enough to melt all source rocks, so the biotites relatively rich in Mg may be considered as representative of the unmelted source. Therefore, biotites from the enclaves show Mg enrichment in comparison to those of the host granite. The biotites from both dark enclaves and intrusive series show a regular variation in the SiO_2 vs Al_2O_3, MgO and FeO diagrams (Fig.4.3), SiO_2 and MgO decrease slightly but FeO increases from the dark enclaves to the granites. These biotite variation trends of biotites suggest that the dark enclaves may be the unmelted source of the Shijiang intrusive series, and their source regions may be the Precambrian metamorphosed sedimentary rocks, because biotites from these rocks display similar chemical characteristics as shown in Table 14 and Fig.4.3.

(2) Biotites from the Sidong granite

The chemical compositions of biotites from two intrusive phases of the Sidong granites can be seen in Table 14. It is evident from these data that the major elements of biotites from the two phases display common features of high FeO (>20 %) and low MgO (<8.0). In the ternary chemical classification of biotite (Foster, 1960; Yang et al., 1986a), all samples from the two phases plot in the Fe-biotite area, with a magnesium-parameter M < 0.45 (M<0.25) (Fig.4.2), and are coincident with those of the Nanling granites.

In general, biotites from the same granite sample present comparable chemical composition, both from different mineral grains and from the center to the margin of individual biotite grains. However,the chemical compositions of biotite vary from different

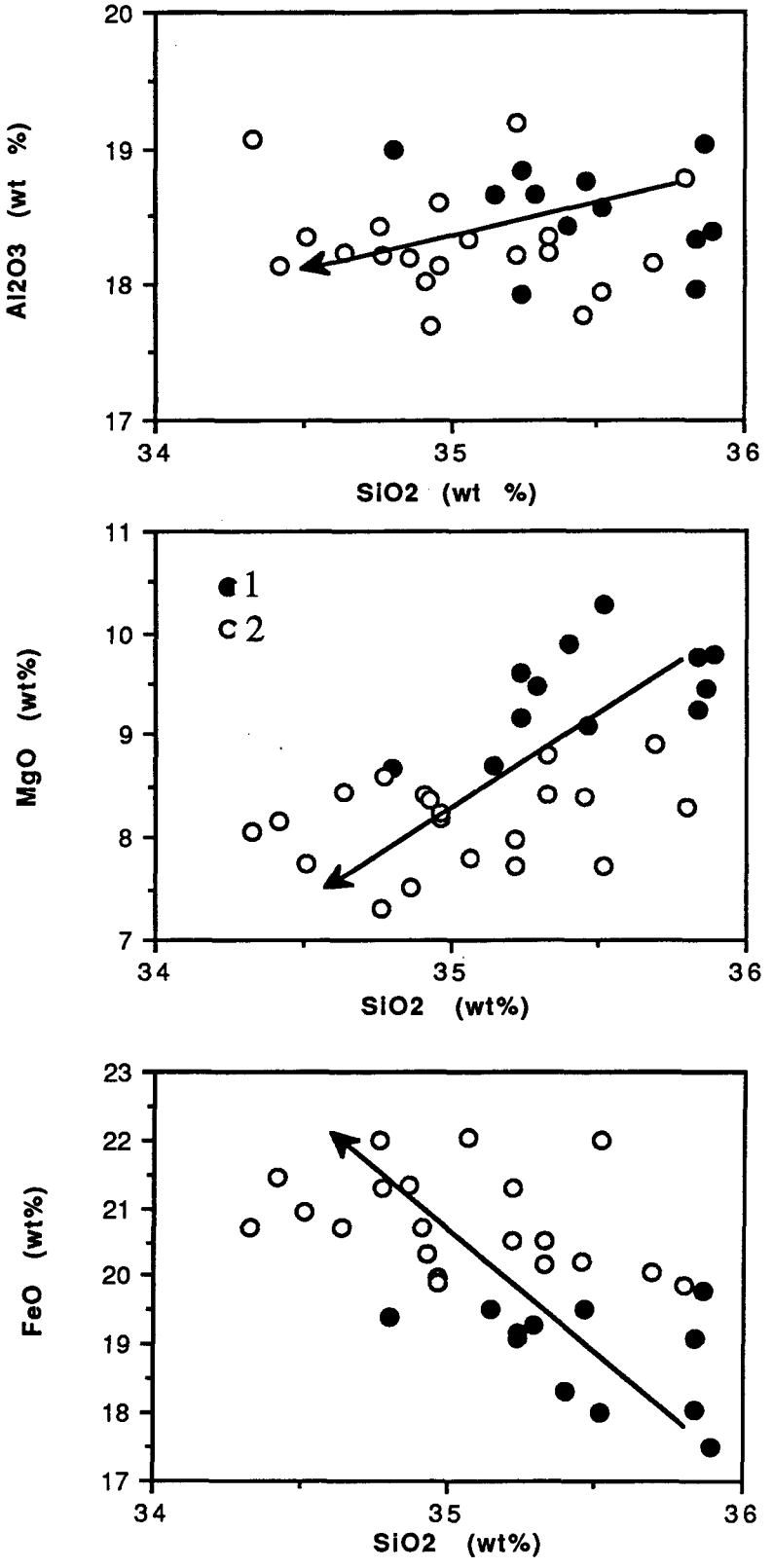

Fig.4.3. Variation of biotites from the Shijiang dark enclave and host granite
1 : Dark enclaves ; 2 : Host granites

intrusive phases in a series. The biotites from the early intrusive phase, coarse-grained granite (sample No. C7-1), contain higher TiO_2 (2.45-2.99), MgO (3.78-4.13), FeO (27.71-28.31), but lower Al_2O_3 (14.17-14.94) and Fe_2O_3 (3.35-3.78) than biotites from the later intrusive phase, medium-fine grained granite (sample No. C7-2), which contain lower TiO_2 (1.59-2.85), MgO (2.89-2.99), FeO (25.69-26.91), but higher Al_2O_3 (15.81-17.08) and Fe_2O_3 (4.63-4.85). It is evident that Al_2O_3 and Fe_2O_3 increase but TiO_2, MgO and FeO decrease from early to late intrusive phases within the pluton. These two intrusive phases probably crystallized at the same temperature, so the decreasing MgO, FeO and TiO_2/Al_2O_3 may reflect magma changes. The increasing ratios of $Fe_2O_3/(Fe_2O_3+FeO)$ may reflect an oxygen fugacity increase with differentiation (Wones, 1965). The calculated chemical formulas of the Sidong biotites are characterized by an aluminum component, Al(VI) about 0.32-0.75 and Al(VI)/Ti >1.0 , demonstrating that the Sidong granites crystallized from a differentiated peraluminous magma.

(3) Shiniutou biotites

The biotites from the Shiniutou granite (No.C17, Table 4.1) are characterized by very low SiO_2 (33.71-34.59), MgO (1.14-1.71) and TiO_2 (1.83-2.68), but very high FeO (27.46-28.68), Fe_2O_3 (4.94-5.18) and Al_2O_3 (16.15-17.97). The ratios of TiO_2/Al_2O_3 and MgO/FeO are low, 0.10-0.15 and 0.04-0.06 respectively. All samples plot in the Fe-biotite area and M values are < 0.45 (M<0.25) in the ternary chemical classification of biotite (Fig.4.2). The chemical compositions of biotites from the Shiniutou are stable in general, reflecting the certain chemical composition of the parent magma of this granite body. The calculated biotite formula (Table 4.1) shows the Shiniutou biotites to have an aluminum component, Al(VI) about 0.56-0.87 and Al(VI)/Ti > 2.24, reflecting a peraluminous magma.

(4) Comparison between biotites from the Caledonian granites

In general, biotites from the Caledonian granites are characterized by high Al_2O_3 but low SiO_2 and TiO_2 contents. Some differences may be seen, for example it is clear from the

diagrams of SiO_2 vs major oxides (Fig.4.4), that the biotites from the Shijiang granites have high Al_2O_3, MgO, MgO/FeO and M value ($0.45<M<0.25$) but low FeO, Fe_2O_3, MnO, TiO_2 and SiO_2, whereas the biotites from the Shiniutou granite contain the highest Al_2O_3, Fe_2O_3, FeO and higher MnO but low MgO, TiO_2, SiO_2, MgO/FeO and M value (<0.25). Those from the Sidong granite are generally similar with Shiniutou, but are rich in Mn. Comparison of the major oxides of biotites from different granites shows that a difference in their MgO/FeO ratio and M value between the Shijiang complex and other granites (the Sidong and Shiniutou) may be mainly due to the chemical composition of the magma. Biotite is the main mafic mineral in these granites, and Mg has the priority over Fe in the biotite crystal structure when the magma crystallizes, so biotite may contain higher Mg if the parent magma is relatively rich in Mg. In addition, the temperature of crystallization may be another factor. Biotite will be Mg rich as Mg has priority at high temperature (Wones, 1965). This factor may not be as important as the chemical composition, because the temperature difference between the Shijiang complex and the others (the Sidong and the Shiniutou) may not be great. Therefore, the source rocks of the Shijiang granites may be more mixed by igneous materials than those of the Sidong and Shiniutou granites, although they all are derived mainly from peraluminous crustal regions.

4-2-2. Chemical compositions of the Hercynian biotites

The chemical compositions of biotites from the Guangning biotite monzogranite and the Yunlougan granodiorite are compared in Table 4.2 (see Appendix III).

(1) Biotites from the Guangning pluton

The biotites from the Guangning granite contain high Al_2O_3 (15.48-16.40 %) and FeO (20.79-22.87), but low SiO_2 (35.00-35.92), TiO_2 (2.47-3.31), MgO (6.78-8.19) and Fe_2O_3 (1.69-2.06), relative to the biotite from the Yunlougan granodiorite (Table 4.2). Similarly, the TiO_2/Al_2O_3 and MgO/FeO ratios are relatively low, 0.16-0.21 and 0.31-0.39 respectively. All samples plot in the Fe-biotite field and the M values are < 0.45 in the ternary chemical classification of biotite (Fig.4.5). The $Fe_2O_3/(Fe_2O_3+FeO)$ ratio is low,

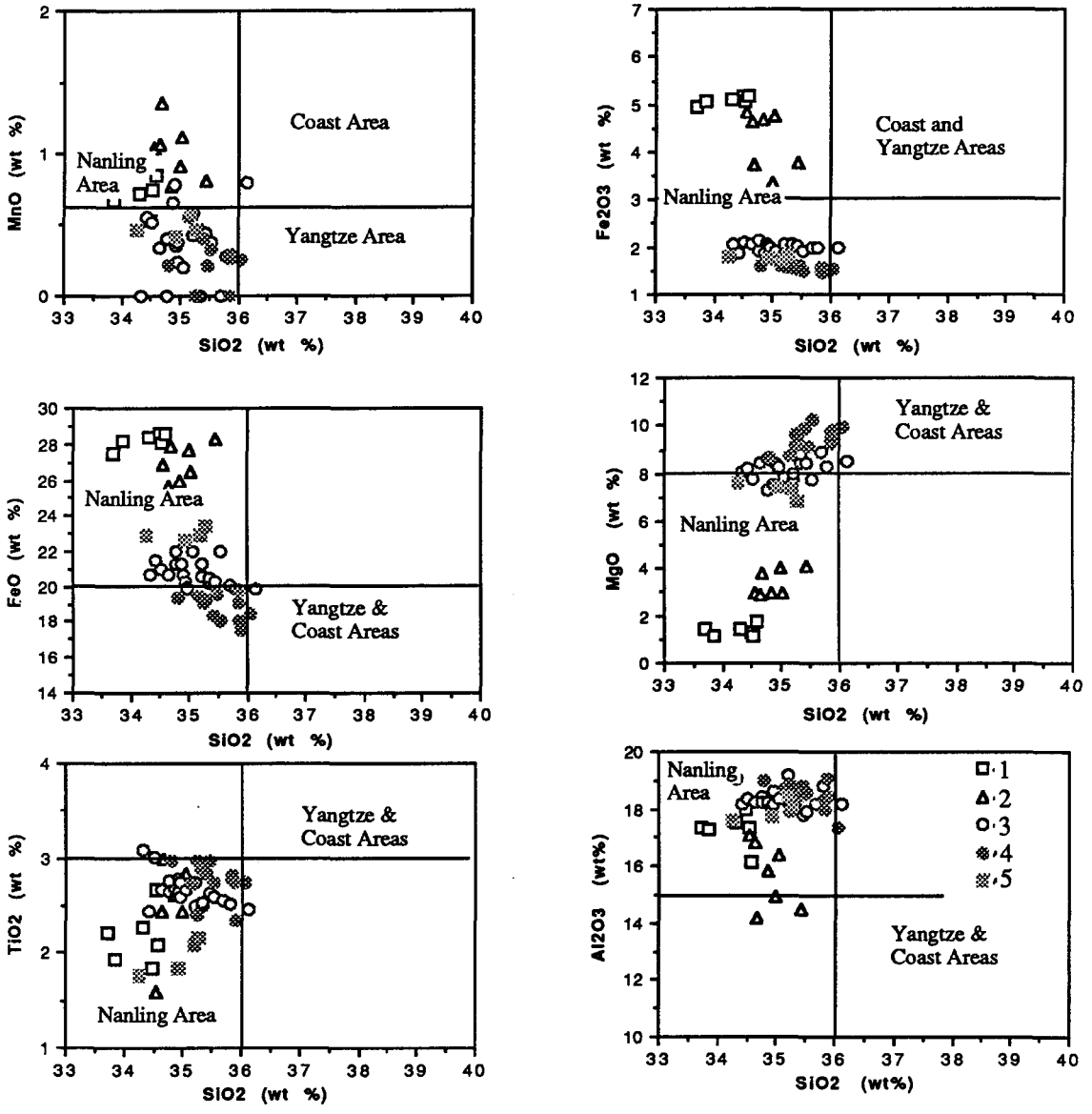

Fig.4.4. Chemical variation of biotites from the Caledonian granites (After Yang, 1992)

1 : Shiniutou (C17); 2 : Sidong (C7-1 & C7-2); 3 : Shijiang complex (C16-2, 3, 4, 5);

4 : Shijiang enclave (C78 & C16-1); 5 : Precambrian sedimentary rock (C42-2)

about 0.08, reflecting a lower fO_2 of the magma. On the other hand, the biotites from the Guangning pluton are aluminous, Al (VI) from 0.39 to 0.53 and Al(VI)/Ti ratios > 1.0, indicating that the biotites crystallized from peraluminous magmas.

(2) Biotites from the Yunlougan granodiorite

In contrast to biotites from the Guangning granite, the biotites from the Yunlougan granodiorite contain higher SiO_2 (36.67-37.90 %), TiO_2 (3.16-3.89) and MgO (8.30-9.34), but lower Al_2O_3 (14.52-14.74) and FeO (19.74-21.06). The TiO_2/Al_2O_3 and MgO/FeO ratios are relatively high, 0.22-0.26 and 0.39-0.46 respectively. All samples plot mainly in the Mg-biotite area but near the limiting line in the ternary chemical classification of biotite (Fig.4.5), and most of their M values are >0.45. In addition, calculated formulas of biotite show that the Yunlougan biotites display slightly aluminous features, although their Al (VI) and Al(VI)/Ti values are relatively low, 0.26-0.36 and 0.67-0.95 respectively. This suggests that the Yunlougan parent magmas may be of igneous origin contaminated by aluminous crustal materials. The $Fe^{3+}/(Fe^{2+}+Fe^{3+})$ ratio is relatively high, about 0.15, indicating a high fO_2 during magma crystallization.

(3) Chemical comparisons of biotites between the Guangning and the Yunlougan

Comparing the data in Table 4.2 and the chemical descriptions of biotites above shows that biotites from the Yunlougan granite contain higher SiO_2, MgO, TiO_2 and Fe_2O_3 but lower FeO, MnO and Al_2O_3 than those from the Guangning granite. The TiO_2/Al_2O_3 and MgO/FeO ratios in the Yunlougan biotite are evidently higher than those in the Guangning biotite. In the SiO_2 vs MgO, FeO, Fe_2O_3, Al_2O_3, TiO_2 and MnO diagrams (Fig.4.6), the biotites from the Guangning and from the Yunlougan are located in two different areas, the Guangning biotites in the higher Al_2O_3, FeO and MnO areas but the Yunlougan biotites in the higher SiO_2, MgO and TiO_2 areas. Similarly, in the ternary chemical classification of biotite, the Guangning granite is characterized by Fe-biotite, whereas the Yunlougan by Mg-biotite (Fig.4.5).

about 0.08, reflecting a lower fO_2 of the magma. On the other hand, the biotites from the Guangning pluton are aluminous, Al (VI) from 0.39 to 0.53 and Al(VI)/Ti ratios > 1.0, indicating that the biotites crystallized from a peraluminous magmas.

(2) Biotites from the Yunlougan granodiorite

In contrast to biotites from the Guangning granite, the biotites from the Yunlougan granodiorite contain higher SiO_2 (36.67-37.90 %), TiO_2 (3.16-3.89) and MgO (8.30-9.34), but lower Al_2O_3 (14.52-14.74) and FeO (19.74-21.06). The TiO_2/Al_2O_3 and MgO/FeO ratios are relatively high, 0.22-0.26 and 0.39-0.46 respectively. All samples plot mainly in the Mg-biotite area but near the limiting line in the ternary chemical classification of biotite (Fig.4.5), and most of their M values are >0.45. In addition, calculated formulas of biotite show that the Yunlougan biotites display slightly peraluminous features, although their Al (VI) and Al(VI)/Ti values are relatively low, 0.26-0.36 and 0.67-0.95 respectively. This suggests that the Yunlougan parent magmas may be of igneous origin contaminated by peraluminous crustal materials. The $Fe^{3+}/(Fe^{2+}+Fe^{3+})$ ratio is relatively high, about 0.15, indicating a high fO_2 during magma crystallization.

(3) Chemical comparisons of biotites between the Guangning and the Yunlougan

Comparing the data in Table 4.2 and the chemical descriptions of biotites above shows that biotites from the Yunlougan granite contain higher SiO_2, MgO, TiO_2 and Fe_2O_3 but lower FeO, MnO and Al_2O_3 than those from the Guangning granite. The TiO_2/Al_2O_3 and MgO/FeO ratios in the Yunlougan biotite are evidently higher than those in the Guangning biotite. In the SiO_2 vs MgO, FeO, Fe_2O_3, Al_2O_3, TiO_2 and MnO diagrams (Fig.4.6), the biotites from the Guangning and from the Yunlougan are located in two different areas, the Guangning biotites in the higher Al_2O_3, FeO and MnO areas but the Yunlougan biotites in the higher SiO_2, MgO and TiO_2 areas. Similarly, in the ternary chemical classification of biotite, the Guangning granite is characterized by Fe-biotite, whereas the Yunlougan by Mg-biotite (Fig.4.5).

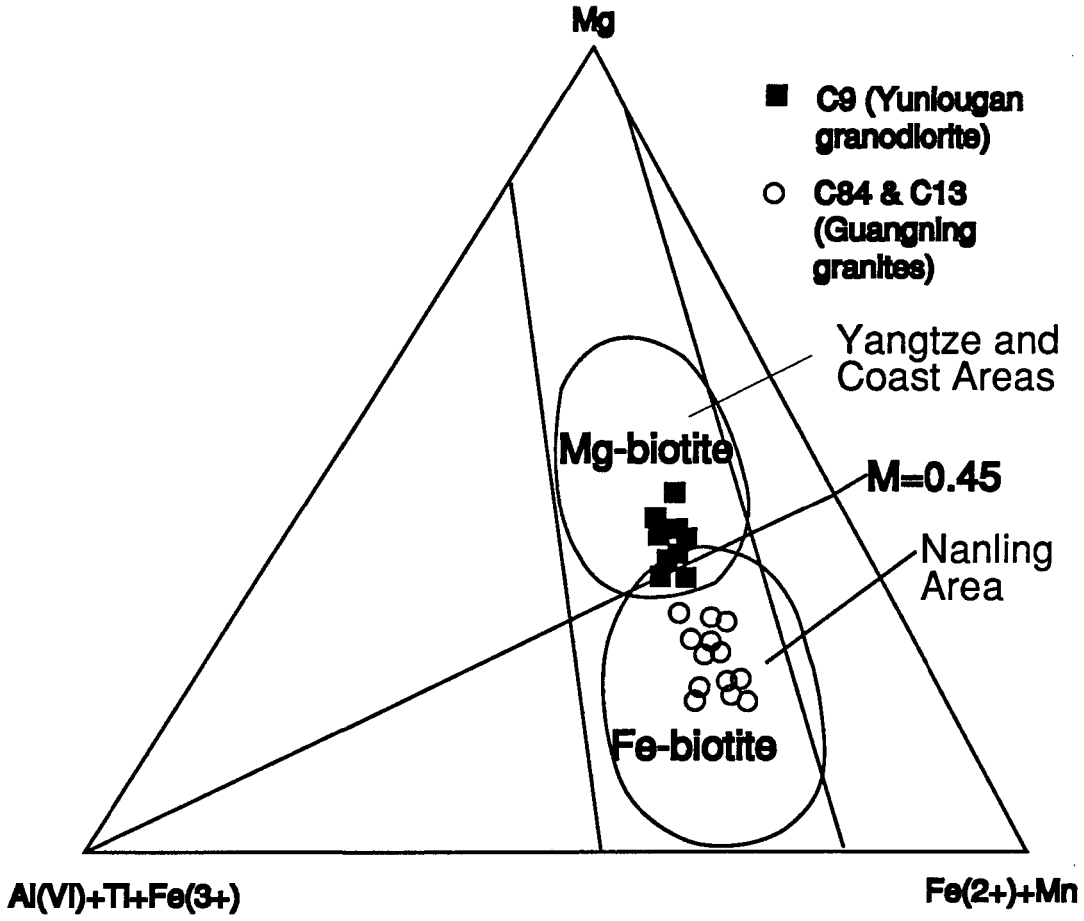

Fig.4.5. Biotite from the different Hercynian granites on the ternary chemical classification (After Foster, 1960 and Yang et al., 1986a)

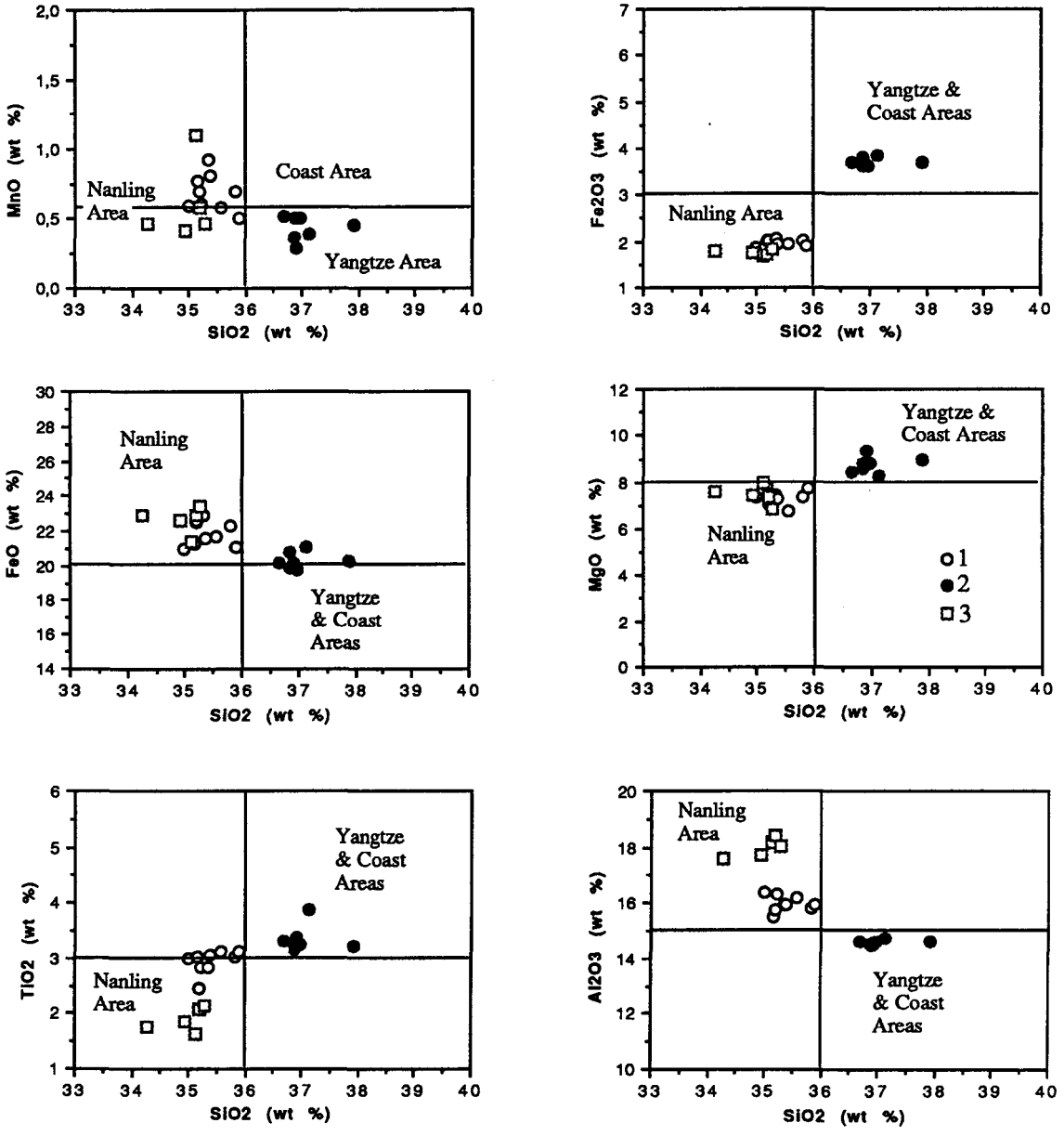

Fig. 4.6. Chemical comparison between biotites from the different Hercynian plutons (after Yang, 1992). 1 : Guangning (C84 & C13); 2 : Yunlougan (C9-1); 3 : Precambrian sedimentary rock

Comparing the chemical features of biotites with those from South China shows that the biotites from the Guangning pluton are generally similar to those from the Nanling granites, whereas biotites from the Yunlougan similar to the Yangtze and Coast granites (Figs.4.5 and 4.6). According to the biotite, it is reasonable to suppose that the Guangning biotite granite is derived from crustal source regions (S-type), whereas the Yunlougan granodiorite may be crystallized from mantle-derived magmas.

4-2-3. Chemical compositions of the Indosinian biotites

The chemical compositions of biotites from the Wuchun megacryst monzogranite and tonalitic enclaves are listed in Table 16 (see Appendix III).

(1) Biotites from the Wuchun megacryst monzogranite

In contrast to biotites from the Caledonian granites, the chemical compositions of biotites from the megacryst monzogranite (Table 16) are characterized by higher SiO_2 (35.91-36.52), TiO_2 (3.21-4.77), MgO (7.12-8.25), Fe_2O_3 (5.13-5.56) and MnO (0.76-0.99), but lower Al_2O_3 (13.14-14.51) and FeO (19.87-21.57). The TiO_2/Al_2O_3 ratios are higher, 0.26-0.36, and the MgO/FeO are moderate, 0.37-0.40. The $Fe_2O_3/(Fe_2O_3+FeO)$ ratios are high, 0.65-0.80, reflecting a higher fO_2 of the magma. The calculated biotite formula display slight aluminous features and their Al (VI) and Al(VI)/Ti values are very low, 0.07-0.29 and 0.12-0.76 respectively, reflecting a metaluminous magma. The samples plot in the transitional area between Fe-biotite area and Mg-biotite area in the ternary chemical classification of biotite (Fig.4.7), and most M values are < 0.45, but the MnO content of these biotites is high. These features usually indicate that biotites are crystallized from a more differentiated magma in which the Mg is very low. In addition, the high Mn may also reduce the M values of biotite.

(2) Biotites from the Wuchun granodioritic enclaves

The biotites from the granodioritic enclaves contain higher SiO_2 (36.71-37.75 %), MgO (8.95-9.70) and TiO_2 (3.08-3.58), but Al_2O_3 (12.98-14.37) and FeO (19.05-20.03), similar to the biotites from the host megacryst monzogranite (Table 16), The TiO_2/Al_2O_3 and MgO/FeO ratios are high, 0.21-0.28 and 0.45-0.51 respectively. The samples plot in the Mg-biotite area in the ternary chemical classification of biotite (Fig.4.7), and their M values are > 0.45. The Al (VI) and Al(VI)/Ti values (0.18-0.32 and 0.44-0.91 respectively) are higher than those in biotites from the monzogranite, reflecting magma evolution from slightly peraluminous to aluminous undersaturation.

Compared to the biotites from the host megacryst monzogranite, MnO content (0.56-0.77) in biotite from the tonalitic enclaves is relatively low. This also indicates evolutionary trend from granodioritic enclave to host monzogranite. These relations can be shown in a series of diagrams such as SiO_2 vs MgO, FeO, TiO_2, Al_2O_3, MnO, TiO_2/Al_2O_3 and MgO/FeO, (Fig.4.8). It is clear that the biotites from the enclaves are distributed in the areas of higher SiO_2, MgO but lower MnO, FeO and TiO_2/Al_2O_3 relative to those from the monzogranite, but they are related to the same genetic type. Consequently, the geochemical features of biotite further endorse the genetic relationship between the granodioritic enclaves and the host monzogranite.

4-2-4. Chemical composition of the Yanshanian biotites

The chemical compositions of biotites from the Shihui alkali feldspar granite complex and their granodioritic enclaves are compared in Table 17 (see Appendix III).

(1) Biotites from the Sihui alkali-feldspar granites

It is evident that the chemical compositions of biotites from the Sihui alkali feldspar granites are characterized by very high SiO_2 (37.05-38.71), TiO_2 (3.00-5.13), MnO (0.79-1.85), Fe_2O_3 (5.43-6.21) but very low Al_2O_3 (11.77-13.40) and FeO (17.62-20.11). MgO varies widely, 7.63-11.01. The TiO_2/Al_2O_3 and MgO/FeO ratios are generally high, 0.24-

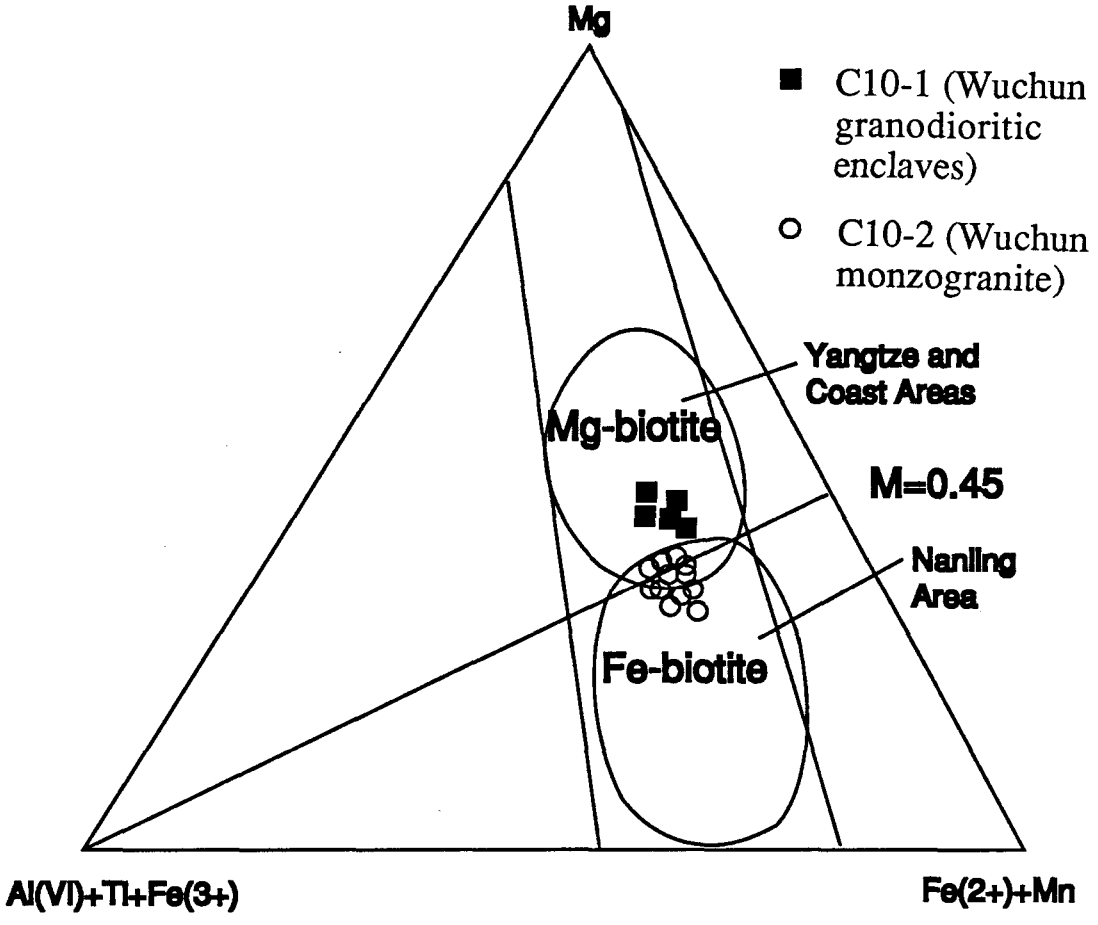

Fig.4.7. Biotites from the Indosinian granites and their enclaves on the ternary chemical classification
(After Foster 1960 and Yang et al., 1986a)

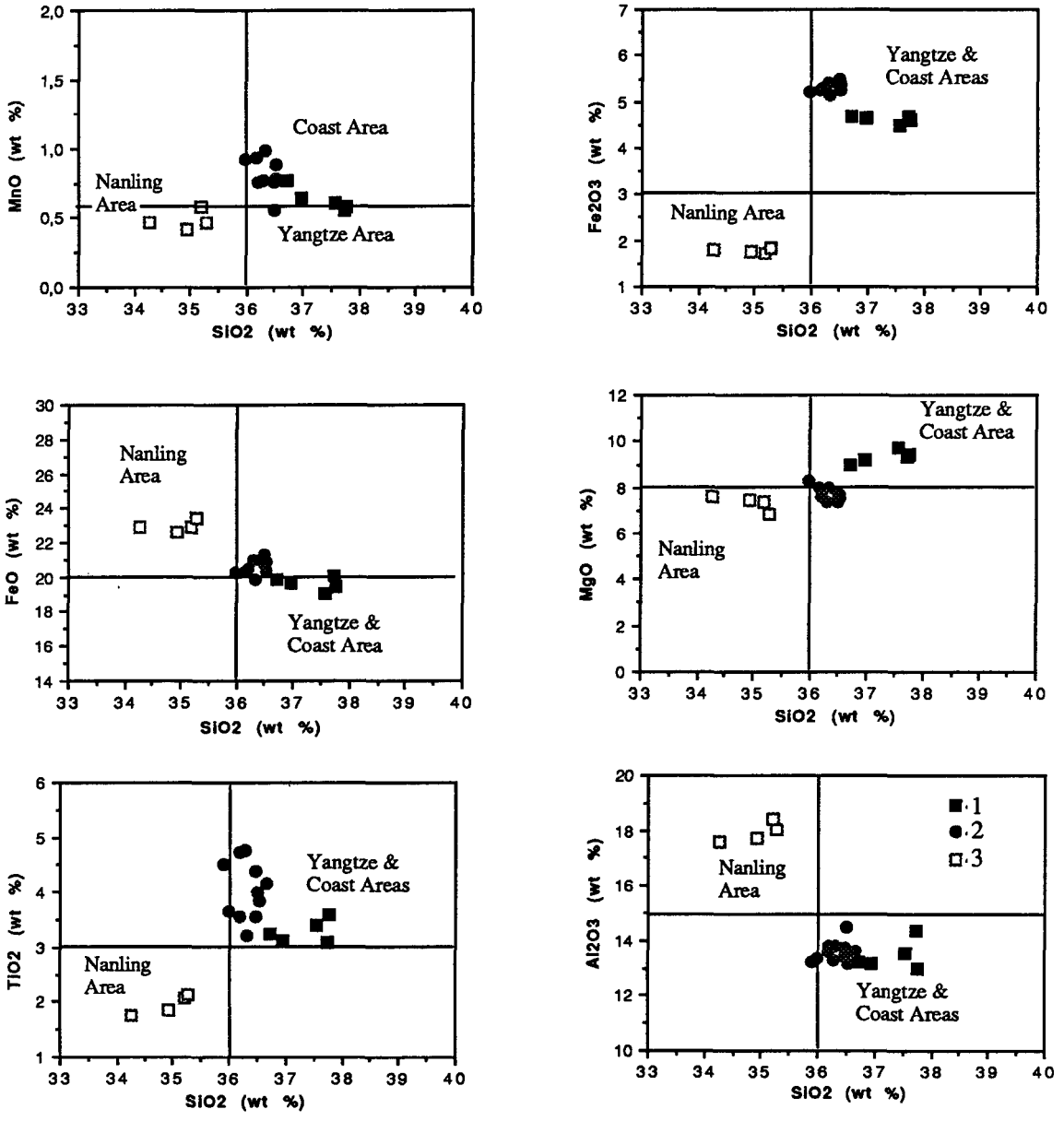

Fig. 4.8. Chemical variation of biotites from the Indosinian granites and enclaves (After Yang, 1992) 1 : Wuchun granodioritic enclave (C10-1); 2 : Wuchun monzogranite; 3 : Precambrian sedimentary rock (C42-2)

0.42 and 0.38-0.60, respectively. All samples plot in the Mg-biotite area in the ternary chemical classification of biotite (Fig.4.9), and their M values (> 0.45) are similar to those from the Yangtze and Coast granites of South China. In addition, these biotites contain very low aluminum and their Al (VI) and Al(VI)/Ti values are close to 0. These chemical features of biotites imply that they are crystallized from a more differentiated magma. On the other hand, their $Fe_2O_3/(Fe_2O_3+FeO)$ ratios are very high, 0.23-0.24 , reflecting a higher fO_2 of the magma.

(2) Biotites from the Sihui granodioritic enclaves

The chemical compositions of biotites from the granodioritic enclaves (Table 17) are characterized by high TiO_2 (3.92-4.95), MgO (9.75-13.06) and SiO_2 (36.78-39.06), but very low Al_2O_3 (10.85-13.16) and FeO (15.34-18.38). The TiO_2/Al_2O_3 and MgO/FeO ratios are very high, 0.33-0.42 and 0.53-0.84, respectively. All samples plot in the Mg-biotite area in the ternary chemical classification of biotite (Fig.4.9), and their M values are > 0.45, similar to those from the Yangtze and Coast granites of South China. These biotites, too, contain little aluminum, and most of Al (VI) and Al(VI)/Ti values are very low (< 0), reflecting aluminum undersaturation in the magma. The $Fe_2O_3/(Fe_2O_3+FeO)$ ratios are high, about 0.22, implying a high fO_2 state.

(3) Geochemical evolution of biotites in the Sihui granite complex

The granodioritic enclaves are considered to be an early intrusive phase of the Sihui complex, and the chemical features of biotites from the granodioritic enclaves support this conclusion. It is evident from Table 17 that the biotites from the enclaves show relatively higher MgO/FeO and TiO_2/Al_2O_3 ratios but lower MnO content than those from the host alkali feldspar granites. Similarly, the evolutionary trends may also be reflected in the SiO_2 vs MgO, FeO, TiO_2, Al_2O_3, Fe_2O_3 and MnO diagrams (Fig.4.10), showing that MnO increases regularly with SiO_2 but other elements decrease from the granodioritic enclaves to alkali feldspar granites, obeying the normal evolutionary trends of magmatic differentiation, so, the granodioritic enclaves probably represent an early intrusive phase.

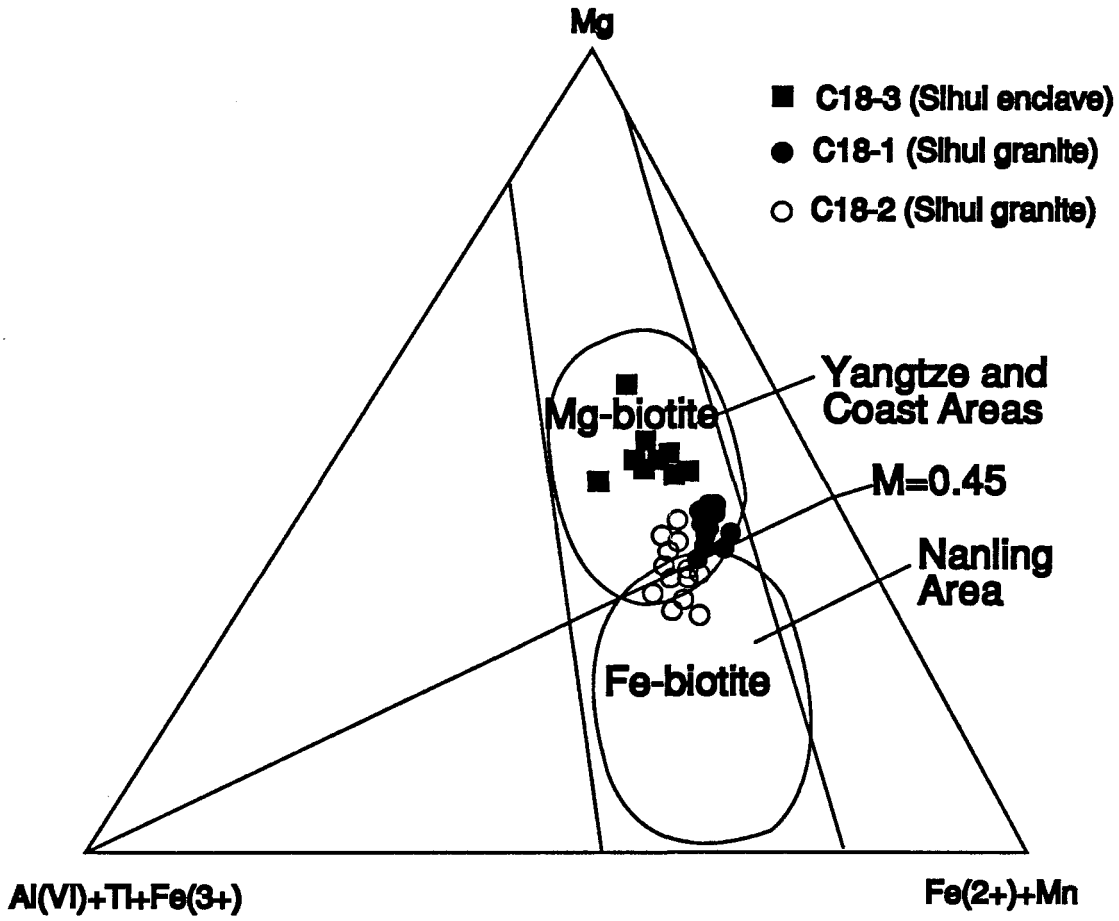

Fig. 4.9. Biotites from the Yanshanian granites and their enclaves on the ternary chemical classification
(After Foster 1960 and Yang et al. 1986a)

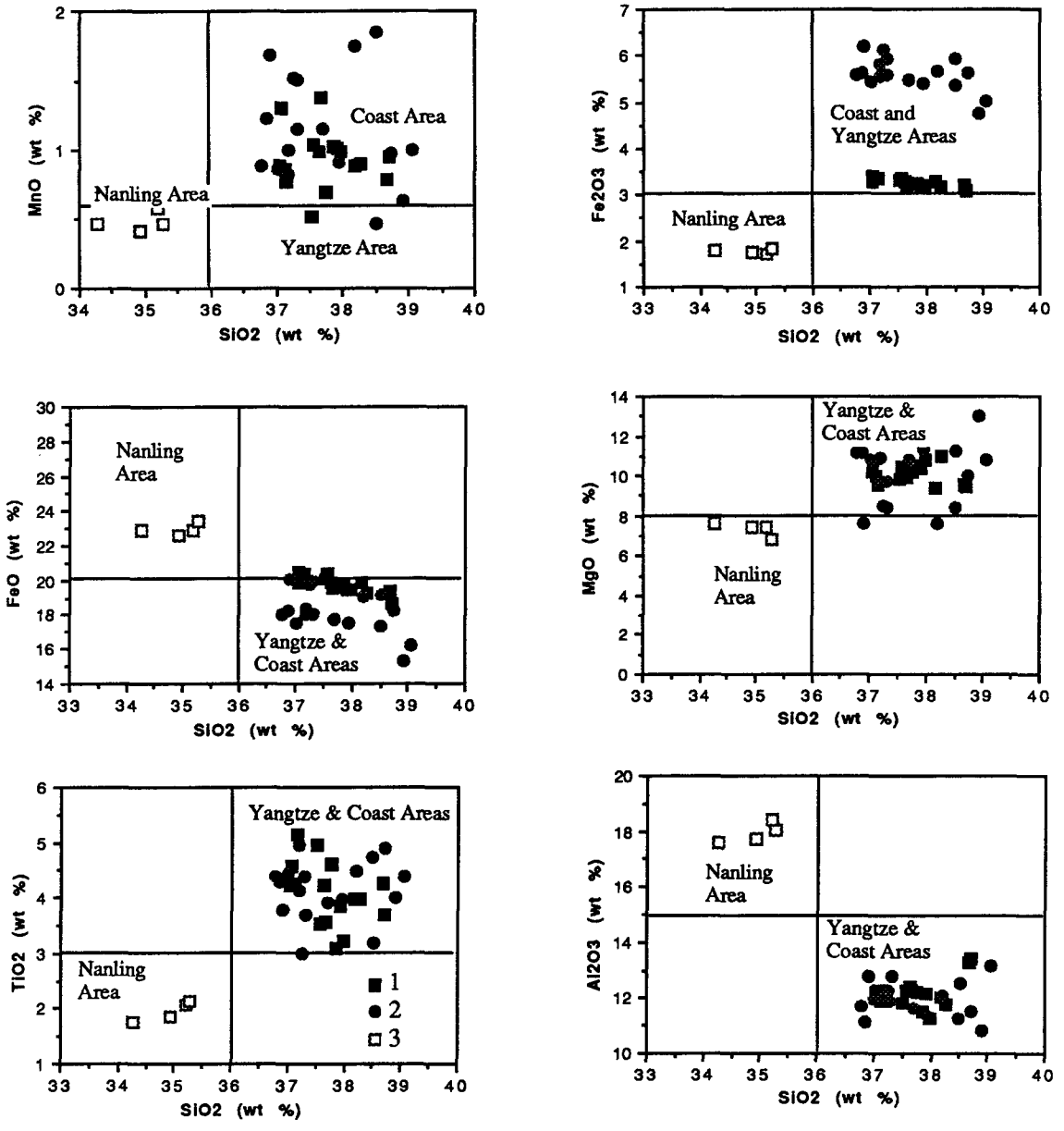

Fig.4.10. Chemical variation of biotites from the Yanshanian granites and enclaves (After Yang, 1992) 1 : Sihui granodioritic enclave (C18-3); 2 : Sihui alkali-feldspar granite (C18-1, C18-2); 3 : Precambrian sedimentary rock (C42-2)

All biotites from both the granodioritic enclave and alkali-feldspar granite have very low aluminum contents, and in their calculated formula, the total Al contents are evidently low and Al(VI) < 0. Such Al-poor biotites usually result from highly differentiated magmas. Although these biotites are characterized by a higher MgO content, all samples are located in the highest SiO_2 and MnO area. Silica-rich and alkali-rich biotite and amphibole usually indicate a continental margin environment (Jakes and White, 1972) and crystallize only from alkaline liquids and during the late magmatic or post-magmatic stage (Giret et al., 1980; Wones and Gilbert, 1982). In general, the biotites are similar to those from the Coast granites of South China, and their high SiO_2 and MnO contents demonstrate that the Sihui alkali feldspar granites may be derived from a highly differentiated magma probably emplaced at a relatively high level, because these biotites contain high Fe_2O_3 contents.

4-3. Comparison between biotites from the Huangtongjiang gabbro and from the Precambrian sedimentary rock

The analyzed biotites from the Huangtongjiang gabbro are listed in Table 18 (see Appendix III), as they may be compared with biotites from granites in the Hetai Area, in order to identify probable source rocks for the different types of granite magma.

It is evident from Table 18 that the biotites from the Huangtongjiang are characterized by high SiO_2 (37.06-37.38), MgO (12.91-13.40) and TiO_2 (3.07-3.93) but low FeO (15.42-15.75), Fe_2O_3 (2.50-2.55) and Al_2O_3 (14.49-15.20). The MnO contents are very low, 0.00-0.33. The TiO_2/Al_2O_3 and MgO/FeO ratios are high, 0.21-0.27 and 0.83-0.87 respectively. All samples plot in the Mg-biotite area in the ternary chemical classification of biotite (Fig.11), and their M values (0.61-0.62) are > 0.45 . On the other hand, their Al (VI) and Al(VI)/Ti values are relatively low, 0.18-0.26 and 0.42-0.67 respectively, reflecting a metaluminous basaltic magma.

In contrast to biotites from the Huangtongjiang gabbro, those from the Precambrian metamorphosed sedimentary rocks contain low SiO_2 (34.26-35.28), TiO_2 (1.75-2.15), MgO (6.82-7.64) and Fe_2O_3 (1.74-1.84) but high Al_2O_3 (17.59-18.40), FeO (22.56-23.46). The MgO/FeO and TiO_2/Al_2O_3 ratios are very low, 0.83-0.87 and 0.21-0.27 respectively.

All samples are plotted in the Fe-biotite area in the ternary chemical classification of biotite, and thier M values are < 0.45 (Fig.4.11). These biotites are alumina-rich and their Al (VI) and Al(VI)/Ti values are very high, 0.65-0.73 and 2.76-3.24 respectively, reflecting a extremely peraluminous chemical environment.

The chemical features of biotites of the Huangtongjiang gabbro differ markedly from those of the Precambrian sedimentary rocks. Such contrasting chemical difference in biotites images the chemical features of their source rocks, and they can be identified in some diagrams such as SiO_2 vs MgO, FeO, TiO_2, Al_2O_3, Fe_2O_3 and MnO (Fig.4.12). Biotites from the Huangtongjiang gabbro are distributed in the high SiO_2, MgO, TiO_2 and M areas, whereas those from the Precambrian sedimentary rocks occur in the high Al_2O_3, FeO but low M areas. It is possible that the chemical features of biotites represent different chemical backgrounds of source rocks. Of course, the chemical features of the Huangtongjiang gabbro represent true igneous sources such as basaltic magmas (I-type), whereas the Precambrian sedimentary rocks are the chemical background of peraluminous crustal source rocks (S-type).

4-4. Comparison between biotites from the different enclaves

The chemical compositions of biotites from different enclaves are compared in Table 19 (see Appendix III). At first, it appears that biotites from the Wuchun and the Sihui enclaves are similar in major oxide contents. The biotites from the Sihui and the Wuchun enclaves all are characterized by high SiO_2, MgO, TiO_2, Fe_2O_3 and MnO, but low Al_2O_3 and FeO. The Al_2O_3/TiO_2 ratios are low but MgO/FeO ratios are high. MnO contents of biotite from the Wuchun enclaves are evidently lower than those from the Sihui enclaves. In the SiO_2 vs selected oxide diagrams (Fig.4.13), biotites from the Shijiang enclaves are distributed mainly in the areas of low SiO_2, TiO_2, MnO, FeO and Fe_2O_3 but high Al_2O_3 and MgO, coincident with biotite of the Nanling granites, whereas biotites from the Wuchun enclaves occur mainly in the areas of high SiO_2, TiO_2, MgO and Fe_2O_3 but low Al_2O_3, FeO and moderate MnO, similar to biotite of the Yangtze granites, and those from the Sihui enclave mainly in the areas of high SiO_2, MnO, Fe_2O_3,

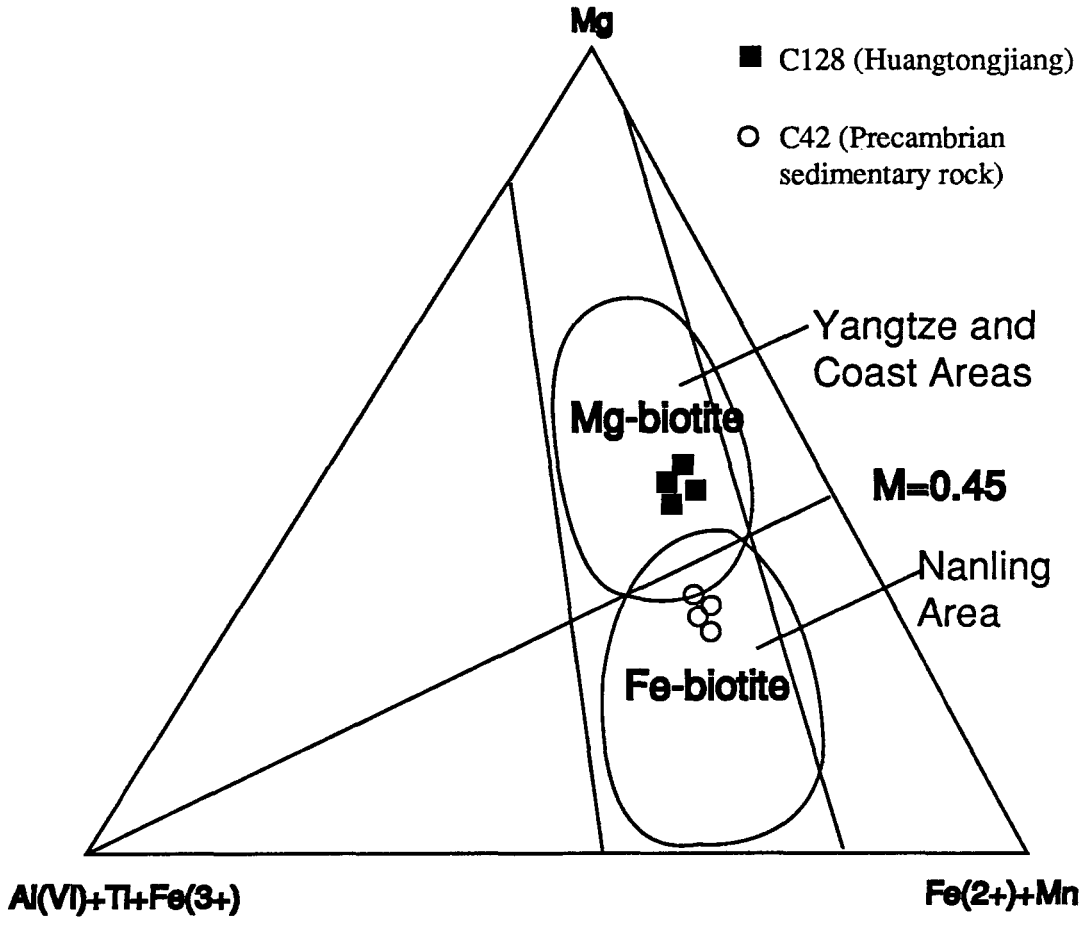

Fig. 4.11. Biotites from the Huangtongjiang gabbro and from Precambrian sedimentary rocks on the ternary chemical classification (After Foster 1960 and Yang et al. 1986a)

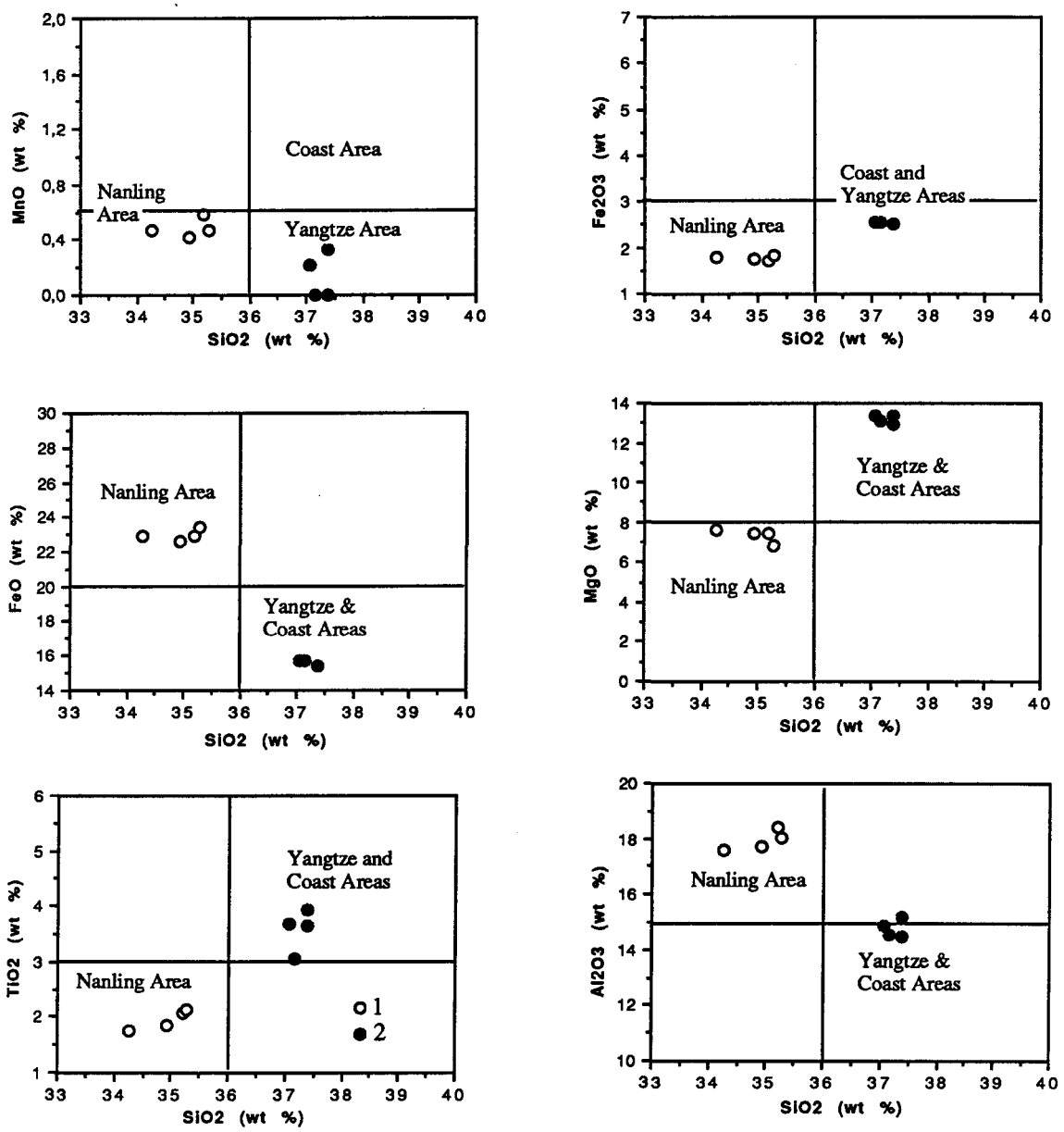

Fig. 4.12. Comparison between biotites from the Huangtongjiang gabbro and from Precambrian sedimentary rock (After Yang, 1992)

1 : Precambrian sedimentary rock (C42-2) ; 2 : Huangtongjiang gabbro (C128)

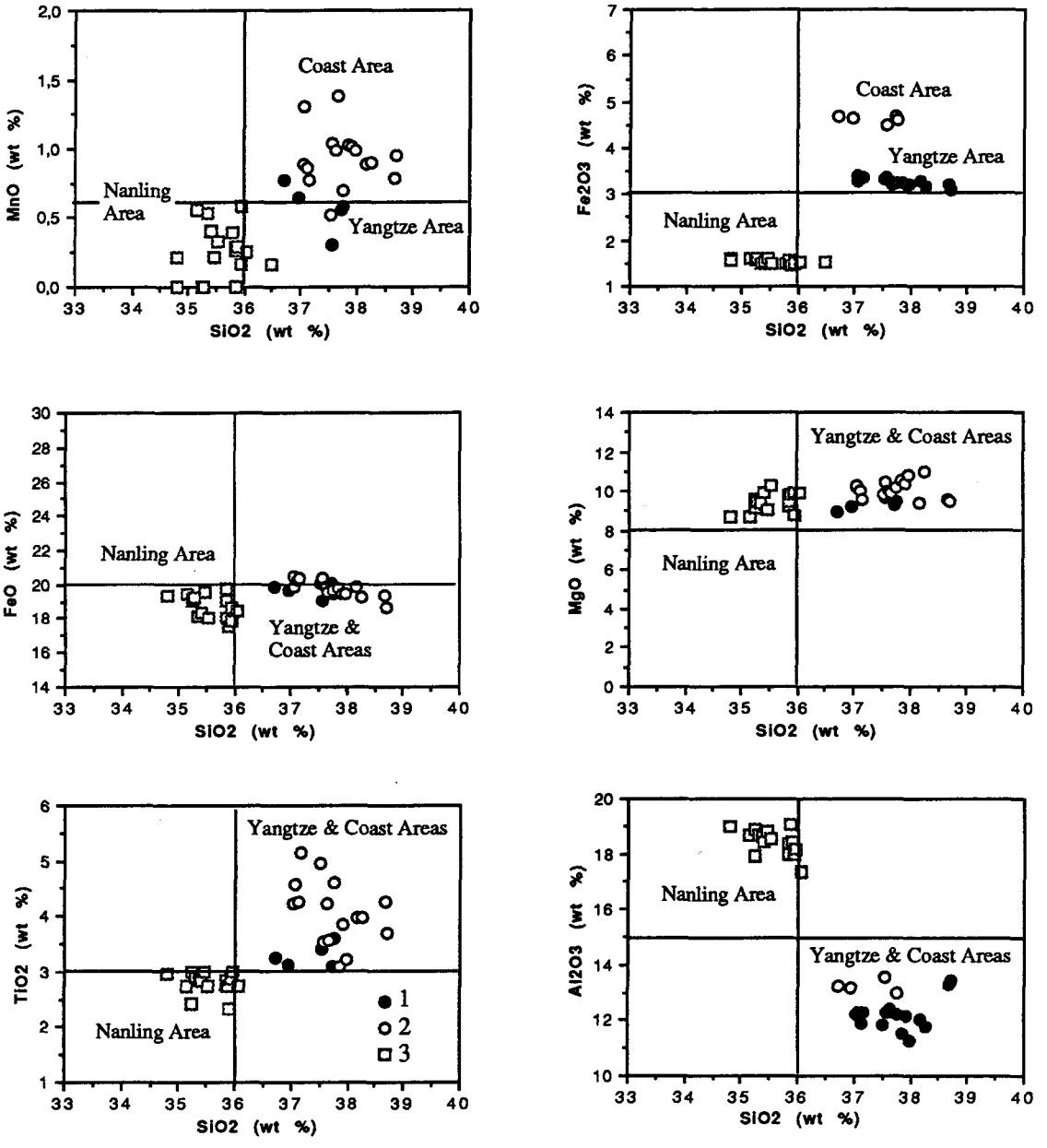

Fig. 4.13. Chemical composition between biotites from different enclaves (After Yang, 1992). 1 : Sihui enclaves (C18-3); 2 : Wuchun enclaves (C10-1) 3 : Shijiang enclaves (C78 & C16-1)

TiO_2 and MgO but low Al_2O_3 and FeO, similar to biotites of the Coast granites. Compared with biotites from the Huangtongjiang gabbro and Precambrian sedimentary rocks in these diagrams (Fig.4.13), it is evident that the biotites from Shijiang enclaves coincide with those from Precambrian sedimentary rocks, whereas the biotites from the Wuchun and the Sihui enclaves are very similar to those from the Huangtongjiang gabbro. The high MnO in biotites from the Sihui enclaves may be the result of more differentiated evolution of mantle-derived magma. Similarly, slightly higher MgO in biotites from Precambrian sedimentary rocks also indicates the participation of igneous materials in Precambrian sediments.

4-5. Geochemical characteristics of biotite for different granite types in the Hetai Area

4-5-1. Major oxide averages of each sample by electron probe analysis

The chemical composition of biotites from individual bodies of different ages show that the chemical features of biotites are closely related to the chemistry of their host granites, and, they may image the chemical background of source rocks and indicate magma evolution, particularly reflecting the evolution of a cognate granite series. The major oxide averages and some trace element contents of biotites from different granites of the Hetai Area are compared in Table 20 (see Appendix III).

Biotites from older granites are characterized by low SiO_2 (<36%), MgO (<8%) and TiO_2 (<3%) but high FeO (>22%) and Al_2O_3 (>15%), and they plot mainly in the Fe-biotite area in the ternary chemical classification of biotite (Fig.4.14) with M values <0.45, coincident with the biotites from the Nanling granites of South China and those from S-type granites; whereas those from the younger granites are characterized by high SiO_2 (>36%), MgO (>8%) and TiO_2 (>3%) but low FeO (<22%) and Al_2O_3 (<15%), and they are distributed mainly in the Mg-biotite area most with M values >0.45, coincident with the biotites from the Yangtze and Coast granites in South China and from I-type granite.

Furthermore, it can be seen from Table 20 and Fig. 4.14 that the biotites from the older granites can be further subdivided. The biotites from the Sidong and Shiniutou granites are characterized by very low MgO (<5%) and M value (<0.25), but high FeO (>25%),

Fe_2O_3 (>3%) and MnO (>0.7%), and those from the Shijiang and Guangning granites have relatively high MgO (>5%) and M value (>0.25), but low FeO (<25%), Fe_2O_3 (<3%). These differences suggest that the source regions of the Shijiang and Guangning granites may be mixed with igneous material. On the other hand, the biotites from the younger granites have a different trend. The biotites from the Sihui (Yanshanian) granites demonstrate the highest SiO_2 (>37.5%), MnO (>0.9%) and Fe_2O_3 (>5%) but the lowest Al_2O_3 (<13%) relative to those from the other younger granites, demonstrating magmatic differentiation.

Comparing all biotite analyses in SiO_2 vs major oxide diagrams (Fig.4.15) shows that the biotites from the older granites are located mainly in the areas of low SiO_2, TiO_2 and MgO but high Al_2O_3 and FeO, and coincide with the biotites from Precambrian sedimentary rocks; whereas the biotites from the younger granites are distributed in the areas of high SiO_2, TiO_2 and MgO but low Al_2O_3 and FeO, coincident with the biotites from the Huangtongjiang gabbro. The biotites from the Yanshanian alkali-feldspar granites show a particularly high SiO_2 and MnO content, and a tendency of MnO increase with the evolution of the granite series. Similarly, their Fe_2O_3 contents are high. When these results are compared to analyzed biotites from different types of granites of South China (Yang et al., 1986a) and other world areas in related diagrams (Fig.4.15), it is clear that the biotites from the older granites plot in the area of biotites from the Nanling granite and from S-type granite, which are characterized by Fe-biotite and peraluminous source rocks. On the other hand, biotites from the younger granites are distributed in the area of biotites from the Yangtze and Coast granites and from I-type granite, which are characterized by Mg-biotite and developed from mantle-derived magma.

4-5-2. Trace element characteristics of biotite

The distributions of certain trace elements such as Li, Zn, Co and Ni in biotite are controlled by crystal chemistry and the substitution of Mg<--Fe(2+)(Co, Ni, Zn and Li) and Si<--Al(IV). They are also influenced by the chemistry of the magma type from which they crystallize. Trace element contents of biotites from the different granites in the Hetai Area

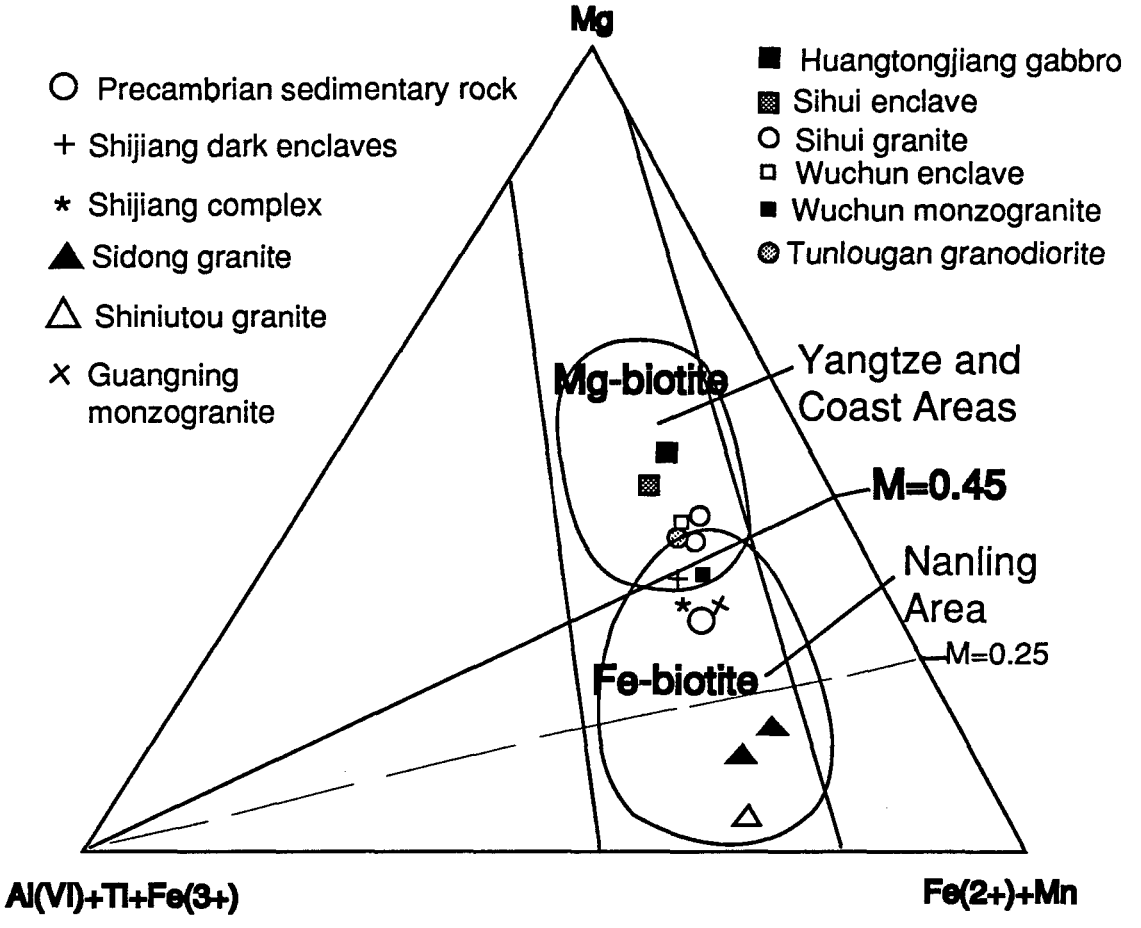

Fig. 4.14. Biotites from the different granites of the Hetai Area on the ternary chemical classification (After Foster 1960 and Yang et al. 1986a)

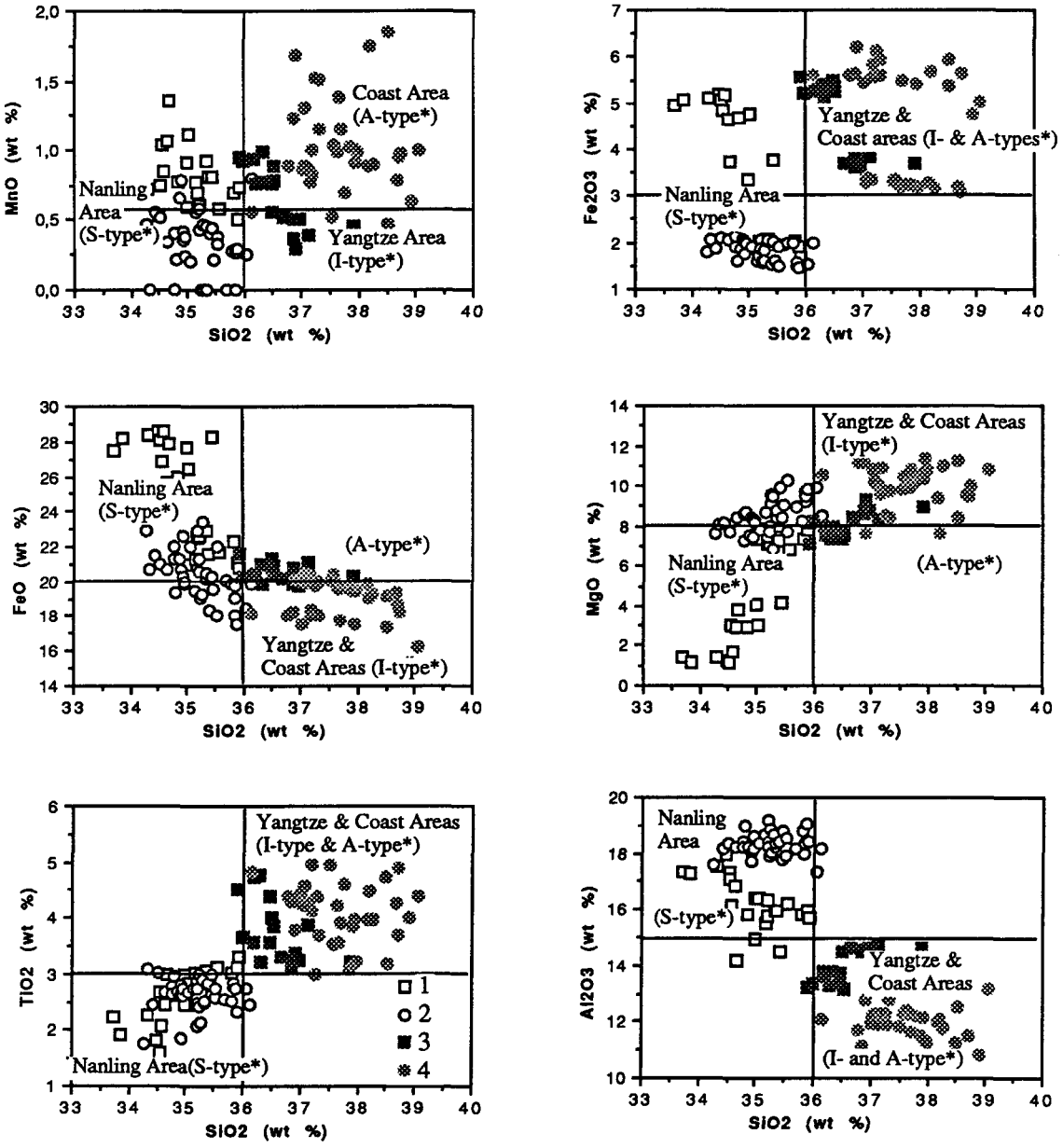

Fig. 4.15. Comparison between biotites from different type granites of the Hetai Area (After Yang, 1992; * data from Dodge et al.,1968; Kanisawa, 1976; Weiss & Troll, 1989; Cocherie et al., 1984; Czamanske, 1986)

1 and 2 : Older granites; 3 and 4 : Younger granite suites

display different trends. As compared in Table 4.7, the Caledonian biotites contain low F (3500-5100 ppm) and Li (128-202) but average Rb (634-734), Zn (425-550), Ni (56-64) and Co (35-37), and similarly, the Hercynian Guangnig biotites F (5500), Li (353), Rb (632), Zn (510), Ni (65) and Co (33). Relative to the Guangning biotites, the Hercynian Yunlougan biotites present even lower F (3000), Li (187), Rb (447) and Zn (425), but higher Ni (84) and Co (39). Whereas the Indosinian biotites and the Yanshanian biotites display regular variations from earlier phase (intermediate-basic enclaves) to later host granites, F (5100->6050), Li (514->697), Rb (734->1000), Zn (450->600) increasing but Ni (98->54) and Co (36->32) decreasing in the Indosinian biotites from the enclave to the host monzogranite, and similarly F (4500->7300), Li (327->1991), Rb (507->1056), Zn (510->1050) increasing but Ni (59->39) and Co (32->24) decreasing in the Yanshanian biotites from the enclave to the host alkali-feldspar granite.

Speer (1982) suggested that the behavior of F in biotite is the key to the behavior of F in many igneous rocks, but his conclusion that Mg-biotite generally contains more F than Fe-biotite seems to be incorrect. For example, the Fe-biotites from the Nanling granites have higher F contents than Mg-biotites from the Yangtze granites, but the Mg-biotites from the Coast alkali-feldspar granites have the highest F contents in South China (Yang et al., 1986a). Similarly, the F contents in biotites from the Hetai granites vary with the magmatic differentiation. The Fe-biotites from the older granites (Table 4.7) have higher F contents than Mg-biotites from the Hercynian Yunlougan and the Indosinian and Yanshanian granodioritic enclaves, but the Mg-biotites from the Indosinian (Wuchun) monzogranite and the Yanshanian (Sihui) alkali-feldspar granite present the highest F contents. F contents in Mg-biotite increase from the earlier intermediate enclave to later host alkali-feldspar granite in the Sihui granite series. Therefore, the F contents of biotites may be closely related to the chemical background of the magma and to magmatic differentiation. The F increase in Mg-biotite in the Sihui granite series suggests a trend of F increase in the more differentiated melts during magma evolution. Li contents are very low in biotites from the older granites, but high in biotites from the younger alkali-feldspar granites. Generally, the distribution of Li, Rb, Zn, Ni and Co as well as F in biotite is closely related to the chemical background of their host rocks and to magma differentiation, and these trace elements in biotites can be regarded as a useful indicator for distinguishing different granite types and evolution.

4-6. Chemical compositions of amphiboles

MgO and FeOt are important components of amphibole and Mg<--Fe and Si <--Al substitutions play a significant role for geochemical change in amphibole during magmatic evolution. In general, the presence of amphibole in granite has a certain significance in indicating granite generation (I-type vs S-type), that is, the chemical features of amphibole may image the geochemical processes of the host granite. Amphibole only occurs in a limited number of granitic bodies in the Hetai Area relative to biotite, and the analyzed amphiboles include only three samples from the Yunlougan granodiorite, the Sihui granodioritic enclaves and the Huangtongjiang gabbro, respectively (Table 21, see Appendix III).

4-6-1. Amphiboles from the Yunlougan granodiorite

The chemical compositions of amphiboles from the Yunlougan granodiorite (Table 21) contain SiO_2 (42.42-49.89), MgO (6.29-11.32), FeOt (19.12-23.68), Al_2O_3 (3.46-9.79), CaO (11.33-12.31), TiO_2 (0.38-1.22), MnO (0.39-0.76), Na_2O (0.37-0.92) and K_2O (0.40-1.35). The MgO/FeOt ratios are from 0.27 to 0.59. The chemical compositions show that the amphiboles inside early zoned plagioclase are different to those in the later polysynthetically twinned plagioclase. It can be seen from Table 4.8 that the amphiboles inside early zoned plagioclase contain higher SiO_2 (47.23-49.89), MgO (9.02-11.32) but lower Al_2O_3 (3.46-6.57), FeOt (19.08-19.65), MnO (0.40-0.54), Na_2O (0-0.37) and K_2O (0.40-0.82), whereas those in the late plagioclase have lower SiO_2 (42.42-43.63), MgO (6.29-6.75) but higher Al_2O_3 (9.37-9.79), FeOt (22.93-23.68), MnO (0.54-0.65), Na_2O (0.50-0.92) and K_2O (1.13-1.35). This means that the amphiboles inside the zoned plagioclase may be the result of early accumulation with plagioclase and indicates that the amphiboles became enriched in Fe, Al, Na and K during magma differentiation.

According to the chemical classification of amphibole (Leake, 1978; Hawthorne, 1981), the amphiboles inside the earlier zoned plagioclase plot mainly in the magnesio-hornblende area but between the Mg-hornblende and Fe-hornblende areas (Fig.

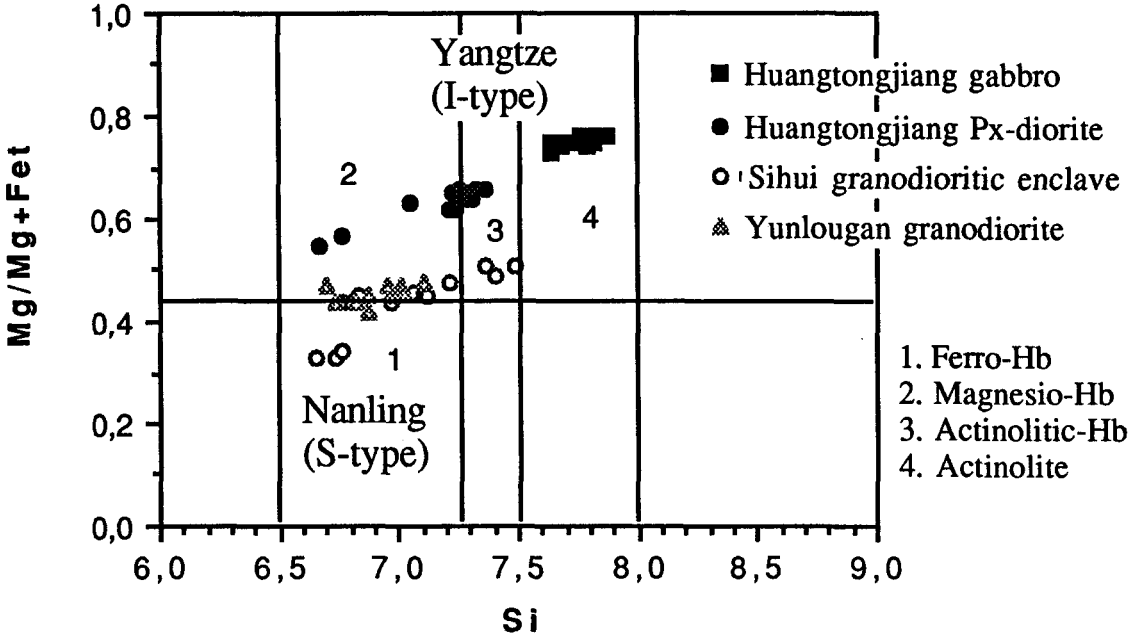

Fig.4.16. Chemical classification of amphibole from the Hetai granites (Modified from the Leake (1978) and Hawthorne (1981))

16). In the SiO_2 vs major oxide diagrams (Fig.4.17), regular differentiation trends can be shown between amphibole from different occurrences, the amphiboles inside early zoned plagioclase plot in the high SiO_2, MgO, but low FeOt, Al_2O_3, Na_2O and K_2O areas, the common amphiboles plot in the moderate area, but the amphiboles in the late polysynthetically twinned plagioclase are located in the low SiO_2, MgO but high FeOt, Al_2O_3, Na_2O and K_2O areas. Such a regular chemical variation not only indicates the chemical evolution of amphibole, but also reflects the magma differentiation trend.

4-6-2. Amphiboles from the Sihui granodioritic enclaves

The amphiboles from the Sihui granodioritic enclaves compared to those from the Yunlougan granodiorite (Table 21) contain similar SiO_2 (43.65-46.01), Al_2O_3 (5.02-7.85), TiO_2 (0.65-1.57), MgO (9.00-10.33), FeOt (18.66-22.24), CaO (10.56-11.31), and K_2O (0.74-0.98), but higher MnO (1.13-1.86) and Na_2O (0.88-1.81) contents. The MgO/FeOt ratios are from 0.41 to 0.52. Most amphiboles plot in the actinolitic-Hb and magnesio-Hb areas, but some in the Fe-hornblende area (Fig. 4.16). Clearly, these amphiboles have high MnO and Na_2O contents, although the host rock is similar to the Yunlougan granodiorite in bulk chemistry. Wones (1981) regarded OH- contents in amphibole and biotite as intensive variable indicators of granitic magma evolution, and interpreted the intrinsic properties which may reflect magma source and significant change during the history of a given magma. Besides the OH^- indication, MnO and Na_2O contents in amphibole and biotite may also be used as an indicator of magma source and significant change during differentiation for a given granitic pluton. The higher MnO and Na_2O in amphiboles from the Sihui granodioritic enclaves may indicate that the differentiated magma may produce geochemical features such as higher alkali components, although their source magma is characterized by calc-alkaline properties (I-type). This trend is reflected by the chemical features of biotite mentioned above. According to Jakes and White (1972) and (Yang, 1992), the more differentiated magma may result in higher MnO, Na_2O and SiO_2 contents of mafic minerals (amphibole and biotite) during magmatic evolution.

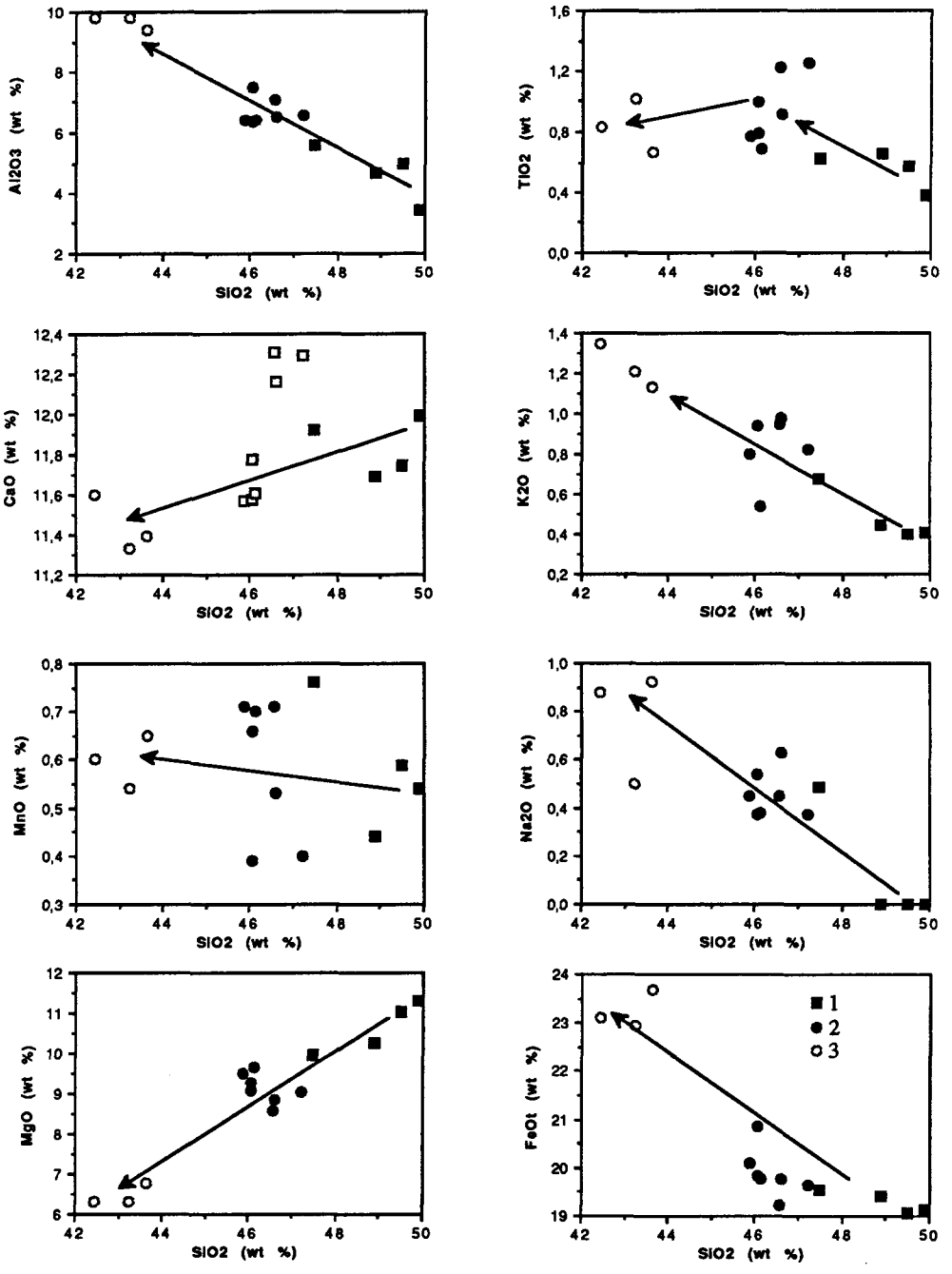

Fig. 4. 17. Chemical variation of amphiboles from the Yunlougan granodiorite

1 : Amphibole in zoned plagioclase; 2 : Common amphibole

3 : Amphibole in polysynthetic plagioclase

4-6-3. Amphiboles from the Huangtongjiang gabbro

The amphiboles from the Huangtongjiang gabbro are characterized by high SiO_2 (49.17-55.37), MgO (12.57-17.54) but low Al_2O_3 (1.80-7.89), TiO_2 (0-0.63), FeOt (9.35-14.24), MnO (0-0.59) and K_2O (0.11-0.33). The Na_2O contents are moderate but variable, from 0.00 to 1.16. The MgO/FeOt ratios are very high, from 0.94 to 1.77. All analyzed samples plot in the actinolite, actinolitic-Hb and magnesio-Hb areas (Fig.4.16) according to the chemical classification (Leake, 1978; Hawthorne, 1981).

Apart from these amphiboles, there is a second type of amphibole with different chemical composition. This later amphibole usually occurs in small grains and coexists with polysynthetically twinned plagioclase. These late amphiboles present relatively low SiO_2 (44.93-48.45), MgO (10.79-12.83) but higher Al_2O_3 (8.60-11.89), FeOt (13.67-15.92), TiO_2 (0.31-0.89), Na_2O (1.07-1.32) and K_2O (0.39-0.61) (Table 4.8). These amphiboles are located in the magnesio-Hb area (Fig. 16). The chemical relations between the late amphiboles and the other amphiboles can be examined in the SiO_2 vs major oxide diagrams (Fig.4.18), and where they display a regular variation from gabbro to pyroxene diorite, indicating a regular chemical variation. This chemical change between the two different amphiboles may be controlled by the evolved magma which may be significantly changed during the differentiation from a common magma.

4-6-4. Comparison between amphiboles from different granitic plutons

The chemical compositions of amphiboles from different granitic plutons (Table 21) show a varied distribution, and the individual variation trends of different amphiboles from different plutons can be seen in the SiO_2 vs major major oxide diagrams and their derived ratios (Fig.4.19). Amphiboles from the Huangtongjiang gabbro are distributed in the highest SiO_2, MgO but lowest Al_2O_3, FeOt, TiO_2, MnO, K_2O and MgO/FeOt areas, and those from the Yunlougan granodiorite generally plot in the intermediate area, althouth they vary considerably. Amphiboles from the Sihui granodioritic enclaves are generally similar to those from the Yunlougan granite, but the former are distributed mainly in the MnO and Na_2O rich areas. The Huangtongjiang amphiboles are characterized by high MgO/FeOt but

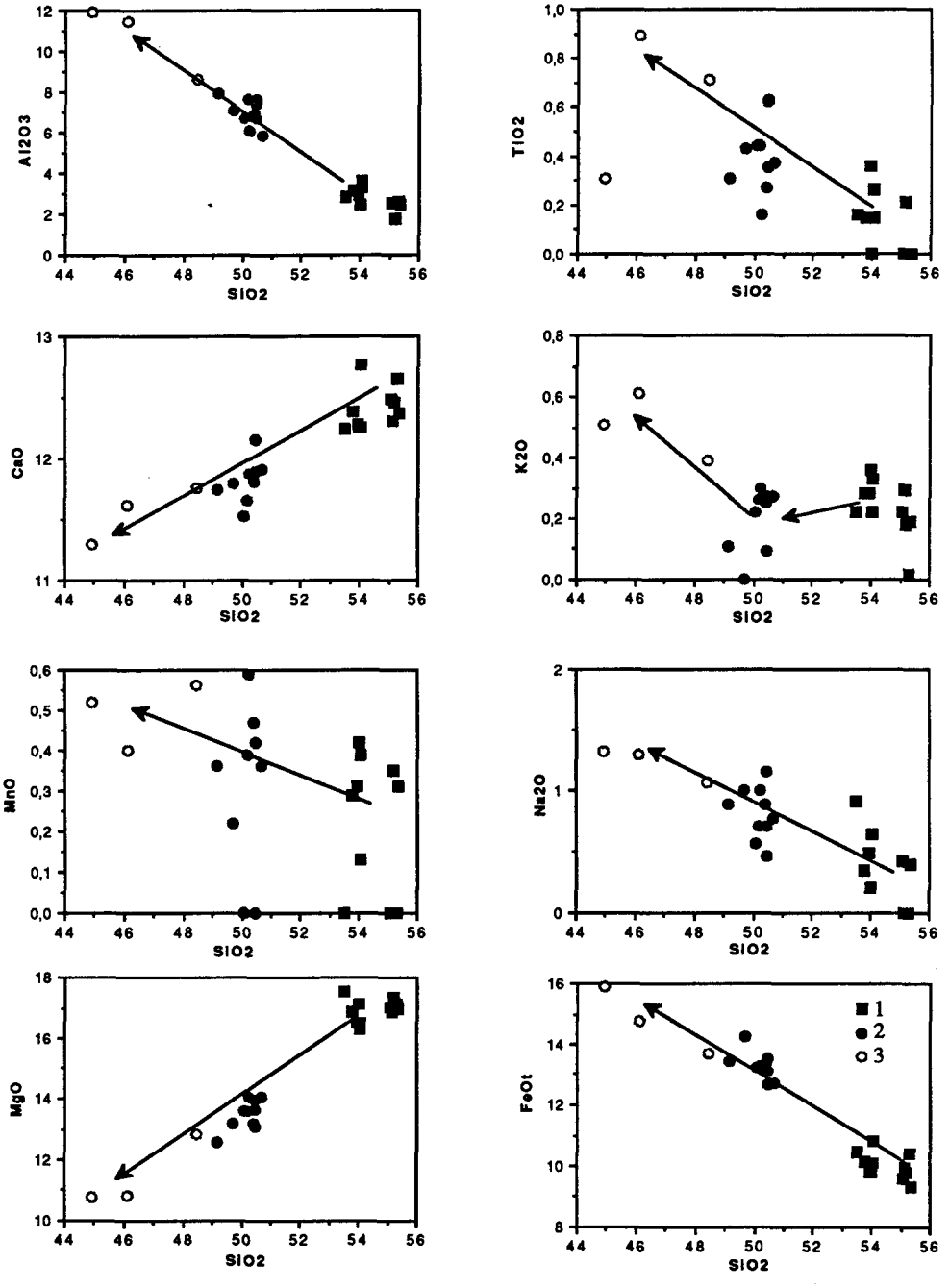

Fig. 4.18. Chemical variation of amphiboles from the Huangtongjiang gabbro
1 : Amphiboles from gabbro (C160-2); 2 : amphiboles from pyroxene diorite (C128); 3 : Amphiboles in matrix plagioclase

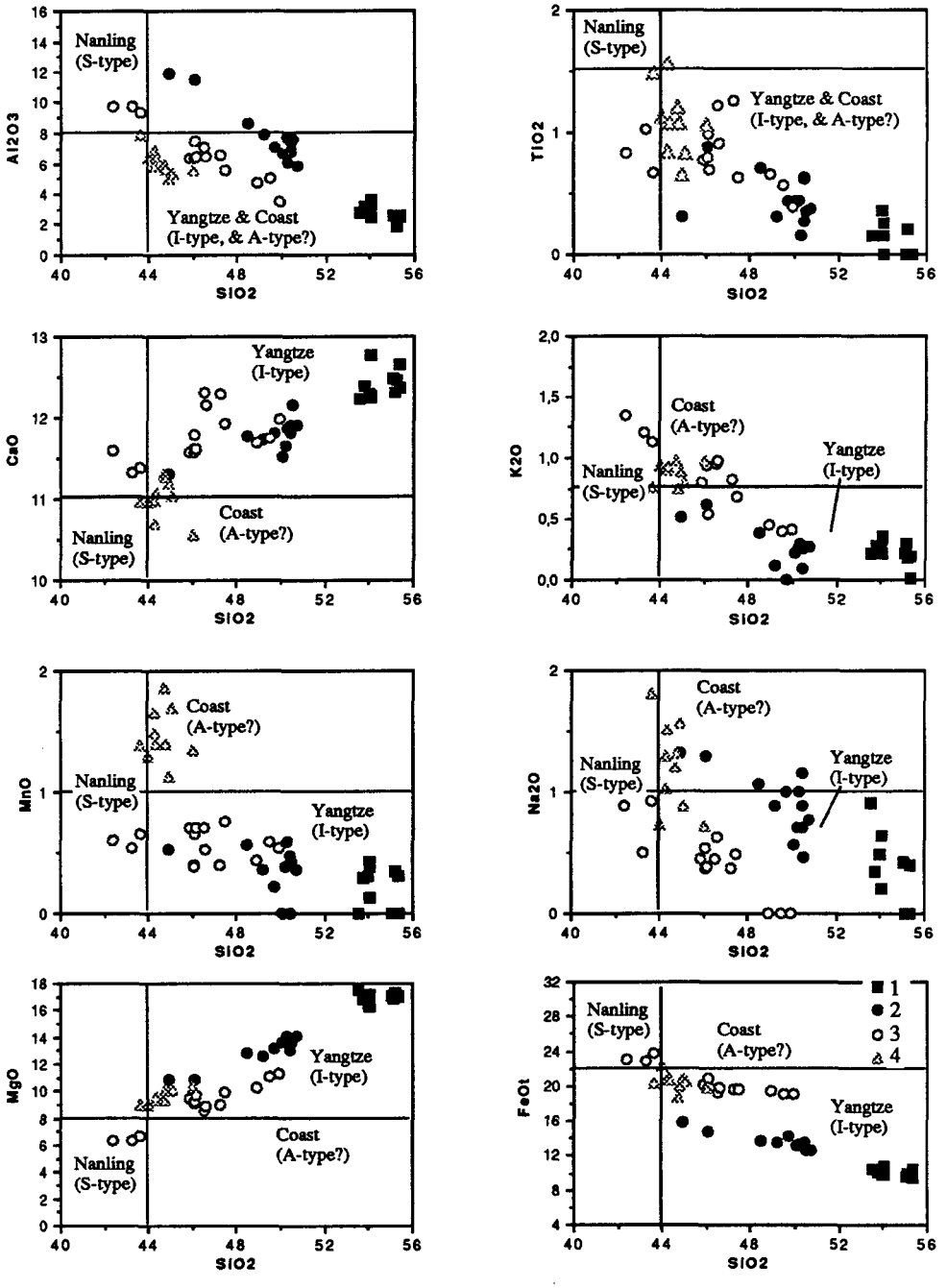

Fig. 4.19. Comparison between amphiboles from the granites of Hetai Area and South China (After Yang, 1992)

1 : Huangtongjiang gabbro (C160-2); 2 : Huangtongjiang pyroxene diorite (C128); 3 : Sihui enclave (C18-3); 4 : Yunlougan granodiorite (C9-1)

low Al, Mn and K, generally similar with the amphiboles from the calc-alkali basaltic rocks (Wones and Gilbert, 1982). Those from the Yunlougan granite reflect intermediate chemical features, whereas the amphiboles from the Sihui enclaves are dominated by higher alkali components and Mn, suggesting that they crystallized from more differentiated magmas with higher alkali-contents although their parent magma may be derived from the same source regions as the Huangtongjiang and the Yunlougan.

The MgO/FeOt ratios of mafic minerals are usually regarded as an indicator of magma crystallization temperature according to the experimental studies of amphibole stability by Wones et al. (1982). The amphiboles from the Huangtongjiang gabbro are characterized by the high MgO/FeOt ratios, whereas those from the Yunlougan and the Sihui have a relatively low MgO/FeOt, and the later amphiboles from the Yunlougan have the lowest MgO/FeOt ratio. This amphibole variation trend further indicates that magma evolution may produce decreasing Mg/Fe ratios in mafic minerals, but increasing alkali contents during the differentiation. In the chemical classification (Fig.4.16) amphiboles from the Huangtongjiang gabbro are located in the high Mg/(Mg+Fet) value (> 0.5) area, and those from the Yunlougan and the Sihui plot in the relatively low Mg/(Mg+Fet) value area (< 0.6), displaying a regular evolution from actinolitic hornblende-->Mg-hornblende-->Fe-hornblende with the evolution from basic to intermediate in the host rocks. In general, the chemical variation trend of amphibole show that the younger granites are the result of magma derived from the mantle.

4-7. Chemical characteristics of feldspar from the Hetai granites

The analyzed feldspars include both plagioclase and alkali feldspar. The feldspars from the individual granite bodies were determined by the electron probe and also the chemical compositions of some zoned feldspars were analyzed from center to margin of single mineral grains. The chemical variations of feldspars within a granite series are also examined to indicate significant changes during the magma evolution.

Plagioclase consists mainly of Si, Al, Ca, Na and K, and the substitution relation between these elements such as Si (4+) + Na (+) (K+) = Al (3+) + Ca (2+) may reflect magma differentiation. In particular, the relative proportion between Ca and Na contents in plagioclase is represented by An value which is an important parameter for indicatng chemical features and temperature of magma crystallization. The anorthite content is positively correlated with temperature during magma crystallization (Smith, 1983). The significant chemical change of feldspars from different type granites is represented in the following section.

4-7-1. Chemical characteristics of feldspar from the Caledonian granites

The chemical composition of feldspars from the Caledonian granites, including the Shijiang, Sidong and Shiniutou, are compiled in Table 22 (see Appendix III). The plagioclases from the Shijiang granite contain lower SiO_2 (61.77-65.25) and Na_2O (8.38-10.11) but higher Al_2O_3 (21.56-24.47) and CaO (3.26-6.09), than those from both the Sidong and Shiniutou, which display similar tendencies, having higher SiO_2 (64.94-69.26) and Na_2O (10.43-11.36) but lower Al_2O_3 (18.68-20.63) and CaO (0.93-3.41). Anorthite contents of plagioclase from the Shijiang granite are usually 30-22, higher than those (An=15-4) from the Sidong and Shiniutou granites. In the SiO_2 vs oxide and ratio diagrams (Fig.4.20), the plagioclases from the Shijiang are located in the lower SiO_2 and Na_2O but higher Al_2O_3 and CaO areas, but those from the Sidong and the Shiniutou plot in contrasting areas. However, the K_2O contents in the Shijiang plagioclases are slightly higher than the Sidong and Shiniutou.

The chemical variation of plagioclase presents normal evolution from the center to margin of single mineral grains. For example, as shown in Table 22, the center of zoned plagioclase from the Sidong granite always has lower SiO_2 and Na_2O but higher An, CaO and Al_2O_3 than the margin. The gradually decreasing An but increasing SiO_2/Al_2O_3 ratios with the zone developing from center to margin of plagioclase indicate ordinary magmatic evolution. Therefore, An contents of plagioclase not only are positively correlated with temperature of the magma crystallization, but also reflect the chemistry of magma which controls the chemistry of the plagioclase. The difference of chemical composition between plagioclases from the Shijiang and from the Sidong and the Shiniutou, for example, may be due to both different crystallizing temperature and chemical features of the magmas. The An

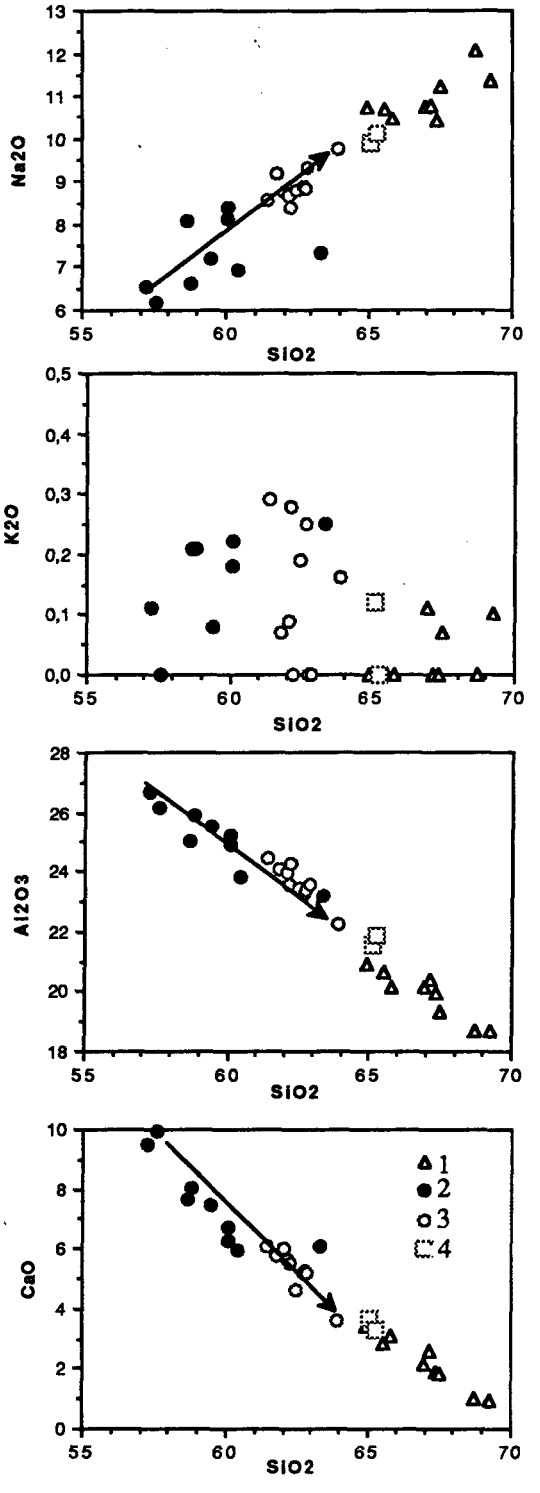

Fig. 4.20. Chemical variation of plagioclase from the Caledonian granites

1 : Sidong & Shiniutou granites; 2 : Shijiang dark enclave; 3 : Shijiang complex;

4 : Precambrian sedimentary rock

content difference suggest that the crystallizing temperature and calcium contents of the Shijiang granite are higher than the Sidong and Shiniutou. In addition, the chemical evolution of plagioclases from the different intrusive phases in the complex also display regular variations. Anorthite content, CaO and Al_2O_3 decrease but SiO_2 and Na_2O gradually increase from dark enclaves to the granitic complex in the SiO_2 vs oxide diagrams of the Shijiang complex (Fig.4.20).

4-7-2. Plagioclases from the Hercynian granites

The Hercynian granites include two different plutons, the Yunlougan granodiorite and the Guangning biotite monzogranite. The different types of granite is reflected in the chemistry of their plagioclase. The chemical compositions of plagioclases from the Hercynian granites are compared in the Table 23 (see Appendix III). It is evident from Table 23 that plagioclase from the Yunlougan are characterized by higher An (45-35), Al_2O_3 (24.10-25.47) and CaO (7.18-9.09) but lower SiO_2 (58.09-60.96) and Na_2O (6.67-7.79) relative to those from the Guangning, which contain higher SiO_2 (61.95-65.52) and Na_2O (7.71-10.05) but lower An (30-15), Al_2O_3 (20.64-23.11) and CaO (3.77-6.39). In the SiO_2 vs An and oxide diagrams (Fig.4.21), plagioclase from the Yunlougan granodiorite are located in lower SiO_2 and Na_2O but higher An, Al_2O_3 and CaO areas, whereas those from the Guangning plot in contrasting area. The obvious chemical difference between plagioclases from different granites may be mainly due to the geochemical properties of parent magmas and their crystallizing temperatures, although their bulk rocks have a similar chemical compositions except for CaO as shown in the Table 4. The plagioclases from the Yunlougan have An 45-35, demonstrating that they were crystallized from Ca-rich magma at relatively high temperature; whereas the plagioclases from the Guangning only have An 30-15, indicating that they were produced by lower Ca magma at lower temperatures. In addition, the zoned plagioclases all display a normal evolution of decreasing An and Al_2O_3 but increasing SiO_2 towards the rim in both the Yunlougan or the Guangning plutons as shown in Table 23.

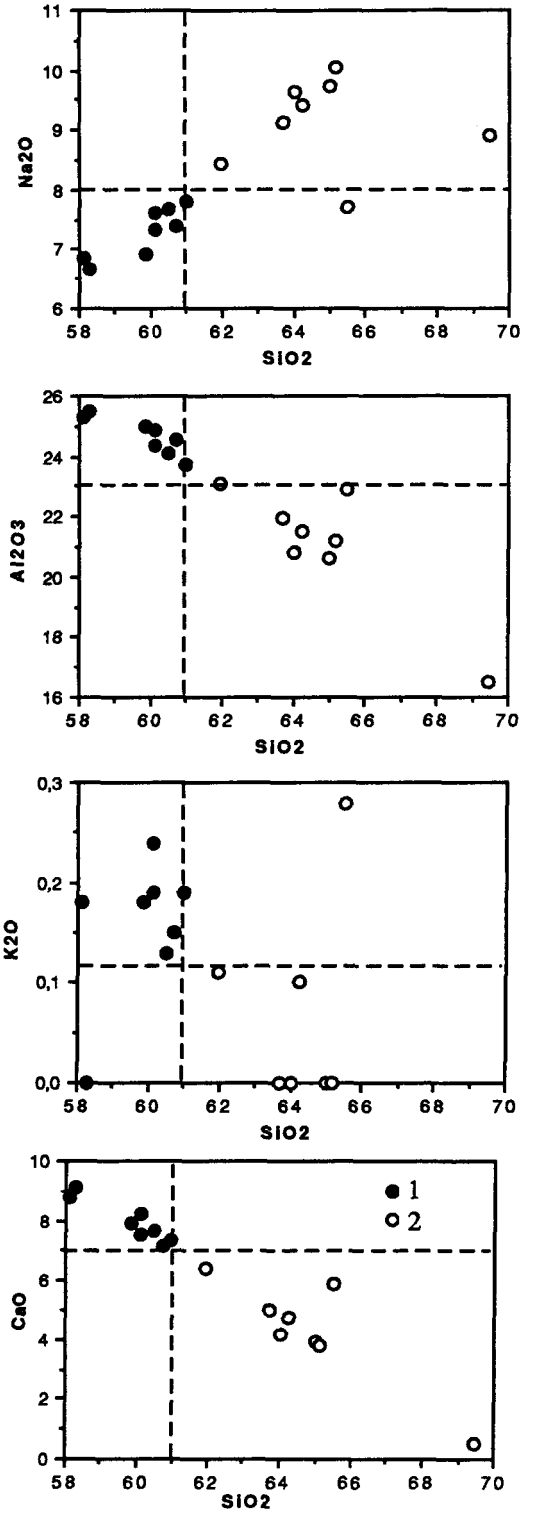

Fig. 4.21. Comparison between plagioclases from the different Hercynian plutons
1 : Yunlougan granodiorite; 2 : Guangning monzogranite

4-7-3. Plagioclase from the Indosinian granites

Plagioclase plays an important role in the evolution of the Wuchun pluton. The large zoned megacrysts occur widely in the host monzogranite. The granodioritic enclaves contain plagioclase xenocrysts, which occur as glomeroporphyritic aggregates and are different from the groundmass plagioclase. The host monzogranite contains more cumulus plagioclase phenocrysts, and these plagioclase phenocrysts are usually large and characterized by a plagioclase core with an albite and K-feldspar margin, forming the giant zoned phenocrysts and a rapakivi-like texture .

It is clear that the plagioclase xenocrysts from the granodioritic enclaves (Table 24, see Appendix III) contain higher An (60-45), Al_2O_3 (23.44-24.78) and CaO (9.11-10.01) but lower SiO_2 (56.07-56.69) and Na_2O (3.70-7.33) than the groundmass plagioclases which have An (35-25), Al_2O_3 (22.32-23.95), CaO (5.31-6.91), SiO_2 (61.34-62.80) and Na_2O (7.83-9.07). In addition, K_2O contents in plagioclase xenocrysts are evidently higher (1.95-5.87) than those in groundmass plagioclases (0.14-0.51), and this may be due to the fact that the crystallizing temperature of plagioclase xenocrysts is higher than the groundmass plagioclases, because $KAlSi_3O_8$ has a wider solid solution with $CaAl_2Si_2O_8$ and $NaAlSi_3O_8$ under high temperature condition in the ternary system (Yund & Tullis, 1983; Green and Usdansky, 1986). Therefore, it is likely that these plagioclase xenocrysts are earlier cumulus minerals which are carried by the rising granitic magmas. The parent magma may be more basic in chemical composition than granodioritic enclaves and monzogranite. The An content of the xenocrysts is 60-45, similar to the plagioclase xenocrysts from mafic magmatic enclaves in some granites of the Sierra Nevada batholith, California (Barbarin, 1990), and is different from the matrix plagioclase with an An content of 35-25.

The zoned plagioclase phenocrysts in the host monzogranite (Table 24) can be divided into two parts, the high Ca core and the high Na margin. The high Ca phenocryst core resulted from earlier crystallization and orientation within the magma foliation during the emplacement of the magma. The Na-rich margin forms an outer rim, which usually contains myrmekite. As shown in Table 24, the plagioclase phenocryst core is characterized by higher An (35-25), CaO (6.78-8.58) and Al_2O_3 (23.61-24.77) but lower SiO_2 (58.39-61.34) and Na_2O (6.95- 8.50), greatly differing from the margin which contains higher

SiO_2 (63.13-69.92) and Na_2O (8.56-12.19) but lower An (15-0), CaO (0.27-5.77) and Al_2O_3 (17.70-22.16), nearly pure albite. Similarly, the K_2O contents of the core (0.16-0.40) are higher than those in the margin (0-0.26), demonstrating that the crystallizing temperature of the core is higher than that of the margin. This obvious chemical difference in these large zoned feldspar phenocrysts further demonstrates that magma differentiation is characterized by the accumulation of Ca-rich plagioclase (phenocryst core) at an earlier stage, and then the differentiated magma richer in Na (and K) continued rising and crystallized between the Ca-rich plagioclase phenocrysts, forming the low Ca but high Na outer rim. This significant feldspar change indicates magma evolution and demonstrates that the generation of the megacryst monzogranite may be explained by ordinary magma differentiation but not by alkaline replacement (Dai, 1986).

The genetic relations between the granodioritic enclaves and host monzogranite are reflected in the SiO_2 vs An and oxide diagrams of plagioclase (Fig.4.22). It is evident from Fig.4.22 that the xenocrysts plot in the highest An, CaO and Al_2O_3 but lower SiO_2 and Na_2O areas. The common plagioclases from the granodioritic enclaves, however, are in the higher An, CaO and Al_2O_3 but lower SiO_2 and Na_2O areas, coincident with the cumulus zoned phenocryst core plagioclases from the host monzogranite, whereas the margins are located in the albite area (An < 10). The variation from the xenocrysts, core plagioclase to margin albite displays a regular trend, indicating normal processes of magma differentiation took place. Therefore, it is reasonable to infer that the entire magma evolved from basic (basalt ?) --> intermediate --> acid --> alkali magma.

4-7-4. Plagioclase from the Sihui granites

The Sihui granites contain granodioritic enclaves in a biotite alkali-feldspar granite. The plagioclases from both are analyzed and their chemical compositions are listed in Table 25 (see Appendix III).

The zoned plagioclases from the granodioritic enclaves display a normal variation in An contents and major oxides from center to margin as shown in Table 25 and Fig.4.23. The center of zoned plagioclases is characterized by higher An (45-30), CaO and Al_2O_3 but lower SiO_2 and Na_2O; whereas the margin is characterized by higher SiO_2 and Na_2O but

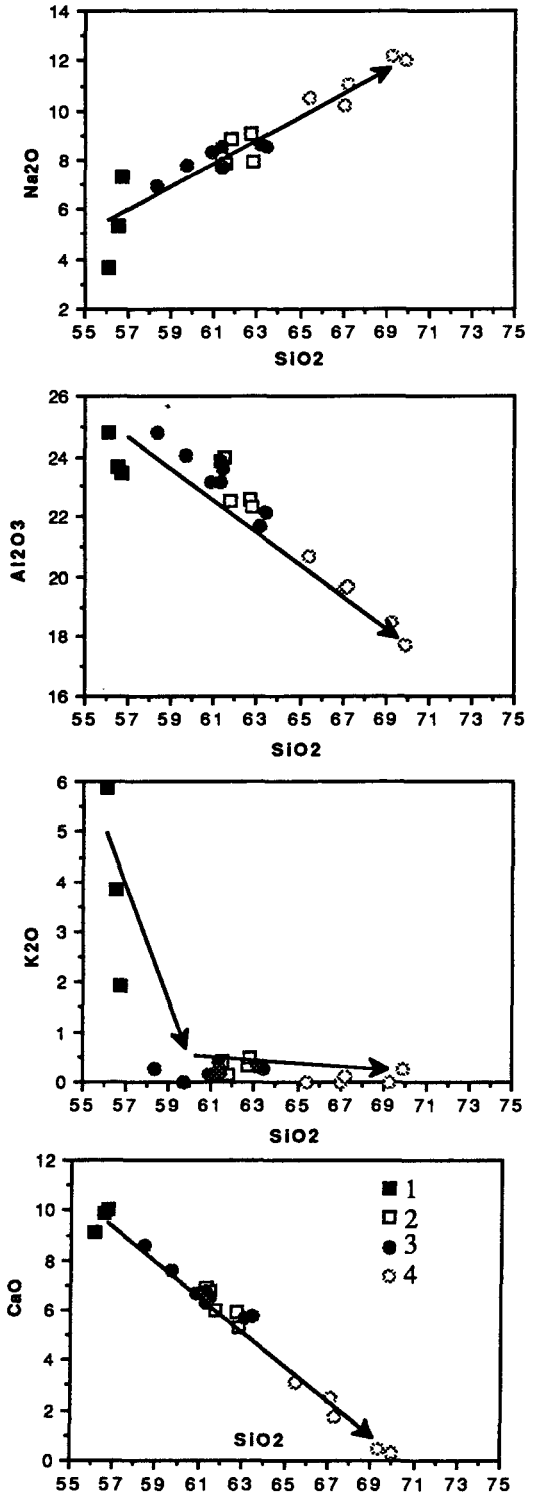

Fig. 4.22. Chemical variation of plagioclase from the Indosinian granite suite

1 : Plagioclase xenocryst from the Wuchun enclave; 2 : Common plagioclase from Wuchun enclave; 3 : Core of plagioclase from the Wuchun monzogranite; 4 : Margin of plagioclase from the Wuchun monzogranite

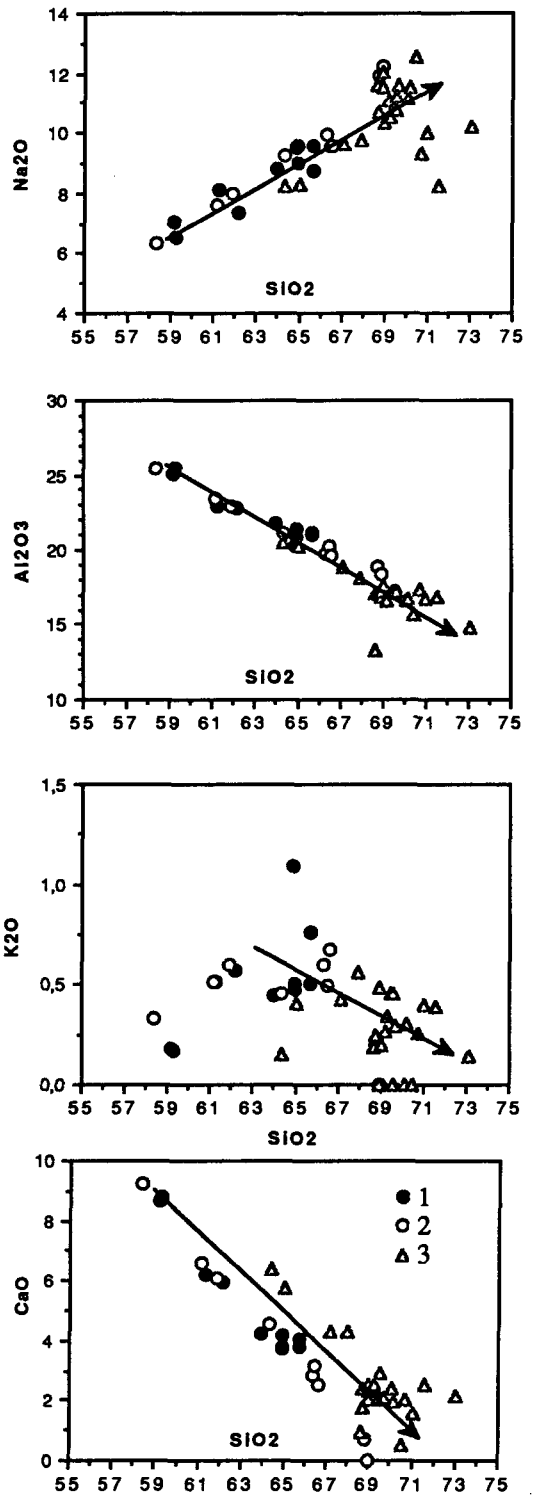

Fig. 4.23. Chemical variation of plagioclase from the Yanshanian granite suite

1 : Plagioclase from the Sihui enclave; 2 : Core of plagioclase from the Sihui alkali-feldspar granite; 3 : Margin of plagioclase from the Sihui alkali-feldspar granite

lower An (30-15), CaO and Al_2O_3. The margin is more similar to the polysynthetically twinned matrix plagioclase (An=30-15). In general, the An contents gradually decrease from center (An=45-30) to margin (30-15), reflecting ordinary magmatic differentiation.

The zoned plagioclase phenocrysts are widely developed in the alkali-feldspar granites. These patchy zoned plagioclase phenocrysts display cumulus features and usually contain a growth zone of albite and K-feldspar, forming an outer alkaline feldspar rim. The patchy zoned phenocrysts contain higher An (45-30), Al_2O_3 and CaO, but lower SiO_2 and Na_2O than their margins, An (20-0), which are similar to common polysynthetically twinned plagioclases (Table 25). In addition, the K-feldspar in the margin contains higher Na_2O (about 2.10-3.89) contents, indicating a solid solution at high magma crystallization temperature (Yund & Tullis, 1983).

Clearly, the chemical compositions of plagioclase whether from the granodioritic enclave or from the host K-feldspar granite display regular variations, and all demonstrate normal magma crystallization. Their textural features and chemical trends suggest that central cores of plagioclase grains may have resulted from accumulation at an earlier stage, and then the differentiated magma richer in Na and K continue to crystallize, forming the outer alkaline rims on the cumulus plagioclases.

4-7-5. Comparison between plagioclase from the Huangtongjiang gabbro and from the Precambrian sedimentary rocks

The chemical compositions of plagioclases from the Huangtongjiang gabbro and from the Precambrian sedimentary rocks are compared in Table 26 (see Appendix III). It is evident that the plagioclases from the Huangtongjiang gabbro are characterized by higher An (67-55), CaO (11.08-13.67) and Al_2O_3 (28.71-30.88) but lower Na_2O (3.66-4.99) and SiO_2 (52.00-54.71), whereas those from the Precambrian sedimentary rocks have lower An (20-15), CaO (3.26-3.6) and Al_2O_3 (21.56-21.87) but higher Na_2O (9.92-10.11) and SiO_2 (65.08-65.25).

4-7-6. Geochemical variation of plagioclase from granites of different ages

The chemical variations of plagioclase can be represented by relative changes of An contents, and the plagioclases from different granites plot in the An-Ab-Or ternary diagram (Fig.4.24). It can be seen that the plagioclases from the older granites are located mainly in the oligoclase and albite fields, whereas those from the younger granites vary from labradorite through andesine and oligoclase to albite with granitic evolution from gabbro --> granodiorite --> monzogranite --> alkali-feldspar granite. Furthermore, the plagioclases from the Shijiang and Guangning granites contain more calcic plagioclase (oligoclase) than those (oligoclase and albite) from the Sidong and Shiniutou granites, although the bulk chemical compositions of later intrusive phases of the Shijiang are comparable to the Sidong and Shiniutou granites. The Hercynian granites have evident chemical differences between plagioclases from the Guangning biotite monzogranite and from the Yunlougan granodiorite. The plagioclases with lower An content from the Guangning monzogranite may possibly reflect a Ca-poor parent magma crystallizing at a lower temperature, whereas the plagioclases with higher An from the Yunlougan granodiorite indicate a Ca-rich parent magma crystallizing at a higher temperature. The chemical variations of plagioclases from different intrusive phases of the Indosinian and Yanshanian granites may be mainly the result of magma differentiation. Accumulation of Ca-rich plagioclases plays an important role during magma differentiation. As the Ca-rich plagioclases crystallized in the early stage, the differentiated magmas become richer in Na and K, and later crystallization formed the alkaline feldspar growth zones on the anorthitic core. The dark enclaves are an earlier intrusive phase, and the glomerporphyritic xenocrysts in the Wuchun granodioritic enclaves demonstrate the parent magmas may have evolved from a basic magma.

Plagioclases from the dark enclaves of the Shijiang granites, on the other hand, are located in the andesine area (Fig.4.24), and their anorthite contents are higher than those from the Shijiang granites. This may further imply that the dark enclaves are the unmelted source rock of the Shijiang granites. Comparing the chemical features of all plagioclases shows that plagioclase from the older granites are coincident to Precambrian metasedimentary rocks, indicating that their source rocks may be derived from the Precambrian sedimentary basement;whereas those from the intermediate-basic phases of the

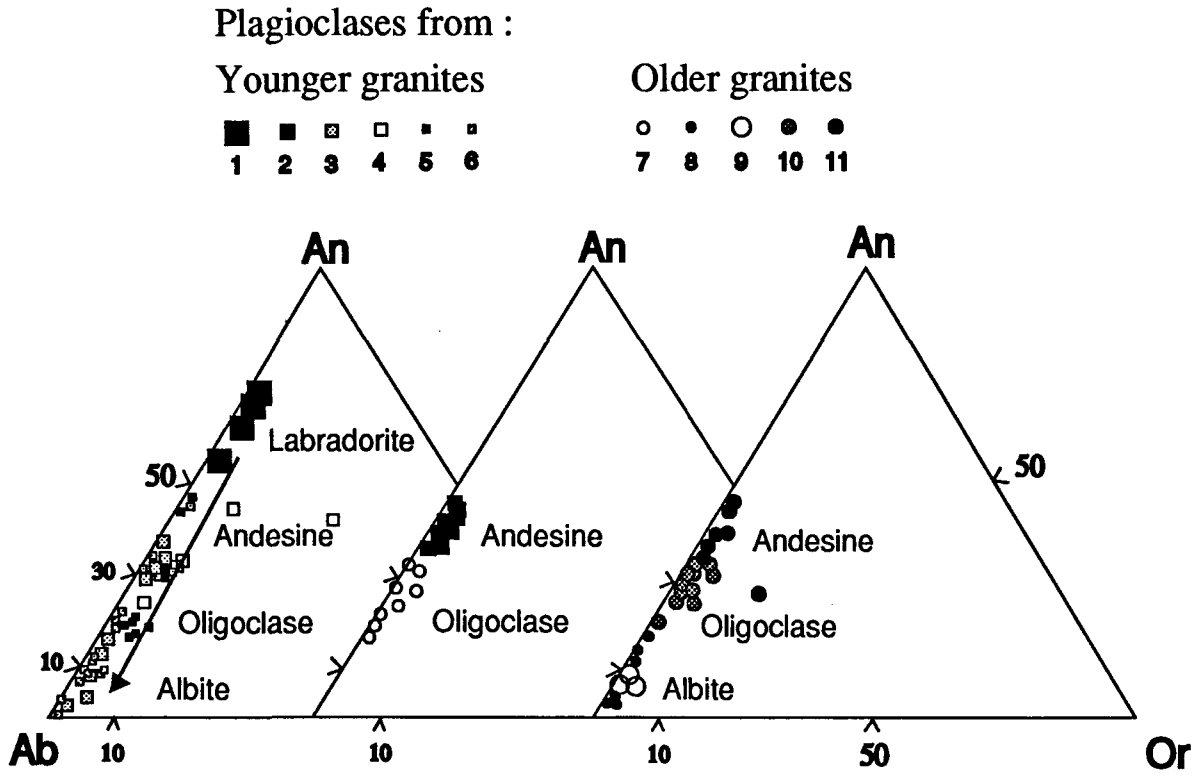

Plagioclases from : 1. Huangtongjiang gabbro; 2. Yunlougan granodiorite; 3. Wuchun granodioritic enclaves
4. Wuchun megacryst monzogranite; 5. Sihui granodioritic enclaves;
6. Sihui alkali-feldspar granite;
7. Guangning biotite monzogranite; 8. Sidong granite; 9. Shiniutou granite;
10. Shijiang granite; 11. Shijiang dark enclaves

Fig. 4.24. Chemical variation of plagioclases on the An-Ab-Or ternary diagram (After Ribbe, 1983)

younger granites are similar to Huangtongjiang gabbro and their later plagioclases with lower Ca but higher Na reflect the degree of differentiation of the magma.

4-8. Mineral criteria for identifying different granite types

The chemical compositions of biotite, amphibole and plagioclase from the different granites of the Hetai Area show different geochemical trends and significant differences reflecting the geochemical background features and magma evolution of different type granites. Generally, the geochemical features of biotite, amphibole and plagioclase from the different granites of the Hetai Area is compared in the following table (Table 4.1).

It can be seen from Table 4.1 that the older granites are characterized mainly by Fe-biotite plagioclase with lower anorthite content (An < 30, most =15-5) and a lack of hornblende, whereas the younger granites are characterized by Mg-biotite, Mg-hornblende and actinolite, and plagioclase with higher anorthite content (An=70-30), which becomes rich in sodium and potassium in the later stage (monzogranite and alkali-feldspar granite) because of magma differentiation. Clearly, the different chemical features of these minerals indicate the different genetic type of their granites. Comparison with results for other areas (Speer, 1982; Yang et al., 1986a and 1992) in Table 4.1 shows that the biotites from the older granites are similar to the Nanling granites (S-type) in South China and may be derived mainly from the crustal source magmas with a peraluminous component; whereas the younger granites are similar with Yangtze granites and Coast granites (I-type, and A-type?) and may be evolved mainly from an upper mantle (and lower crustal) basaltic magma.

Table 4.1. Comparison of biotite and amphibole from different granites of the Hetai Area and South China

Type	Older	(S-type)		Younger		(I-type)		Younger	(A-type?)	
Area	Hetai	Nanling*		Hetai		Yangtze*		Hetai	Coast*	
Rock	Biotite granite			Granodiorite and gabbro				Alkali-feldspar granite		
Mineral	Biotite	Amphibole	Biotite	Amphibole	Biotite	Amphibole	Biotite	Amphibole	Biotite	Amphibole	Biotite	Amphibole
Colour	Brown-red		Brown-red		Brown-green		Brown-green		Brown-green			
SiO2 (%)	most < 36				most > 37	> 44		> 44	> 37			> 44
Al2O3	> 15		> 15	< 44	< 15	< 8	< 15	> 10	< 14		< 15	< 8
TiO2	< 3		< 3	> 1.1	>3	< 1.5	> 3	< 1.5	> 3		about 3	< 1.5
MgO	most < 8		< 8	< 10	> 8	> 8	> 8	> 10			> 8	< 8
FeOt				> 18								
FeO	most > 20		> 20		most < 20	< 20	< 20	< 18			< 20	> 20
MnO	large scale		large scale	0.2-0.8	< 0.8	large scale	0.1-1.1	< 0.6	> 0.8		0.7-3.5	0.3-6.8
Na2O				1.2-2.5		large scale		0.2-2.0				
K2O				> 0.8								
CaO												
MgO/FeO	most < 0.50		< 0.50		most > 0.45		> 0.45		most > 0.45		> 0.45	< 0.2
MgO/FeOt				< 0.6				> 0.6				
F (ppm)	3500-5500				3000-5100				6050-7300			
Li	100-360		>1000		180-514		94		697-1991		540	
Rb	632-734		>1000		447-732		782		1000-1056		875	
Zn	425-550		810		425-510		410		600-1050		940	
Co	56-65		38		59-98		58		39-54		37	
Ni	33-37		78		32-39		120		24-32		63	

* Data from Yang (1986 and 1992)

CHAPTER V

TEMPERATURE AND PRESSURE ESTIMATES

5-1. Introduction

The relationship of mineral assemblages in granitic rocks to the intensive variables of the original magma have been discussed in many papers (Ishihara, 1977; Didier et al., 1982; Chappell and White, 1974; Yang et al.1986a). For example, certain granites of Japan are classified as Magnetite-series or Ilmenite-series as a result of different oxygen fugacity during the evolution of the granitic magma (Ishihara, 1977) based on the species of opaque minerals; White and Chappell (1983) emphasized that S-type granites contain more Al-rich minerals such as cordierite, muscovite, andalusite, sillimanite or almandine because of aluminum saturation of the magma. The Nanling granites of South China are characterized by Al-silicate + Fe-biotite (+ little Fe-hornblende) assemblage, derived from crustal source regions (S-type). The Yangtze and the Coast granites are characterized by Ca-rich silicate + Mg-biotite + Mg-hornblende assemblage, derived from lower crustal and upper mantle source regions (Wang et al., 1984c; Zhang et al., 1984; Yang et al., 1986a). The DTA (differential thermal analysis) of biotite show that Fe-biotite from the Nanling granites displays a weak heat absorption valley on the DTA curve at lower temperature (1150 °C), wheras Mg-biotite from the Yangtze and Coast granites has a strong valley at a higher temperature (1200 °C), indicating a difference of magma crystallization temperature between different types of granite (Yang et al., 1986a). Al in amphibole has been used as a geobarometer for magma emplacement (Hammarstrom and Zen, 1986). Therefore, the chemical data of Mg and Fe^{2+} in biotite and Al in amphibole are used for estimating the petrogenetic conditions (T and P) of different granites in the Hetai Area.

Silicate melt inclusions are very useful for discussing granite generation, because they result only from the silicate magmatic crystallization, rather than from granitization. Consequently, silicate melt inclusion must be identified based on their petrographic features, and their formation conditions may be estimated for understanding magma crystallization. Silicate melt inclusions found in the Hetai granites, not only in younger granites but also in older granites, may be regarded as important evidence for magmatic granite. Furthermore, the temperature of homogenization of silicate melt inclusions are tested by heating experiments and may also be used to establish the temperature of magma crystallization and for distinguishing different granites. Some fluid inclusion data have been obtained and are compared with data from gold deposits in the Hetai Area.

5-2. T and P estimates of granites based on biotite and amphibole

The chemical compositions of biotite and amphibole are closely related to magmatic evolution during granite formation (Wones, 1965 and 1981). The relation between Fe^{2+} and Mg in biotite and Al contents in amphibole in particular are considered as useful parameters for estimating temperature (T) and pressure of magma crystallization of granite. The analyzed biotite and amphibole samples will be used to estimate the temperature and pressure of crystallization for the different granites of the Hetai Area.

5-2-1. Temperature estimate based on Mg and Fe^{2+} in biotite

There is a close relation between T and $Fe^{2+}/(Mg+Fe^{2+})$ ratio in biotite relative to different buffering conditions based on the experimental result of biotite stability by Wones (1965). Biotites from different granites are characterized by different ratios of $Fe^{2+}/(Mg+Fe^{2+})$ and temperature (T) correlates inversely to this ratio. Biotites from the Huangtongjiang pyroxene diorite, Yunlougan granodiorite, Wuchun granodioritic enclaves and monzogranite and Sihui granodioritic enclaves and alkali-feldspar granite have lower $Fe^{2+}/(Mg+Fe^{2+})$ ratios than biotites from the Shijiang, Sidong and Shiniu biotite granites and Guangning monzogranite (Table 5.1). The temperature estimates are also controlled by

Table 5.1. Temperature estimate by biotite, granites of the Hetai Area

Age	Sample	Location	Fe2+/(Mg+Fe2+)	Buffer condition*	T (°C)
Caledonian	C16-2,3,4,5	Shijiang	0.58	Fe_2SiO_4-SiO_2-Fe_3O_4	800-850
	C7-1	Sidong	0.79	Fe_2SiO_4-SiO_2-Fe_3O_4	750-800
	C7-2	Sidong	0.82		700-750
	C17	Shiniutou	0.91	Ni-NiO	700-750
Hercynian	C84, C13	Guangning	0.61	Ni-NiO	800-850
Hercynian	C9-1	Yunlougan	0.55	Ni-NiO & Fe_3O_4-Fe_2O_3	850-900
Indosinian	C10-1	Wuchun	0.52	Fe_3O_4-Fe_2O_3	850-900
	C10-2	Wuchun	0.58	Fe_3O_4-Fe_2O_3	850-900
Yanshanian	C18-3	Sihui	0.45	Fe_3O_4-Fe_2O_3	900-950
	C18-1	Sihui	0.48	Fe_3O_4-Fe_2O_3	850-900
	C18-2	Sihui	0.53	Fe_3O_4-Fe_2O_3	850-900
	C128	Huangtongjiang	0.45	Ni-NiO & Fe_3O_4-Fe_2O_3	900-950

* Based on Wones (1965)

different buffering conditions, which are roughly reflected by the Fe^{3+} content of the biotite, and which depend on the oxidation-reduction state of the magma. So, Fe^{3+} in biotite is an important parameter for estimating buffering conditions in the experiments on biotite stability as shown by Wones (1965). Biotites from the Sihui K-feldspar granite and Wuchun monzogranites have the highest Fe^{3+} based on wet chemical analyses, and they plot near the Fe_3O_4-Fe_2O_3 buffer line in the buffering diagram (Wones, 1965). Biotites from the Yunlougan granodiorite, Huangtongjiang pyroxene diorite and their enclaves plot near the Ni-NiO buffer line, whereas biotites from the Sidong, Shijiang, Shiniutou and Guangning biotite granites plot near the Fe_2SiO_4-SiO_2-Fe_3O_4 buffering line. The magma crystallization temperatures of the different granites can be estimated from the diagrams of T vs $Fe^{2+}/(Mg+Fe^{2+})$ (Wones, 1965), and these are compiled in Table 5.1. It can be seen that the estimated magma crystallization temperature for different intrusions are different, the Huangtongjiang pyroxene diorite being highest (900-950 °C), the Yunlougan granodiorite about 850-900 °C, the Wuchun granites about 850-900 °C, and the Sihui complex about 850-900 °C; whereas the Sidong and Shiniutou granites about 700-750 °C, and the Shijiang complex and Guangning monzogranite about 800-850 °C. Clearly, the crystallization temperatures of the Yunlougan granodiorite and the Wuchun and the Sihui granite suites are higher than those of the Caledonian Shijiang, Sidong and Shiniutou and the Hercynian Guangning granites.

5-2-2. Pressure estimates based on Al content in amphibole

Pressure is the most difficult intensive variable to estimate in granites, although Tuttle and Bowen (1958) indicated that for a given pressure the composition of a liquid coexisting with H_2O vapor, quartz and alkali feldspar may be shown to have a unique composition. Wones (1981) considered that one of the most important relations is the muscovite + quartz curve, which puts a limit on the minimum pressure at which two mica granites crystallize. In the Hetai Area, the different granites are characterized by different mineral assemblages and their estimated temperatures (based on biotite) show some variations. If it can be assumed that the granites crystallized from a water-saturated magma, the minimum pressures roughly estimated by means of P-T diagram by Tuttle and Bowen (1958) suggest that the minimum pressures of the older granites (Sidong, Shiniutou,

Shijiang and Guangning granites) may be higher than those of the younger granites (Yunlougan, Wuchun and Sihui granites and Huangtongjiang gabbro) based on their estimated temperature data. This, however, is only a relative measurement.

An empirical igneous geobarometer for estimating pressures of magma emplacement and crystallization based on Al content of amphibole was first suggested by Hammarstron and Zen (1986). They considered that amphibole data collected from plutonic complexes and from phase equilibrium experiments using natural rocks or synthetic analogue compositions show a similar Al(t)-Al(IV) trend and systematic pressure effects in that high-pressure calcic amphibole have high Al(t). The relation between Al(t) in hornblende and pressure for data from calc-alkaline plutons is

$$P\ (\pm 1.86\ \text{kbar}) = -3.92 + 5.03\ \text{Al (t)}, \qquad r^2 = 0.80 \quad .....(1)$$

$$P\ (\pm 2.11\text{kbar}) = 2.01\ \lg 1.27\ \text{Al (t)}, \qquad r^2 = 0.77 \quad .....(2)$$

In equation (1), the Al (t) content of hornblende is suggested as a pressure indicator accurate to within ±1.86 kbars for crystallization of plutonic rocks of appropriate bulk composition and mineral assemblage.

Subsequently, Hollister et al. (1987) tested the proposed hornblende geobarometer of Hammarstrom and Zen and suggested the equation

$$P\ (\pm 1\ \text{kbar}) = -4.76 + 5.64\ \text{Al (t)}, \qquad r^2 = 0.97 \quad .....(3)$$

This equation decreases the pressure error from the ±1.86 kbars suggested by Hammarstrom and Zen (1986) to ± 1 kbars.

Schmidt (1992) calibrated the Al-in-hornblende barometer experimentally under water-saturated conditions at pressures of 2.5-13 kbars and temperatures of 700-655 °C, and suggested that the relation between pressure and Al (t) content in hornblende fits the equation:

$$P\ (\pm 0.6\ \text{kbar}) = -3.01 + 4.76\ \text{Al (t)}, \qquad r^2 = 0.99 \quad .....(4)$$

This equation further decreases the error of pressure from ± 1 kbar suggested by Hollister et al. (1987) to ± 0.6 kbar.

However, the estimated pressure values may occur as < 0 , when the limiting Al(t) contents in amphibole are less than 0.78, 0.84 and 0.63 with respect to equations (1), (3) and (4). Therefore, equations (1), (3) and (4) may be not used for some intrusions, because the Al(t) contents in amphibole from these intrusions are too low. For example, the Al (t) content in amphibole from shallow intrusions such as the Coast granites in South China is usually low. In this situation, equation (2) may be used.

Pressure values are derived from the Al (t) content of amphibole from some of the granites in the Hetai Area. Equations (1), (3) and (4) were used to calculate most of the pressure values. In addition, some samples of lower Al (t) content are estimated by equation (2), because Al(t) content in these amphiboles is less than the limiting value for equations (1), (3) and (4). The calculated results are listed in Table 5.2. It can be seen that the calculated results by equation (4) are higher than those by equations (1) and (3), which are generally similar (Table 5.2). So, the calculated results by equations (1) and (3) are used to estimate the depth of magma emplacement. On the other hand, some samples show an evolution trend of Al (t) in amphiboles from the same pluton, and in this situation, only representative Al (t) contents are chosen to calculate the pressure parameter. For example, the Al (t) contents of amphibole inside earlier zoned plagioclase from the Yunlougan granodiorite are lower than those in contact with the outer rims of the plagioclase. According to the pressure calculations, it may be estimated that the solidification of the Yunlougan granodiorite occurred at a depth between 6-10 km, the Sihui granodioritic enclave at 3-8 km depth, and the Huangtongjiang gabbro at less than 3 km depth. Furthermore, compared with amphiboles from the Yangtze, the Nanling and the Coast granites in South China, it is clear from Table 5.2 that the amphiboles from the Yunlougan, the Sihui and the Huangtongjiang plutons are similar to those of the Yangtze and the Coast granites.

Table 5.2. Pressure estimate by Al in amphibole from granites of the Hetai Area and South China

Age	Sample	Rock	Location	Al (t)	P1* (kbar)	P3* (kbar)	P2* (kbar)	Depth (km)
Hercynian	C9-1	Granodiorite	Yunlougan	1.12-1.34	1.71-2.82	1.56-2.80		6.0-10.0
Yanshanian	C18-3	Enclave	Sihui	0.92-1.25	0.71-2.37	0.43-2.29		3.0-8.0
	C128	Px-diorite	Huangtongjiang	1.00-1.37	1.11-2.97	0.88-2.97		3.0-10.0
	C160-2	Gabbro	Huangtongjiang	0.30-0.61			0.11-0.47	< 3.0
Yanshanian			Yangtze Area	0.82-1.45	< 3.37	< 3.42		< 12.0
Yanshanian			Coast Area	< 0.60			< 0.50	< 2.0
Caledonian-Yanshanian			Nanling Area	1.39-1.92	3.07-5.74	3.08-6.07		11.0-22.0

*P1=-3.92+5.03 Al(t); P2=2.01 Lg1.27 Al(t); P3=-4.76+5.64 Al(t)

5-3. Silicate melt inclusions in the different Hetai granites

In contrast to the numerous studies on fluid inclusions, very little is known about silicate melt inclusions in intrusive rocks. The presence of silicate melt inclusions in eruptive and shallow intrusive rocks may provide useful data for magma evolution (Roedder, 1977, 1979, 1984 and 1992; Lu et al., 1990; Frezzotti,1992). The studies of Frezzotti (1992) on silicate melt inclusions established a possible model for fluid evolution with a hydrosaline melt exsolving from the magma at a late stage. He found that devitrified silicate melt inclusions are present in some magmatic miarolitic quartz from the Mount Genis granite, a post-tectonic intrusion, and examined the compositions of silicate melt inclusion and the effect of shallow emplacement on volatile evolution. His studies indicated that these magmatic remnants show initial melting at 680-720 °C and the presence of two immiscible fluid phases of mixed hydrosaline melt and silicate melt in some inclusions based on heating experiments and electron microprobe analyses. He considered that brines can occur by direct magmatic immiscibility in the magmatic late-stage.

Silicate melt inclusions in deeply emplaced granitic rocks have been ignored because they are more difficult to identify than those in volcanic and shallow intrusive rocks. Silicate melt inclusions have not been studied in granites of the Hetai Area, although detailed studies of silicate melt inclusions as magmatic remnants could give direct evidence about magmatic evolution and mineralization. In this work special attention has been paid to silicate melt inclusions in different granites of the Hetai Area in order to constrain granitic magmatism. Silicate melt inclusions have been found not only in relatively shallow intrusive bodies (the Sihui and Wuchun granites) but also in intrusives such as the Shijiang and the Guangning granites, which were considered to be the result of granitization (Mo, 1987 and 1989; Dai,1986). The presence of the silicate melt inclusions is useful in reconstructing the granite genesis.

5-3-1. Petrographic features of silicate melt inclusions

The petrographic features of silicate melt inclusions have been described and compared between the older granites and younger granites. The identification of silicate melt inclusions in the granites is difficult, because silicate melt inclusions commonly devitrify

and undergo a change of shape. The original appearance of these magmatic remnants in the Hetai granites may be altered or destroyed by later devitrification, because some of the Hetai granites were metamorphosed. Therefore, it is necessary to describe petrographic features of the silicate melt inclusions first.

Silicate melt inclusions in the Hetai granites are commonly present in quartz grains (Fig.5.1). They have a regular elliptical or polygonal shape, with dimensions from 0.05 mm to 0.20 mm, and occur as apparently isolated inclusions, most likely corresponding to growth zones of the quartz crystals. These microsystems commonly consist of glass, daughter minerals and some bubbles, and the glassy parts are speckled or spidery in appearance because of advanced devitrification (Fig. 5.1). Under crossed nicols, silicate melt inclusions show negative crystal form and a different interference colour from the host minerals (quartz and plagioclase). Optical identification of daughter minerals in silicate melt inclusions is very difficult, because the devitrified silicate melt inclusions are usually nearly opaque. Some needle-shaped apatites occur around and in some silicate melt inclusions. Frezzotti (1992) used Raman analysis to identify slightly anisotropic daughter phases K-feldspar and Na-rich plagioclase occur in silicate melt inclusions from the Mount Genis granite.

The silicate melt inclusions in the Sihui and Wuchun granites are common but smaller, about 0.05--0.15 mm in diameter (Fig.5.1a and b), than those in the Shijiang and Guangning granites, about 0.10-0.20 mm (Fig.5.1c and d). In addition, the silicate melt inclusions in the Sihui and Wuchun are usually polygonal in shape and display clear contacts with the host mineral (Fig.5.1a and b), whereas those in the Shijiang and Guangning granites are ellipsoidal with relatively vague contacts (Fig.5.1c and d). These differences may be the result of different crystallizing conditions during trapping of the silicate melt inclusions. More silicate melt inclusions may indicate that granitic magmas of the Sihui and Wuchun granites were emplaced at a shallower depth under lower pressure. The Shijiang and Guangning granites consolidated in a deeper environment under higher pressure, and magma crystallization was slower. Therefore, silicate melt inclusions are less numerous in the S-type granite environment.

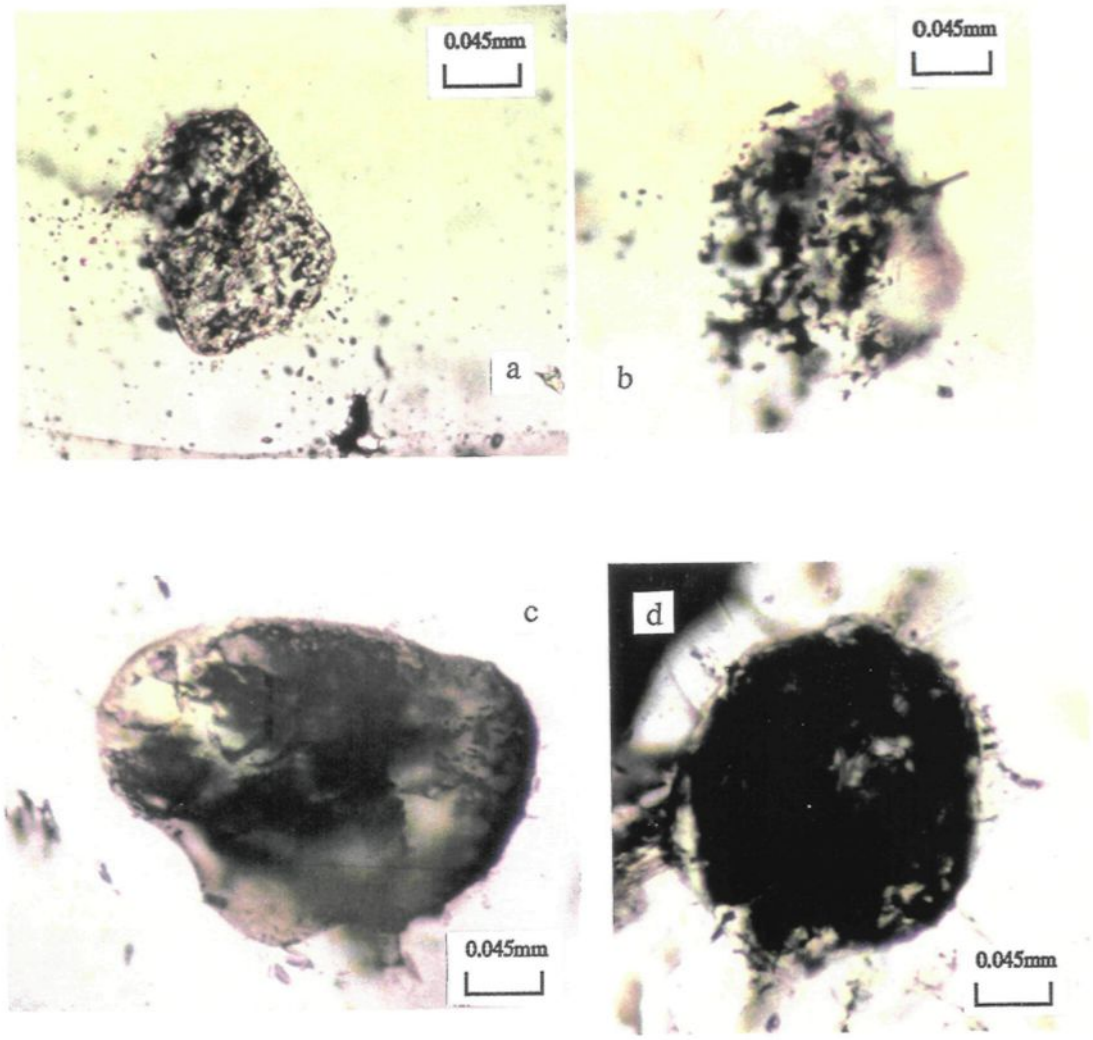

Fig. 5.1. Silicate melt inclusions in the Hetai granites.

Younger granites :

a : Wuchun monzogranite (C10-2); b : Sihui alkali-feldspar granite (C18-2);

Older granites :

c : Shijiang granite (C78-3); d : Guangning monzogranite (C84);

Silicate melt inclusions in older granites of the Hetai area possibly underwent a complicated evolution after their trapping. Frezzotti (1992) considered that petrographic studies may interpret the evolution of silicate melt inclusions after trapping. Clearly, devitrification is the most important phenomenon and the degree of devitrification is often proportional to the inclusion size. For the Hetai granites, the degree of devitrification of silicate melt inclusions is relatively high, usually about 40-50 % relative to the size of silicate melt inclusion. Silicate melt inclusions in the shallow intrusives such as the Sihui granite and the Wuchun granite are more devitrified and more polygonal shaped than those of the Shijiang and Guangning granites, demonstrating that the silicate-glass evolution is not only controlled by temperature change but also pressure during the cooling process after trapping, because the devitrification degree of glass from shallow emplaced granites is higher than deep emplaced granites. The temperature of the shallow intrusions may decrease more quickly than that of the deep intrusions, so the trapped silicate melt inclusions may easily recrystallize during the cooling process. The temperature decrease of the Sihui and Wuchun granites may be more quickly than the Shijiang and Guangning granites.

5-3-2. Change in silicate melt inclusions at high temperature

The trapping temperature of silicate melt inclusions was determined by reheating the silicate melt inclusions. The samples with silicate melt inclusions were heated to a certain temperature for 48 hours, and then were quenched in water and their changes were observed under the microscope. The heating temperature for all samples began at 600 °C, and after heating for 48 hours, and continued at 50 °C increments. Two facts were observed when temperatures reached 700 °C : (1) the refractive index of the glass diminished and the bubbles began to disappear and silicate melt inclusions became a little more transparent in some samples such as those from the Shijiang and Guangning granites; or (2) no change occurred as in the Sihui and Wuchun samples. With further increase of temperature to 750 °C, more bubbles disappear and silicate melt inclusion in the samples of the Shijiang and Guangning granites became more transparent. The bubbles start to disappear and silicate melt inclusion shows a little transparency in the Sihui and Wuchun samples. At 850 °C, most bubbles disappear and silicate melt inclusion are nearly transparent in the Shijiang and Guangning samples. But at 950 °C, most bubbles disappear and silicate melt inclusion are

nearly transparent in the Sihui and Wuchun granites. In general, the heating process resulted in disappearing bubbles and increasing transparency of the glass of silicate melt inclusion, as well as a rounding of the outline of silicate melt inclusion. Their changes between initial and final states are compared (Fig.5.2).

The homogenization temperatures are compared in Table 5.3. It is evident that the temperatures of silicate melt inclusions in the Sihui granite (900-950 °C) and in the Wuchun granites (900-950 °C) are higher than those in the Shijiang granite (800-850 °C) and Guangning granite (800-850 °C). The more common silicate melt inclusions in the Sihui and Wuchun granites may result from a more differentiated magma under low pressure, whereas the fewer silicate melt inclusions from the Shijiang and Guangning granites possibly reflect magma emplacement in a deep environment under high pressure. Therefore, the magma crystallization temperatures of the Sihui and Wuchun granites are higher than those of the Shijiang and Guangning granites, but their pressures are lower. These can be compared with the data of estimated temperature and pressure based on the chemical compositions of biotite and amphibole.

5-4. Fluid inclusions in granites

Fluid inclusions are commonly used as an important measure of the evolution of volatiles in granites and the genesis of related ore deposits (Roedder, 1984). They can provide information on the temperature, pressure, density and composition of the fluid at the time of trapping during mineralization. For example, Shelton et al. (1988) studied fluid inclusions in gold vein deposits of the Jungwon Gold Area in the Republic of Korea and indicated that gold was deposited between 375-290 °C from relatively dilute fluids containing 15-25 mole percent CO_2, similar to nearby Late Jurassic granodiorite.

Fluid inclusion studies on the evolution of volatiles in gold ore deposits of the Hetai Area have been studied based on the features of fluid inclusions in quartz (Chen et al. 1988; Fu, 1989; Dai, 1986; Zhou, 1992). The mineralizing fluids related to the Hetai gold deposits have been considered related to the hydrothermal fluids by magma evolution (Fu, 1989) or controlled by the metamorphic hydrothermal fluids (Chen et al., 1988 and Dai, 1986; Zhou,

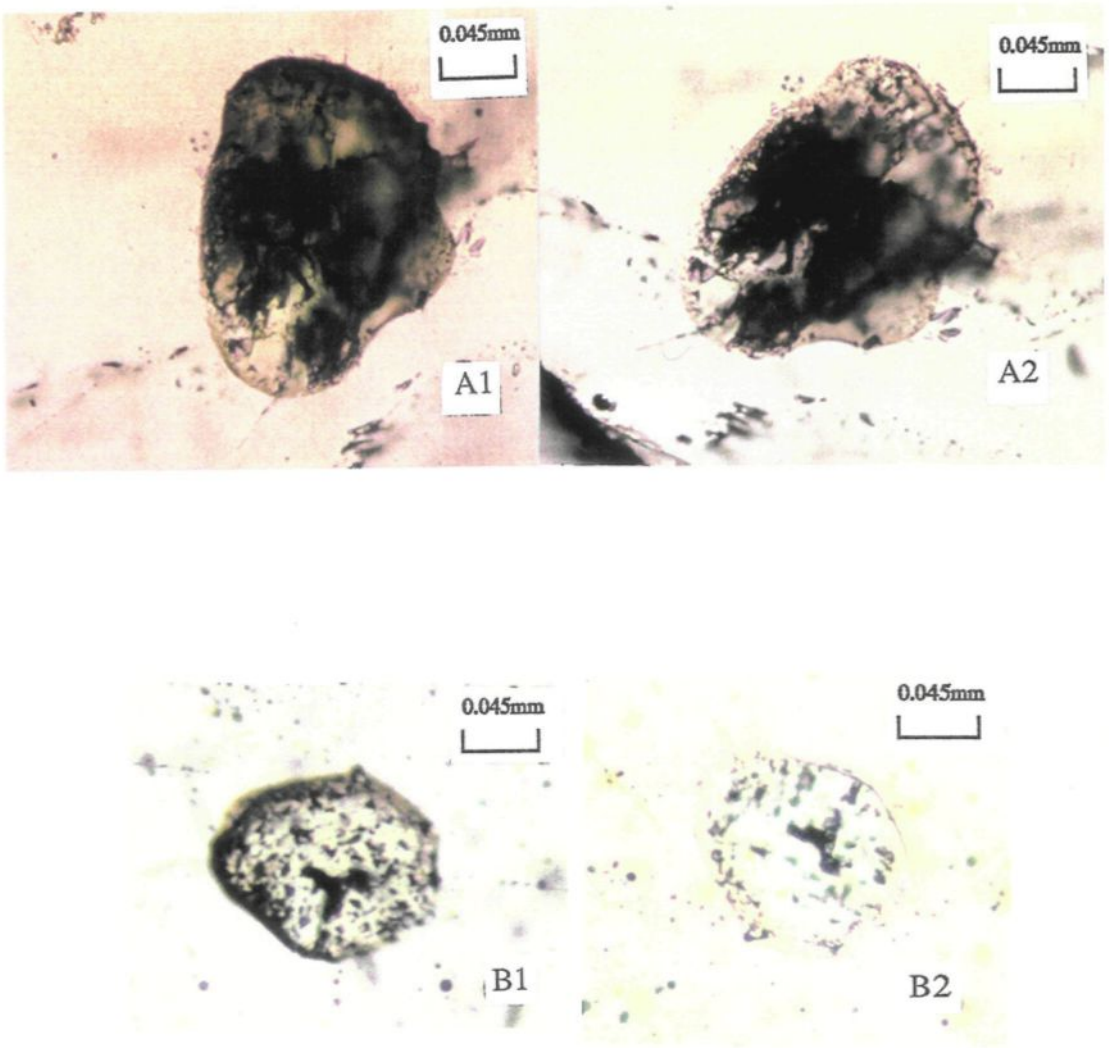

Fig. 5.2. Comparisons between original and heated melt silicate inclusions in different granites.

A : Shijiang (Older granite)

A1 : original ; A2 : heated one (850 °C, more transparent)

B : Sihui granites (Younger granite)

B1 : Sihui original ; B2 : Sihui heated (950 °C, transparent)

Table 5.3. Temperature of Homogenization (Th) of silicate melt inclusion in granites of the Hetai Area

Age	Sample	Location	Host mineral	Number of measument	Size (mm)	Shape	Th (°C)
Caledonian	C78-3	Shijiang	Quartz	4	0.10-0.20	elliptical	800-850
Hercynian	C84, C13	Guangning	Quartz	4	0.12-0.20	elliptical	800-850
Indosinian	C10-2	Wuchun	Quartz	4	0.06-0.15	polygonal	900-950
Yanshanian	C18-2	Sihui	Quartz	6	0.05-0.15	polygonal	900-950

1992).

A limited number of fluid inclusions in quartz and plagioclase from some granite samples of the Hetai Area were determined and are compared (Table 5.4). The determinations of fluid inclusions were performed by means of freezing method and the salinities were estimated from the data (Lu et al., 1990). The selected fluid inclusions are secondary inclusions after magma consolidation, but certain trends can be seen in the salinity data of fluid inclusions from different granites.

Table 5.4 shows the different salinities of fluid inclusions from different granites and the salinities in older granites are higher than those in younger granites. The fluid inclusions in the Caledonian and Hercynian granites have higher salinities, from 5.3-> 9.8 (NaCl wt %), whereas those in the Yunlougan granodiorite and Wuchun monzogranite (Indosinian) show lower salinities, from 3.0-> 4.3, and those from the Sihui granites (Yanshanian) are from 6.6 -> 8.0. In general, the chemical compositions of fluid inclusions in older granites belong to a moderate-salinity (5.3-9.8 % NaCl) aqueous type, but those in the younger granites may belong to a low-salinity (3.0-8.0 % NaCl) H_2O-CO_2 type. The homogenization temperatures of all samples are nearly similar, varying from 160-> 282 °C. The low homogenization temperature of these fluid inclusions also suggests that they are secondary fluid inclusions. Because only a very limited numbers of fluid inclusions in granites were examined in this work, the data is not sufficient to discuss the volatile evolution.

Fluid inclusion data from the Hetai gold deposits shows that they generally have CO_2 contents of about 6.95-32.29 (ml/100g) and NaCl about 1.06-9.26 (wt%) and homogenization temperature about 190-280 °C (Chen et al., 1988). Zhou (1992) suggested that there are three compositional types of fluid inclusions in the Hetai gold deposits, a CO_2-dominated one, a low-salinity (1.5-6.0 % NaCl) CO_2-H_2O one, and a moderate-salinity (6-14 % NaCl) aqueous one. These fluid inclusions show similar homogenization temperatures to those of the Hetai gold deposits but are different in chemical composition (Table 5.4).

Table 5.4. Salinity and homogenization temperature of fluid inclusions in different granites and in the Hetai ore deposits

Age	Sample	Location	Host mineral	Number	Tm,ice (°C)	Salinity (wt%)	Th (°C)	Reference
Caledonian	C78-3	Shijiang	Quartz	8	-3.8	6.1	280	
	C7-2	Sidong	Plagioclase	4	-5.8	8.8	193	
Hercynian	C84	Guangning	Quartz	6	-3.7	6.1	210	
Hercynian	C9-1	Yunlougan	Quartz	5	-2.2	3.6	205	
Indosinian	C10-2	Wuchun	Quartz	11	-2.2	3.7	266	
Yanshanian	C18-2	Sihui	Quartz	11	-4.6	7.3	208	
	C18-3	Sihui	Quartz	8	-4.2	6.8	215	
Gold-deposits		Hetai	Quartz			1.06-9.26	280-190	Chen et al.,1988
Gold-deposits		Hetai	Quartz			1.5-14.0	310-130	Zhou, Y.,1992

CHAPTER VI

DISCUSSION AND CONCLUSIONS

6-1. Discussion

Granites of the Hetai Area intruded during the Caledonian, Hercynian, Indosinian and Yanshanian periods (Table 1.2), but their ages are not precisely known and they must be studied by precise methods. The Guangning granite (253 ± 36 Ma) may belong to the Hercynian but is not quite Indosinian (Chen and Wu, 1989; Ye, 1990). Similarly, the Shijiang granite (373 ± 45 Ma) may be Hercynian rather than Caledonian. The Guangning and the Shijiang granites show much geochemical and mineralogical similarity and were probably produced during the same orogenic period. The Yunlougan granodiorite, in addition, may be produced between the Hercynian and Indosinian orogenic periods. Except for these examples, the granites, as defined by their ages, generally reflect the relationship between granitic magmatism and orogenic evolution of the Hetai Area. The Caledonian and the Yanshanian granitic magmatisms in the whole of South China (Institute of Geochemistry, Academia Sinica, 1979), are represented in the orogenic evolution of the Hetai Area. The Caledonian and the Yanshanian granites are a result of magmatism during specific orogenic periods, and their geochemical features are the result of their orogenic derivation. The geochemical differences between the various suites show that they belong to different geotectonic types. The older granites display peraluminous features and their magmatism may be related with geotectonic environment of a continent-continent collision such as the Himalaya type (Harris et al., 1986; Debon et al., 1986; Condie, 1989). In contrast, the younger granites are mafic and their geochemical trend is better associated with geotectonic evolution from a subduction to extension environment.

The deformation of the older granites is obviously stronger than that affecting the Indosinian and the Yanshanian granites. The strong solid-state deformation gives the false impression that the Caledonian and the Hercynian granites are formed by granitization of Precambrian sedimentary rocks, and magmatic processes were largely ignored in earlier discussions of granite petrogenesis. In fact, the main petrographic features such as the preferred orientation of primary igneous minerals are in reality flow foliations of aligned zoned plagioclase and euhedral K-feldspar, which generally do not grow as euhedral crystals in unmelted metamorphic rocks (Vernon, 1986). These typical igneous microstructures demonstrate that magmatic events are responsible for the genesis of the Caledonian and the Hercynian granites. The superimposed solid-state deformation has modified the primary magmatic flow foliations, and produced zones of gneissic, augen and mylonitic structures in the deformed granites. The solid-state deformation changed the primary igneous crystals into broken, finer-grained aggregates with mylonitic microstructure, showing that a physical mechanism rather than a chemical mechanism operated. There is no evident chemical change during the solid-state deformation, because dynamic deformation, more rapid than melting and crystallizing processes, is not commonly maintained long enough to cause obvious chemical transformation. Therefore, both deformed and undeformed granites inherit the geochemical characteristics of their source magmas and the geochemical changes of granites are controlled mainly by magmatic evolution.

Geochemical classification of granite can be used to distinguish the different possible source regions of granitic magma. In general, the older granites display different geochemical features from the younger granites in the Hetai Area. The older granites are characterized by a peraluminous composition, reflecting the geochemical characteristics of crustal source rocks, whereas the younger granites are characterized by a mafic and calc-alkaliine----> alkaline evolution, demonstrating the geochemical features of magma source derived from upper mantle (or lower crust). However, the criteria for granite classification are relative because of the geochemical non-uniformity and different geotectonic background. Comparing the Hetai granites with given geochemical criteria from the Lachlan Fold Belt (White and Chappell, 1977 and 1983) and from the Southeast Asian Area (Cobbing et al., 1986) shows that the I-S classification line of the K_2O-Na_2O diagram changes for different areas. The Hetai granites show a comparatively larger K_2O variation than other areas. This may be caused by two factors : (1) that the older granites resulted from melting of Precambrian sedimentary basement source rocks, and (2) the younger

granites evolved from differentiated magma. The magmatic differentiations also result in some elements such as Rb, Sr, V, Sc and Nb varying in a large scale so that later stage granites differ greatly from their early intrusive phases. These may be the reason why the different granites of the Hetai Area cannot be clearly separated in the Rb-(Nb+Y) and Rb-(Ta+Yb) diagrams of Pearce et al. (1984). On the other hand, the (Nb+Ta) - Rb/Sr, - Sc and - V diagrams distinguish the various granite types well and discriminate the significant changes of magma evolution in the Hetai Area. Comparing the Hetai granites with those of typical areas such as the Lachlan Foldbelt of Australia, Japan and East Malaysia in these geochemical diagrams shows that the different granite types can be distinguished in the (Nb+Ta)-Rb/Sr, -Sc and -V diagrams.

The geotectonic discriminations of different granites by Pearce et al. (1984), Maniar and Piccoli (1990) and Brown et al. (1984) may be applied to the Hetai granites. In general, the older granites are peraluminous (A/CNK > 1.05) and have higher LILE and moderate HFSE contents, suggesting a continent-continent collision environment. In contrast, the younger granite suites are characterized by aluminous undersaturation (A/CNK < 1.05) and by significant change of LILE and HFSE from low to high with calc-alkali --> alkali granite series evolution, demonstrating a tectonic evolution from a subduction environment to an extension environment.

The study of the chemical characteristics of mafic minerals and plagioclase may also establish criteria to discriminate between different granite types and magma evolution. In general, the significant differences of biotite from different granitic rocks are represented by the relative proportion of Mg to Fe^{2+} (and Mn), so the Mg--Fe^{2+}+Mn--Al^{VI} +Fe^{3+}+Ti ternary classification and the parameter M are useful indicators for distinguishing different granite types in the Hetai and other areas. The M value of biotite usually decreases because of Mn increase in biotite from late stage granites such as the Wuchun monzogranite and the Sihui alkali-feldspar granite, but Mg/Fe^{2+} ratios are still high in these biotites. The Mg/Fe^{2+} ratio in biotite is controlled mainly by crystallization temperature (Wones et al., 1965). The chemical compositions of biotites from different granites suggest that magma composition also affects Mg/Fe^{2+} ratio and M value, because biotites from the Yangtze granites always have higher Mg/Fe^{2+} ratio than those from the Nanling granites (Yang et al.,1986; Hong, 1982). Similarly, biotites from the Caledonian granites have a lower Mg/Fe^{2+} ratio (<0.55) and M value (<0.45) than those from the Yanshanian and Indosinian granite suites and the

Huangtongjiang gabbro (>0.55 and >0.45 respectively). These are the result of different magma compositions and crystallizing temperatures, because the Caledonian granites have both lower MgO/(MgO+FeO) ratio and crystallizing temperature than the Yanshanian and Indosinian granite suites and the Huangtongjiang gabbro. In addition, the Al_2O_3 content and Al(VI)/Ti ratio of biotite are an important parameter for distinguishing different granite types, which are controlled by the chemistry of magma and the crystallizing pressure. Biotite from the Caledonian granites has higher Al_2O_3 and Al(VI)/Ti than that from the Yanshanian and Indosinian granite suites. The MgO/FeOt ratio in amphibole is controlled by crystallization temperature and its geochemistry, but Al_2O_3 content is closely related to magma crystallizing pressure as well as the geochemical composition. Mg-hornblende and actinolite occur in the Yunlougan granodiorite, the Indosinian and Yanshanian granodioritic enclaves and the Huangtongjiang gabbro, but no amphibole occurs in the Caledonian granites.

Changes in MnO, Na_2O and SiO_2 contents of biotite and amphibole document magma evolution of different granite series. SiO_2 contents in biotite and amphibole may be controlled mainly by the crystallization temperature and pressure, but show no close relation with SiO_2 content of the magma (Jakes and white, 1972), because SiO_2 in biotite form the Caledonian granites is lower than that from Yanshanian, Indosinian granite suites and the Huangtongjiang gabbro. Similarly, SiO_2 content of amphibole from the Nanling granite is lower than that of the Yangtze and Coast granites, although the Yangtze granites and the Coast granites contain greatly contrasting SiO_2 contents (Yang, 1992). The MnO and Na_2O in biotite and amphibole are controlled mainly by the geochemistry of the magma, and increase with the magma evolution in granites of the Hetai Area and South China (Yang, 1992).

The anorthite content of plagioclase is controlled by the crystallization temperature of magma, and An content becomes lower as temperature decreases during the process of magmatic differentiation. Aside from the temperature factor, the anorthite contents of plagioclase display significant differences between the different granites in the Hetai Area. The plagioclases from the Caledonian and Hercynian biotite granites generally have lower anorthite (An=35-5), whereas those from the Hercynian Yunlougan granodiorite, Indosinian and Yanshanian early phases (granodioritic enclaves) and the Huangtongjiang gabbro have higher anorthite contents (An=70-30). This difference suggests that An values of plagioclase

are also controlled by geochemistry of the magma. In addition, the An values of plagioclase from the later stage granites (such as the Sihui alkali-feldspar granites) become very low (An=15-0), but the crystallizing temperature of these granites is higher (T=900-950 °C). Clearly, the decreasing An values of plagioclase in the later stage granites are caused mainly by the geochemical change (CaO decrease relative to Na_2O) with magmatic evolution.

Silicate melt inclusions in different granites in the Hetai Area indicate directly that the Hetai granites are derived from magma and are not produced by solid-state granitization. The difference in the silicate melt inclusions between different granites results from different temperature and pressure of crystallization of magma. The high temperature but low pressure may be favourable to producing silicate melt inclusions. Silicate melt inclusions are more widely distributed in the later stage granites, and are more abundant in the Wuchun monzogranite and Sihui alkali-feldspar granites (younger granites) than in the Shijiang and Guangning granites (older granites). The homogenization temperature data of silicate melt inclusions show that the crystallizing temperatures of the Yanshanian and Indosinian granite suites are higher (950-900 °C) than those of the Caledonian Shijiang and Hercynian Guangning granites (800-850 °C).

Au shows variable concentration between different granites in the Hetai Area, and higher contents are found in the Huangtongjiang gabbro, the Hercynian Yunlougan granodiorite, the Indosinian and the Yanshanian granite suites than the Caledonian and the Hercynian granites. This Au distribution indicates that Au enrichment may be related to the magmas of upper mantle derivation and their more differentiated products. In addition, the ages of gold mineralization in the Hetai Area are mainly in the Yanshanian period (Chen et al., 1991), at which time granites widely intruded in this area, so, attention should be paid to the relationship between gold mineralization and granites derived from deeper source magmas.

The geochemistry of granites and their minerals shows that there are three different types of granite developed in the Hetai Area and a significant change from the Caledonian, through the Hercynian and the Indosinian to the Yanshanian corresponds to different orogenic situations. The geochemical characteristics of whole rocks as well as biotite (amphibole) of the older (Caledonian and Hercynian) granites are similar to S-type granites, and suggest their derivation from peraluminous crustal source regions and emplacement as

relatively low temperature magma in a high pressure environment. In contrast, the Hercynian (Yunlougan) granodiorite and the Indosinian and Yanshanian granodioritic enclaves as well as the Huangtongjiang gabbro show I-type or mantle source characteristics. They are high temperature magmas which were intruded under conditions of relatively low pressure. The Yanshanian alkali-feldspar granite and the Indosinian monzogranite characterize high SiO_2-K_2O geochemical features of the more differentiated deeper source magmas and suggest emplacement under low pressure conditions. By comparison with South China and other typical world areas, the older granites may have been produced by a continent-continent collision event in the Early Paleozoic, whereas the younger intermediate granites appear to result from subduction events at a continental margin (Nanling continent), and the alkali-feldspar granites may be produced by a subsequent extensional event in which more differentiated deeper magmas were emplaced in the Late Mezozoic period.

The Caledonian and the Hercynian granites are distributed mainly in the inland area, whereas the Yanshanian alkali-feldspar granites occur near the coastal area (Figs. 1.4 and 1.5). The geotectonic environment of granites in the Hetai Area may be modelled (Fig.6.1) on the basis of their geochemical characteristics and the temporal-spatial distribution : (1) In the Early Paleozoic orogenic period, a continent-continent collision occurred and the Precambrian sedimentary basement folded, thickened and melted. The magma was emplaced at about 20 km depth and formed the older (Caledonian and some Hercynian) granites. (2) The collision event in the Early Mesozoic orogenic period was replaced by the subduction because of the oceanic plate (Gunanhai, Hsu et al., 1990) moving beneath the Nanling continent, and produced the Yunlougan granodiorite (I-type). These early granites were strongly deformed because of late dynamic structure movement. (3) The geotectonic evolution in the Middle-Late Mesozoic orogenic period is dominated by subduction of the oceanic plate beneath the continent, and the Indosinian and the early Yanshanian intrusions as well as the Huangtongjiang gabbro may be produced from the subduction zone derived magmas. (4) In the Late Mesozoic, extension was produced by a change in the subduction angle, and the more differentiated magmas emplaced along the extension zone, producing shallow level alkali-feldspar granites such as the Yanshanian Sihui alkali-feldspar granite. So, from NW to SE in the Hetai Area (Fig.1.5), the granites gradually become younger from the Caledonian through the Hercynian and Indosinian to the Yanshanian, and the geotectonic evolution develops from collision --> subduction --> extension environments with geochemical tendency of granites from peraluminous (S-type) -> mafic and calc-alkali

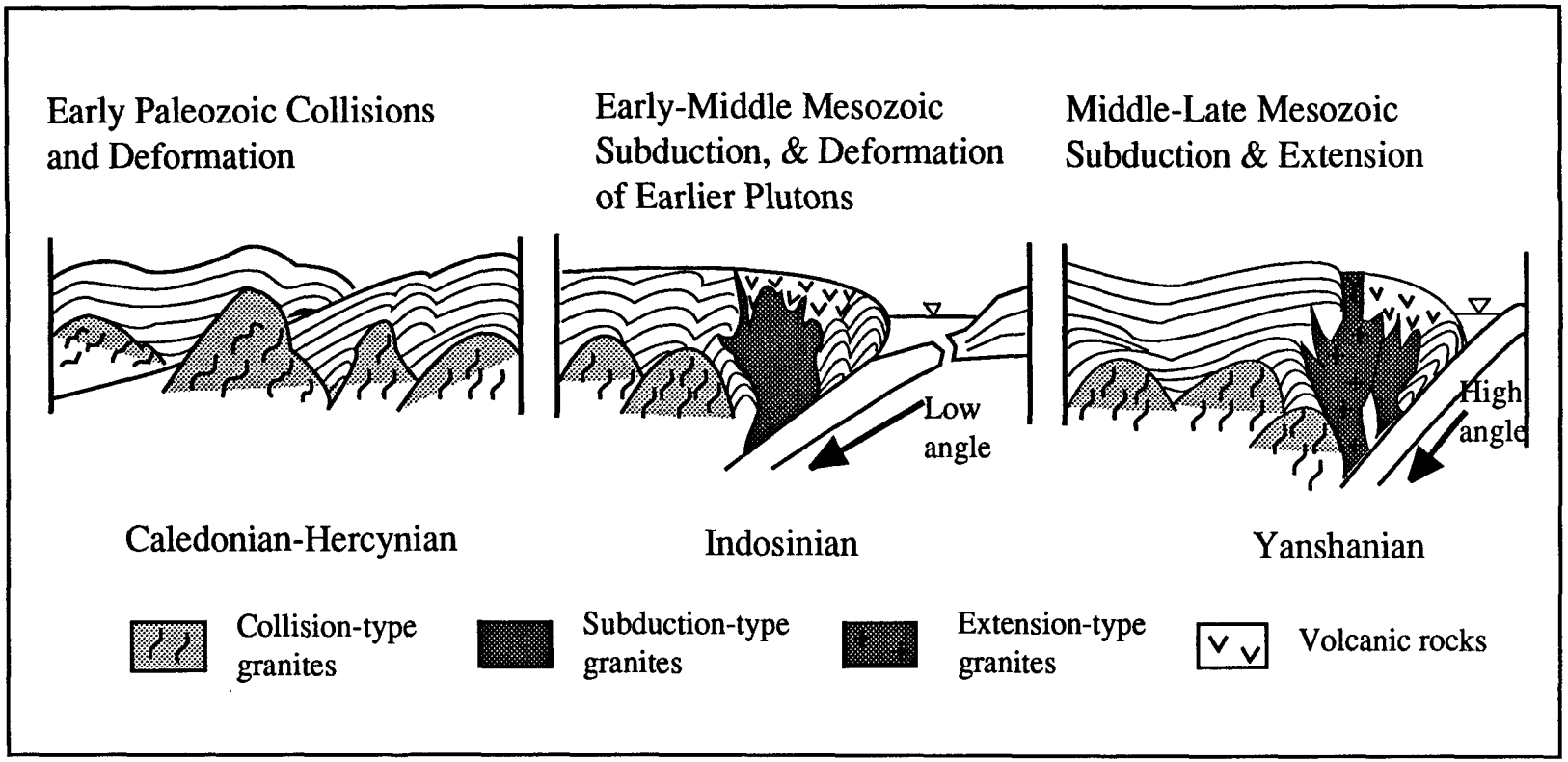

Fig. 6.1. Model of geotectonic evolution of different granite types of the Hetai Area (not to scale)

features of granites, but the collision-type (S-type) granites are derived from different source region, unlike the subduction- and extension-type granites.

6-2. Conclusions

1. The petrographic characteristics of the Caledonian and Hercynian granites show that they are magmatic rocks which have had solid-state deformation superimposed on original magmatic fabrics. The younger granites such as the Indosinian and Yanshanian granites have magmatic fabrics with only minor local ductile deformation.

2. The Caledonian and most Hercynian granites belong to the S-type or collision-type granite; whereas the Hercynian, the Indosinian and the Yanshanian intermediate-basic granitic rocks are I-type of subduction derived granites; finally the Yanshanian and the Indosinian alkali-feldspar granites are the result of differentiation of I-type magmas which present some geochemical features of A-type granite, and are believed to have formed in an extension environment.

3. The chemical compositions of biotite, amphibole and plagioclase show significant variations which may be used for distinguishing different granite types. The Fe-biotites from the Caledonian and the most Hercynian granites indicate derivation from aluminous source rocks of the upper crust. The Mg-biotites formed in the Hercynian, the Indosinian and the Yanshanian intermediate-basic and alkali-feldspar granites that crystallized from deeper derived magmas. Ca-rich plagioclase xenocrysts in intermediate-basic enclaves further suggest that the source magmas of the Indosinian and the Yanshanian granites are closely related to basaltic magma evolution. Estimates of temperature and pressure based on biotite and amphibole show that the Caledonian and the Hercynian magmas had lower crystallizing temperature but were emplaced at a deeper level of the crust than the Yanshanian and the Indosinian granites. The Caledonian and Hercynian granites from the Hetai Area are parts of the Nanling granites (S-type), whereas the Indosinian and Yanshanian granites are similar to the Yangtze granites (I-type) and the Coast granites (I-type -->A-type ?) based on mafic mineral geochemistry.

4. Silicate melt inclusions provide further evidence that the Hetai granites are magmatic products. The homogenization temperatures of silicate melt inclusions from different granites indicate crystallization temperatures for the Yanshanian and the Indosinian granites, which are higher than those of the Caledonian and the Hercynian granites.

5. Au distributions in different type granites in the Hetai Area suggest that the granites derived from basic magmas are Au enriched compared to those derived from upper crustal source regions. Au enrichment of magmas may occur in the evolution stage from calc-alkali to alkali differentiation of basic magma. Some Hetai gold mineralization may possibly be related to basic magmatism.

6. The temporal-spatial distribution of the different granites reflects the orogenic evolution of the Hetai Area. A Caledonian continental collision folded, thickened and melted the Precambrian sedimentary rocks, producing the Caledonian granites. The older granites were strongly deformed because of later subduction and extension movements. In the Middle-Late Mesozoic periods, the geotectonic evolution was dominated first by subduction environments, resulting in the Indosinian and Yanshanian calc-alkali granite series. The final Yanshanian period resulted in the alkali-granite series, produced in an extension environment.

Some problems remain to be addressed. The ages of the Hetai granites need to be determined by precise U-Pb methods in order to constrain the formation of the plutons in this study, as well as to simply comparisons with new tectonic, subduction-related models. The structural geology is another problem, as regional structures have not been studied systematically and the relationship between granite deformation and regional structures has not been established in detail. Isotope systems, particularly Sm-Nd may be a useful method to determine the some of the granite plutons, and may be particularly useful in examining the older granites.

REFERENCES

Ague, J. J., 1989. The distribution of Fe and Mg between biotite and amphibole in granitic rocks : Effects of temperature, pressure, and amphibole composition. Geochemical Journal, 23; 279-293.

Barbarin, B., 1990. Plagioclase xenocrysts and mafic magmatic enclaves in some granitoids of the Sierra Nevada batholith, California. Journal of Geophysical Research, 95; 17747-17756.

Barriere, M., 1981. On curved laminae, graded layers, convection currents and dynamic crystal sorting in the Ploumanac'h (Brittany) subalkaline granite. Contributions to Mineralogy and Petrology, 77; 214-224.

Bateman, P. C., Busacca, A. J. and Sawka, W. N., 1983. Cretaceous deformation in the western foothills of the Sierra Nevada, California. Geological Society of America Bulletin, 94; 30-42.

Bateman, R., 1985. Aureole deformation by flattening around a diapir during in situ ballooning : the Cannibal Creek granite, Journal of Geology, 93; 293-310.

Blundy, J. D. and Sparks, PS. J., 1992. Petrogenesis of mafic inclusions in granitoids of the Adamello Massif, Italy. Journal of Petrology, 33. 1039-1104.

Bowden, P., Batchelor, R. A., Chappell, B. W., Didier, J. and Lameyre, J., 1984. Petrological, geochemical and source criteria for the classification of granitic rocks: a discussion. Physics of the Earth and Planetary Interiors, 35; 1-11.

Bowden, P. and Kinnaird, J. A., 1984. The petrology and geochemistry of alkaline granites from Nigeria. Physics of the Earth and Planetary Interiors, 35; 199-211.

Brown, G. C., Thorpe, R. S. and Webb, P. C., 1984. The geochemical characteristics of granitoids in contrasting arcs and comments on magma sources. Journal of Geological Society of London, 141; 413-426.

Cantagrel, J. M., Didier, J. and Gourgaud, A., 1984. Magma mixing : origin of

intermediate rocks and enclaves from volcanism to plutonism. Physics of the Earth and Planetary Interiors, 35; 63-76.

Chappell, B. W., and White, A. J. R., 1974. Two contrasting granite types. Pacific Geology, 8; 173-174.

Chappell, B. W., 1984. Source rocks of I- and S-type granites in the Lachlan Fold Belt, southeastern Australia. Philosophical Transactions Royal Society of London, A310; 693-707.

Chen, C. T., Ji, M. J. and Hu, X. T., 1988. The metallogical conditions of gold deposit in Hetai Area, Guangdong Province. Guangdong Geology, 3; 1-16 (in chinese).

Chen, H. and Li, H., 1991. Fluid inclusion Rb-Sr isochron dating of gold deposits in Yunkai Uplift Area. Mineral Deposits, 10; 333-341 (in chinese).

Chen, T. P. and Wu, J. Y., 1989. Age of the Shiniutou granitic complex of Gaoyao County, Western Guangdong. Guangdong Geology, 4; 21-34 (in chinese).

Chen, Y. D., Price, R. C. and White, A. J. R., 1989. Inclusions in three S-type granites from southeastern Australia. Journal of Petrology, 30; 1181-1218.

Chen, Y. D., Price, R. C. and White, A. J. R., 1990. Mafic inclusions from the Glenbog and Blue Gum granite suites, southeastern Australia. Journal of Geophysical Research, 95; 17757-17785.

Chi, G. X., 1992. Polygenetic control of the localization of proximal versus distal deposits in the Xinlu tin-polymetallic ore field, Guangxi, southern China. Unpublished Ph. D. thesis, Université du Québec à Chicoutimi.

Cobbing, E. J., Mallick, D. I. J., Pitfield, P. E. J. and Teoh, L. H., 1986. The granites of the Southeast Asian Tin Belt. Journal of the Geological Society, 143; 537-550.

Cocherie, A., Rossi, Ph. and Le Bel, L., 1984. The Variscan calc-alkalic plutonism of western Corsica : mineralogy and major and trace element geochemistry. Physics of the Earth and Planetary Interiors, 35; 145-178.

Collins, W. J., Beams, S. D., White, A. J. R. and Chappell, B. W., 1982. Nature and origin of A-type granites with particular reference to Southeastern Australia. Contributions to Mineralogy and Petrology, 80; 189-200.

Condie, K. C., 1989. Plate tectonics and crustal evolution (third edition), Pergamon Press.

Czamanske, G. K., 1986. Chemistry of rock-forming minerals of the Cretaceous-Paleocene batholith in southwestern Japan and implications for magma

genesis. Journal of Geophysical Research, 81; 10431-10469.

Dai, A. H., 1986. Geochemistry of the Hetai Gold Deposits, western Guangdong Province. Unpublished M. Sc. thesis, Dept. of Geology, Nanjing University (in Chinese)

Debon, F., Lefort, P., Sheppard, S. M. F. and Sonet, J., 1986. The four plutonic belts of the Transhimalaya-Himalaya : a chemical, mineralogical, isotopic and chronological synthesis along a Tibet-Nepal section. Journal of Petrology, 27; 219-250.

Department of Geology, Nanjing University, 1981. Different age granites and related mineralizations of South China. Science Press, Beijing (in chinese).

Didier, J., Duthou, J. L. and Lameyre, J., 1982. Mantle and crustal granites : genetic classification of orogenic granites and the nature of their enclaves. Journal of Volcanology and Geothermal Research, 14; 125-132.

Dodge, F. C. W., Papike, J. J. and Mays, R. E., 1968. Hornblendes from granitic rocks of the Central Sierra Nevada Botholith, California. Journal of Petrology, 9; 378-410.

Dodge, F. C. W., Papike, J. J. and Mays, R. E., 1969. Hornblendes from granitic rocks of the Central Sierra Nevada batholith, California. Journal of Petrology, 9; 378-410.

Farrow, C. E. G. and Barr, S. M., 1992. Petrology of high-Al-hornblende- and magmatic-epidote-bearing plutons in the southeastern Cape Breton Highlands, Nova Scotia. Canadian Mineralogist, 30; 377-392.

Feeley, T. C. and Grunder, A. L., 1991. Mantle contribution to the evolution of Middle Tertiary silicic magmatism during early stages of extension : the Egan Range volcanic complex, east-central Nevada. Contributions to Mineralogy and Petrology, 10; 154-169.

Foster, M. D., 1960, Interpretation of the composition of trioctahedral micas. U.S.Geological Survey of Professional Paper., 354-B. 11-40.

Frezzotti, M. L., 1992. Magmatic immiscibility and fluid phase evolution in the Mount Genis granite (southeastern Sardinia, Italy). Geochimica et Cosmochimica Acta, 56; 21-33.

Fu, L., 1988. Preliminary investigation on "fracture-metamorphism" and gold mineralization laying emphasis on Hetai Gold Mine, Gaoyao County. Guangdong Geology, 3; 31-44 (in chinese).

Fu, L., 1989. Discussion on the genesis of Hetai Gold Deposit. Guangdong Geology, 4; 35-43 (in chinese).

Giret, A., Bonin, B. and Leger, J. M., 1980. Amphibole compositional trends in oversaturated and undersaturated alkaline plutonic ring-complexs. Canadian Mineralogist, 18. 481-495.

Green, N. L. and Usdansky, S. I., 1986. Ternary feldspar mixing relations and thermobarometry. American Mineralogist, 71; 1100-1108.

Groves, D. F., 1972. The geochemical evolution of tin-bearing granites in the Blue Tier batholith, Tasmania. Economic Geology, 67; 443-457.

Guo L. Z, 1984. The terrain structure of southeastern China. Journal of Nanjing University, 1; 732-739 (in chinese).

Hammarstrom, J. M. and Zen, E-An, 1986. Alumium in hornblende : An empirical igneous geobarometer. American Mineralogist, 71; 1297-1313.

Hanson, G. N., 1978. The application of trace elements to the petrogenesis of igneous rocks of granitic composition. Earth and Planetary Science Letters, 38; 26-43.

Harris, N. B. W., Pearce, J. A. and Tindle, A. G., 1986. Geochemical characteristics of collision-zone magmatism. Collision Tectonics. Geological Society Special Publication, 19; 67-81.

Hawthorne, F. C., 1981. Crystal chemistry of the amphiboles, Amphiboles and other hydrous pyriboles-mineralogy. Reviews in mineralogy, 9A; 1-9.

He, M. X., 1987. Geophysical characteristics and deep structure of the Guangdong Province. Guangdong Geology, 2; 21-28 (in chinese).

Heinrich, E. W., 1946. Studies in the mica group. Journal of Sciences, 244. 836-848.

Henderson, P., 1984. Rare earth element geochemistry. Developmemts in Geochemistry, London. 63-107.

Henderson, C. M. B., Pendlebury, K. and Foland, K. A., 1989. Mineralogy and petrology of the Red Hill alkaline igneous complex, New Hampshire, U.S.A.. Journal of Petrology, 30; 627-666.

Hibbard, M. J., 1979. Myrmekite as a marker between preaqueous and postaqueous phase saturation in granitic systems. Geological Society of America Bulletin, 90; 1047-1062.

Hibbard, M. J., 1987. Deformation of incompletely crystallized magma systems:

granitic gneisses and their tectonic implications. Journal of Geology, 95; 543-561.

Hollister, L. S., Grisson, G. C., Peters, E. K. and Sisson, V. B., 1987. Confirmation of the empirical correlation of Al in hornblende with pressure of solidification of calc-alkaline plutons. American Mineralogist, 72; 231-239.

Hong, D. W., 1982. Biotite and mineralization series of granites in South China. Acta Geological Sinica, 2; 149-164 (in chinese).

Hsu, K. J., Li, J. L., Chen, H. H., Wang, Q. C., Sun, S. and Sengor, A. M. C., 1990. Tectonics of South China : Key to understanding west Pacific geology. Tectonophysics, 183; 9-39.

Huang, L., 1988. Characteristics and genesis of granitic rocks in Hetai Gold Mine. Guangdong Geology, 3; 45-54 (in chinese).

Institute of Geochemistry, Academia Sinica, 1979. Geochemistry of granitoid rocks in South China. Science Press, Beijing (in chinese).

Ishihara,S., 1977. The magnetite-series and ilmenite-series granitic rocks, Mining Geology, 27; 293-305.

Ishihara,S. and Terashima,S., 1977, Chemical variation of the cretaceous granitoids across southeastern Japan. Journal of the Geological Society of Japan, 83; 1-18.

Jahn, B. M., Zhou, X. H. and Li, J. L., 1990. Formation and tectonic evolution of Southeastern China and Taiwan : Isotopic and geochemical constraints. Tectonophysics, 183; 145-160.

Jakes, P. and White, A. J. R., 1972. Hornblendes from calc-alkaline volcanic rocks of island arcs and continental margins. American Mineralogist, 57; 887-902.

Kanisawa, S., 1972. Coexisting biotites and hornblendes from some granitic rocks in Southern Kitakami, Japan. Journal of the Japanese Association of Mineralogists, Petrologists and Economic Geologists, 67; 332-344.

Kanisawa, S., 1976. Chemistry of biotites and hornblendes of some granitic rocks in the San'in Zone, southwest Japan. Journal of the Geological society of Japan, 82; 543-548.

Kleemann, G. J. and Twist, D., 1989. The compositionally-zoned sheet-like granite pluton of the Bushveld complex : evidence bearing on the nature of A-type magmatism. Journal of Petrology, 30; 1383-1414.

Leake, B. E., 1978. Nomenclature of amphiboles. Canadian Mineralogist, 16; 501-520.

Li, X., Tatsumoto, M., Premo, W. R. and Gui, X., 1989. Age and origin of the Tanghu granite, southeast China : results from U-Pb single zircon and Nd isotopes. Geology, 17; 395-399.

Ling, J., 1986. Geological characteristics of the Hetai gold deposits, Guangdong Province. Guangdong Geology, 1; 56-68 (in chinese).

Ling, J., 1988. Structural and metallogenic characteristics of the ductile shear zone of Gaocun gold mine, Hetai, Gaoyao County. Guangdong Geology, 3; 17-24 (in chinese).

Liu, Y. J., Chao, L. M., Li, Z. L., Wang, H. N., Zu, T. Q. and Zhang, J. R., 1984. Element geochemistry. Scientical Publication, Beijing, (in chinese).

Lu, H. Z., Li, B. L., Shen, K., Zhao, X. C., Yu, T. J. and Wei, J. X., 1990. Fluid inclusion geochemistry. Geological Publishing House, Beijing (in chinese).

Maniar, P. D. and Piccoli, P. M., 1989. Tectonic discrimination of granitoids. Geological Society of America Bulletin, 101; 635-643.

Mason, D. R., 1978. Compositional variations in ferromagnesian minerals from porphyry copper-generating and barren intrusions of the Western Highlands, Papua, New Guinea. Economic Geology, 73; 878-890.

Mo, Z., 1985. A discussion on the classification of Nanling granites according to geological environment. Geotectonica et Metallogenia, 9; 17-27 (in chinese).

Mo, Z., 1987. Geotectonic development of the Western Guangdong Area and evolution of granitoid rocks. Guangdong Geology, 2; 1-8 (in chinese).

Mo, Z., 1989. Qinlian Movement and Hercynian granite in the area of East Guangxi and West Guangdong. Guangdong Geology, 4; 59-67 (in chinese).

Naney, M. T., 1980. The effect of Fe and Mg on crystallization in granitic systems. American Mineralogist, 65; 639-653.

Nan Y., 1989. Outline of stratigraphy of Guangdong Province : Part I, Late Proterozoic-Paleozoic. Guangdong Geology, 4; 1-22 (in chinese).

Paterson, S. R. and Tobisch, O. T., 1988. Using pluton ages to date regional deformation : Problems with commonly used criteria. Geology, 16; 1108-1111.

Paterson, S. R. and Tobisch, O.T., 1989, Criteria for establishing the relative timing of pluton emplacement and regional deformation. Geology, 17; 475-480.

Paterson, S. R., Vernon, R. H. and Tobisch, O. T., 1989. A review of criteria for the

identification of magmatic and tectonic foliations in granitoids. Journal of Structural Geology, 11; 349-363.

Pearce, J. A., Harris, N. B. W. and Tindle, A. G., 1984. Trace element discrimination diagrams for the tectonic interpretation of granite rocks. Journal of Petrology, 25; 956-983.

Phillips, E. R., 1980. On polygenetic myrmekite. Geological Magasine, 17; 29-36.

Pitcher, W. S., 1987. Granites and yet more granites forty years on. Geologische Rundschau, 76; 51-79.

Reid, J. B. and Hamilton, M. A., 1987. Origin of Sierra Nevadan granite : evidence from small-scale composite dykes. Contributions to Mineralogy and Petrology, 96; 441-454.

Ribbe, P. H., 1983. Exsolution textures in ternary and plagioclase feldspars; interference colors. Review in Mineralogy, 2; 141-176.

Rock, N. M. S., 1987. The need for standardization of normalized multi-element diagrams in geochemistry : a comment. Geochemical Journal, 21; 75-84.

Roedder, E., 1977. Fluid inclusions as a tool in mineral exploration. Economic Geology, 72; 503-525.

Roedder, E., 1979. Origin and significance of magmatic inclusions, Bulletin de minéralogie, Tome 102, 5-6.

Roedder, E., 1984. Fluid inclusions, Reviews in Mineralogy. 12; Mineralogical Society of America.

Roedder, E., 1992. Fluid inclusion evidence for immiscibility in magmatic differentiation. Geochemica et Cosmochimica Acta, 56; 5-20.

Schilmidt, M. W., 1992. Amphibole composition in tonalite as a function of pressure: an experimental calibration of the Al-in-hornblende barometer. Contributions to Mineralogy and Petrology, 110; 304-310.

Sevigny, J. H., Parrish, R. R. and Ghent, E. D., 1989. Petrogenesis of peraluminous granites, Monashee Mountains, southeastern Canadian Cordillera. Journal of Petrology, 30; 557-581.

Shaw, D. M., Cramer, J. J., Higgins, M . D. and Truscott, M. G., 1986. Composition of the Canadian Precambrian Shield and the continental crust of the earth. Dawson, J.B., Carswell,D.A., Hall,J. and Wedepohl,K.H. (editors). The nature of the lower continental crust. Geological Society Special Publication,

24; 275-282.

Shelton, K. L., So, C. and Chang, J., 1988. Gold-rich mesothermal vein deposits of the Republic of Korea : geochemical studies of the Jungwon gold area. Economic Geology, 83; 1221-1237.

Simpson, C. and Wintsch, R. P., 1989. Evidence for deformation-induced K-feldspar replacement by myrmekite. Journal of Metamorphic Geology. 7. 261-275.

Smith, J. V., 1983. Some chemical properties of feldspar. Review in Mineralogy, 2; 281-296.

Speer, J. A., 1982. Micas in igneous rocks. Reviews in Mineralogy, 13; 299-356.

Sutcliffe, R. H., Smith, A. R., Doherty, W. and Barnett, R. L., 1990. Mantle derivation of Archean amphibole-bearing granitoid and associated mafic rocks : evidence from the southern Superior Province, Canada. Contributions to Mineralogy and Petrology, 105; 255-274.

Taylor, S. R.,1979. Chemical composition and evolution of the continental crust : the rare earth element evidence, in The Earth : its origin, structure and evolution. Academic Press, 353-376.

Taylor, S. R. and McLennan, S. M., 1985. The continental crust : its composition and evolution. Blackwell Scientific Publication, London, 256-277.

Tsusue, A., Mizuta, T. and Tamai, T., 1989. Mode of differentiation of granitic magmas in South Korea and Southwest Japan. Geochemical Journal, 23; 271-278.

Tuttle, O. F. and Bowen, N. L., 1958. Origin of granite in the light of experimental studies in the system NaAlSi3O8-KAlSi3O8-SiO2-H2O. Geological Society of America Memoir. 74.

Vernon. R. H., 1968. Microstructures of high-grade metamorphic rocks at Broken Hill, Australia. Journal of Petrology, 9; 1-22.

Vernon, R. H., Williams, V. A. and D'Arcy, W. F., 1983. Grain-size reduction and foliation development in a deformed granitoid batholith. Tectonophysics, 92; 123-145.

Vernon, R. H., 1986. K-feldspar megacrysts in granites-phenocrysts, not porphyroblasts. Earth Science Reviews, 23; 1-63.

Vernon, R. H. and Collins, W. J., 1988. Igneous microstructures in migmatites. Geology, 16; 1126-1129.

Vernon, R. H., 1991. Questions about myrmekite in deformed rocks. Journal of Structural Geology, 13; 979-985.

Vogt, E. T. and Flower, M. F. T., 1989. Genesis of the Kinabalu (Sabah) granitoid at a subduction-collision junction. Contributions to Mineralogy and Petrology, 103; 433-509.

Wager, L. R. and Brown, G. M., 1967. Layered igneous rocks. Oliver and Boyd, Edinburgh.

Wall, V. J, Clemens, J. D. and Clarke, D. B., 1987. Models for granitoid evolution and source compositions. Journal of Geology, 95; 731-749.

Wang, L., Zhu, W., Zhang, S. and Yang, W., 1983. The evolution of two petrogeno-mineralization series and isotopic data from granites in South China. Mining Geology, 33; 295-303.

Wang, L., Zhu, W. and Zhang, S, 1984a, The belt distribution of granites and plate tectonics of South China. Petrological Research, 4; 1-13 (in chinese).

Wang, L., Yang, W. and Zhang, S., 1984b. The distribution map of two different series granites of South China, Hunan Publication.

Wang, L., Zhu, W., Zhang, S. and Yang, W., 1984c, Classification of series and types of granites and their spatial distribution in South China. Developments in Geoscience, Academia Sinica. Scientical Publication, Bejing, 299-309.

Weiss, S. and Troll, G., 1989. The Ballachulish igneous complex, Scotland : petrography, mineral chemistry, and order of crystallization in the Monzodiorite-quartz diorite suite and in the granite. Journal of Petrology, 30; 1069-1115.

White, A. J. R. and Chappell, B. W., 1977, Ultrametamorphism and granitoid genesis. Tectonophysics, 43; 7-22.

White, A. J. R. and Chappell, B. W., 1983. Granitoid types and their distribution in the Lachlan Fold Belt, Southeastern Australia. Geological Society of America Memoir, 159; 21-34.

Wones, D. R., 1965. Stability of biotite : experiment, theory, and application. American Mineralogist, 50; 1228-1272.

Wones, D. R., 1981. Mafic silicates as indicators of intensive variables in granitic magmas. Mining Geology, 31; 191-212.

Wones, D. R. and Gilbert, M. C., 1982. Amphiboles in the igneous environment.

Reviews in mineralogy, 9B; 355-383.

Wyborn, D., Chappell, B. W. and Johnston, R. M., 1981. Three S-type volcanic suites from the Lachlan Fold Belt, southeast Australia. Journal of Geophysical Research, 86; 10335-10348.

Xia, H. and Liang, S., 1985. Ta-Nb, W, Mo and Sn metallogeny related to granites, in The crust : the significance of granite gneisses in the lithosphere. Theophrastus Publications S.A., Athens, 571-587.

Xu, K. Q. and Tu, G. Z. (editors), 1984. Geology and mineralization of granitoids. Scientical and Technical Publication, Jiangsu, Nanjing, 657.

Yang, W., 1986. Chemical characteristics of micas from the granites of South China. Unpublished M. Sc. Institute of Geochemistry, Academia Sinica.

Yang, W., Wang, L., Zhang, S. and Xu, W., 1986a. Micas of the two series of granites in South China, Acta Mineralogica Sinica. 6; 298-307 (in chinese).

Yang, W., Wang, L., Zhang, S. and Xu, W., 1986b. Geochemical characteristics and formation environment of the Coast-type granites in the Fujian-Zhejiang coast area. Geochemica, 4; 307-318 (in chinese).

Yang, W., Wang, L., Zhang, S. and Xu, W., 1988a. On the origin and evolution of granites in South China in terms of trace elements in micas. Acta Mineralogica Sinica, 8; 127-135 (in chinese).

Yang, W., Wang, L., Zhang, S. and Xu, W., 1988b, REE characteristics of micas from two petrogeno-mineralization series granites in South China. Acta Mineralogica Sinica, 8; 336-343.

Yang, W., 1992. Chemical characteristics of biotite and amphibole from granites of South China. Geological Association of Canada, Mineralogical Association of Canada, 17; A120 .

Ye, B., 1989. Isotopic age data from Yunkai Area of Guangdong and Guangxi provinces and their geologic implications. Guangdong Geology, 4; 39-55 (in chinese).

Yuan, Z. and Huang, F., 1990. New view of structural control and minerogenetic features of Gaochun gold deposit in Hetai Ore Field, Western Guangdong. Guangdong Geology, 5; 72-82 (in chinese).

Yund, R. A. and Tullis, J., 1983. Subsolidus phase relations in the alkal feldspars with emphasis on coherent phase. Review in Mineralogy, 2; 141-170.

Zen, E-An and Hammarstrom, J. M., 1984. Magmatic epidote and its petrologic significance. Geology, 12; 515-518.

Zen, E-An and Hammarstrom, J. M., 1986. Reply to comments on "Implications of magmatic epidote-bearing plutons on crustal evolution in the accreted terranes of northwestern North America" and "Magmatic epidote and its petrologic significance". Geology, 14; 188-189.

Zhang, S., Wang, L.and Zhu, W., 1984. Accessory mineral assemblage and trace elements in them for genetic classification of granites in South China, in Geology and Mineralization of Granites. Scientical Publication, Nanjing, 634-644 (in chinese).

Zhang, Z., Zhang, S. and Yuan, H., 1986. Characteristics of S- and Pb- isotope of Hetai gold deposit, Guangdong. Guangdong Geology, 4; 29-39 (in chinese).

Zhou, Y., 1992, Geochemistry and metallogenetic mechanism of the Hetai Gold Field, southern China. Unpublished Ph. D. thesis, Université du Québec à Chicoutimi.

APPENDIX I

DESCRIPTION OF SAMPLES

C1 : Major oxide average of granites of South China

1. Shijiang complex

C16-1 and C78 : Dark biotite-feldspar enclaves in the Shijiang granite, medium-fine grained, deformed, biotite(25%)+ muscovite(5%)+ plagioclase(50%, An =50-30)+ orthoclase (10%)+ quartz(10%)+garnet

C12-1 : Dark biotite-feldspar enclave in the Shijiang granite, deformed, fine-grained, biotite(25%)+ muscovite(5%)+ plagioclase(40%, An=45-30) +orthoclase(15%)+ quartz(15%)+ garnet

C16-2, C16-2a (C16-2-1), C78-1 and C12-2 : Homogeneous coarse-medium biotite granite, strongly deformed, mylonitic structure, biotite(20%)+ muscovite(5%)+ plagioclase(45%, An=30-20), orthoclase(10%)+ quartz(15%)+garnet

C78-3 and C12-3 : Heterogeneous stromatic biotite granite, strongly deformed, mylonitic structure, biotite(15%)+ muscovite(5%)+ plagioclase(40%, An=30-20)+ orthoclase(20%)+ quartz(20%)+garnet

C16-3 : Banded biotite granite, strongly deformed, mylonitic structure, biotite(10%)+ muscovite(5%)+ plagioclase(15%, An=30-10)+ orthoclase(45%)+

quartz(30%)+garnet

C 16-4, C78-5, C12-4 and C12-5: Augen biotite granite, strongly deformed, gneissic and mylonitic structure, biotite(5%)+ muscovite(5%)+ palgioclase(15%, An=25-5)+ orthoclase(50%)+ quartz(30%)+garnet

2. Sidong granitic pluton :

C7-1 and C7-1a : Coarse-grained biotite granite, magmatic flow foliation, deformed, biotite(8%)+ plagioclase(30%, An<15)+ microcline(30%)+ quartz(32%) +muscovite+garnet

C7-2 : Medium-fine-grained biotite granite, magmatic flow foliation, deformed, biotite(5%)+ plagioclase(30%, An<15)+ orthoclase(10%)+ microcline(25%)+ quartz(40%) +muscovite+garnet

3. Shiniutou granitic pluton :

C17 and C22-1 : Banded biotite granite, strongly deformed, mylonitic structure, biotite(3%)+ muscovite(5%)+ plagioclase(20 %, An<15)+ microcline(40%)+ quartz(32%)+ garnet+ apatite+zircon

C22-2 and C22-3 : Gneissic and augen biotite granite, strongly deformed, mylonitic structure, biotite(5%)+ muscovite(5%)+ plagioclase(25%)+ microcline(35%)+ quartz(30%)+ garnet+apatite+ zircon

4. Metamorphosed Precambrian sedimentary rock :

C42, C42a and C42-1 : Metamorphosed biotite-feldspar sandstone, deformed, biotite(30%)+ plagioclase(40%, An=40-30)+ orthoclase(20%)+ quartz(10%) +muscovite+ garnet

5. Guangning granitic pluton :

C84, C84a and C13 : Medium-grained biotite monzogranite, equigranular texture, strongly deformed, mylonitic structure, biotite(8%)+ muscovite(2%)+ plagioclase(35%, An=30-15)+ microcline(25%)+ quartz(30%)+ garnet+

allanite(epidote)

6. Yunlougan pluton

C9-1, C9-1a and C9-1b : Medium-grained granodiorite, equigranular texture, strongly deformed, amphibole(5%)+ biotite(15%)+ plagioclase(60%, An=50-30)+ microcline(10%)+ quartz(15%)+ magnetite+ allanite(epidote)+ sphene

C9-2 : Pegmatite, leuco-dyke, porphyritic structure, very weakly deformed, biotite(<1%)+ muscovite(15%)+ plagioclase(20, An<10)+ orthoclase(40%)+ quartz(25%)

7. Wuchun granite suite :

C10-1 and C10-1a : Granodioritic enclaves in the Wuchun pluton, irregular shape and different sizes, very weakly deformed, containing Ca-rich plagioclase xenocrysts (An=60-45), amphibole(2%)+ biotite(18%)+ plagioclase(55%, An=40-25)+ orthoclase(10%)+ quartz(15%)+ magnetite+sphene+allanite

C10-2 and C10-2a : Megacryst monzogranite, porphyritic structure, very weakly deformed, biotite(5%)+ plagioclase(30, An=35-5)+ orthoclase(35%)+ quartz(30%)+ magnetite+sphene+allanite(epidote)

8. Sihui granite suite :

C18-3 and C18-3a : Granodioritic enclaves, irregular shape and different sizes, magmatic flow foliation with the host granite, porphyric structure, very weakly deformed, amphibole(2%)+ biotite(8%)+ plagioclase(60%, An=45-30)+ orthoclase(10%)+ quartz (20%)+ magnetite+sphene+epidote

C18-1 and C21-1 : Coarse-grained alkali-feldspar granite, porphyritic structure, very weakly deformed, a few amphibole+ biotite(5%)+ plagioclase(20%, An=45-10)+ orthoclase(15%)+ microcline(25%)+ quartz(35%)+ magnetite+sphene+zircon

C18-2, C21-2 and C21-3 : Medium-fine-grained alkali-feldspar granite, porphyritic

structure, very weakly deformed, biotite(<5%)+ plagioclase(15%, An=30-5)+ orthoclase(20%)+ microcline(25%)+ quartz(35%)+ magnetite+sphene+zircon

9. Huangtongjiang gabbro :

C160-2 : Medium-fine-grained diabase gabbro, porphyritic structure, very weakly deformed, pyroxene(5-8%)+ amphibole(35%)+ biotite(5%)+ plagioclase(50%, An=70-50)+ orthoclase(<2%)+ quartz(<2%)+ magnetite+sphene+epidote

C162-1 and C128 : Medium-fine-grained diabase gabbro or pyroxene diorite, porphyritic structure, very weakly deformed, pyroxene(5%)+ amphibole(40%)+ biotite(5%)+ plagioclase(45%)+ orthoclase(3%)+ quartz(2%)+ magnetite+ epidote+ apatite

10. Basic dykes :

C4 : Metamorphosed basic dyke in the Hetai ore deposit field

APPENDIX II

METHODS OF ANALYSES

1. Whole rock analyses of granites

The chemical compositions of different granitic rocks and their enclaves have been systematically analyzed in different methods :

Major oxides SiO2, P2O5, Al2O3, Fe2O3, FeO, MgO, MnO, CaO, Na2O, K2O and H2O by (1) XRF in McGill University, Canada, and (2) some samples by wet chemical analyses in Institute of Geochemistry, Academia Sinica, China;

The Rb, Sr, Ba, Zr, Co, Ni, Cr, V, Pb, Zn and Ga by XRF and XRS analyses in McGill University and Centre de Recherches Minérales, Québec;

The Hf, U, Th, As, Au, La, Ce, Nd, Sm, Eu, Tb, Ho, Yb and Lu by Neutron Activiation in Sciences de la Terre, Université du Québec à Chicoutimi.

Au contents in different granitic rocks of the Hetai Area are determined by means of wet chemical analyse in Institute of Geochemistry, Academia Sinica, China and by neutron activiation in Université du Québec à Chicoutimi, Canada, respectively.

These analyzed samples cover over different intrusive phases, different ages and different tectonic positions, as well as different kinds of enclaves in the Hetai Area, in order to establish a geochemical relation and have a comparison between them.

2. Analyses of biotite, amphibole and plagioclase

Major oxides SiO2, Al2O3, FeOt, MgO, MnO, CaO, Na2O and K2O are determined by means of Electron Microprobe in Sciences de la Terre, Université du Québec à Chicoutimi. Analyses were obtained using a ARL electron microprobe fitted with a Tracor-Noran energy dispersive detector and a 143 eV resolution. The voltage of acceleration is 15 KV and the curant through sample is 9-10 nA. The counter time is controlled between 50-100 seconds.

The Fe2O3 and FeO contents of biotites were calculated based on wet chemical data of same biotite sample analyzed in Institute of Geochemistry, Academia Sinica, China.

Trace elements of biotites were also analyzed by wet chemical method in Institute of Geochemistry, Academia Sinica, China.

3. Silicate melt inclusions and fluid inclusions in granites

Silicate melt inclusions were observed under a Nikon microscope and the heating runs to determine homogenization temperatures were carried out in a furnace with variable temperature from 650 °C to 1000 °C at Department des Sciences Appliquées, Université du Québec à Chicoutimi.

The homogenization temperature of fluid inclusions in granites were measured by the freezing method using an equipment of CHAIXMCCA with variable temperature from -186 °C to +600 °C at Sciences de la Terre, Université du Québec à Chicoutimi.

APPENDIX III

TABLES OF CHEMICAL DATA OF GRANITES AND MINERALS

Table 1. Major oxides of the Caledonian granites.....228-229

Table 2. Trace element compositions of the Caledonian granites 230

Table 3. REE compositions of the Caledonian granites 231

Table 4. Major oxides of the Hercynian granites.....232

Table 5. Trace element analyses of the Hercynian granites.....233

Table 6. REE compositions of the Hercynian granites 234

Table 7. Major oxides of the Indosinian granites.....235

Table 8. Trace element analyses of the Indosinian granites.....236

Table 9. REE compositions of the Indosinian granites.....237

Table 10. Major oxides of the Yanshanian granites.....238

Table 11. Trace element analyses of the Yanshanian granites.....239

Table 12. REE compositions of the Yanshanian granites 240

Table 13. Au contents in different granite types of the Hetai Area 241

Table 14. Chemical compositions of biotites from the Caledonian granites 242-244

Table 15. Chemical analyses of biotites from the Hercynian granites 245

Table 16. Chemical analyses of biotites from the Indosinian granites.....246

Table 17. Chemical analyses of biotites from the Yanshanian granites.....247-248

Table 18. Comparison between biotites from the Huangtongjiang gabbro and metamorphosed Precambrian sedimentary rock.....249

Table 19. Comparison between biotites from the different enclaves 250-251

Table 20. Trace elements and major oxide averages of biotites from granites of the Hetai Area 252

Table 21. Chemical analyses of amphiboles from some granitic plutons of the Hetai Area.....253-255

Table 22. Chemical analyses of plagioclases, Caledonian granites.....256-257

Table 23. Chemical analyses of plagioclases, Hercynian granites.....258

Table 24. Chemical analyses of plagioclases, Indosinian granites.....259

Table 25. Chemical analyses of plagioclases, Yanshanian granites.....260-261

Table 26. Chemical analyses of plagioclases, Huangtongjiang gabbro and metamorphosed Precambrian sedimentary rock 262

Table 1. Major oxides of the Caledonian granites

Sample No.	C1	C42	C42a	C42-1	C78-1	C12-1	C16-1	C16-2	C16-2a	C78-1	C12-2	C12-3	C16-3	C78-3
SiO2	72.05	70.30	69.02	70.88	66.54	67.70	64.34	68.13	67.97	68.31	70.21	69.60	68.35	70.04
Al2O3	13.72	14.82	14.92	14.35	16.47	16.25	16.31	15.69	16.04	15.80	14.83	15.82	15.24	15.14
Fe2O3	0.98	0.72	1.31	0.75	0.38	0.37	1.02	0.16	0.39	0.75	0.25	0.20	0.42	0.21
FeO	1.96	3.82	4.33	3.75	3.38	3.11	4.73	3.42	3.33	3.02	3.02	2.19	3.53	2.74
MgO	0.66	1.01	1.10	1.05	1.89	1.96	2.51	1.79	1.62	1.51	1.23	0.91	1.36	1.19
CaO	1.38	0.99	1.50	1.04	4.27	3.58	3.41	3.14	3.15	2.98	2.94	2.56	2.40	2.20
Na2O	3.22	2.47	2.90	2.54	3.41	3.91	3.14	3.74	3.65	3.44	3.35	3.17	3.82	3.54
K2O	4.54	4.32	3.40	4.36	2.00	1.73	2.71	2.12	2.40	2.80	2.52	4.39	2.68	3.37
H2O+-	0.76	1.08	0.78	1.01	0.49	0.47	0.61	0.55	0.63	0.63	0.46	0.46	0.49	0.58
TiO2	0.28	0.34	0.51	0.41	0.58	0.53	1.00	0.63	0.56	0.57	0.45	0.34	0.58	0.42
P2O5	0.12	0.09	0.09	0.05	0.18	0.16	0.15	0.15	0.14	0.12	0.10	0.08	0.14	0.17
MnO	0.08	0.08	0.11	0.04	0.06	0.09	0.07	0.06	0.05	0.06	0.07	0.04	0.05	0.05
Total	99.75	100.00	99.97	100.20	99.65	99.86	100.00	99.58	99.93	99.99	99.43	99.76	99.06	99.65
K2O/Na2O	1.41	1.75	1.17	1.72	0.59	0.44	0.86	0.57	0.66	0.81	0.75	1.38	0.70	0.95
K2O/P2O5	37.83	48.00	37.78	87.20	11.11	10.80	18.07	14.13	17.14	23.33	25.20	54.88	19.14	19.82
Fe2O3/(Fe2O3+FeO)	0.33	0.16	0.23	0.17	0.10	0.11	0.18	0.04	0.10	0.20	0.08	0.08	0.11	0.07
MgO/(MgO+FeO)	0.25	0.26	0.21	0.22	0.36	0.39	0.35	0.34	0.33	0.33	0.29	0.29	0.28	0.30
Mol.A/CNK		1.27	1.33	1.33	1.06	1.10	1.14	1.12	1.12	1.12	1.09	1.08	1.12	1.12
CIPW weight % norms (analyses recalculated to 100% free of H2O and CO2; cc not calculated)														
qz	31.53	33.64	31.96	33.45	25.51	26.21	22.34	27.17	26.71	27.60	31.40	26.39	27.09	28.87
ab	27.52	21.12	24.74	21.66	29.10	33.29	26.73	31.96	31.10	29.30	28.64	27.01	32.79	30.24
or	27.10	25.80	20.26	25.97	11.92	10.29	16.11	12.65	14.28	16.65	15.05	26.13	16.07	20.10
an	6.12	4.37	6.91	4.87	20.18	16.82	16.03	14.74	14.82	14.09	14.08	12.26	11.15	9.90
mt	1.44	1.05	1.91	1.10	0.56	0.54	1.49	0.23	0.57	1.09	0.37	0.29	0.62	0.31
il	0.54	0.65	0.98	0.78	1.11	1.01	1.91	1.21	1.07	1.09	0.86	0.65	1.12	0.81
ap	0.28	0.21	0.21	0.12	0.42	0.37	0.35	0.35	0.33	0.28	0.23	0.19	0.33	0.40
cm	1.30	4.54	3.99	3.71	1.37	1.83	2.38	1.91	2.06	1.99	1.50	1.40	2.06	2.10
ag	0.74	0.59	0.57	0.62	0.47	0.51	0.50	0.54	0.54	0.55	0.56	0.63	0.60	0.63
DI	86.16	80.56	76.96	81.08	66.53	69.79	65.18	71.78	72.10	73.55	75.09	79.53	75.95	79.21

Table 1 continued

Sample	C16-4	C78-5	C12-5	C12-4	C7-1a	C7-1	C7-2	C17	C22-1	C22-2	C22-3
SiO2	72.17	72.10	74.36	73.63	73.55	76.02	76.66	76.25	74.37	74.61	72.65
Al2O3	14.56	14.71	13.37	14.00	13.59	12.72	12.74	12.99	12.33	14.56	13.75
Fe2O3	0.27	0.13	0.08	0.01	0.54	0.15	0.27	0.15	0.81	0.28	0.33
FeO	1.70	1.57	1.55	1.17	1.67	1.10	0.68	0.91	1.29	0.66	1.52
MgO	0.62	0.45	0.54	0.24	0.50	0.04	0.01	0.01	0.34	0.22	0.89
CaO	1.12	1.20	1.48	1.02	2.00	1.18	0.87	0.58	1.06	0.92	1.39
Na2O	2.27	2.96	2.56	2.92	3.22	3.73	3.58	2.82	2.39	2.69	0.79
K2O	5.95	5.34	5.29	6.05	4.07	3.88	4.92	5.18	4.64	4.20	4.29
H2O+-	0.74	0.64	0.31	0.38	0.26	0.20	0.23	0.90	1.72	1.97	4.14
TiO2	0.30	0.26	0.21	0.14	0.14	0.13	0.13	0.07	0.24	0.05	0.26
P2O5	0.13	0.14	0.05	0.09	0.03	0.03	0.03	0.13	0.14	0.15	0.14
MnO	0.02	0.02	0.03	0.02	0.10	0.03	0.02	0.03	0.03	0.02	0.04
Total	99.85	99.52	99.83	99.67	99.67	99.21	100.10	100.00	99.36	100.33	100.19
K2O/Na2O	2.62	1.80	2.07	2.07	1.26	1.04	1.37	1.84	1.94	1.56	5.43
K2O/P2O5	45.90	38.14	105.80	67.22	135.67	129.33	164.00	39.85	33.14	28.00	30.64
Fe2O3/(Fe2O3+FeO)	0.14	0.08	0.05	0.01	0.24	0.12	0.28	0.14	0.39	0.30	0.18
MgO/(MgO+FeO)	0.27	0.22	0.26	0.17	0.02	0.04	0.01	0.01	0.21	0.25	0.37
	1.17	1.03	1.06	1.05	1.01	1.02	0.99	1.23	1.13	1.36	1.61
CIPW weight % norms (analyses recalculated to 100% free of H2O and CO2; cc not calculated)											
qz	32.41	30.86	34.42	30.53	33.32	36.54	34.86	38.80	40.67	41.26	48.66
ab	19.38	25.33	21.77	24.88	27.41	31.88	30.32	24.07	20.71	23.14	6.96
or	35.48	31.92	31.41	36.01	24.20	23.16	29.10	30.88	28.08	25.23	26.40
an	4.75	5.10	7.05	4.50	9.78	5.71	4.12	2.05	4.45	3.64	6.23
mt	0.39	0.19	0.12	0.01	0.79	0.22	0.39	0.22	1.20	0.41	0.50
il	0.57	0.50	0.40	0.27	0.27	0.25	0.25	0.13	0.47	0.10	0.51
ap	0.30	0.33	0.12	0.21	0.07	0.07	0.07	0.30	0.33	0.35	0.34
cm	2.68	2.24	0.87	1.02	0.32	0.31	0.02	2.02	1.83	4.35	5.85
ag	0.70	0.72	0.74	0.81	0.71	0.81	0.88	0.79	0.73	0.62	0.43
DI	87.27	88.10	87.60	91.43	84.92	91.58	94.28	93.75	89.46	89.64	82.02

Table 2. Trace element compositions of the Caledonian granites in the Hetai Area (ppm)

LOCATION	No	Co	Ni	Cr	Sc	V	Cu	Zn	Pb	Ba	Sr	Rb	Nb	Ta	Ga	Zr	Hf	Y	U	Th	Rb/Sr
Hetai	C42	61	53	10	4.8	56	19	37	17	101	61	179	7	3.5	18	112	3.0	20	2.5	12.0	2.93
	C42a	66	59	10	5.5	52	10	32	17	110	62	150	8	4.0	19	120	2.5	22	4.0	12.0	2.42
	C42-1	58	50	15	5.6	60	15	42	22	110	77	160	9	3.2	19	120	2.5	21	3.5	11.0	2.17
Shijiang	C78	61	49	50	15.0	75	15	58	12	271	157	150	11	3.4	23	158	4.4	9	0.8	6.7	0.96
	C12-1	57	62	66	8.6	59	16	47	4	343	161	141	9	3.2	26	155	6.6	15	2.0	10.6	0.90
	C16-1	58	44	55	14.8	115	25	78	12	233	117	159	12	3.1	25	149	5.0	16	1.5	11.5	1.36
Shijiang	C16-2	45	61	96	10.7	88	596	67	17	171	127	166	10	2.8	23	150	5.2	14	4.1	14.3	1.31
	C16-2a	54	14	10	10.6	79	25	52	20	461	136	149	11	3.3	22	132	4.1	18	3.8	12.9	1.10
	C78-1	49	81	120	9.9	76	49	62	21	446	129	146	11	3.1	21	124	4.2	18	3.1	14.6	1.13
	C12-2	51	12	30	9.6	66	10	38	23	386	108	118	10	3.4	22	137	5.3		7.7	24.5	1.09
	C12-3	42	21	31	6.6	43	27	27	39	940	134	133	8	2.7	19	87	3.9	20	5.6	17.5	0.99
	C16-3	54	49	45	9.3	65	25	77	20	213	107	179	13	3.5	23	153	4.2	18	3.7	15.0	1.67
	C78-3	53	30	59	6.6	64	84	53	28	243	90	182	14	4.1	23	96	3.5	12	4.8	11.4	2.02
	C16-4	52	15	10	4.7	36	28	35	37	606	84	209	9	3.1	19	125	4.4	14	5.7	26.7	2.49
	C78-5	65	14	59	4.0	49	20	21	38	467	85	195	9	3.8	19	125	3.8	13	5.5	24.1	2.29
	C12-5	72	17	50	4.8	33	15	10	44	548	94	190	7	4.3	16	39	1.9	36	14.0	24.5	2.02
	C12-4	61	15	35	4.0	31	696	23	48	413	69	186	7	3.3	15	62	1.4	31	10.3	24.5	2.70
Sidong	C7-1a	62	14	15	2.5	12	10	12	16	908	22	144	8	3.0	13	95	0.6	11	5.0	12.0	6.55
	C7-1	64	11	10	3.4	10	24	10	17	864	27	125	4	3.9	12	100	6.1	13	4.5	8.3	4.63
	C7-2	67	14	10	1.2	16	37	10	15	919	27	154	3	4.0	15	85	6.2	10	5.6	19.8	5.70
Shiniutou	C17	56	41	35	3.0	18	361	17	20	70	18	369	9	4.4	20	41	3.0	24	17.7	12.1	20.50
	C22-1	59	18	10	5.2	34	31	10	15	292	53	241	10	4.4	19	100	4.7	40	5.4	18.8	4.55
	C22-2	55	20	10	4.8	15	245	10	14	118	36	256	6	3.3	26	44	3.5	8	51.1	9.7	7.11
	C22-3	59	25	10	5.2	31	25	10	6	261	27	281	11	3.7	18	110	3.5	39	7.0	20.0	10.41

Table 3. REE compositions of the Caledonian granites in the Hetai Area (ppm)

LOCATION	No.	La	Ce	Nd	Sm	Eu	Tb	Ho	Yb	Lu	La/Sm	La/Yb
Hetai	C42	12.36	20.46	10.76	2.39	0.29	0.66	0.77	2.62	0.52	5.17	4.71
Shijiang	C78	23.27	44.33	19.86	3.52	1.19	0.47	0.33	0.80	0.14	6.61	18.38
	C12-1	27.16	55.64	25.63	4.91	1.17	0.67	0.58	1.45	0.27	5.53	18.73
	C16-1	25.80	44.53	23.26	4.31	1.05	0.58	0.72	1.36	0.19	5.99	18.97
Shijiang	C16-2	30.35	56.56	25.99	5.15	1.07	0.62	0.72	1.56	0.26	5.89	19.46
	C16-2a	28.19	52.74	27.16	5.56	1.25	0.81	0.96	2.40	0.37	5.07	11.75
	C78-1	30.69	55.55	20.91	4.72	1.08	0.79	0.74	2.17	0.32	6.50	14.14
	C12-2	37.86	77.31	26.69	7.73	1.03	2.02	2.30	3.37	1.23	4.90	5.16
	C12-3	27.85	55.34	20.55	4.54	0.88	0.81	0.66	2.52	0.42	6.13	11.05
	C16-3	30.49	60.12	27.32	5.32	0.97	0.72	0.89	1.83	0.29	5.73	16.66
	C78-3	24.15	44.81	22.20	6.27	1.11	0.82	1.02	1.38	0.22	3.85	17.50
	C16-4	54.02	108.80	44.76	11.60	1.16	1.80	1.31	2.95	0.36	4.66	27.70
	C12-5	15.08	30.76	14.53	4.53	0.78	1.11	1.51	4.16	0.76	3.33	3.63
	C12-4	17.68	33.59	16.13	4.19	0.66	1.02	1.41	4.42	0.62	4.22	4.00
	C78-5	33.88	66.50	35.36	7.20	1.03	1.13	0.88	2.43	0.31	4.71	13.90
Sidon	C7-1	9.90	17.46	8.11	1.61	0.36	0.43	0.58	2.09	0.35	6.15	4.74
	C7-2	10.31	16.13	6.99	1.43	0.50	0.31	0.47	1.78	0.36	7.21	5.79
Shiniutou	C17	8.69	18.74	9.64	3.96	0.14	0.86	1.34	2.57	0.46	2.19	3.38
	C22-1	27.61	56.20	21.96	5.88	0.57	1.38	1.48	4.04	0.64	4.70	6.83
	C22-2	3.93	8.20	6.80	2.79	0.22	0.66	2.49	1.41	0.31	1.41	2.79
	C22-3	25.19	50.39	28.48	5.62	0.69	1.21	1.79	3.93	0.64	4.48	6.41

Table 4. Major oxides of the Hercynian granites

Sample	C13	C84	C84-a	C9-2	C9-1a	C9-1b	C9-1
SiO2	71.74	70.95	69.13	73.31	66.29	65.26	67.31
Al2O3	14.72	14.95	15.88	13.34	16.75	15.88	15.36
Fe2O3	0.33	0.59	0.53	0.01	0.71	1.38	0.54
FeO	1.80	2.22	2.21	1.11	4.36	4.21	4.03
MgO	0.66	1.02	0.90	0.30	1.70	1.80	1.90
CaO	1.69	2.54	2.60	0.58	3.00	4.30	3.83
Na2O	3.37	3.35	3.18	2.24	3.16	3.08	3.16
K2O	4.23	3.64	3.73	7.13	2.39	2.27	2.33
H2O+-	0.56	0.49	0.48	0.82	0.25	0.75	0.53
TiO2	0.31	0.41	0.37	0.14	0.53	0.60	0.68
P2O5	0.15	0.14	0.15	0.06	0.16	0.16	0.16
MnO	0.05	0.05	0.10	0.02	0.11	0.11	0.08
Total	99.61	100.40	99.26	99.06	99.41	99.80	99.91
K2O/Na2O	1.26	1.09	1.17	3.18	0.76	0.74	0.74
K2O/P2O5	28.20	26.00	16.21	118.83	14.93	14.19	14.56
Fe2O3/(Fe2O3+FeO)	0.15	0.21	0.19	0.01	0.14	0.25	0.12
MgO/(MgO+FeO)	0.27	0.31	0.29	0.21	0.28	0.30	0.32
Mol. A/CNK	1.11	1.07	1.14	1.07	1.04	1.03	1.06
CIPW weight % norms (analyses recalculated to 100% free of H2O and CO2; cc not calculated)							
qz	30.87	29.64	28.76	31.18	27.41	24.80	26.87
ab	28.79	28.39	27.24	19.29	26.97	26.31	26.91
or	25.24	21.54	22.32	42.89	14.24	13.54	13.86
an	7.48	11.70	12.07	2.53	13.95	20.48	18.07
mt	0.48	0.86	0.78	0.01	1.04	2.02	0.79
il	0.59	0.78	0.71	0.27	1.02	1.15	1.30
ap	0.35	0.32	0.35	0.14	0.37	0.37	0.37
cm	1.90	1.22	2.27	1.04	3.93	0.93	1.07
ag	0.69	0.63	0.58	0.85	0.46	0.47	0.50
DI	84.90	79.57	78.32	93.37	68.62	64.66	67.63

Table 5. Trace element compositions of the Hercynian granites in the Hetai Area

LOCATION	No.	Co	Ni	Cr	Sc	V	Cu	Zn	Pb	Ba	Sr	Rb	Nb	Ta	Ga	Zr	Hf	Y	U	Th	Rb/Sr
Guangning	C13	60	13	12	5.9	44	19	38	32	437	74	225	12	4.9	20	88	3.5	16	15.0	16.5	3.04
	C84	51	30	43	7.7	57	19	44	27	303	83	186	10	3.4	21	107	3.3	19	6.9	15.3	2.24
	C84a	52	31	33	6.5	33	14	65	28	335	72	197	12	3.2	21	90	3.5	18	8.0	15.5	2.74
Yunlougan	C9-2	67	38	18	3.2	32	13	10	59	1244	90	198	5	4.0	14	2	1.5	13	4.7	4.5	2.20
Yunlougan	C9-1a	69	29	50	14.0	93	52	85	16	403	172	110	10	2.0	20	192	5.0	31	3.0	15.0	0.64
	C9-1b	68	29	42	12.0	93	56	82	14	513	177	117	9	3.0	22	188	6.0	30	5.0	16.0	0.66
	C9-1	67	27	34	13.3	96	54	54	15	745	161	112	12	3.6	21	189	5.6	29	2.8	18.3	0.70

Table 6. REE compositions of the Hercynian granites in the Hetai Area (ppm)

LOCATION	No.	La	Ce	Nd	Sm	Eu	Tb	Ho	Yb	Lu	La/Sm	La/Yb
Guangning	C13	23.62	45.05	17.76	4.50	0.73	0.73	0.84	1.73	0.28	5.25	13.65
	C84	21.92	50.39	23.48	4.65	0.84	0.68	0.90	2.17	0.37	4.71	10.10
Yunlougan	C9-2	3.00	6.50	6.20	1.68	0.68	0.42	0.48	1.66	0.32	1.79	1.81
Yunlougan	C9-1	46.71	82.33	35.21	6.42	1.06	1.00	0.94	2.98	0.48	7.28	15.67

Table 7. Major oxides of the Indosinian granites and Huangtongjiang gabbro

Sample	C10-1a	C10-1	C10-2	C10-2a	C160-2	C162-1	C128	C128a
SiO2	63.19	64.65	71.39	70.38	51.48	52.67	49.42	56.18
Al2O3	16.32	15.76	14.54	14.44	15.14	16.51	16.77	16.40
Fe2O3	1.01	0.90	0.52	0.67	1.38	1.66	2.13	2.20
FeO	4.50	4.48	1.89	2.12	4.85	5.49	6.88	5.94
MgO	2.70	2.27	0.52	0.50	9.38	7.34	7.97	5.40
CaO	3.81	3.75	2.08	2.30	12.78	10.53	11.32	6.20
Na2O	3.80	3.78	3.63	3.51	1.90	3.19	2.57	3.50
K2O	2.10	2.32	4.37	4.40	0.51	0.77	0.61	1.61
H2O+-	1.02	0.54	0.49	0.22	1.44	1.16	1.07	1.44
TiO2	0.73	0.77	0.33	0.29	0.66	0.68	1.14	0.62
P2O5	0.23	0.25	0.12	0.12	0.03	0.06	0.07	0.05
MnO	0.18	0.18	0.08	0.11	0.13	0.14	0.16	0.16
Total	99.59	99.65	99.96	99.06	99.68	100.20	100.10	99.70
K2O/Na2O	0.55	0.61	1.20	1.25	0.27	0.24	0.24	0.46
K2O/P2O5	9.13	9.28	36.42	36.67	17.00	12.83	8.71	32.20
Fe2O3/(Fe2O3+FeO)	0.18	0.17	0.22	0.24	0.22	0.23	0.24	0.27
MgO/(MgO+FeO)	0.38	0.34	0.22	0.19	0.66	0.57	0.54	0.48
Mol. A/CNK	1.06	1.02	0.99	0.98	0.52	0.65	0.66	0.88
CIPW weight % norms (analyses recalculated to 100% free of H2O and CO2; cc not calculated)								
qz	18.79	20.27	27.60	26.70	0.95	0.00	0.00	6.09
ab	32.62	32.27	30.88	30.05	16.37	27.25	21.96	30.14
or	12.59	13.83	25.96	26.31	3.07	4.59	3.64	9.68
an	17.65	17.12	9.59	10.75	31.84	28.73	32.73	24.71
di					25.98	19.05	19.00	5.10
ol					0.00	1.81	7.95	0.00
mt	1.49	1.32	0.76	0.98	2.04	2.43	3.12	3.25
il	1.41	1.48	0.63	0.56	1.28	1.30	2.19	1.20
ap	0.54	0.58	0.28	0.28	0.07	0.14	0.16	0.12
cm	1.44	0.82	0.35	0.01	0.00	0.00	0.00	0.00
ag	0.52	0.55	0.74	0.73	0.24	0.37	0.29	0.46
DI	64.00	66.37	84.44	83.06	20.39	31.85	25.60	45.91

Table 8. Trace element compositions of the Indosinian granites in the Hetai Area (ppm)

LOCATION	No	Co	Ni	Cr	Sc	V	Cu	Zn	Pb	Ba	Sr	Rb	Nb	Ta	Ga	Zr	Hf	Y	U	Th	Rb/Sr
Houangtong.	C160-2	59	130	284	41.1	162	81	38	4	144	126	25	3	1.2	16	24	1.2	18	0.5	2.0	0.20
	C162-1	42	62	83	31.5	183	81	45	9	56	128	32	4	0.9	16	41	1.4	16	1.1	4.5	0.25
	C128	54	95	271	33.3	197	10	61	6	39	113	24	4	0.9	19	59	2.5	26	0.5	1.7	0.21
	C128a	51	89	88	25.5	121	18	135	8	330	77	59	7	3.0	18	55	1.8	19	1.5	2.5	0.77
Wuchun	C10-1a	32	89	120	8.6	92	24	133	15	293	287	282	19	7.0	21	150	4.0	15	58.0	12.0	0.98
	C10-1	44	61	116	10.7	99	16	92	13	275	243	248	16	3.1	22	141	4.6	17	71.6	11.4	1.02
	C10-2	90	76	19	5.3	54	862	42	28	301	190	230	19	6.8	21	105	4.0	15	10.1	17.1	1.21
	C10-2a	45	54	20	4.0	52	810	82	28	348	178	239	16	8.0	22	110	4.5	16	15.0	18.0	1.34

Table 9. REE compositions of the Indosinian granites in the Hetai Area (ppm)

LOCATION	No.	La	Ce	Nd	Sm	Eu	Tb	Ho	Yb	Lu	La/Sm	La/Yb
Huangtongjiang	C160-2	5.27	13.18	8.89	2.56	0.91	0.62	0.80	2.38	0.37	2.06	2.21
	C162-1	5.48	12.80	6.95	1.83	0.78	0.47	0.63	1.63	0.29	2.99	3.36
	C128	5.83	13.95	11.15	3.59	1.42	0.77	1.10	3.07	0.43	1.62	1.90
Wuchun	C10-1	27.80	51.78	16.24	4.96	0.96	0.67	0.73	1.98	0.40	5.60	14.04
	C10-2	17.75	39.79	16.95	3.49	0.77	0.60	0.79	2.15	0.41	5.09	8.26

Table 10. Major oxides of the Yanshanian granites

Sample	C18-3a	C18-3	C21-1	C18-1	C18-2	C21-2	C21-3
SiO2	64.11	67.29	73.99	74.89	75.78	76.49	75.93
Al2O3	16.96	15.88	13.66	13.18	12.71	13.34	13.47
Fe2O3	2.63	1.80	0.22	0.65	0.75	0.01	0.01
FeO	3.30	2.31	1.27	0.90	0.37	0.67	0.51
MgO	1.10	1.05	0.02	0.29	0.04	0.01	0.01
CaO	3.80	3.26	1.30	1.22	0.79	1.00	0.91
Na2O	4.06	4.88	3.88	3.48	3.40	4.55	4.36
K2O	2.07	1.90	4.39	4.75	4.97	3.68	4.23
H2O+-	0.74	0.56	0.45	0.29	0.31	0.33	0.30
TiO2	0.67	0.66	0.22	0.23	0.15	0.08	0.07
P2O5	0.20	0.19	0.06	0.06	0.04	0.01	0.01
MnO	0.12	0.13	0.07	0.06	0.06	0.03	0.01
Total	99.76	99.91	99.53	100.00	99.37	100.20	99.82
K2O/Na2O	1.07	0.39	1.13	1.36	1.46	0.81	0.97
K2O/P2O5	10.35	10.00	73.17	79.17	124.25	368.00	423.00
Fe2O3/(Fe2O3+FeO)	0.44	0.44	0.15	0.42	0.67	0.01	0.02
MgO/(MgO+FeO)	0.25	0.31	0.02	0.24	0.10	0.01	0.02
Mol. A/CNK	1.06	0.99	1.01	1.01	1.02	0.99	1.01
CIPW weight % norms (analyses recalculated to 100% free of H2O and CO2; cc not calculated)							
qz	22.20	22.90	31.39	33.30	35.68	33.33	32.22
ab	34.69	41.56	33.14	29.53	29.04	38.55	37.07
or	12.35	11.30	26.18	28.15	29.65	21.78	25.12
an	17.72	15.03	6.11	5.68	3.69	4.90	4.47
di							
ol							
mt	3.85	2.63	0.32	0.95	0.96	0.01	0.01
il	1.29	1.26	0.42	0.44	0.29	0.15	0.13
ap	0.47	0.44	0.14	0.14	0.09	0.02	0.02
cm	1.63	0.33	0.31	0.24	0.40	0.08	0.09
ag	0.53	0.64	0.82	0.82	0.86	0.86	0.87
DI	69.25	75.76	90.71	90.99	94.37	93.66	94.41

Table 11. Trace element compositions of the Yanshanian granites in the Hetai Area (ppm)

LOCATION	No.	Co	Ni	Cr	Sc	V	Cu	Zn	Pb	Ba	Sr	Rb	Nb	Ta	Ga	Zr	Hf	Y	U	Th	Rb/Sr
Huangtong.	C160-2	59	130	284	41.1	162	81	38	4	144	126	25	3	1.2	16	24	1.2	18	0.5	2.0	0.20
	C162-1	42	62	83	31.5	183	81	45	9	56	128	32	4	0.9	16	41	1.4	16	1.1	4.5	0.25
	C128	54	95	271	33.3	197	10	61	6	39	113	24	4	0.9	19	59	2.5	26	0.5	1.7	0.21
	C128a	51	89	88	25.5	121	18	135	8	330	77	59	7	3.0	18	55	1.8	19	1.5	2.5	0.77
Sihui	C18-3a	39	54	10	11.1	96	14	90	14	655	260	149	19	7.0	21	250	8.0	46	12.0	19.0	0.57
	C18-3	58	10	10	9.4	83	30	54	14	398	243	137	13	3.8	21	253	8.3	45	11.8	17.8	0.56
	C21-1	99	31	10	8.2	37	318	36	30	352	85	272	20	8.2	24	119	4.9	46	15.6	36.8	3.20
	C18-1	73	24	27	4.8	34	21	10	19	440	105	216	23	4.0	16	99	4.5	19	6.5	36.6	2.06
	C18-2	75	10	10	3.9	27	21	10	25	215	62	262	22	4.6	18	83	4.4	12	6.0	29.8	4.23
	C21-2	94	24	10	2.7	10	36	10	36	56	19	220	44	10.2	26	23	3.2	55	28.7	17.0	11.58
	C21-3	98	13	10	1.8	19	31	10	41	19	22	238	61	11.4	23	22	2.8	63	37.2	19.2	10.82

Table 12. REE compositions of the Yanshanian granites in the Hetai Area (ppm)

LOCATION	No.	La	Ce	Nd	Sm	Eu	Tb	Ho	Yb	Lu	La/Sm	La/Yb
Huangtongjiang	C160-2	5.27	13.18	8.89	2.56	0.91	0.62	0.80	2.38	0.37	2.06	2.21
	C162-1	5.48	12.80	6.95	1.83	0.78	0.47	0.63	1.63	0.29	2.99	3.36
	C128	5.83	13.95	11.15	3.59	1.42	0.77	1.10	3.07	0.43	1.62	1.90
Sihui	E18-3	42.72	84.67	33.05	6.85	1.18	1.17	1.43	5.77	1.13	6.24	7.40
	C21-1	38.24	74.60	29.61	8.33	0.69	1.59	1.73	5.11	0.68	4.59	7.48
	C18-1	29.29	56.49	23.45	4.17	0.55	0.70	0.82	2.38	0.48	7.02	12.31
	C18-2	24.76	41.35	11.62	2.96	0.52	0.63	0.71	2.13	0.42	8.36	11.62
	C21-2	6.42	14.24	8.90	4.52	0.41	1.76	2.72	6.45	1.11	1.42	1.00
	C21-3	5.75	11.28	10.37	4.60	0.54	2.10	3.77	7.94	1.38	1.25	0.72

Table 13. Au contents in different granites of the Hetai Area

Age	Location	Sample	Au (ppb)	SiO2 (%)	K2O (%)	V (ppm)	Sc (ppm)	K2O/Na2O	Mg*	Rb/Sr	Nb+Ta (ppm)
Precambrian	Hetai	C42	2.6	70.30	4.32	56.00	4.80	1.75	0.26	2.93	10.54
		C42a	2.5	69.02	3.40	52.00	5.50	1.17	0.21	2.42	12.00
		42-1	3.6	70.88	4.36	60.00	5.60	1.72	0.22	2.17	12.20
Caledonian	Shijiang	C78	0.4	66.54	2.00	75.00	14.99	0.59	0.36	0.96	14.38
		C12-1	2.5	67.70	1.73	59.00	8.61	0.44	0.39	0.90	12.23
		C16-1	0.0	64.34	2.71	115.00	14.79	0.86	0.35	1.36	15.10
Caledonian	Shijiang	C16-2	0.3	68.13	2.12	88.00	10.70	0.57	0.34	1.31	12.81
		C16-2a	3.1	67.97	2.40	79.00	10.64	0.66	0.33	1.10	14.26
		C16-3	0.9	68.35	2.68	65.00	9.25	0.70	0.28	1.67	16.49
		C16-4	1.3	72.17	5.95	36.00	4.72	2.62	0.27	2.49	12.08
		C78-1	1.5	68.31	2.80	76.00	9.86	0.81	0.33	1.13	14.07
		C78-3	2.6	70.04	3.37	64.00	6.64	0.95	0.30	2.02	18.12
		C78-5	1.4	72.10	5.34	49.00	4.00	1.80	0.22	2.29	12.83
		C12-2	1.1	70.21	2.52	66.00	9.56	0.75	0.29	1.09	13.44
		C12-3	1.2	69.60	4.39	43.00	6.56	1.38	0.29	0.99	10.70
		C12-5	1.3	74.36	5.29	33.00	4.80	2.07	0.26	2.02	10.26
		C12-4	2.5	73.63	6.05	31.00	4.02	2.07	0.17	2.70	10.30
Caledonian	Sidong	C7-1a	5.4	73.55	4.07	12.00	2.50	1.26	0.02	6.55	11.00
		C7-1	2.0	76.02	3.88	10.00	3.44	1.04	0.04	4.63	7.91
		C7-2	2.4	76.66	4.92	16.00	1.18	1.37	0.01	5.70	7.02
Caledonian	Shiniutou	C17	3.7	76.25	5.18	18.00	2.95	1.84	0.01	20.50	13.42
		C22-1	4.3	74.37	4.64	34.00	5.21	1.94	0.21	4.55	14.40
		C22-2	1.8	74.61	4.20	15.00	4.76	1.56	0.25	7.11	9.30
		C22-3	42.9	72.65	4.29	31.00	5.20	5.43	0.37	10.40	14.68
Hercynian	Yunlougan	C9-2	0.9	73.31	7.13	32.00	3.21	3.18	0.21	2.20	9.02
Hercynian	Guangning	C13	0.8	71.74	4.23	44.00	5.94	1.26	0.27	3.04	16.86
		C84	2.1	70.95	3.64	57.00	7.73	1.09	0.31	2.24	13.39
		C84a	4.5	69.13	3.73	33.00	6.50	1.17	0.29	2.74	15.20
	Hetai	C4	52.7	65.04	10.14	93.00	12.27	19.13	0.32	12.93	11.90
	Huang-tongjiang	C160-2	15.0	51.48	0.51	162.00	41.12	0.27	0.66	0.20	4.30
		C162-1	14.5	52.67	0.77	183.00	31.49	0.24	0.57	0.25	4.85
		C128	7.5	49.42	0.61	197.00	33.27	0.24	0.54	0.21	4.85
		C128a	10.0	56.18	1.61	121.00	25.50	0.46	0.48	0.77	10.00
Hercynian	Yunlougan	C9-1a	11.0	66.29	2.39	93.00	14.00	0.76	0.28	0.64	12.00
		C9-1b	12.0	65.26	2.27	93.00	12.00	0.74	0.30	0.66	12.00
		C9-1	8.2	67.31	2.33	96.00	13.29	0.74	0.32	0.70	15.56
Indosinian	Wuchun	C10-1a	13.0	63.19	2.10	92.00	8.60	0.55	0.38	0.98	26.00
		C10-1	4.1	64.65	2.32	99.00	10.65	0.61	0.34	1.02	19.12
	Wuchun	C10-2	9.6	71.39	4.37	54.00	5.32	1.20	0.22	1.21	25.80
		C10-2a	11.0	70.38	4.40	52.00	4.00	1.25	0.19	1.34	24.00
Yanshanian	Sihui	C18-3a	6.8	64.11	2.07	96.00	11.10	1.07	0.25	0.57	26.00
		C18-3	1.6	67.29	1.90	83.00	9.41	0.39	0.31	0.56	15.82
	Sihui	C18-1	3.6	74.89	4.75	34.00	4.80	1.36	0.24	2.06	26.97
		C18-2	4.6	75.78	4.97	27.00	3.92	1.46	0.10	4.23	26.60
		C21-1	6.6	73.99	4.39	27.00	8.21	1.13	0.02	3.20	28.22
		C21-2	6.0	76.49	3.68	10.00	2.70	0.81	0.01	11.60	54.19
		C21-3	3.3	75.93	4.23	19.00	1.84	0.97	0.02	10.80	72.35

Mg*=MgO/(MgO+FeO)

Table 14. Chemical compositions of biotites from the Caledonian granites

LOCATION	Shiniutou						Sidong			Sidong				Shijiang				
Sample No.	C17						C7-1			C7-2				C16-2				
SiO2	34.59	34.31	33.71	33.84	34.48	34.53	35.43	35.00	34.67	35.04	34.85	34.54	34.65	34.51	35.45	34.64	34.91	34.77
Al2O3	16.15	17.53	17.36	17.26	17.97	17.37	14.49	14.94	14.17	16.37	15.81	17.06	16.81	18.35	17.77	18.24	18.03	18.22
TiO2	2.08	2.28	2.22	1.93	1.83	2.68	2.85	2.45	2.99	2.85	2.62	1.59	2.44	3.02	2.64	2.67	2.65	2.66
FeOt	30.93	30.72	29.69	30.50	30.94	30.39	29.81	29.38	29.59	28.60	28.09	29.09	27.77	21.89	21.14	21.64	21.66	22.24
MgO	1.71	1.42	1.42	1.14	1.28	1.14	4.13	4.06	3.78	2.99	2.96	2.97	2.89	7.75	8.40	8.44	8.41	8.59
MnO	0.85	0.72	0.73	0.67	0.53	0.75	0.81	0.91	1.35	1.11	0.77	1.04	1.06	0.52	0.44	0.34	0.79	0.00
CaO	0.26	0.33	0.34	0.31	0.42	0.35	0.44	0.42	0.00	0.37	0.32	0.53	0.40	0.00	0.00	0.00	0.00	0.00
Na2O	0.00	0.00	0.00	0.00	0.00	0.00	0.00	0.00	0.00	0.00	0.00	0.00	0.17	0.00	0.00	0.57	0.00	0.26
K2O	9.36	9.13	9.05	9.08	9.17	9.35	9.18	9.66	9.90	9.72	9.62	8.59	9.48	9.97	9.55	9.58	9.79	9.68
Total	96.34	96.74	95.02	95.01	96.99	96.90	97.14	96.97	96.45	97.06	95.38	95.55	95.77	96.31	95.54	96.12	96.37	96.53
Fe2O3	5.18	5.12	4.94	5.08	5.16	5.07	3.78	3.35	3.75	4.77	4.68	4.85	4.63	2.09	2.02	2.07	2.07	2.13
FeO	28.60	28.42	27.46	28.21	28.62	28.11	28.31	27.71	27.90	26.45	25.98	26.91	25.69	20.95	20.23	20.71	20.73	21.28
MgO/FeO	0.06	0.05	0.05	0.04	0.04	0.04	0.15	0.15	0.14	0.11	0.11	0.11	0.11	0.37	0.42	0.41	0.41	0.40
TiO2/Al2O3	0.13	0.13	0.13	0.11	0.10	0.15	0.20	0.16	0.21	0.17	0.17	0.09	0.15	0.16	0.15	0.15	0.15	0.15
Fe2O3/(Fe2O3+FeO)	0.15	0.15	0.15	0.15	0.15	0.15	0.12	0.11	0.12	0.15	0.15	0.15	0.15	0.09	0.09	0.09	0.09	0.09
Si	5.59	5.48	5.49	5.51	5.50	5.51	5.61	5.58	5.58	5.54	5.60	5.53	5.53	5.31	5.45	5.32	5.36	5.33
Al(iv)	2.42	2.52	2.51	2.49	2.50	2.49	2.39	2.42	2.42	2.46	2.40	2.47	2.47	2.69	2.55	2.68	2.64	2.67
Al(vi)	0.56	0.79	0.82	0.83	0.87	0.77	0.32	0.38	0.47	0.59	0.60	0.75	0.70	0.64	0.67	0.62	0.62	0.62
Ti	0.25	0.27	0.27	0.24	0.22	0.32	0.34	0.29	0.36	0.34	0.32	0.19	0.29	0.35	0.30	0.31	0.31	0.31
Mg	0.41	0.34	0.35	0.28	0.30	0.27	0.98	0.96	0.91	0.70	0.71	0.71	0.69	1.78	1.92	1.93	1.93	1.96
Fe(t)	4.18	4.11	4.04	4.16	4.13	4.05	3.95	3.91	3.98	3.78	3.78	3.90	3.71	2.82	2.72	2.78	2.78	2.85
Fe(3+)	0.59	0.57	0.56	0.58	0.58	0.57	0.42	0.42	0.43	0.53	0.53	0.54	0.52	0.24	0.23	0.24	0.24	0.25
Fe(2+)	3.58	3.54	3.48	3.58	3.54	3.48	3.53	3.49	3.55	3.25	3.25	3.35	3.19	2.58	2.49	2.54	2.54	2.60
Mn	0.41	0.10	0.10	0.09	0.30	0.10	0.11	0.12	0.18	0.15	0.11	0.14	0.14	0.07	0.06	0.04	0.10	0.00
K	1.93	1.86	1.88	1.89	1.87	1.90	1.86	1.96	2.03	1.96	1.97	1.76	1.93	1.96	1.87	1.88	1.92	1.89
Na	0.00	0.00	0.00	0.00	0.00	0.00	0.00	0.00	0.00	0.00	0.00	0.00	0.05	0.00	0.00	0.17	0.00	0.08
Ca	0.05	0.06	0.06	0.06	0.07	0.06	0.07	0.07	0.00	0.06	0.06	0.09	0.07	0.00	0.00	0.00	0.00	0.00
M=Mg/(Mg+Fe2++Mn)	0.09	0.08	0.08	0.07	0.08	0.07	0.21	0.21	0.20	0.17	0.17	0.17	0.17	0.40	0.43	0.43	0.43	0.43
Al(vi)/Ti	2.24	2.93	3.04	3.46	3.95	2.41	0.94	1.31	1.31	1.74	1.88	3.95	2.41	1.83	2.23	2.00	2.00	2.00

Table 14 continued

Shijiang C16-3						Shijiang C16-4						Shijiang C16-5				Shijiang Dark Enclave C78					
34.96	34.93	34.33	35.33	34.96	35.33	34.42	34.76	35.52	34.86	35.22	35.06	35.80	36.12	35.22	35.69	35.89	35.52	35.84	35.24	36.05	35.40
18.15	17.69	19.08	18.24	18.61	18.36	18.14	18.44	17.94	18.20	18.22	18.34	18.79	18.14	19.18	18.16	18.40	18.57	17.97	17.93	17.37	18.43
2.75	2.79	3.09	2.50	2.60	2.53	2.45	2.76	2.59	2.67	2.75	2.68	2.52	2.46	2.50	2.55	2.34	2.74	2.82	2.98	2.74	2.85
20.88	21.24	21.65	21.10	20.80	21.43	22.30	22.85	22.86	22.18	22.12	22.91	20.75	20.73	21.46	20.95	18.15	18.66	18.72	19.80	19.13	19.00
8.18	8.36	8.05	8.43	8.25	8.81	8.17	7.30	7.71	7.51	7.72	7.79	8.28	8.53	7.97	8.91	9.80	10.29	9.75	9.61	9.93	9.88
0.24	0.35	0.00	0.45	0.38	0.00	0.56	0.40	0.38	0.66	0.43	0.20	0.28	0.80	0.58	0.00	0.29	0.33	0.00	0.00	0.25	0.40
0.00	0.00	0.00	0.00	0.00	0.00	0.00	0.00	0.00	0.00	0.00	0.00	0.00	0.00	0.58	0.00	0.00	0.00	0.00	0.00	0.00	0.00
0.00	0.00	0.00	0.00	0.23	0.00	0.22	0.00	0.00	0.00	0.00	0.00	0.00	0.34	0.00	0.23	0.49	0.22	0.00	0.26	0.00	0.00
10.02	9.81	9.76	9.77	9.98	10.32	9.77	9.52	9.29	9.62	10.21	9.76	9.46	9.84	9.83	9.82	9.91	10.03	9.94	9.99	9.71	9.91
95.24	95.27	95.96	95.83	95.93	96.78	96.03	96.02	96.42	95.69	96.66	96.75	95.89	96.96	96.75	96.32	95.26	96.36	95.05	96.03	95.36	95.95
2.00	2.03	2.07	2.02	1.99	2.05	1.88	1.93	1.93	1.87	1.87	1.93	1.98	1.98	2.05	2.00	1.45	1.49	1.50	1.58	1.53	1.52
19.98	20.31	20.72	20.19	19.91	20.51	21.45	21.98	22.00	21.34	21.28	22.04	19.86	19.84	20.54	20.05	17.50	18.00	18.05	19.09	18.44	18.32
0.41	0.41	0.39	0.42	0.41	0.43	0.38	0.33	0.35	0.35	0.36	0.35	0.42	0.43	0.39	0.44	0.56	0.57	0.54	0.50	0.54	0.54
0.15	0.16	0.16	0.14	0.14	0.14	0.14	0.15	0.14	0.15	0.15	0.15	0.13	0.14	0.13	0.14	0.13	0.15	0.16	0.17	0.16	0.15
0.09	0.09	0.09	0.09	0.09	0.09	0.08	0.08	0.08	0.08	0.08	0.08	0.09	0.09	0.09	0.09	0.08	0.08	0.08	0.08	0.80	0.08
5.40	5.41	5.27	5.42	5.37	5.38	5.32	5.36	5.45	5.39	5.39	5.37	5.45	5.47	5.35	5.43	5.46	5.36	5.47	5.37	5.49	5.37
2.60	2.59	2.73	2.58	2.63	2.62	2.68	2.64	2.55	2.61	2.61	2.63	2.55	2.53	2.65	2.57	2.54	2.64	2.53	2.63	2.51	2.63
0.70	0.64	0.72	0.71	0.74	0.67	0.62	0.71	0.69	0.70	0.68	0.68	0.82	0.71	0.79	0.69	0.76	0.66	0.70	0.59	0.60	0.60
0.32	0.32	0.36	0.29	0.30	0.29	0.28	0.32	0.30	0.31	0.32	0.31	0.29	0.28	0.29	0.29	0.27	0.31	0.32	0.34	0.31	0.33
1.88	1.93	1.84	1.93	1.89	2.00	1.88	1.68	1.76	1.73	1.76	1.78	1.88	1.93	1.81	2.02	2.22	2.31	2.22	2.18	2.26	2.34
2.70	2.75	2.78	2.70	2.67	2.73	2.88	2.95	2.93	2.87	2.83	2.93	2.64	2.62	2.73	2.67	2.31	2.35	2.39	2.52	2.44	2.41
0.23	0.24	0.24	0.23	0.23	0.24	0.22	0.22	0.22	0.21	0.21	0.22	0.23	0.23	0.24	0.23	0.16	0.16	0.17	0.18	0.17	0.17
2.47	2.51	2.54	2.47	2.34	2.49	2.66	2.73	2.71	2.66	2.62	2.71	2.41	2.39	2.49	2.44	2.15	2.19	2.22	2.34	2.27	2.24
0.03	0.05	0.00	0.06	0.05	0.00	0.07	0.05	0.05	0.09	0.06	0.03	0.04	0.10	0.08	0.00	0.04	0.04	0.00	0.00	0.03	0.05
1.98	1.94	1.91	1.91	1.95	2.00	1.93	1.87	1.82	1.90	1.99	1.91	1.84	1.90	1.91	1.91	1.92	1.93	1.93	1.94	1.89	1.92
0.00	0.00	0.00	0.00	0.07	0.00	0.07	0.00	0.00	0.00	0.00	0.00	0.00	0.10	0.00	0.07	0.14	0.06	0.00	0.08	0.00	0.00
0.00	0.00	0.00	0.00	0.00	0.00	0.00	0.00	0.00	0.00	0.00	0.00	0.00	0.00	0.00	0.00	0.00	0.00	0.00	0.00	0.00	0.00
0.43	0.43	0.42	0.43	0.44	0.44	0.41	0.38	0.39	0.39	0.40	0.39	0.42	0.44	0.41	0.45	0.49	0.49	0.48	0.46	0.48	0.49
2.19	2.00	2.00	2.45	2.47	2.31	2.21	2.22	2.30	2.26	2.12	2.19	2.83	2.54	2.72	2.38	2.81	2.13	2.19	1.74	1.94	1.82

Table 14 continued

Shijiang Dark Enclave C16-1							Hetai C42			
35.86	35.29	35.46	35.15	35.24	35.84	34.80	34.93	34.26	35.20	35.28
19.03	18.67	18.77	18.66	18.83	18.33	18.99	1.84	1.75	2.09	2.15
2.75	2.90	2.98	2.73	2.41	2.78	2.97	17.72	17.59	18.40	18.03
19.48	20.01	20.25	20.29	19.90	19.81	20.11	23.35	23.71	23.06	24.29
9.45	9.47	9.08	8.71	9.17	9.24	8.67	7.43	7.62	7.40	6.82
0.29	0.00	0.22	0.56	0.00	0.26	0.22	0.42	0.47	0.58	0.47
0.00	0.00	0.00	0.00	0.00	0.00	0.00	0.00	0.00	0.00	0.00
0.00	0.00	0.00	0.41	0.00	0.00	0.36	0.00	0.00	0.19	0.00
10.06	9.92	10.02	10.14	9.77	9.59	9.97	10.28	9.50	9.84	10.21
96.91	96.26	96.93	96.79	95.32	95.85	96.14	95.97	94.90	96.76	97.26
1.56	1.60	1.62	1.62	1.59	1.58	1.61	1.76	1.79	1.74	1.84
19.78	19.29	19.52	19.50	19.18	19.10	19.39	22.56	22.90	22.96	23.46
0.48	0.49	0.47	0.45	0.48	0.48	0.45	0.33	0.33	0.32	0.29
0.14	0.16	0.16	0.15	0.13	0.15	0.16	0.10	0.10	0.11	0.12
0.07	0.08	0.08	0.08	0.08	0.08	0.08	0.07	0.07	0.07	0.07
5.38	5.35	5.36	5.34	5.39	5.44	5.31	5.43	5.39	5.40	5.42
2.62	2.65	2.64	2.66	2.61	2.56	2.69	2.57	2.61	2.60	2.58
0.75	0.69	0.70	0.68	0.78	0.71	0.72	0.68	0.65	0.73	0.69
0.31	0.33	0.34	0.31	0.28	0.32	0.34	0.21	0.21	0.24	0.25
2.12	2.14	2.05	1.97	2.09	2.09	1.97	1.72	1.79	1.69	1.56
2.44	2.54	2.56	2.58	2.54	2.51	2.56	3.04	3.12	2.96	3.12
0.16	0.19	0.18	0.18	0.19	0.17	0.18	0.21	0.22	0.21	0.22
2.28	2.35	2.38	2.40	2.35	2.34	2.38	2.93	2.90	2.75	2.90
0.04	0.00	0.03	0.07	0.00	0.03	0.03	0.08	0.08	0.08	0.06
1.93	1.92	1.93	1.97	1.91	1.86	1.94	2.04	1.90	1.93	2.00
0.00	0.00	0.00	0.12	0.00	0.00	0.11	0.00	0.00	0.00	0.00
0.00	0.00	0.00	0.00	0.00	0.00	0.00	0.00	0.00	0.06	0.00
0.46	0.48	0.46	0.44	0.47	0.47	0.45	0.37	0.38	0.42	0.35
2.42	2.09	2.06	2.19	2.79	2.22	2.12	3.24	3.10	3.04	2.76

Table 15. Chemical analyses of biotites from the Hercynian granites

LOCATION	Guangning					Guangning					Yunlougan						
Sample No.	C13					C84					C9-1						
SiO2	35.22	35.81	35.20	35.33	35.00	35.56	35.16	35.92	35.89	35.38	36.86	36.97	37.12	36.67	37.90	36.91	36.86
Al2O3	16.32	15.85	15.76	15.96	16.40	16.21	15.48	15.70	15.97	15.94	14.50	14.59	14.74	14.64	14.63	14.52	14.53
TiO2	2.84	3.04	2.47	2.82	2.99	3.13	3.02	3.31	3.12	3.07	3.24	3.24	3.89	3.32	3.20	3.38	3.16
FeOt	23.56	23.17	23.44	23.80	21.80	22.59	22.20	21.63	21.89	22.40	22.51	21.36	22.79	21.83	21.95	21.80	21.48
MgO	7.07	7.33	7.10	7.48	7.39	6.78	7.86	8.19	7.76	7.27	8.56	8.79	8.30	8.46	8.93	9.34	8.79
MnO	0.61	0.70	0.69	0.92	0.59	0.58	0.77	0.74	0.50	0.81	0.50	0.51	0.39	0.52	0.46	0.29	0.37
CaO	0.41	0.55	0.56	0.66	0.68	0.38	0.49	0.54	0.36	0.51	0.38	0.28	0.35	0.31	0.25	0.51	0.36
Na2O	0.30	0.00	0.00	0.00	0.00	0.00	0.00	0.00	0.00	0.00	0.00	0.00	0.00	0.00	0.00	0.00	0.00
K2O	10.12	9.62	9.39	9.23	9.32	9.96	9.90	9.73	9.98	9.41	9.71	9.63	9.51	9.56	9.77	9.49	9.96
Total	96.83	96.06	94.62	96.46	94.38	95.61	94.88	96.12	95.66	94.79	96.28	95.67	97.09	95.31	97.09	96.61	95.66
Fe2O3	2.04	2.01	2.03	2.06	1.89	1.96	1.92	1.69	1.90	1.94	3.80	3.61	3.84	3.69	3.71	3.68	3.63
FeO	22.64	22.27	22.53	22.87	20.95	21.71	21.33	20.79	21.04	21.56	20.80	19.74	21.06	20.17	20.28	20.14	19.85
MgO/FeO	0.31	0.33	0.32	0.33	0.35	0.31	0.37	0.39	0.37	0.34	0.41	0.45	0.39	0.42	0.44	0.46	0.44
TiO2/Al2O3	0.17	0.19	0.16	0.18	0.18	0.19	0.20	0.21	0.20	0.19	0.22	0.22	0.26	0.23	0.22	0.23	0.22
Fe2O3/(Fe2O3+FeO)	0.08	0.08	0.08	0.08	0.08	0.08	0.08	0.08	0.08	0.08	0.15	0.15	0.15	0.15	0.15	0.15	0.15
Si	5.46	5.56	5.56	5.48	5.49	5.54	5.53	5.54	5.56	5.55	5.68	5.70	5.66	5.68	5.75	5.64	5.70
Al(iv)	2.54	2.45	2.44	2.52	2.51	2.45	2.48	2.46	2.44	2.45	2.32	2.30	2.34	2.32	2.25	2.36	2.30
Al(vi)	0.45	0.45	0.49	0.40	0.53	0.53	0.39	0.39	0.48	0.49	0.31	0.35	0.31	0.36	0.36	0.26	0.35
Ti	0.33	0.35	0.29	0.33	0.35	0.37	0.36	0.38	0.36	0.36	0.38	0.38	0.45	0.39	0.37	0.39	0.37
Mg	1.63	1.69	1.67	1.73	1.73	1.58	1.84	1.88	1.79	1.70	1.97	2.02	1.89	1.96	2.02	2.13	2.03
Fe(t)	3.06	3.01	3.09	3.09	2.86	2.94	2.92	2.79	2.84	2.94	2.90	2.75	2.90	2.83	2.78	2.79	2.78
Fe(3+)	0.23	0.23	0.24	0.24	0.21	0.22	0.22	0.21	0.22	0.23	0.41	0.40	0.41	0.40	0.39	0.39	0.39
Fe(2+)	2.82	2.77	2.85	2.84	2.65	2.72	2.69	2.58	2.62	2.71	2.49	2.35	2.49	2.43	2.39	2.39	2.38
Mn	0.08	0.09	0.09	0.12	0.08	0.08	0.10	0.10	0.07	0.11	0.07	0.06	0.05	0.07	0.06	0.04	0.05
K	2.00	1.90	1.89	1.83	1.87	1.98	1.99	1.91	1.79	1.88	1.91	1.89	1.85	1.89	1.89	1.85	1.96
Na	0.09	0.00	0.00	0.00	0.00	0.00	0.00	0.00	0.00	0.00	0.00	0.00	0.00	0.00	0.00	0.00	0.00
Ca	0.07	0.09	0.10	0.11	0.12	0.06	0.08	0.09	0.06	0.09	0.06	0.05	0.06	0.05	0.04	0.08	0.06
M=Mg/(Mg+Fe2+ +Mn)	0.36	0.37	0.36	0.37	0.39	0.36	0.40	0.41	0.40	0.38	0.44	0.46	0.43	0.44	0.45	0.47	0.46
Al(VI)/Ti	1.36	1.29	1.69	1.21	1.51	1.43	1.08	1.03	1.33	1.36	0.82	0.92	0.67	0.92	1.00	0.67	0.95

Table 16. Chemical analyses of biotites from the Indosinian granites

LOCATION	Wuchun					Wuchun									
Sample No.	C10-1					C10-2									
SiO2	37.73	37.75	37.55	36.71	36.95	36.51	36.20	35.91	36.32	36.52	35.99	36.18	36.47	36.48	36.28
Al2O3	14.37	12.98	13.53	13.22	13.18	14.51	13.77	13.20	13.79	13.14	13.34	13.63	13.74	13.40	13.29
TiO2	3.08	3.58	3.42	3.26	3.12	4.02	4.75	4.51	3.21	3.86	3.67	3.55	4.39	3.55	4.77
FeOt	22.13	21.56	21.07	21.96	21.76	22.77	22.90	24.07	22.18	23.30	22.65	22.71	23.76	23.20	23.45
MgO	9.34	9.45	9.70	8.95	9.19	7.55	7.56	7.12	7.96	7.70	8.25	8.01	7.39	7.74	7.33
MnO	0.56	0.58	0.31	0.77	0.64	0.89	0.76	0.95	0.99	0.78	0.93	0.94	0.56	0.76	0.77
CaO	0.41	0.26	0.37	0.49	0.51	0.43	0.41	0.50	0.13	0.57	0.39	0.24	0.36	0.34	0.70
Na2O	0.00	0.00	0.00	0.00	0.00	0.00	0.64	0.00	0.00	0.00	0.00	0.00	0.00	0.00	0.00
K2O	9.02	9.42	9.72	9.74	9.74	9.64	9.45	9.63	9.41	9.68	9.56	9.21	9.35	9.59	9.95
Total	96.75	95.67	95.67	95.10	95.10	96.31	96.44	95.89	94.29	95.55	94.99	94.45	96.02	95.33	96.55
Fe2O3	4.67	4.60	4.49	4.68	4.64	5.26	5.29	5.56	5.13	5.38	5.23	5.25	5.49	5.36	5.42
FeO	20.03	19.49	19.05	19.85	19.67	20.40	20.50	21.57	19.87	20.88	20.29	20.35	21.29	20.79	21.01
MgO/FeO	0.47	0.48	0.51	0.45	0.47	0.37	0.37	0.33	0.40	0.37	0.41	0.39	0.35	0.37	0.35
TiO2/Al2O3	0.21	0.28	0.25	0.25	0.24	0.28	0.34	0.34	0.23	0.29	0.28	0.26	0.32	0.26	0.36
Fe2O3/(Fe2O3+FeO)	0.19	0.19	0.19	0.19	0.19	0.20	0.21	0.20	0.21	0.20	0.20	0.21	0.21	0.20	0.21
Si	5.74	5.82	5.77	5.74	5.76	5.64	5.61	5.64	5.73	5.72	5.66	5.70	5.67	5.72	5.64
Al(iv)	2.26	2.18	2.23	2.26	2.24	2.36	2.39	2.36	2.27	2.28	2.34	2.30	2.33	2.28	2.36
Al(vi)	0.32	0.18	0.22	0.17	0.18	0.28	0.12	0.08	0.29	0.15	0.13	0.23	0.19	0.19	0.07
Ti	0.35	0.41	0.40	0.38	0.37	0.47	0.55	0.53	0.38	0.45	0.43	0.42	0.51	0.42	0.56
Mg	2.12	2.17	2.22	2.09	2.14	1.74	1.75	1.67	1.87	1.80	1.94	1.88	1.71	1.81	1.70
Fe(t)	2.82	2.78	2.71	2.87	2.84	2.94	2.97	3.16	2.93	3.05	2.98	2.99	3.09	3.04	3.05
Fe(3+)	0.49	0.49	0.47	0.50	0.49	0.55	0.56	0.59	0.55	0.57	0.56	0.57	0.58	0.58	0.56
Fe(2+)	2.32	2.39	2.23	2.37	2.34	2.39	2.41	2.56	2.37	2.48	2.42	2.42	2.50	2.46	2.48
Mn	0.07	0.08	0.04	0.10	0.09	0.12	0.10	0.13	0.13	0.10	0.12	0.13	0.07	0.10	0.10
K	1.75	1.85	1.91	1.94	1.94	1.90	1.87	1.93	1.89	1.93	1.92	1.85	1.85	1.92	1.97
Na	0.00	0.00	0.00	0.00	0.00	0.00	0.19	0.00	0.00	0.00	0.00	0.00	0.00	0.00	0.00
Ca	0.07	0.04	0.06	0.08	0.09	0.07	0.07	0.09	0.02	0.10	0.07	0.04	0.06	0.06	0.12
M=Mg/(Mg+Fe2+ +M	0.47	0.47	0.49	0.46	0.47	0.41	0.41	0.38	0.43	0.41	0.43	0.43	0.40	0.41	0.40
Al(VI)/Ti	0.91	0.44	0.55	0.45	0.49	0.60	0.22	0.15	0.76	0.31	0.30	0.55	0.35	0.45	0.12

Table 17. Chemical analyses of biotites from the Yanshanian granites

LOCATION	Sihui													Sihui		
Sample No.	C18-3													C18-1		
SiO2	38.72	37.30	39.06	37.70	37.18	37.95	37.01	36.86	38.50	36.78	36.15	37.19	38.91	38.17	38.71	38.66
Al2O3	11.55	11.87	13.16	11.63	12.05	11.34	11.99	11.15	11.26	11.69	12.09	12.07	10.85	12.05	13.40	13.32
TiO2	4.90	4.40	4.38	3.92	4.13	3.97	4.44	4.29	4.75	4.38	4.84	4.95	4.01	3.99	3.68	4.27
FeOt	20.82	20.62	18.50	20.16	20.53	19.96	20.14	20.79	19.80	20.58	20.67	21.50	17.52	21.32	20.06	20.80
MgO	10.05	9.76	10.80	10.77	10.88	11.30	10.80	11.17	11.27	11.14	10.58	9.75	13.06	9.39	9.44	9.59
MnO	0.98	1.15	1.00	1.15	0.82	0.91	0.86	1.23	0.47	0.88	0.56	1.00	0.63	0.89	0.95	0.79
CaO	0.92	0.57	0.37	0.30	0.00	0.28	0.51	0.32	0.31	0.30	0.56	0.26	0.20	0.39	0.36	0.41
Na2O	0.00	0.00	0.00	0.00	0.00	0.00	0.00	0.00	0.00	0.00	0.00	0.00	0.00	0.00	0.00	0.00
K2O	9.03	9.80	8.73	9.89	9.74	9.90	9.35	9.59	9.87	9.83	9.69	9.30	9.77	9.02	8.87	8.84
Total	96.97	95.57	96.00	95.63	95.62	95.60	95.30	95.58	96.37	95.72	95.29	96.04	95.16	95.22	95.70	96.87
Fe2O3	5.23	5.18	4.65	5.06	5.16	5.01	5.06	5.22	4.93	5.17	5.19	5.40	4.40	5.78	5.43	5.64
FeO	18.47	18.29	18.41	17.88	18.21	17.70	17.86	18.44	17.58	18.25	18.23	19.07	15.54	18.72	17.62	18.26
MgO/FeO	0.54	0.53	0.59	0.60	0.60	0.64	0.60	0.61	0.64	0.61	0.58	0.51	0.84	0.50	0.54	0.53
TiO2/Al2O3	0.42	0.37	0.33	0.34	0.34	0.35	0.37	0.38	0.42	0.37	0.40	0.41	0.37	0.33	0.27	0.32
Fe2O3/(Fe2O3+FeO)	0.22	0.22	0.22	0.22	0.22	0.22	0.22	0.22	0.22	0.22	0.22	0.22	0.22	0.24	0.24	0.24
Si	5.87	5.79	5.87	5.83	5.75	5.85	5.73	5.73	5.86	5.70	5.63	5.73	5.93	5.90	5.90	5.84
Al(iv)	2.06	2.17	2.13	2.12	2.20	2.06	2.19	2.05	2.02	2.13	2.22	2.19	1.95	2.10	2.10	2.16
Al(vi)	0.00	0.00	0.20	0.00	0.00	0.00	0.00	0.00	0.00	0.00	0.00	0.00	0.00	0.08	0.31	0.21
Ti	0.56	0.51	0.50	0.46	0.48	0.46	0.52	0.50	0.54	0.51	0.57	0.57	0.46	0.46	0.42	0.49
Mg	2.27	2.26	2.42	2.48	2.51	2.60	2.49	2.59	2.56	2.57	2.46	2.24	2.97	2.16	2.15	2.16
Fe(t)	2.64	2.67	2.33	2.61	2.66	2.57	2.61	2.70	2.52	2.67	2.69	2.77	2.23	2.75	2.56	2.63
Fe(3+)	0.53	0.54	0.43	0.53	0.54	0.52	0.55	0.56	0.52	0.54	0.55	0.57	0.46	0.60	0.55	0.57
Fe(2+)	2.11	2.13	1.90	2.08	2.12	2.05	2.06	2.14	2.00	2.12	2.14	2.20	1.77	2.15	2.01	2.05
Mn	0.13	0.15	0.13	0.15	0.11	0.12	0.11	0.16	0.06	0.12	0.07	0.13	0.08	0.12	0.12	0.10
K	1.75	1.94	1.68	1.95	1.92	1.95	1.85	1.90	1.92	1.94	1.92	1.83	1.90	1.78	1.73	1.70
Na	0.00	0.00	0.00	0.00	0.00	0.00	0.00	0.00	0.00	0.00	0.00	0.00	0.00	0.00	0.00	0.00
Ca	0.15	0.09	0.06	0.05	0.00	0.05	0.09	0.05	0.05	0.05	0.09	0.04	0.03	0.06	0.06	0.07
M=Mg/(Mg+Fe2+ +Mn)	0.50	0.49	0.54	0.52	0.52	0.54	0.53	0.52	0.55	0.53	0.52	0.46	0.61	0.49	0.50	0.50
Al(VI)/Ti	0.00	0.00	0.41	0.00	0.00	0.00	0.00	0.00	0.00	0.00	0.00	0.00	0.00	0.17	0.74	0.44

Table 17 continued

Sihui
C18-2

37.57	38.26	37.05	37.16	37.07	37.75	37.52	37.91	37.64	37.66	37.13	37.97	37.86	38.19	37.32	37.25	36.90	38.52
12.25	11.77	12.19	12.26	12.30	12.20	11.84	12.13	12.39	12.31	11.90	11.24	11.49	12.10	12.81	12.26	12.81	12.56
3.54	3.97	4.22	5.13	4.57	4.62	4.97	3.86	4.23	3.56	4.25	3.22	3.10	4.49	3.68	3.00	3.78	3.19
21.90	20.73	22.00	21.87	21.34	21.16	21.51	20.95	21.38	20.99	21.75	20.93	21.21	21.67	22.67	22.54	22.90	21.86
10.43	11.01	10.23	9.59	10.25	10.22	9.85	10.37	9.98	9.89	10.03	10.85	10.57	7.64	8.43	8.50	7.63	8.40
1.04	0.90	0.88	0.77	1.31	0.69	0.52	1.01	0.99	1.38	0.86	0.99	1.02	1.75	1.51	1.52	1.68	1.85
0.37	0.24	0.38	0.35	0.27	0.35	0.43	0.38	0.39	0.35	0.38	0.30	0.36	0.45	0.52	0.26	0.30	0.18
0.00	0.00	0.00	0.00	0.00	0.00	0.00	0.00	0.32	0.00	0.00	0.00	0.00	0.00	0.00	0.00	0.00	0.00
9.50	9.37	9.52	9.56	9.28	9.70	9.47	9.51	9.67	9.60	9.05	9.40	9.21	9.62	9.67	9.44	9.21	9.91
96.77	96.41	96.52	96.81	96.57	96.94	96.25	96.40	97.32	95.92	95.44	95.10	94.99	96.07	96.88	94.77	95.29	96.68
5.94	5.62	5.96	5.93	5.79	5.74	5.83	5.68	5.80	5.69	5.90	5.67	5.75	5.68	5.94	6.11	6.21	5.93
19.23	18.20	19.32	19.29	18.74	18.58	18.89	18.40	18.78	18.43	19.10	18.58	18.62	19.11	19.99	19.79	20.11	19.19
0.54	0.60	0.53	0.50	0.55	0.55	0.52	0.56	0.53	0.54	0.53	0.54	0.55	0.40	0.42	0.43	0.38	0.44
0.29	0.34	0.35	0.42	0.37	0.38	0.42	0.32	0.34	0.29	0.36	0.34	0.33	0.37	0.29	0.24	0.30	0.25
0.24	0.24	0.24	0.24	0.24	0.24	0.24	0.24	0.24	0.24	0.24	0.24	0.24	0.23	0.23	0.24	0.24	0.24
5.77	5.84	5.71	5.70	5.70	5.76	5.77	5.81	5.74	5.82	5.76	5.90	5.89	5.91	5.76	5.86	5.79	5.92
2.22	2.12	2.21	2.22	2.23	2.20	2.15	2.19	2.22	2.18	2.18	2.06	2.11	2.09	2.24	2.14	2.21	2.08
0.00	0.00	0.00	0.00	0.00	0.00	0.00	0.00	0.00	0.06	0.00	0.00	0.00	0.02	0.09	0.14	0.15	0.19
0.41	0.46	0.49	0.59	0.53	0.53	0.58	0.45	0.49	0.41	0.50	0.38	0.36	0.52	0.43	0.36	0.45	0.37
2.39	2.51	2.35	2.19	2.35	2.33	2.26	2.37	2.27	2.28	2.32	2.52	2.45	1.76	1.94	1.99	1.79	1.92
2.81	2.65	2.83	2.81	2.74	2.70	2.77	2.69	2.73	2.71	2.82	2.72	2.76	2.81	2.93	2.97	3.00	2.81
0.61	0.58	0.62	0.61	0.60	0.59	0.60	0.58	0.59	0.58	0.61	0.59	0.60	0.61	0.64	0.65	0.66	0.62
2.00	2.07	2.21	2.20	2.14	2.11	2.17	2.11	2.14	2.13	2.21	2.13	2.16	2.10	2.28	2.31	2.34	2.18
0.14	0.12	0.12	0.10	0.17	0.09	0.07	0.13	0.13	0.18	0.11	0.13	0.13	0.23	0.20	0.20	0.22	0.24
1.86	1.83	1.87	1.87	1.82	1.89	1.86	1.86	1.88	1.89	1.79	1.86	1.83	1.90	1.90	1.99	1.84	1.92
0.00	0.00	0.00	0.00	0.00	0.00	0.00	0.00	0.09	0.00	0.00	0.00	0.00	0.00	0.00	0.00	0.00	0.00
0.06	0.04	0.06	0.06	0.05	0.06	0.07	0.06	0.06	0.00	0.06	0.05	0.06	0.07	0.09	0.04	0.05	0.03
0.53	0.53	0.50	0.47	0.50	0.51	0.50	0.51	0.50	0.50	0.50	0.53	0.52	0.42	0.44	0.44	0.41	0.44
0.00	0.00	0.00	0.00	0.00	0.00	0.00	0.00	0.00	0.00	0.00	0.15	0.00	0.04	0.21	0.39	0.33	0.51

Table 18. Comparison between biotites from the Huangtongjiang gabbro and metamorphosed Precambrian sedimentary rock

LOCATION	Hetai				Huangtongjiang			
Sample No.	C42 (Metamorphosed Precambrian sedimentary rock)				C128 (Gabbro)			
SiO2	34.93	34.26	35.20	35.28	37.38	37.16	37.37	37.06
Al2O3	17.72	17.59	18.40	18.03	14.49	14.54	15.20	14.89
TiO2	1.84	1.75	2.09	2.15	3.93	3.07	3.67	3.70
FeOt	23.35	23.71	23.06	24.29	16.54	16.90	16.59	16.83
MgO	7.43	7.62	7.40	6.82	12.91	13.14	13.40	13.34
MnO	0.42	0.47	0.58	0.47	0.00	0.00	0.33	0.22
CaO	0.00	0.00	0.00	0.00	0.00	0.00	0.00	0.00
Na2O	0.00	0.00	0.19	0.00	0.34	0.23	0.00	0.00
K2O	10.28	9.50	9.84	10.21	10.07	10.11	9.83	10.24
Total	95.97	94.90	96.76	97.26	95.66	96.16	96.47	96.39
Fe2O3	1.76	1.79	1.74	1.84	2.50	2.55	2.51	2.54
FeO	22.56	22.90	22.96	23.46	15.42	15.75	15.46	15.69
MgO/FeO	0.33	0.33	0.32	0.29	0.84	0.83	0.87	0.85
TiO2/Al2O3	0.10	0.10	0.11	0.12	0.27	0.21	0.24	0.25
Fe2O3/(Fe2O3+FeO)	0.07	0.07	0.07	0.07	0.14	0.14	0.14	0.14
Si	5.43	5.39	5.40	5.42	5.61	5.56	5.55	5.54
Al(iv)	2.57	2.61	2.60	2.58	2.39	2.44	2.45	2.46
Al(vi)	0.68	0.65	0.73	0.69	0.22	0.18	0.26	0.21
Ti	0.21	0.21	0.24	0.25	0.42	0.43	0.39	0.33
Mg	1.72	1.79	1.69	1.56	2.89	2.93	2.97	2.97
Fe(t)	3.04	3.12	2.96	3.12	2.07	2.11	2.06	2.10
Fe(3+)	0.21	0.22	0.21	0.22	0.26	0.27	0.26	0.27
Fe(2+)	2.93	2.90	2.75	2.90	1.81	1.84	1.80	1.83
Mn	0.06	0.06	0.08	0.06	0.00	0.00	0.04	0.03
K	2.04	1.90	1.93	2.00	1.93	1.93	1.86	1.95
Na	0.00	0.00	0.06	0.00	0.00	0.00	0.00	0.00
Ca	0.00	0.00	0.00	0.00	0.10	0.07	0.00	0.00
M=Mg/(Mg+Fe2+ +Mn)	0.37	0.38	0.42	0.35	0.61	0.61	0.62	0.62
Al(VI)/Ti	3.24	3.10	3.04	2.76	0.52	0.42	0.67	0.64

Table 19. Comparison between biotites from different enclaves

LOCATION	Shijiang dark enclave							Shijiang dark enclave						Wuchun granodioritic enclave				
Sample No.	C78							C16-1						C10-1				
SiO2	35.89	35.52	35.84	35.24	36.05	35.40	35.86	35.29	35.46	35.15	35.24	35.84	34.80	37.73	37.75	37.55	36.71	36.95
Al2O3	18.40	18.57	17.97	17.93	17.37	18.43	19.03	18.67	18.77	18.66	18.83	18.33	18.99	14.37	12.98	13.53	13.22	13.18
TiO2	2.34	2.74	2.82	2.98	2.74	2.85	2.75	2.90	2.98	2.73	2.41	2.78	2.97	3.08	3.58	3.42	3.26	3.12
FeOt	18.15	18.66	18.72	19.80	19.13	19.00	19.48	20.01	20.25	20.29	19.90	19.81	20.11	22.13	21.56	21.07	21.96	21.76
MgO	9.80	10.29	9.75	9.61	9.93	9.88	9.45	9.47	9.08	8.71	9.17	9.24	8.67	9.34	9.45	9.70	8.95	9.19
MnO	0.29	0.33	0.00	0.00	0.25	0.40	0.29	0.00	0.22	0.56	0.00	0.26	0.22	0.56	0.58	0.31	0.77	0.64
CaO	0.00	0.00	0.00	0.00	0.00	0.00	0.00	0.00	0.00	0.00	0.00	0.00	0.00	0.41	0.26	0.37	0.49	0.51
Na2O	0.49	0.22	0.00	0.26	0.00	0.00	0.00	0.00	0.00	0.41	0.00	0.00	0.36	0.00	0.00	0.00	0.00	0.00
K2O	9.91	10.03	9.94	9.99	9.71	9.91	10.06	9.92	10.02	10.14	9.77	9.59	9.97	9.02	9.42	9.72	9.74	9.74
Total	95.26	96.36	95.05	96.03	95.36	95.95	96.91	96.26	96.93	96.79	95.32	95.85	96.14	96.75	95.67	95.67	95.10	95.10
Fe2O3	1.45	1.49	1.50	1.58	1.53	1.52	1.56	1.60	1.62	1.62	1.59	1.58	1.61	4.67	4.60	4.49	4.68	4.64
FeO	17.50	18.00	18.05	19.09	18.44	18.32	19.78	19.29	19.52	19.50	19.18	19.10	19.39	20.03	19.49	19.05	19.85	19.67
MgO/FeO	0.56	0.57	0.54	0.50	0.54	0.54	0.48	0.49	0.47	0.45	0.48	0.48	0.45	0.47	0.48	0.51	0.45	0.47
TiO2/Al2O3	0.13	0.15	0.16	0.17	0.16	0.15	0.14	0.16	0.16	0.15	0.13	0.15	0.16	0.21	0.28	0.25	0.25	0.24
Fe2O3/(Fe2O3+FeO)	0.08	0.08	0.08	0.08	0.80	0.08	0.07	0.08	0.08	0.08	0.08	0.08	0.08	0.19	0.19	0.19	0.19	0.19
Si	5.46	5.36	5.47	5.37	5.49	5.37	5.38	5.35	5.36	5.34	5.39	5.44	5.31	5.74	5.82	5.77	5.74	5.76
Al(iv)	2.54	2.64	2.53	2.63	2.51	2.63	2.62	2.65	2.64	2.66	2.61	2.56	2.69	2.26	2.18	2.23	2.26	2.24
Al(vi)	0.76	0.66	0.70	0.59	0.60	0.60	0.75	0.69	0.70	0.68	0.78	0.71	0.72	0.32	0.18	0.22	0.17	0.18
Ti	0.27	0.31	0.32	0.34	0.31	0.33	0.31	0.33	0.34	0.31	0.28	0.32	0.34	0.35	0.41	0.40	0.38	0.37
Mg	2.22	2.31	2.22	2.18	2.26	2.34	2.12	2.14	2.05	1.97	2.09	2.09	1.97	2.12	2.17	2.22	2.09	2.14
Fe(t)	2.31	2.35	2.39	2.52	2.44	2.41	2.44	2.54	2.56	2.58	2.54	2.51	2.56	2.82	2.78	2.71	2.87	2.84
Fe(3+)	0.16	0.16	0.17	0.18	0.17	0.17	0.16	0.19	0.18	0.18	0.19	0.17	0.18	0.49	0.49	0.47	0.50	0.49
Fe(2+)	2.15	2.19	2.22	2.34	2.27	2.24	2.28	2.35	2.38	2.40	2.35	2.34	2.38	2.32	2.39	2.23	2.37	2.34
Mn	0.04	0.04	0.00	0.00	0.03	0.05	0.04	0.00	0.03	0.07	0.00	0.03	0.03	0.07	0.08	0.04	0.10	0.09
K	1.92	1.93	1.93	1.94	1.89	1.92	1.93	1.92	1.93	1.97	1.91	1.86	1.94	1.75	1.85	1.91	1.94	1.94
Na	0.14	0.06	0.00	0.08	0.00	0.00	0.00	0.00	0.00	0.12	0.00	0.00	0.11	0.00	0.00	0.00	0.00	0.00
Ca	0.00	0.00	0.00	0.00	0.00	0.00	0.00	0.00	0.00	0.00	0.00	0.00	0.00	0.07	0.04	0.06	0.08	0.09
M=Mg/(Mg+Fe2++Mn)	0.49	0.49	0.48	0.46	0.48	0.49	0.46	0.48	0.46	0.44	0.47	0.47	0.45	0.47	0.47	0.49	0.46	0.47
Al(vi)/Ti	2.81	2.13	2.19	1.74	1.94	1.82	2.42	2.09	2.06	2.19	2.79	2.22	2.12	0.91	0.44	0.55	0.45	0.49

Table 19 continued

Sihui granodioritic
C18-3

38.72	37.30	39.06	37.70	37.18	37.95	37.01	36.86	38.50	36.78	36.15	37.19	38.91
11.55	11.87	13.16	11.63	12.05	11.34	11.99	11.15	11.26	11.69	12.09	12.07	10.85
4.90	4.40	4.38	3.92	4.13	3.97	4.44	4.29	4.75	4.38	4.84	4.95	4.01
20.82	20.62	18.50	20.16	20.53	19.96	20.14	20.79	19.80	20.58	20.67	21.50	17.52
10.05	9.76	10.80	10.77	10.88	11.30	10.80	11.17	11.27	11.14	10.58	9.75	13.06
0.98	1.15	1.00	1.15	0.82	0.91	0.86	1.23	0.47	0.88	0.56	1.00	0.63
0.92	0.57	0.37	0.30	0.00	0.28	0.51	0.32	0.31	0.30	0.56	0.26	0.20
0.00	0.00	0.00	0.00	0.00	0.00	0.00	0.00	0.00	0.00	0.00	0.00	0.00
9.03	9.80	8.73	9.89	9.74	9.90	9.35	9.59	9.87	9.83	9.69	9.30	9.77
96.97	95.57	96.00	95.63	95.62	95.60	95.30	95.58	96.37	95.72	95.29	96.04	95.16
5.23	5.18	4.65	5.06	5.16	5.01	5.06	5.22	4.93	5.17	5.19	5.40	4.40
18.47	18.29	18.41	17.88	18.21	17.70	17.86	18.44	17.58	18.25	18.23	19.07	15.54
0.54	0.53	0.59	0.60	0.60	0.64	0.60	0.61	0.64	0.61	0.58	0.51	0.84
0.42	0.37	0.33	0.34	0.34	0.35	0.37	0.38	0.42	0.37	0.40	0.41	0.37
0.22	0.22	0.22	0.22	0.22	0.22	0.22	0.22	0.22	0.22	0.22	0.22	0.22
5.87	5.79	5.87	5.83	5.75	5.85	5.73	5.73	5.86	5.70	5.63	5.73	5.93
2.06	2.17	2.13	2.12	2.20	2.06	2.19	2.05	2.02	2.13	2.22	2.19	1.95
0.00	0.00	0.20	0.00	0.00	0.00	0.00	0.00	0.00	0.00	0.00	0.00	0.00
0.56	0.51	0.50	0.46	0.48	0.46	0.52	0.50	0.54	0.51	0.57	0.57	0.46
2.27	2.26	2.42	2.48	2.51	2.60	2.49	2.59	2.56	2.57	2.46	2.24	2.97
2.64	2.67	2.33	2.61	2.66	2.57	2.61	2.70	2.52	2.67	2.69	2.77	2.23
0.53	0.54	0.43	0.53	0.54	0.52	0.55	0.56	0.52	0.54	0.55	0.57	0.46
2.11	2.13	1.90	2.08	2.12	2.05	2.06	2.14	2.00	2.12	2.14	2.20	1.77
0.13	0.15	0.13	0.15	0.11	0.12	0.11	0.16	0.06	0.12	0.07	0.13	0.08
1.75	1.94	1.68	1.95	1.92	1.95	1.85	1.90	1.92	1.94	1.92	1.83	1.90
0.00	0.00	0.00	0.00	0.00	0.00	0.00	0.00	0.00	0.00	0.00	0.00	0.00
0.15	0.09	0.06	0.05	0.00	0.05	0.09	0.05	0.05	0.05	0.09	0.04	0.03
0.50	0.49	0.54	0.52	0.52	0.54	0.53	0.52	0.55	0.53	0.52	0.46	0.61
0.00	0.00	0.41	0.00	0.00	0.00	0.00	0.00	0.00	0.00	0.00	0.00	0.00

Table 20. Trace elements and major oxide averages of biotites from different granites of the Hetai Area

Age	Precambrian	Caledonian					Hercynian		Indosinian		Yanshanian			
LOCATION	Hetai	Shiniutou	Sidong	Sidong	Shijiang	Shijiang	Guangning	Yunlougan	Wuchun	Wuchun	Sihui	Sihui	Sihui	Huangtongjiang
Sample No.	C42	C17	C7-1	C7-2	C78&C16	C16-2,3,4,5	C13&C84	C9-1	C10-1	C10-2	C18-3	C18-1	C18-2	C128
SiO2	34.92	37.24	35.03	34.77	35.51	35.08	35.44	37.04	37.34	36.29	37.64	37.76	37.8	37.24
Al2O3	17.94	17.27	14.53	16.51	18.46	18.32	15.97	14.59	13.46	13.58	11.75	12.19	12.34	14.78
TiO2	1.96	2.17	2.76	2.38	2.77	2.65	2.97	3.35	3.29	4.03	4.41	4.07	3.86	3.59
FeOt	23.6	30.53	29.59	28.39	19.49	21.7	22.69	21.96	21.7	23.1	20.12	21.24	21.99	16.72
MgO	7.32	1.35	3.99	2.95	9.47	8.14	7.4	9.74	9.33	7.66	10.87	10.11	8.61	13.2
MnO	0.49	0.71	1.02	1	0.22	0.35	0.69	0.43	0.63	0.83	0.9	0.94	1.48	0.14
CaO	0	0.34	0.29	0.41	0	0.03	0.52	0.35	0.41	0.41	0.38	0.36	0.43	0
Na2O	0.05	0	0	0.04	0.13	0.08	0.03	0	0	0.06	0	0.02	0	0.14
K2O	9.96	9.19	9.58	9.35	9.92	9.8	9.66	9.66	9.53	9.55	9.58	9.35	9.47	10.06
Total	96.22	96.17	96.85	95.94	96.02	96.19	95.55	96.24	95.72	95.58	95.76	96.2	96.12	96.17
Fe2O3	1.78	5.09	3.63	4.73	1.56	1.99	1.95	3.71	4.62	5.34	5.05	5.76	5.84	2.53
FeO	22.97	28.24	27.97	26.26	18.86	20.8	21.8	20.29	19.62	20.7	17.99	18.67	19.37	15.58
MgO/FeO	0.32	0.05	0.14	0.11	0.5	0.39	0.34	0.48	0.48	0.37	0.6	0.54	0.44	0.85
TiO2/Al2O3	0.11	0.13	0.19	0.14	0.15	0.14	0.19	0.23	0.24	0.3	0.38	0.33	0.31	0.24
Fe2O3/(Fe2O3+FeO)	0.07	0.15	0.11	0.15	0.08	0.09	0.08	0.15	0.19	0.21	0.22	0.24	0.24	0.14
Si	5.41	5.51	5.59	5.55	5.39	5.38	5.53	5.69	5.77	5.67	5.79	5.8	5.85	5.76
Al(iv)	2.59	2.49	2.41	2.45	2.61	2.62	2.47	2.31	2.23	2.33	2.11	2.17	2.14	2.24
Al(vi)	0.69	0.77	0.39	0.66	0.69	0.69	0.46	0.33	0.21	0.17	0.2	0.11	0.12	0.22
Ti	0.23	0.26	0.33	0.29	0.32	0.31	0.35	0.39	0.38	0.47	0.51	0.47	0.45	0.39
Mg	1.69	0.33	0.95	0.7	2.15	1.86	1.72	2	2.15	1.79	2.49	2.32	1.98	2.94
Fe(t)	3.06	4.11	3.95	3.79	2.47	2.78	2.96	2.82	2.8	3.02	2.59	2.73	2.84	2.09
Fe(3+)	0.22	0.58	0.42	0.53	0.17	0.23	0.23	0.4	0.49	0.57	0.53	0.59	0.62	0.27
Fe(2+)	2.87	3.53	3.52	3.26	2.3	2.55	2.73	2.42	2.33	2.45	2.06	2.12	2.21	1.82
Mn	0.07	0.19	0.14	0.14	0.03	0.05	0.09	0.06	0.09	0.11	0.12	0.12	0.19	0.02
K	1.97	1.89	1.95	1.91	1.92	1.92	1.91	1.89	1.88	1.9	1.88	1.83	1.88	1.92
Na	0.02	0	0	0.01	0.04	0.03	0.01	0	0	0.02	0	0.01	0	0
Ca	0	0.06	0.05	0.07	0	0	0.09	0.06	0.07	0.07	0.06	0.06	0.07	0.04
M=Mg/(Mg+Fe2+ +Mn)	0.38	0.08	0.21	0.17	0.47	0.42	0.38	0.45	0.47	0.41	0.53	0.51	0.45	0.62
Al(VI)/Ti	3	2.96	1.18	2.28	2.12	2.23	1.31	0.85	0.55	0.36	0.39	0.23	0.27	0.56
F (ppm)			5100	4400	3600	3500	5500	3000	5100	6050	4500	7300	7300	
Li			198	128	152	202	353	187	514	697	327	1256	1991	
Rb			655	634	659	734	632	447	732	1000	507	1056	1056	
Zn			425	500	375	550	510	425	450	600	510	800	1050	
Ni			64	64	69	56	65	84	98	54	59	39	44	
Co			36	37	39	35	33	39	36	32	32	26	24	

Table 21. Chemical analyses of amphiboles from granitic plutons in the Hetai Area

Location	Yunlougan														Sihui			
Age	Hercynian														Yanshanian			
Sample No	Granodiorite, C9-1														Granodioritic enclave, C18-3			
Occurence								In zoned plagioclase				In polysynthetic plagioclase						
SiO2	46.55	46.59	47.23	46.12	45.87	46.06	46.06	47.46	49.89	48.88	49.50	43.24	42.42	43.63	44.68	44.26	44.32	43.99
TiO2	1.22	0.91	1.25	0.69	0.77	0.99	0.79	0.63	0.38	0.66	0.57	1.02	0.83	0.67	1.21	0.84	1.08	1.13
Al2O3	7.07	6.51	6.57	6.42	6.41	6.35	7.49	5.57	3.46	4.67	4.99	9.79	9.79	9.37	5.92	5.87	6.50	6.39
FeOt	19.24	19.76	19.65	19.78	20.10	19.83	20.86	19.56	19.12	19.41	19.08	22.93	23.10	23.68	18.66	20.62	20.76	22.24
MgO	8.57	8.86	9.02	9.65	9.49	9.07	9.26	9.96	11.32	10.26	11.04	6.29	6.31	6.75	9.32	9.31	9.57	9.02
MnO	0.71	0.53	0.40	0.70	0.71	0.39	0.66	0.76	0.54	0.44	0.59	0.54	0.60	0.65	1.86	1.65	1.40	1.30
CaO	12.31	12.16	12.29	11.61	11.57	11.58	11.78	11.92	11.99	11.69	11.75	11.33	11.60	11.39	11.31	10.69	11.07	10.97
Na2O	0.45	0.63	0.37	0.38	0.45	0.54	0.37	0.49	0.00	0.00	0.00	0.50	0.88	0.92	1.20	1.30	1.51	0.73
K2O	0.95	0.98	0.82	0.54	0.80	0.94	0.94	0.68	0.41	0.45	0.40	1.21	1.35	1.13	0.97	0.92	0.92	0.93
Total	97.27	97.17	97.67	96.04	96.17	95.74	98.22	97.05	97.31	96.45	97.90	96.85	96.88	98.19	95.35	95.45	97.13	96.70
MgO/FeOt	0.45	0.45	0.46	0.49	0.47	0.46	0.44	0.51	0.59	0.53	0.58	0.27	0.27	0.28	0.50	0.45	0.46	0.41
(O=23)																		
Si	6.76	6.80	6.83	7.10	7.07	7.12	6.97	7.22	7.49	7.41	7.37	6.73	6.65	6.76	6.70	6.97	6.87	6.87
Al	1.21	1.12	1.12	1.16	1.17	1.16	1.34	1.00	0.61	0.83	0.88	1.80	1.81	1.70	1.05	1.09	1.19	1.18
Ti	0.13	0.10	0.14	0.08	0.09	0.11	0.09	0.07	0.04	0.08	0.06	0.12	0.10	0.08	0.14	0.10	0.13	0.13
Mg	1.86	1.93	1.94	2.21	2.18	2.09	2.09	2.26	2.53	2.32	2.45	1.46	1.47	1.55	2.08	2.19	2.21	2.10
Fe	2.34	2.41	2.37	2.55	2.59	2.56	2.64	2.49	2.40	2.46	2.38	2.99	3.03	3.05	2.34	2.72	2.69	2.91
Mn	0.09	0.07	0.05	0.09	0.09	0.05	0.09	0.10	0.07	0.06	0.07	0.07	0.08	0.08	0.24	0.22	0.18	0.17
Ca	1.92	1.90	1.90	1.91	1.91	1.92	1.91	1.94	1.93	1.90	1.88	1.89	1.95	1.88	1.82	1.80	1.84	1.84
Na	0.13	0.18	0.10	0.11	0.13	0.16	0.11	0.14	0.00	0.00	0.00	0.15	0.27	0.27	0.35	0.40	0.45	0.22
K	0.18	0.18	0.15	0.11	0.16	0.18	0.18	0.13	0.08	0.09	0.08	0.24	0.27	0.22	0.19	0.18	0.18	0.19
P1* (kbar)	2.17	1.71	1.71	1.91	1.97	1.91	2.82	1.11				5.13	5.15	4.63	1.36	1.56	2.07	2.02
P2*									0.47	0.87	0.98							
P3**	2.06	1.56	1.56	1.78	1.84	1.78	2.80	0.88				5.39	5.41	4.83	1.16	1.39	1.95	1.94
P4***	2.75	2.32	2.32	2.51	2.56	2.51	4.37	1.75				5.56	5.58	5.08	2.00	2.18	2.65	2.61
Depth (km)#	8.00	6.00	6.00	7.00	7.00	6.00	10.00								4.00	5.00	7.00	7.00

* After Hammarstron and Zen (1986); ** After Hollister et al. (1987); *** After Schmidt (1992); # After Wyllie (1971)

Table 21 continued

Sihui					Huangtongjiang										
C18-3					Gabbro, C160-2										
44.77	46.01	44.94	45.06	44.25	54.05	53.96	54.01	55.32	54.04	55.37	53.76	55.09	55.20	55.12	53.52
1.08	1.07	0.65	0.83	1.57	0.26	0.36	0.00	0.00	0.15	0.00	0.15	0.00	0.00	0.21	0.16
5.64	5.57	5.02	5.36	6.89	3.64	2.89	2.46	2.61	3.32	2.44	3.13	2.52	1.80	2.55	2.81
20.00	19.72	20.80	20.60	21.06	10.84	9.79	9.78	10.41	10.08	9.35	10.14	9.60	9.80	9.95	10.48
10.10	10.33	10.05	10.14	9.39	16.53	16.49	17.14	17.12	16.32	16.98	16.87	17.03	17.35	16.87	17.54
1.40	1.34	1.13	1.69	1.49	0.13	0.31	0.42	0.00	0.39	0.31	0.29	0.00	0.35	0.00	0.00
11.26	10.56	11.19	11.03	10.99	12.26	12.28	12.25	12.65	12.77	12.37	12.39	12.49	12.46	12.31	12.24
1.32	0.72	1.57	0.88	1.03	0.64	0.49	0.20	0.00	0.64	0.40	0.35	0.42	0.00	0.00	0.91
0.74	0.98	0.89	0.80	0.90	0.33	0.28	0.36	0.01	0.22	0.19	0.28	0.22	0.18	0.29	0.22
96.31	96.31	96.25	96.37	97.57	98.68	96.95	96.72	98.49	98.07	97.40	97.37	97.52	97.13	97.51	97.88
0.51	0.52	0.48	0.49	0.45	1.52	1.68	1.75	1.64	1.62	1.82	1.66	1.77	1.77	1.70	1.67
6.96	7.10	7.02	7.01	6.82	7.64	7.74	7.76	7.79	7.68	7.85	7.68	7.81	7.87	7.82	7.63
1.03	1.01	0.92	0.98	1.25	0.61	0.49	0.42	0.43	0.56	0.41	0.53	0.42	0.30	0.43	0.47
0.13	0.12	0.08	0.10	0.18	0.03	0.04	0.00	0.00	0.02	0.00	0.02	0.00	0.00	0.02	0.02
2.34	2.38	2.34	2.35	2.16	3.48	3.52	3.67	3.59	3.46	3.59	3.59	3.60	3.69	3.57	3.73
2.60	2.54	2.72	2.68	2.71	1.28	1.17	1.18	1.23	1.20	1.11	1.21	1.14	1.17	1.18	1.25
0.18	0.18	0.15	0.22	0.19	0.02	0.04	0.05	0.00	0.05	0.04	0.04	0.00	0.04	0.00	0.00
1.88	1.74	1.87	1.84	1.81	1.86	1.89	1.89	1.91	1.94	1.88	1.90	1.90	1.90	1.87	1.87
0.40	0.22	0.48	0.26	0.31	0.18	0.14	0.06	0.00	0.18	0.11	0.10	0.12	0.00	0.00	0.25
0.15	0.19	0.18	0.16	0.18	0.06	0.05	0.07	0.02	0.04	0.03	0.05	0.04	0.03	0.05	0.04
1.26	1.16	0.71	1.01	2.37	0.47	0.30	0.22	0.23	0.40	0.21	0.35	0.22	0.11	0.23	0.28
1.05	0.94	0.43	0.77	2.29											
1.89	1.80	1.37	1.65	2.94											
4.00	4.00	3.00	3.00	8.00	2.00	1.00	1.00	1.00	2.00	1.00	1.00	1.00	1.00	1.00	1.00

Table 21 continued

Huangtongjiang										Huangtongjiang		
pyroxene diorite, C128										C128 In polysynthetic plagioclase		
50.26	50.21	50.46	50.06	49.17	50.48	50.43	49.71	50.44	50.70	48.45	46.10	44.93
0.16	0.44	0.63	0.44	0.31	0.35	0.27	0.43	0.62	0.37	0.71	0.89	0.31
6.04	7.65	7.37	6.66	7.89	7.64	6.91	7.05	6.72	5.82	8.60	11.44	11.89
13.19	13.29	13.13	13.22	13.43	12.66	13.37	14.24	13.55	12.70	13.67	14.79	15.92
14.06	13.61	13.09	13.61	12.57	13.65	13.19	13.18	13.94	14.05	12.83	10.82	10.79
0.59	0.39	0.42	0.00	0.36	0.42	0.47	0.22	0.00	0.36	0.56	0.40	0.52
11.87	11.66	11.88	11.52	11.74	12.16	11.81	11.80	11.90	11.91	11.76	11.61	11.30
1.00	0.71	0.71	0.57	0.88	0.46	0.88	1.00	1.16	0.77	1.07	1.29	1.32
0.30	0.26	0.09	0.22	0.11	0.27	0.25	0.00	0.25	0.27	0.39	0.61	0.51
97.47	98.22	97.79	96.98	96.46	98.40	97.93	97.82	98.64	97.23	98.04	98.09	97.50
1.07	1.02	1.00	1.03	0.94	1.08	0.99	0.93	1.03	1.11	0.94	0.73	0.68
7.32	7.23	7.29	7.30	7.22	7.25	7.31	7.24	7.26	7.37	7.05	6.77	6.67
1.04	1.30	1.25	1.14	1.37	1.29	1.18	1.21	1.14	1.00	1.48	1.98	2.08
0.02	0.05	0.07	0.05	0.03	0.04	0.03	0.05	0.07	0.04	0.08	0.10	0.04
3.06	2.92	2.82	2.96	2.75	2.92	2.85	2.86	2.99	3.05	2.78	2.37	2.39
1.61	1.60	1.59	1.61	1.65	1.52	1.62	1.73	1.63	1.54	1.66	1.82	1.98
0.07	0.05	0.05	0.00	0.05	0.05	0.06	0.03	0.00	0.04	0.07	0.05	0.07
1.85	1.80	1.84	1.80	1.85	1.87	1.83	1.84	1.84	1.86	1.83	1.83	1.80
0.28	0.20	0.20	0.16	0.25	0.13	0.25	0.28	0.32	0.22	0.30	0.37	0.38
0.06	0.05	0.02	0.04	0.02	0.05	0.05	0.04	0.05	0.05	0.07	0.11	0.10
1.31	2.62	2.37	1.81	2.97	2.57	2.02	2.17	1.81	1.11	3.52	6.04	5.64
1.11	2.57	2.29	1.67	2.97	2.52	1.90	2.06	1.67	0.88	3.59	6.41	6.97
1.94	3.18	2.94	2.42	3.51	3.13	2.61	2.75	2.42	1.75	4.03	6.41	6.89
4.00	10.00	9.00	6.00	10.00	9.00	7.00	8.00	6.00	3.00			

Table 22. Chemical analyses of plagioclases from the Caledonian granites

Location	Shiniutou		Sidong					Sidong	Shijiang							
Sample No.	C17		C7-1					C7-2	C78 (Dark enclave)					C16-1 (Dark enclave)		
SiO2	66.95	67.37	67.49	67.15	68.74	64.94	65.51	65.81	69.26	57.57	60.06	57.24	59.44	58.80	58.68	60.10	60.42
Al2O3	20.15	19.99	19.36	20.43	18.70	20.90	20.63	20.14	18.68	26.18	24.92	26.65	25.52	25.89	25.00	25.24	23.80
TiO2	0.00	0.00	0.00	0.00	0.00	0.00	0.00	0.00	0.00	0.18	0.00	0.00	0.18	0.00	0.00	0.00	0.00
FeOt	0.00	0.00	0.00	0.00	0.00	0.00	0.00	0.00	0.00	0.00	0.00	0.00	0.00	0.00	0.00	0.00	0.00
MgO	0.00	0.00	0.00	0.00	0.00	0.00	0.00	0.00	0.00	0.00	0.00	0.00	0.00	0.00	0.00	0.00	0.00
MnO	0.00	0.00	0.00	0.00	0.00	0.30	0.00	0.00	0.00	0.19	0.00	0.00	0.00	0.00	0.00	0.00	0.00
CaO	2.18	1.93	1.82	2.59	1.00	3.41	2.85	3.13	0.93	9.95	6.27	9.47	7.45	8.05	7.66	6.68	5.95
Na2O	10.75	10.43	11.23	10.77	12.06	10.75	10.70	10.48	11.36	6.17	8.14	6.51	7.20	6.63	8.08	8.40	6.95
K2O	0.11	0.00	0.07	0.00	0.00	0.00	0.00	0.00	0.10	0.00	0.22	0.11	0.08	0.21	0.21	0.18	2.42
Total	100.14	99.72	99.97	100.94	100.50	100.29	99.69	99.56	100.33	100.25	99.61	99.98	99.87	99.59	99.64	100.61	99.55
SiO2/Al2O3	3.32	3.37	3.49	3.29	3.68	3.11	3.18	3.27	3.71	2.20	2.41	2.15	2.33	2.27	2.35	2.38	2.54
Na2O/CaO	4.93	5.40	6.17	4.16	12.06	3.29	3.75	3.35	12.22	0.62	1.30	0.69	0.97	0.82	1.05	1.26	1.17
Si	11.75	11.83	11.86	11.70	12.00	11.47	11.59	11.65	12.07	10.32	10.74	10.28	10.61	10.54	10.56	10.67	10.89
Al	4.17	4.14	4.01	4.20	3.85	4.35	4.30	4.20	3.84	5.53	5.25	5.64	5.37	5.47	5.30	5.28	5.05
Ca	0.41	0.36	0.34	0.48	0.19	0.65	0.54	0.59	0.17	1.91	1.20	1.82	1.42	1.55	1.48	1.27	1.15
Na	3.66	3.55	3.83	3.64	10.48	3.68	3.67	3.60	3.84	2.15	2.82	2.27	2.49	2.30	2.82	2.89	2.43
K	0.03	0.00	0.02	0.00	0.00	0.00	0.00	0.00	0.02	0.00	0.05	0.02	0.02	0.05	0.05	0.04	0.56
Ab	89.30	90.80	89.30	88.30	95.60	84.90	87.20	85.90	95.00	53.00	69.30	55.20	63.40	59.00	64.80	68.80	58.70
An	10.00	9.20	7.90	11.70	4.40	15.10	12.80	14.10	4.00	47.00	29.50	44.30	36.10	39.70	34.00	30.20	27.80
Or	0.70	0.00	2.80	0.00	0.00	0.00	0.00	0.00	1.00	0.00	1.20	0.50	0.50	1.30	1.20	1.00	13.50

Table 22 continued

Shijaing C16-2	Shijiang C16-2	C16-3		C16-5	C16-5	C16-4			
62.70	62.87	61.77	62.15	61.40	62.06	62.77	62.22	62.46	63.91
23.26	23.56	24.08	23.57	24.47	23.97	23.39	24.28	23.46	22.24
0.00	0.00	0.00	0.15	0.00	0.00	0.00	0.00	0.21	0.00
0.00	0.00	0.00	0.00	0.00	0.00	0.00	0.00	0.00	0.27
0.00	0.00	0.00	0.00	0.00	0.00	0.00	0.00	0.00	0.00
0.00	0.00	0.00	0.00	0.00	0.00	0.00	0.00	0.17	0.00
5.19	5.19	5.77	5.62	6.09	6.03	5.27	5.51	4.65	3.63
8.90	9.34	9.18	8.67	8.58	8.75	8.83	8.38	8.77	9.77
0.25	0.00	0.07	0.28	0.29	0.09	0.00	0.00	0.19	0.16
100.30	100.97	100.87	100.44	100.83	100.90	100.26	100.39	99.91	99.99
2.70	2.67	2.57	2.64	2.51	2.59	2.68	2.56	2.66	2.87
1.71	1.80	1.59	1.54	1.41	1.45	1.68	1.52	1.89	2.69
11.09	11.05	10.91	11.00	10.85	10.94	11.09	10.98	11.08	11.31
4.85	4.88	5.01	4.92	5.10	4.98	4.87	5.05	4.91	4.64
0.98	0.98	1.09	1.07	1.15	1.14	1.00	1.04	0.88	0.69
3.05	3.18	3.14	2.98	2.94	2.99	3.03	2.87	3.01	3.35
0.06	0.00	0.17	0.06	0.07	0.02	0.00	0.00	0.04	0.04
74.60	76.40	71.40	72.50	70.70	72.00	75.20	73.40	74.70	82.10
24.00	23.60	24.80	26.00	27.60	27.50	24.80	26.60	21.80	16.90
1.40	0.00	3.80	1.50	1.70	0.50	0.00	0.00	3.50	1.00

Table 23. Chemical comparison between plagioclases from the Hercynian granites

Location	Yunlougan								Guangning				Guangning			
Sample No.	C9-1								C13				C84			
Position														Center	Middle	Margin
SiO2	58.09	59.83	60.50	58.25	60.10	60.96	60.74	60.13	65.15	65.00	65.52	64.03	64.27	61.95	63.71	69.48
Al2O3	25.30	25.01	24.10	25.47	24.83	23.72	24.56	24.34	21.16	20.64	22.91	20.82	21.51	23.11	21.94	16.51
TiO2	0.00	0.00	0.00	0.00	0.00	0.29	0.00	0.13	0.00	0.00	0.21	0.00	0.00	0.00	0.00	0.00
FeOt	0.00	0.00	0.00	0.00	0.00	0.00	0.00	0.00	0.00	0.00	0.25	0.38	0.00	0.00	0.00	0.00
MgO	0.00	0.00	0.00	0.00	0.00	0.00	0.00	0.00	0.00	0.00	0.00	0.00	0.00	0.00	0.00	0.00
MnO	0.00	0.00	0.00	0.00	0.00	0.00	0.00	0.00	0.00	0.00	0.00	0.00	0.00	0.29	0.00	0.43
CaO	8.82	7.89	7.67	9.09	8.25	7.34	7.18	7.55	3.77	3.95	5.87	4.18	4.76	6.39	5.03	0.53
Na2O	6.87	6.92	7.67	6.67	7.32	7.79	7.38	7.62	10.05	9.75	7.71	9.64	9.42	8.43	9.14	8.92
K2O	0.18	0.18	0.13	0.00	0.24	0.19	0.15	0.19	0.00	0.00	0.28	0.00	0.10	0.11	0.00	4.38
Total	99.25	99.83	100.07	99.47	100.73	100.29	100.01	99.96	100.14	99.34	99.75	99.06	100.06	100.28	99.82	100.25
SiO2/Al2O3	2.30	2.39	2.51	2.29	2.42	2.57	2.47	2.47	3.08	3.15	2.86	3.08	2.99	2.68	2.90	4.21
Na2O/CaO	0.78	0.88	1.00	0.73	0.89	1.06	1.03	1.01	2.67	2.47	1.31	2.31	1.98	1.32	1.82	16.83
Si	10.49	10.69	10.80	10.49	10.67	10.85	10.81	10.74	11.49	11.54	11.11	11.45	11.37	11.01	11.30	12.20
Al	5.39	5.26	5.07	5.40	5.20	4.97	5.15	5.13	4.40	4.32	4.80	4.39	4.48	4.84	4.59	3.52
Ca	1.71	1.51	1.47	1.75	1.57	1.40	1.37	1.45	0.71	0.75	1.12	0.80	0.90	1.22	0.96	0.10
Na	2.41	2.40	2.65	2.33	2.52	2.69	2.54	2.64	3.44	3.36	2.66	3.34	3.23	2.90	3.14	3.04
K	0.04	0.04	0.03	0.00	0.05	0.04	0.04	0.04	0.00	0.00	0.06	0.00	0.02	0.03	0.00	0.98
Ab	57.90	60.80	63.90	57.10	60.90	65.10	64.30	63.90	82.90	81.80	69.30	80.70	77.80	69.90	76.60	72.00
An	41.00	38.20	35.40	42.90	37.90	33.90	34.70	35.10	17.10	18.20	29.20	19.30	21.70	29.40	23.40	2.30
Or	1.10	1.00	0.70	0.00	1.20	0.00	1.00	1.00	0.00	0.00	1.50	0.00	0.50	0.70	0.00	5.70

Table 24. Chemical analyses of plagioclases from the Indosinian granites

Location	Wuchun		Wuchun			Wuchun								
Sample No.	C10-1		C10-1			C10-2								
Position	Xenocryst	Xenocryst	Ordinary plagioclase			Core	Middle	Margin				Core	Middle	Margin
SiO2	56.69	56.07	61.34	61.52	62.73	59.72	61.29	69.31	65.43	67.26	67.03	61.45	63.43	69.92
Al2O3	23.44	24.78	23.83	23.95	22.59	24.01	23.83	18.48	20.69	19.68	19.59	23.61	22.16	17.70
TiO2	0.19	0.00	0.00	0.00	0.00	0.00	0.00	0.00	0.00	0.00	0.00	0.00	0.00	0.00
FeOt	0.28	0.00	0.26	0.00	0.00	0.00	0.00	0.00	0.00	0.00	0.26	0.00	0.00	0.00
MgO	0.00	0.00	0.00	0.00	0.00	0.00	0.00	0.00	0.00	0.00	0.00	0.00	0.00	0.00
MnO	0.00	0.00	0.37	0.26	0.00	0.00	0.00	0.00	0.00	0.00	0.00	0.00	0.00	0.00
CaO	10.01	9.11	6.91	6.76	5.89	7.62	6.78	0.45	3.14	1.72	2.52	6.53	5.77	0.27
Na2O	7.33	3.70	8.06	7.83	9.07	7.77	8.50	12.19	10.51	11.01	10.22	7.68	8.56	12.06
K2O	1.95	5.87	0.14	0.43	0.34	0.00	0.40	0.00	0.00	0.10	0.00	0.20	0.25	0.26
Total	99.89	99.71	100.91	100.75	100.63	99.13	100.79	100.44	99.78	99.76	99.62	99.47	100.17	100.21
SiO2/Al2O3	2.42	2.26	2.57	2.57	2.78	2.49	2.57	3.75	3.16	3.42	3.42	2.60	2.86	3.95
Na2O/CaO	0.73	0.41	1.17	1.16	1.54	1.02	1.25	27.09	3.35	6.40	4.06	1.18	1.48	44.67
Si	10.40	10.69	10.87	10.89	11.11	10.76	10.87	12.08	11.57	11.83	11.82	10.97	11.23	12.21
Al	5.07	5.89	4.97	5.00	4.71	5.10	4.98	3.80	4.31	4.08	4.07	4.97	4.63	3.64
Ca	1.97	1.86	1.31	1.28	1.12	1.47	1.29	0.08	0.60	0.33	0.48	1.25	1.09	0.05
Na	2.11	1.37	2.77	2.69	3.11	2.72	2.92	4.12	3.60	3.75	3.49	2.66	2.94	4.08
K	0.46	1.43	0.03	0.10	0.08	0.00	0.09	0.00	0.00	0.02	0.00	0.04	0.06	0.06
An	43.40	40.00	31.90	31.40	26.50	35.10	30.00	1.90	14.30	8.00	12.10	31.60	26.60	2.10
Ab	46.50	29.40	67.40	66.10	72.20	64.90	67.90	98.10	85.70	91.00	87.90	67.30	71.90	95.80
Or	10.10	30.60	0.70	2.50	0.30	0.00	2.10	0.00	0.00	1.00	0.00	1.10	1.50	2.10

Table 25. Chemical analyses of feldspars from the Yanshanian granites

Location	Sihui										Sihui				
Sample No.	C18-3, Granodioritic enclave										C18-1				
Position	core	margir	core	margin				core	middle	margin			core	middle	margin
SiO2	59.26	64.92	59.18	64.87	63.92	64.91	65.71	61.28	62.16	65.72	68.93	68.76	58.37	61.14	61.87
Al2O3	25.38	21.44	25.04	20.28	21.83	20.92	21.00	22.92	22.80	21.18	18.35	18.90	25.44	23.37	22.92
TiO2	0.29	0.23	0.00	0.00	0.00	0.00	0.00	0.37	0.24	0.00	0.00	0.00	0.00	0.00	0.00
FeOt	0.00	0.00	0.25	0.00	0.00	0.00	0.00	0.26	0.58	0.40	0.23	0.00	0.16	0.00	0.36
MgO	0.00	0.00	0.00	0.00	0.00	0.00	0.00	0.00	0.00	0.00	0.00	0.00	0.00	0.00	0.00
MnO	0.00	0.00	0.23	0.00	0.00	0.00	0.00	0.29	0.00	0.00	0.00	0.00	0.00	0.00	0.00
CaO	8.77	4.18	8.70	3.73	4.27	3.82	3.82	6.18	5.97	4.08	0.00	0.71	9.26	6.61	6.06
Na2O	6.53	9.00	7.04	9.48	8.83	9.58	9.58	8.13	7.37	8.75	12.20	11.91	6.32	7.60	7.96
K2O	0.17	0.47	0.18	1.09	0.45	0.50	0.50	0.51	0.57	0.76	0.00	0.20	0.33	0.51	0.60
Total	100.38	100.25	100.62	99.46	99.30	100.62	100.62	99.99	99.67	100.89	99.71	100.48	99.89	99.23	99.84
SiO2/Al2O3	2.33	3.03	2.36	3.20	2.93	3.10	3.13	2.67	2.73	3.10	3.76	3.64	2.29	2.62	2.70
Na2O/CaO	0.74	2.15	0.81	2.54	2.07	2.51	2.51	1.32	1.23	2.14	20.00	18.00	0.68	1.15	1.31
Si	10.56	11.44	10.56	11.57	11.37	11.54	11.54	10.95	11.09	11.52	12.10	12.00	10.62	10.97	11.04
Al	5.33	4.45	5.27	4.26	4.58	4.35	4.35	4.84	4.79	4.37	3.80	3.89	5.45	4.94	4.83
Ca	1.67	0.79	1.66	0.71	0.81	0.72	0.72	1.18	1.14	0.77	0.00	0.13	1.80	1.27	1.16
Na	2.25	3.08	2.43	3.28	3.05	3.26	3.26	2.82	2.54	2.97	4.15	4.03	2.23	2.64	2.76
K	0.04	0.11	0.04	0.25	0.10	0.11	0.11	0.11	0.13	0.17	0.00	0.04	0.08	0.12	0.14
Ab	56.80	77.40	58.80	77.40	77.00	77.90	79.70	68.60	66.70	76.00	100.00	96.00	54.30	65.50	68.00
An	42.20	19.80	40.20	16.70	20.50	18.90	7.60	28.70	29.90	19.70	0.00	3.10	43.80	31.40	28.60
Or	0.00	2.80	0.00	5.90	2.50	3.20	2.70	2.70	3.40	4.30	0.00	0.90	1.90	3.10	3.40

Table 25 continued

Sihui C21-1			C21-1					Sihui C18-2				C21-2		C21-3			
core	middle	margir	center	middle	margin			core	margin							center	margin
64.33	65.00	67.14	67.98	69.26	69.53	68.93	71.03	64.31	66.33	66.58	66.47	68.68	70.16	68.99	73.06	69.19	70.46
20.48	20.21	18.87	18.05	17.08	17.19	16.88	16.68	21.14	19.81	19.64	20.23	17.15	16.72	17.56	14.81	16.52	15.68
0.00	0.00	0.00	0.00	0.00	0.00	0.00	0.00	0.00	0.00	0.00	0.00	0.34	0.00	0.00	0.00	0.31	0.00
0.00	0.24	0.00	0.00	0.00	0.00	0.30	0.00	0.00	0.00	0.28	0.00	0.00	0.00	0.46	0.00	0.00	0.00
0.00	0.00	0.00	0.00	0.00	0.00	0.00	0.00	0.00	0.00	0.00	0.00	0.00	0.00	0.00	0.00	0.00	0.00
0.00	0.00	0.00	0.00	0.00	0.00	0.00	0.00	0.00	0.00	0.00	0.00	0.00	0.00	0.00	0.23	0.00	0.24
6.40	5.77	4.33	4.31	2.55	2.89	2.36	1.56	4.54	2.82	2.53	3.14	1.75	1.98	2.00	2.14	2.49	0.48
8.21	8.29	9.65	9.75	10.49	11.24	11.54	10.01	9.27	9.92	9.55	9.58	11.57	11.55	10.31	10.20	11.12	12.55
0.15	0.41	0.43	0.56	0.34	0.00	0.48	0.40	0.46	0.60	0.67	0.49	0.19	0.30	0.20	0.14	0.27	0.00
99.56	99.93	100.42	100.65	99.71	100.85	100.50	99.67	99.52	99.49	99.25	99.91	99.67	100.70	99.52	100.58	99.90	99.41
3.14	3.22	3.56	3.77	4.06	4.04	4.08	4.26	3.04	3.35	3.39	3.29	4.00	4.20	3.93	4.93	4.19	4.49
1.28	1.44	2.23	2.26	4.11	3.89	0.65	6.42	2.04	3.52	3.77	3.05	6.61	5.83	5.16	4.77	4.47	26.15
11.45	11.53	11.82	11.93	12.19	12.13	12.12	12.41	11.36	11.75	11.80	11.71	12.12	12.24	12.15	12.65	12.19	12.42
4.30	4.22	3.91	3.73	3.54	3.53	3.50	3.43	4.48	4.13	4.10	4.20	3.57	3.44	3.65	3.02	3.43	3.26
1.22	1.10	0.82	0.81	0.48	0.54	0.45	0.29	0.88	0.54	0.48	0.59	0.33	0.37	0.38	0.40	0.47	0.09
2.83	2.85	3.29	3.32	3.58	3.80	3.93	3.39	3.24	3.41	3.28	3.27	3.96	3.91	3.52	3.42	3.80	4.29
0.03	0.09	0.10	0.13	0.08	0.00	0.11	0.09	0.11	0.14	0.15	0.11	0.04	0.07	0.04	0.03	0.06	0.00
69.40	70.50	78.10	77.90	86.50	87.60	87.50	89.90	76.60	83.40	83.90	82.40	91.50	89.90	89.30	88.80	87.80	97.90
29.90	27.20	20.00	19.00	11.60	12.40	10.00	7.70	20.80	13.30	12.30	14.90	7.60	8.50	8.90	10.40	10.90	2.10
0.70	2.30	1.90	3.10	1.90	0.00	2.50	2.40	2.60	3.30	3.80	2.70	0.90	1.60	1.80	0.80	1.30	0.00

Table 26. Chemical comparison between plagioclases from the Huangtongjiang gabbro and metamorphosed Precambrian sedimentary rock

Location	Huangtongjiang	Huangtongjiang		Hetai	
Sample No.	C160-2	C128		C42	
SiO2	54.71	52.00	52.60	52.81	65.08	65.25
Al2O3	28.71	30.33	30.88	30.44	21.56	21.87
TiO2	0.00	0.00	0.00	0.00	0.00	0.13
FeOt	0.00	0.00	0.00	0.00	0.00	0.00
MgO	0.00	0.00	0.00	0.00	0.00	0.00
MnO	0.00	0.00	0.00	0.00	0.27	0.30
CaO	11.08	13.09	13.67	12.71	3.66	3.26
Na2O	4.99	3.92	3.66	4.25	9.92	10.11
K2O	0.00	0.00	0.11	0.00	0.12	0.00
Total	99.49	99.34	100.93	100.20	100.61	100.92
SiO2/Al2O3	1.91	1.71	1.70	1.73	3.02	2.98
Na2O/CaO	0.45	0.30	0.27	0.33	2.71	3.10
Si	9.90	9.48	9.45	9.54	11.43	11.40
Al	6.12	6.52	6.54	6.48	4.46	4.51
Ca	2.15	2.56	2.63	2.46	0.69	0.61
Na	1.75	1.39	1.28	1.49	3.39	3.43
K	0.00	0.00	0.03	0.00	0.03	0.00
An	55.10	64.70	66.80	62.30	16.80	15.10
Ab	44.90	35.30	32.50	37.70	82.50	84.90
Or	0.00	0.00	0.70	0.00	0.70	0.00